DAA/Ames NCC2-106

Department of AERONAUTICS and ASTRONAUTICS
STANFORD UNIVERSITY

OPTIMAL LANDING
OF A HELICOPTER IN AUTOROTATION

A DISSERTATION

SUBMITTED TO

THE DEPARTMENT OF AERONAUTICS AND ASTRONAUTICS

AND THE COMMITTEE ON GRADUATE STUDIES

OF STANFORD UNIVERSITY

IN PARTIAL FULFILLMENT OF THE REQUIREMENTS

FOR THE DEGREE OF

DOCTOR OF PHILOSOPHY

By

Allan Yeow-Nam Lee

July 1985

OPTIMAL LANDING
OF A HELICOPTER IN AUTOROTATION

A DISSERTATION

SUBMITTED TO

THE DEPARTMENT OF AERONAUTICS AND ASTRONAUTICS

AND THE COMMITTEE ON GRADUATE STUDIES

OF STANFORD UNIVERSITY

IN PARTIAL FULFILLMENT OF THE REQUIREMENTS

FOR THE DEGREE OF

DOCTOR OF PHILOSOPHY

By

Allan Yeow-Nam Lee

July 1985

OPTIMAL LANDING OF A HELICOPTER IN AUTOROTATION

Allan Yeow-Nam Lee, Ph.D.

Stanford University, 1985

Gliding descent in autorotation is a maneuver used by helicopter pilots in case of engine failure. It requires considerable skill, and since it is seldom practiced, it is considered quite dangerous. In fact, during certification, a region of low altitude and low velocity (the H-V restriction zone) is established where it is considered impossible to make a safe descent.

The landing of a helicopter in autorotation is formulated as a nonlinear optimal control problem. A simplified point-mass model of an OH-58A helicopter is used in the study. The model considers as its states the helicopter vertical and horizontal velocities, vertical and horizontal displacements (from the point at which engine-failure occurred), and the rotor angular speed. It provides an empirical approximation for the induced velocity in the vortex-ring state. The cost function of the optimal control problem is a weighted sum of the squared horizontal and vertical components of the helicopter velocity at touchdown. The control (horizontal and vertical components of the thrust coefficient) required to minimize the cost function is obtained using nonlinear optimal control theory.

A unique feature in the present problem formulation is the addition of path inequality constraints on both the control and the state vectors. The control variable inequality constraint is a reflection of the limitation on the rotor thrust coefficient.

The state variable inequality constraint is an upper bound on the vertical sink-rate of the helicopter during descent. "Slack" variables are employed to convert these path inequality constraints into path equality constraints. The resultant two-point boundary-value problem with path equality constraints is successfully solved using the Sequential Gradient Restoration Technique.

Optimal trajectories are calculated for entry conditions well within the H-V restriction curve, with the helicopter initially in hover or in forward flight. Solutions are essentially discontinuous, i.e., they consist of variable subarcs which are connected at suitable corners. Subarcs are those which satisfy either the Eulerian equations, the upper bound on the thrust coefficient, or the bound on the maximum rate of descent. The optimal solutions exhibited similar control techniques as are used by helicopter pilots in actual autorotational landings. The results indicate the need to drop the collective pitch immediately after engine failure. During the landing flare phase, the thrust vector is rotated to the rear in order to decelerate the forward motion of the vehicle. The stored rotational energy of the rotor is traded for additional thrust to cushion the landing at touchdown. The study indicates that, subject to pilot acceptability, a substantial reduction could be made in the H-V restriction zone using optimal control techniques, thus providing a benchmark for comparisons with other control techniques.

These optimization techniques could also be used to:

(1) help instruct pilots on good autorotation technique.

(2) reduce the risk/time/effort involved in establishing the H-V restriction zones by flight tests.

(3) provide an objective comparison of the autorotation capabilities of different helicopter models.

(4) assess the influence of vehicle parameters on autorotation during preliminary design.

Approved for publication:

By _____
For Major Department

By _____
Dean of Graduate Studies and Research

I certify that I have read this thesis and that in my opinion it is fully adequate, in scope and quality, as a dissertation for the degree of Doctor of Philosophy.

_____

(Principal Adviser)

I certify that I have read this thesis and that in my opinion it is fully adequate, in scope and quality, as a dissertation for the degree of Doctor of Philosophy.

_____

I certify that I have read this thesis and that in my opinion it is fully adequate, in scope and quality, as a dissertation for the degree of Doctor of Philosophy.

_____

Approved for the University Committee on Graduate Studies:

_____

Dean of Graduate Studies and Research

Abstract

Gliding descent in autorotation is a maneuver used by helicopter pilots in case of engine failure. It requires considerable skill, and since it is seldom practiced, it is considered quite dangerous. In fact, during certification, a region of low altitude and low velocity (the H-V restriction zone) is established where it is considered impossible to make a safe descent.

The landing of a helicopter in autorotation is formulated as a nonlinear optimal control problem. A simplified point-mass model of an OH-58A helicopter is used in the study. The model considers as its states the helicopter vertical and horizontal velocities, vertical and horizontal displacements (from the point at which engine-failure occurred), and the rotor angular speed. It provides an empirical approximation for the induced velocity in the vortex-ring state. The cost function of the optimal control problem is a weighted sum of the squared horizontal and vertical components of the helicopter velocity at touchdown. The control (horizontal and vertical components of the thrust coefficient) required to minimize the cost function is obtained using nonlinear optimal control theory.

A unique feature in the present problem formulation is the addition of path inequality constraints on both the control and the state vectors. The control variable inequality constraint is a reflection of the limitation on the rotor thrust coefficient. The state variable inequality constraint is an upper bound on the vertical sink-rate of the helicopter during descent. "Slack" variables are employed to convert these path inequality constraints into path equality constraints. The resultant two-point boundary-value problem with path equality constraints is successfully solved using the Sequential Gradient Restoration Technique.

Optimal trajectories are calculated for entry conditions well within the H-V restriction curve, with the helicopter initially in hover or in forward flight. Solutions are essentially discontinuous, i.e., they consist of variable subarcs which are connected at suitable corners. Subarcs are those which satisfy either the Eulerian equations, the upper bound on the thrust coefficient, or the bound on the maximum rate of descent. The optimal solutions exhibited similar control techniques as are used by helicopter pilots in actual autorotational landings. The results indicate the need to drop the collective pitch immediately after engine failure. During the landing flare phase, the thrust vector is rotated to the rear in order to decelerate the forward motion of the vehicle. The stored rotational energy of the rotor is traded for additional thrust to cushion the landing at touchdown. The study indicates that, subject to pilot acceptability, a substantial reduction could be made in the H-V restriction zone using optimal control techniques, thus providing a benchmark for comparisons with other control techniques.

These optimization techniques could also be used to:

(1) help instruct pilots on good autorotation technique.

(2) reduce the risk/time/effort involved in establishing the H-V restriction zones by flight tests.

(3) provide an objective comparison of the autorotation capabilities of different helicopter models.

(4) assess the influence of vehicle parameters on autorotation during preliminary design.

Acknowledgements

First and foremost, I wish to thank Professor Arthur E. Bryson, Jr. for his help and friendship. He suggested the research described in this thesis and provided me with the technical expertise that has made this dissertation possible. He has also been a constant source of energy and inspiration for me throughout my graduate study at Stanford University.

I would also like to thank Professors Daniel B. DeBra and John V. Breakwell for their assistance and guidance during the initial phase of my research.

Special thanks must be given to Senior Research Associate William S. Hindson for all the hours of valuable discussions. His experience with operations of helicopters has helped me to bridge the gap between theory and practice.

I am greatly indebted to my wife, Helen for her endless moral support and her tireless patience. She was a constant source of joy and inspiration when I needed it most. To my family, I want to express both my love and gratitude. Without their unflagging support and encouragement throughout all of my educational experiences, I would never have been able to reach the stage that this dissertation represents for me.

I also appreciate the encouragement and suggestions offered by many of my friends. I would particularly like to thank William A. Decker and Dr. Robert T.N. Chen of NASA Ames Research Center, who contributed to numerous fruitful technical discussions.

I gratefully acknowledge financial support from the National Aeronautics and Space Administration under Grant NCC 2-106.

Table of Contents

List of Figures

List of Tables

List of Symbols

a	Rotor blade two-dimensional lift curve slope
A	Rotor disk area, πR^2
A(τ)	A function defined in Equation (13) of Section (3.3)
B(τ)	A function defined in Equation (13) of Section (3.3)
c	Rotor blade chord
C	A vector defined in Equation (13) of Section (3.3)
c_d	Rotor blade section drag coefficient (at zero lift)
c_0	Nondimensional parameter defined in Equation (37) of Section (2.4)
c_{pro}	Equivalent profile drag coefficient
C_Q	Rotor torque coefficient
C_T	Rotor thrust coefficient
$(\frac{C_T}{\sigma})_s$	Rotor stall limit
C_x	Horizontal thrust coefficient
C_z	Vertical thrust coefficient
D	Helicopter parasite drag
$\bar{d}_f$	Nondimensional horizontal distance defined in

	Equation (51) of Section (2.6)
f_e	Helicopter equivalent flat plate area
f_G	Ground effect factor in induced velocity
f_I	Induced velocity parameter
$\bar{f}$	Nondimensional parameter defined in Equation (37) of Section (2.4)
g	Acceleration due to gravity
$\vec{g}$	A vector defined by Equations (22) and (23) of Section (3.2)
g_0	Nondimensional parameter defined in Equation (37) of Section (2.4)
h	Helicopter vertical displacement
h_0	Height at which engine of the helicopter fails
H	Hamiltonian function
[H]	A matrix defined in Equation (11) of Section (3.4)
$\bar{h}_f$	Nondimensional vertical distance defined in Equation (51) of Section (2.6)
I	Optimal control cost function
I_b	Rotor blade flap inertia
I_R	Total rotor rotational inertia, NI_b
J	Augmented cost function
i_0	Nondimensional parameter defined in Equation (37) of Section (2.4)
K_{ind}	Empirical factor in the induced velcoity
k_0	Nondimensional parameter defined in Equation (37) of Section (2.4)

$[K]_{(\,)}$	Diagonal gain matrix
K.E.	Kinetic energy of a helicopter
L	Integral cost function
m	Helicopter mass
m	Order of the control vector $\vec{U}$
m_0	Nondimensional parameter defined in Equation (37) of Section (2.4)
n	Order of the state vector $\vec{X}$
N	Number of blades
N	Current iteration number
n_s	Stall parameter
p	Order of the unknown parameter vector $\vec{\pi}$
P	Feasibility condition
[P]	A matrix defined in Equation (11) of Section (3.4)
P_i	Induced power
P_M	Momentum Power
p_0	Nondimensional parameter defined in Equation (37) of Section (2.4)
P_{pro}	Profile power
P_R	Power required on the main rotor to generate lift, propulsive thrust and to overcome blade profile drag
P_S	Power supplied by the engine
P.E.	Potential energy of a helicopter
q	Order of the terminal constraint vector $\vec{\psi}$
Q	Rotor torque
Q	Optimality condition

[Q]	A matrix defined in Equation (11) of Section (3.4)
$[Q_{ij}]$	A matrix defined by Equation (24) of Section (3.2)
r	Order of the equality constraint vector $\vec{S}$
$r^{(i)}$	A scalar defined in Equation (6a) of Section (3.2)
R	Rotor blade radius
[R]	A matrix defined in Equation (11) of Section (3.4)
R.E.	Rotational energy of a helicopter
$\vec{S}$	Equality constraint vector
[S]	A "square-root" matrix defined in Equation (17) of Section (3.2)
t	Time
T	Rotor thrust
[T]	A matrix defined in Equation (11) of Section (3.4)
T.E.	Total energy of a helicopter
TPP	Tip Path Plane of the rotor disk
u	Horizontal component of helicopter velocity
u_i, $i = 1,...,4$	Normalized control components
$\vec{U}$	Control vector
$\bar{u}_0$	Nondimensional parameter defined in Equation (49) of Section (2.6)
V	Helicopter flight path velocity
$\bar{V}$	Normalized vertical sink rate of a helicopter
w	Vertical component of helicopter velocity
W	Helicopter gross weight, mg
$[W_x]$	Weighting factor in the cost function
x	Helicopter horizontal displacement

x_i, $i = 1,...,6$	Normalized state components
$\vec{X}$	State vector
$\bar{x}_1$	Nondimensional parameter defined in Equation (15) of Section (2.3)
$\bar{x}_2$	Nondimensional parameter defined in Equation (16) of Section (2.3)

Greek Symbols

α	Angle between the rotor thrust vector and the vertical
γ	Rotor Lock number
θ	Angle between the helicopter's flight path velocity from horizontal
θ_{75}	Rotor collective pitch angle at 75 percent chord
λ	Rotor inflow ratio (tip-path plane refernece)
$\vec{\lambda}$	Lagrange multiplier variable vector
$[\Lambda]$	Neighboring optimal feedback gain matrix
μ	Rotor advance ratio (tip-path plane refernece)
μ	Lagrange multiplier
ν	Rotor induced velocity
ν_h	Induced velocity at hover
ϕ	Terminal cost function
Φ	Augmented terminal cost function
$\vec{\pi}$	Control parameter vector
$\vec{\psi}$	Terminal constraint vector
ρ	Air density

$\vec{\rho}$	Lagrange multiplier variable vector
σ	Rotor solidity ratio
τ	Induced velocity time lag, seconds
τ	Normalized time defined in Equation (28) of Section (2.4)
τ_f	Terminal value of τ
Ω	Rotor angular speed
Ω_o	Nominal angular speed of the rotor
ξ	Normalized time defined in Equation (55) of Section (2.8)
$\vec{\pi}$	Unknown parameter vector

Notations

[ ]	Matrix notation
$[A]_{[B]}$	$\partial[A]/\partial[B]$
$[A]_{[B][C]}$	$\frac{\partial}{\partial[C]}([A]_{[B]})^T$ where [A] [B] and [C] are either scalar or matrix
$(\cdot)_1$	Value of $(\cdot)$ evaluated at $\tau = 1$
$[\ ]^T$	Transpose of a matrix [ ]
$N_{[A]}(\vec{B})$	Weighted norm function defined in Equation (15a) of Section (3.2), $\vec{B}^T[A]\vec{B}$
$\delta(\cdot)$	First variation of $(\cdot)$
$(\ )'$	Differentiation with respect to normalized time τ
$(\ )^{\nabla}$	Differentiation with respect to normalized time ξ
$\Delta(\cdot)$	Perturbation of $(\cdot)$; see Equations (11) and (12) of Section (3.3)

$\tilde{(\cdot)}$	Varied function of $(\cdot)$; see Equations (11) and (12) of Section (3.3)
$det[A]$	Determinant of matrix $[A]$

Chapter 1

Introduction

§1.1 Background and Motivations of Research

The unique autorotation capability of the helicopter is an inherent safety feature which is heavily relied upon during power failure emergencies. However, the autorotation maneuver, which places great demands on pilot skill, is an unfamiliar task to most helicopter pilots. The vulnerability to power failure has received renewed interest lately, due to the increased military tactical emphasis on nap-of-earth (NOE) operations which require helicopter flight within the restricted areas of the height-velocity curve.

Fig. (1.1.1) shows a typical height-velocity restriction diagram. The "avoid" area of this curve defines a region of height and speed combinations from which a given helicopter, operated by a pilot of "average" skill, cannot make a safe landing should the power source fail. Outside of the avoid area, the pilot has sufficient leeway to trade height and air speed to maintain adequate energy in the rotor to arrest the sink rate at touch down, and thus accomplish a safe landing.

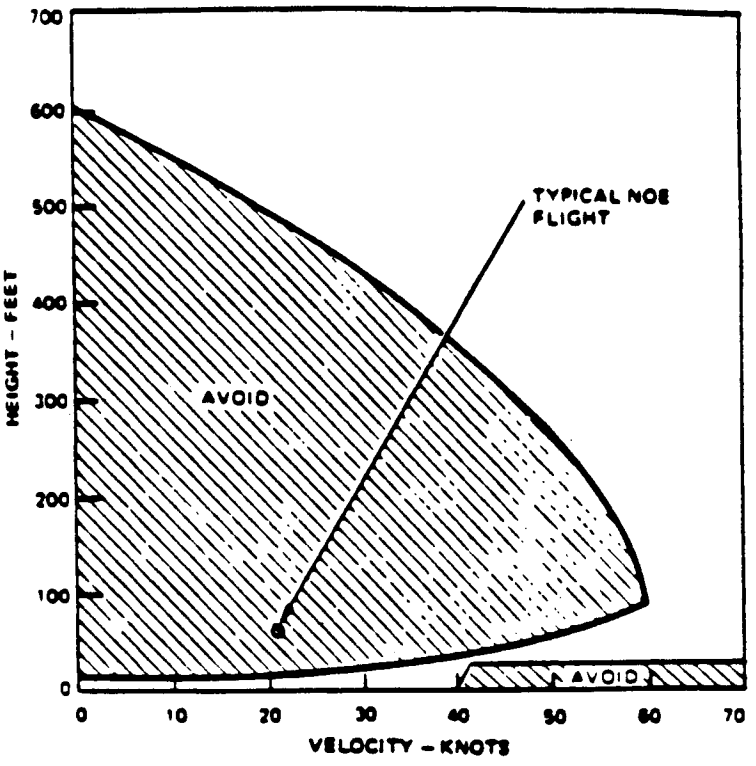

Figure 1.1.1 Typical height-velocity envelope

While the frequency of emergency autorotative landings has decreased over the past several years due to improvements in the reliability and maintenance of helicopter engines. the percentage of unsuccessful landings resulting from emergency autorotations has remained high. United States Army Safety Center accident statistics reveal that at least 27 percent of all autorotative landings involving single engine helicopters result in some degree of vehicle damage or personnel injury [Reference 1]. Fig. (1.1.2) shows that most of these emergency landings are related to engine failure.

§1.2 The Autorotation Maneuver and Related Research

The transient dynamics and control of a helicopter after engine failure have been studied both analytically [2,3], and experimentally [4-10]. The immediate and obvious effects of power loss are rotor rpm decay and out-of-trim rotational accelerations (notably, left yaw). From the standpoint of minimizing rotor rpm decay, the collective pitch must be reduced immediately. This is especially true when collective pitch and consequent torque are high. Heavy weight, high altitude, hover and vertical climb are therefore critical conditions.

Typically, the maneuver of the helicopter, from pilot recognition of engine failure to touchdown, can be divided into three phases. The entry phase consists mainly of the arresting angular motion of the vehicle and main-rotor rpm decay. During the steady-state descent phase, air flows upward through the rotor disk. The increase in angle of attack on the rotor blades offsets the reduction in the collective pitch angle. Total aerodynamic force is increased and inclined forward so equilibrium is established. Potential energy of the vehicle can also be traded for kinetic energy in order to attain desired steady-state descent airspeed that correspond to minimum sink rate or minimum descent angle.

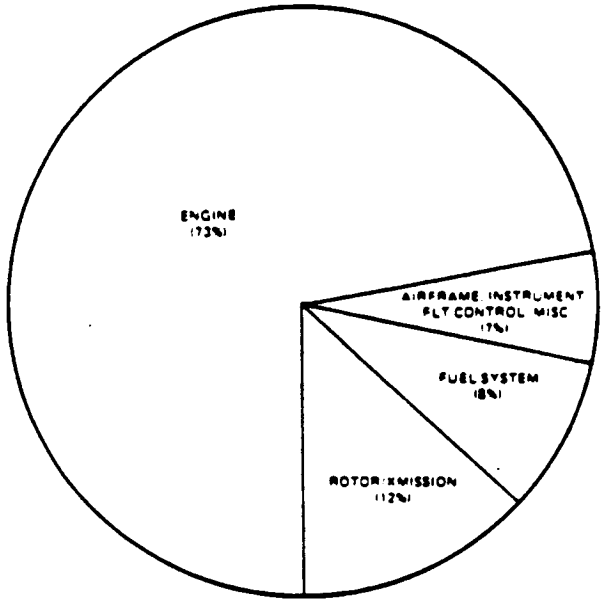

Figure 1.1.2 Emergency autorotation cause related factors

To perform the final phase of an autorotative landing, the pilot must reduce airspeed and sink rate just before touchdown. Both of these actions can be accomplished by moving the pilot's cyclic control stick to the rear. The rearward oriented rotor disk allows a larger volume of air to flow through it, resulting in an increase in the total lifting force. The increased aft-directed thrust will reduce both the airspeed and sink rate. Kinetic energy of the vehicle has been converted into lift (in the forms of profile and induced power losses), as well as rotor energy. Finally, the collective is raised to convert the stored rotor energy into lift which further cushions the landing.

Various methods and devices have been proposed to improve helicopter autorotational characteristics. One passive autorotation augmentation concept is to store energy in the helicopter main rotor by using blades with high inertia. Flight demonstration of the concept, the High Energy Rotor System (HERS), was conducted by Bell Helicopter and documented in references [11,12]. In addition to reducing the H-V restriction curves, the HERS can also provide increased maneuverability and performance. However, the high payload weight penalty makes HERS unattractive for all single engine helicopters.

Active autorotation augmentation concepts have also been explored. References [1,13 and 14] list tip jets, flywheel and auxiliary turbines as the three most promising concepts that can provide an additional source of energy to the system with payload weight penalty of only 3 to 8 percent. Based upon simulation results, these authors conclude that the autorotative characteristics of single engine helicopter can be substantially improved.

In comparison with the concepts of active energy addition and passive energy storage, the concept of optimal control management as a means of improving autorotation characteristics of a helicopter has received relatively little attention. Here,

improved autorotation performance is achieved only by the management of available energy. No supplemental energy is used.

Johnson [15] used nonlinear optimal control theory to study the autorotative descent and landing of a helicopter in hover. He found that the optimal descent is purely vertical. A comparison of the optimal control procedure with flight tests showed sufficient correlation to verify the basic features of the mathematical model used.

§1.3 Objectives of Research

The primary objective of the research is to study the possible reduction in height-velocity restrictions for the autorotational landing of a helicopter using optimal control techniques.

A secondary objective is to develop numerical optimization algorithms that incorporate the practical constraints that are involved in executing the maneuver.

§1.4 Outline of Thesis

In Chapter 2, the control of a helicopter after engine failure is formulated as an optimal control problem using a simplified point mass model representing an OH-58A helicopter equipped with high inertia blades. The formulation contains path inequality constraints, reflecting limitations on the rotor thrust coefficient and vertical sink rates acceptable to pilots.

In Chapter 3 the numerical optimization algorithms used to solve the problems posed in Chapter 2 are described.

In Chapter 4, results obtained for optimal autorotative landings of the modeled helicopter with entry conditions both inside and outside of the height-velocity restriction curve are presented. These results are compared with those obtained from the HERS flight tests [12], that used a similar helicopter to the one modeled for the research.

Finally, in Chapter 5 we discuss the potential usefulness of the optimal procedure in the reduction, or even elimination, of the height-velocity restriction curve. Areas of further research are also recommended.

The major contribution of this research is in the formulation of a general optimal autorotative descent problem with path inequality constraints, reflecting limitations on the thrust coefficient and vertical sink rate. This problem was successfully solved using the Sequential Gradient Restoration (SGR) technique.

In the course of the research, the potential usefulness of two other numerical optimization techniques was identified and algorithms developed. The Combined Parameter and Function (CPF) optimization algorithm extends the capability of FCNOPT [16] to include an unknown parameter vector in the formulation of the optimal control problem. The algorithm SECOND computes neighboring feedback control laws for optimal control problems with path equality constraints.

In addition to its potential usefulness in the reduction of height- velocity restriction for helicopter flight, the optimal control procedure can also be used for:

(1) assessing the influence of basic parameters on the helicopter autorotation characteristics during the preliminary design process;

(2) reducing the time and risk involved in the establishment of the H-V restriction curves during the helicopter certification process;

and (3) providing an objective comparison of the autorotation capability of different helicopter designs.

Chapter 2

Problem Formulation

In this chapter, the landing of a helicopter after engine failure is formulated as a dynamic optimization problem. The assumptions made in the derivation of the dynamic model are stated first. The cost function of the optimal control problem is formulated as a weighted sum of the square of sink rate and forward speed at touchdown. Path inequality constraints, reflecting limitations on the thrust coefficient and sink rate, are then introduced. Finally, the end conditions are added to complete the formulation.

§2.1 The Need to Simplify

The solution of a high-order nonlinear optimal control problem is a difficult task. Practical engineering problems, like this one, need to be simplified before current optimization techniques can be applied. Practical considerations suggest the use of an approximate mathematical model of low order which can describe the dynamic system within some tolerable degree of error. Solutions obtained from a simplified model of the system often provide a good physical understanding of the problem. More accurate models can then be used, if necessary, to include secondary effects which were ignored in the simplified model.

§2.2 Basic Assumptions

We simplify the problem here by :

(A) considering only motion in a vertical plane:

(B) using a point mass model:

(C) using a simplified induced velocity model where:

(1) dynamics of induced velocity are neglected:

(2) triangular induced velocity distribution is assumed over the rotor disk:

(3) an empirical determination of induced velocity in the vortex ring state is used;

(D) modeling power losses as follows:

(1) compressibility and tail rotor power losses have been neglected;

(2) parasite drag of the fuselage is modeled as an equivalent flat plate area;

(3) mean profile drag coefficient is assumed constant and independent of the angle of attack on the rotor's blades.

(4) ground effect is neglected;

(E) neglecting winds and variations in air density.

Motion in a vertical plane was assumed to keep the number of state variable low for the optimization codes. Extension of the point-mass model to three-dimensional motions would be straight forward and would include two additional states (heading angle and lateral position), and two additional controls (lateral component of thrust coefficient and yawrate).

Justification of assumption (B) is made through a comparison of the experimentally determined steady state sink rate of an OH-58A helicopter in autorotation [12] with that computed using the point mass model (cf. Appendix A). Figure (2.2.1) shows that the computed steady state sink rate falls between the upper and lower bounds of the experimentally determined data. Therefore the neglected pitching motion of the helicopter in the point mass model does not enter the dynamic performance equations in a significant way.

The modeling of induced velocity for a helicopter operating in the vortex ring state is a difficult task. The approximate formula given by Johnson [15], based upon experimental results obtained by Washizu et al [17], is used in the present research work. Since the vortex ring state is a condition with high induced power loss, it is avoided during autorotation in any event. The error introduced by the approximation should be minimal.

No attempt has been made to incorporate an equation to describe the time rate of change of induced velocity. A simple first order inflow lag was developed in references [19,20] and could be used to refine the present formulation.

It is well known that the power required to hover near the ground is less than that required for hover out of ground effect [21]. However, this performance benefit of operating near the ground diminishes rapidly as the airspeed increases [22]. Ground-based simulator experiments on the control of a helicopter after engine failure and autorotation landings have shown only a minor role played by ground effect in the overall autorotational performance of a helicopter [23]. Ground effect is therefore neglected in the present study.

Finally, it is difficult to include the effect of atmospheric disturbances in an open-loop optimal control problem. However, neighboring feedback control laws could

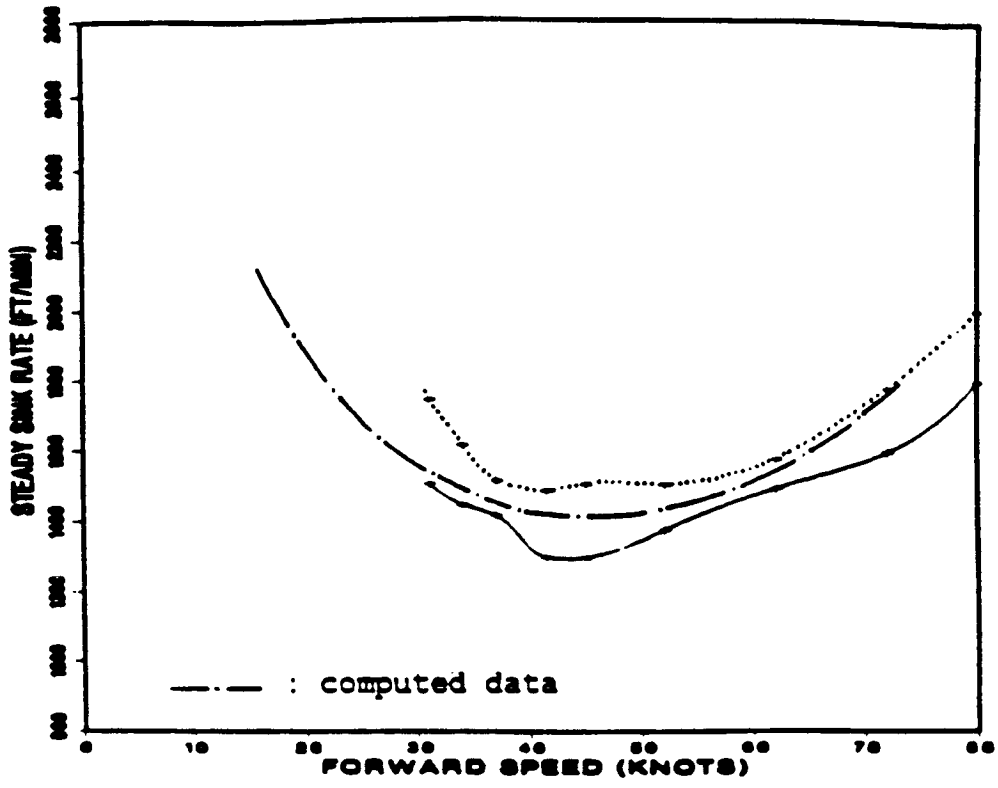

Figure 2.2.1 A comparison of computed sink rate with experimental results of Reference (18)

be computed along the nominal optimal path, to convert the open-loop solution into closed-loop feedback laws. Deterministic effects of steady wind could easily be incorporated in the model.

§2.3 Equations of Motion

2.3.1 General Considerations and Coordinate System Used.

The problem considered here is to find the controls after engine failure to arrive at the ground with acceptably small forward and vertical velocity. The helicopter is assumed to be in equilibrium level flight at the time of engine failure, with rotor speed Ω, forward speed u, and height h_0.

It is convenient to define the aircraft position from the point of engine failure by the coordinates h and x in the vertical and horizontal direction respectively. Fig. (2.3.2) shows the coordinate system used. The point at which the engine fails is therefore $h = 0$, and $h = h_0$ is the ground.

Various choices of control variables are possible. One choice is the rotor thrust coefficient C_T, and the angle the thrust vector makes with the vertical α. Since α is not well defined when C_T becomes very small, and in anticipation of the small value of C_T when the collective pitch is lowered after engine failure, it is preferable to express the problem in terms of the vertical and horizontal components of C_T:

$$\begin{aligned} C_{T_z} &= C_T \cos\alpha, \\ C_{T_x} &= C_T \sin\alpha. \end{aligned} \tag{1}$$

The collective pitch control required to obtain this thrust may then be obtained from blade element theory as in [24]:

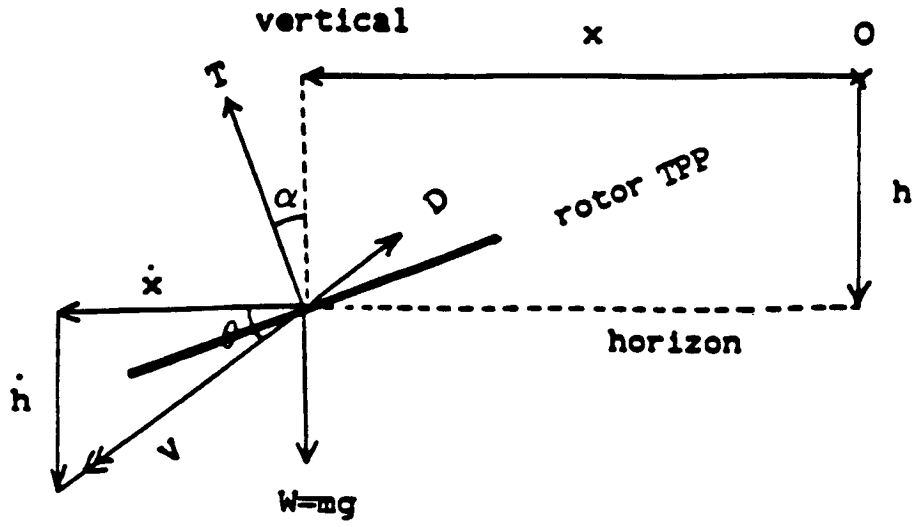

DEFINITIONS

O	:	Point at which engine fails
T	:	Rotor thrust (lb.wt.)
D	:	Parasite drag (lb. wt.)
W	:	Weight of helicopter (lb. wt.)
x	:	Horizontal distance from point of engine failure (ft.)
h	:	Vertical distance from point of engine failure (ft.)
V	:	Velocity of helicopter (ft/sec.)
$\dot{x}$	:	Horizontal component of V (ft/sec.)
$\dot{h}$	:	Vertical component of V (ft/sec.)
θ	:	Angle which V makes with the horizon (rad.)
α	:	Angle between thrust vector and vertical (rad.)

Figure 2.3.2 Coordinate system used

$$\theta_{75} = \frac{(1 + \frac{3}{2}\mu^2)(\frac{6C_T}{a\sigma}) + \frac{3}{2}\lambda(1 - \frac{1}{2}\mu^2)}{(1 - \mu^2 + \frac{9}{4}\mu^4)}, \tag{2}$$

where θ_{75} is the rotor collective pitch angle at 75 percent span, while σ and a are the rotor solidity ratio and rotor blade two dimensional lift curve slope respectively. The quantities μ and λ are respectively the advance and inflow ratios defined in the tip path plane. With reference to Fig. (2.3.2). the advance ratio μ and inflow ratio λ are defined as follows:

$$\begin{aligned} \mu &= \frac{u\cos\alpha + w\sin\alpha}{\Omega R}, \\ \lambda &= \frac{u\sin\alpha - w\cos\alpha + \nu}{\Omega R}. \end{aligned} \tag{2a}$$

Here w is the vertical velocity, and u is the forward velocity of the helicopter with respect to the inertial frame. Ω is the rotor angular velocity, and ν is the induced velocity of the rotor disk. Note that λ is defined positive in the positive direction of w, while μ is defined positive in the negative direction of x.

It is not possible to obtain the longitudinal cyclic pitch control from C_T and α without considering the helicopter pitch attitude, and the rotor flapping also. But the sign and magnitude of C_{T_x} provides information about the orientation of the rotor disk in space.

2.3.2 Dynamic Equations.

With reference to Fig. (2.3.2) , vertical and horizontal force balances give:

$$\begin{aligned} m\dot{w} &= mg - T\cos\alpha + D\sin\theta, \\ m\dot{u} &= T\sin\alpha - D\cos\theta, \end{aligned} \tag{3}$$

Here T is the rotor thrust. The helicopter parasite drag D is defined by an equivalent flat plate area f_e as:

$$\begin{aligned} D &= \frac{1}{2}\rho V^2 f_e \,, \\ &= \frac{1}{2}\rho (u^2 + w^2) f_e \,. \end{aligned} \tag{4}$$

The angle θ which the resultant velocity vector V makes with the horizontal can be eliminated from equation (2) by the relationships:

$$\begin{aligned} \sin\theta &= \frac{w}{\sqrt{u^2 + w^2}} \,, \\ \cos\theta &= \frac{u}{\sqrt{u^2 + w^2}} \,. \end{aligned} \tag{5}$$

Note that θ is undefined when both u and w approach zero. However, the corresponding components of parasite drag in the vertical and horizontal direction also approach zero under these conditions:

$$\begin{aligned} D\sin\theta &= \frac{1}{2}\rho f_e w \sqrt{u^2 + w^2} \longrightarrow 0 \\ D\cos\theta &= \frac{1}{2}\rho f_e u \sqrt{u^2 + w^2} \longrightarrow 0 \end{aligned} \tag{6}$$

2.3.3 The Energy Model.

A unique characteristic of the helicopter, as opposed to a fixed wing aircraft, is in its ability to store energy in the main rotor. The main rotor will accelerate when the torque supplied by the engine exceeds the torque required on the main rotor shaft. The torque balance equation can be expressed simply as:

$$I_R \dot{\Omega} = -Q \,, \tag{6a}$$

$$= -[\rho(\pi R^2)(\Omega R)^2 R] C_Q \,. \tag{6b}$$

and the energy balance equation of the rotor system is given by:

$$I_R \Omega \dot{\Omega} = P_S - P_R \tag{7}$$

Here I_R is the total rotational inertia of the rotor system and C_Q is the torque coefficient. It can be shown that the torque coefficient C_Q is the same as the power coefficient C_P [24]. Therefore, we can substitute C_P into equation (6b) for the torque balance equation. P_S is the power supplied by the engine and available on the main rotor shaft, after losses associated with driving the tail rotor, gearboxes, etc. have been deducted. In the event of complete engine failure, power supplied to the main rotor is reduced to zero (in fact, shaft power may even be negative due to mechanical losses or residual tail-rotor profile losses, etc.). P_R is the power required on the main rotor shaft to generate lift and propulsive thrust, and also to overcome blade profile drag. The induced power (associated with the generation of thrust) and propulsive power (power required to overcome parasite drag on the fuselage and to accelerate the helicopter forward) can be computed using momentum theory. Profile drag on the rotor blades must be obtained by blade element theory.

2.3.4 Momentum Theory.

In the momentum theory approximation, the rotor affects only the air passing through the rotor disc. As the air flows through the rotor disc it experiences a velocity increase $\vec{v}$ perpendicular to the disc (the induced velocity). The thrust generated by the rotor is equal to the rate at which momentum is imparted to the flow:

$$\vec{T} = -\rho \pi R^2 \mid \vec{V} - \vec{v} \mid 2\vec{v} \tag{8}$$

since the total velocity imparted to the air flowing through the disc is $2\vec{v}$ (cf. [25]).

The momentum power, which is the sum of the induced and propulsive powers is simply the rate at which energy is transmitted to the air due to the helicopter flight. It is the scalar product of the thrust and the resultant velocity of the flow through the actuator disk:

$$P_M = \vec{T} \cdot (\vec{V} - \vec{v}) \tag{9}$$

The first term in equation (9). $P_P = \vec{T} \cdot \vec{V}$, represents propulsive power. This is the power required to accelerate or to climb against parasite drag. The term is negative in autorotative flight. The rotor is then like a windmill, extracting energy from the air as it sweeps through it.

The second term, $P_i = -\vec{T} \cdot \vec{v}$, represents the induced power required to produce thrust. It is always positive since the induced velocity vector is always oriented in a direction opposite to the thrust generated.

Momentum theory cannot account for induced power inefficiencies such as tip loss (similar to a rotor with reduced blade size) and those due to non-uniform inflow distribution. A tip loss factor of 0.97 has generally been assumed in helicopter research and has been neglected in the present work for simplicity.

For a given thrust, a uniform inflow distribution minimizes the induced power loss. A non-uniform inflow distribution raises the induced power by a factor of K_{ind} and the actual induced power requirement becomes:

$$P_i = -K_{ind}\,\vec{T} \cdot \vec{v} \tag{10}$$

where K_{ind} is the ratio of non-uniform inflow to uniform inflow induced power requirements. For a triangular downwash distribution, K_{ind} is given by $\frac{2}{5}(\sqrt{2})^3$, or approximately 1.13.

2.3.5 Modeling the Induced Velocity.

The induced velocity ν is approximated by Johnson [15] as:

$$\tau \dot{\nu} - \nu = K_{ind}\, \nu_h\, f_I\, f_G\,. \tag{11}$$

where the symbols are defined below.

The ground effect factor f_G is taken to be unity in the present study. τ is a time constant, approximated by [19]:

$$\tau = \frac{0.21}{|\lambda|\,\Omega_0} \tag{12}$$

Ω_0 is the nominal angular speed of the rotor and is on the order of 37.0 rad/sec for OH-58A helicopters. λ is the inflow ratio which is of the order of 0.04 (for example, λ_{hover}=0.039). The value of τ calculated using equation (12) is on the order of 0.14 seconds and may be neglected in our analysis.

ν_h is a reference velocity defined by:

$$\begin{aligned} {\nu_h}^2 &= \frac{T}{2\rho\pi R^2} \\ &= R^2\Omega^2(\frac{C_T}{2}) \end{aligned} \tag{13}$$

Finally, the induced velocity parameter f_I is defined as the ratio of the actual induced velocity to the reference velocity defined in equation (13). For the determination of f_I, the following expression is used [15]:

$$f_I = \begin{cases} 1.0/\sqrt{(\bar{x}_2 + (\bar{x}_1 + f_I)^2)}, & \text{If } (2\bar{x}_1 + 3)^2 + \bar{x}_2^2 \geq 1.0; \\ \bar{x}_1(0.373\bar{x}_1^2 + 0.598\bar{x}_2^2 - 1.991), & \text{otherwise.} \end{cases} \tag{14}$$

where the parameters $\bar{x}_1$ and $\bar{x}_2$ are defined as follow:

$$\begin{aligned}\bar{x}_1 &= \frac{u\sin\alpha - w\cos\alpha}{v_h}, \\ &= \frac{u\sin\alpha - w\cos\alpha}{R\Omega\sqrt{\frac{C_T}{2}}}.\end{aligned} \tag{15}$$

$$\begin{aligned}\bar{x}_2 &= \frac{u\cos\alpha - w\sin\alpha}{v_h}, \\ &= \frac{u\cos\alpha - w\sin\alpha}{R\Omega\sqrt{\frac{C_T}{2}}}.\end{aligned} \tag{16}$$

The first expression for f_I is the familiar momentum theory result. The second expression is an empirical approximation for the vortex-ring state (where the momentum theory breaks down). The region of roughness in the vortex-ring state is defined approximately by $(2\bar{x}_1 - 3)^2 + \bar{x}_2^2 \leq 1.0$ [17]. An approximate three dimensional picture of the variation of f_I with $\bar{x}_1$ and $\bar{x}_2$ is given in Fig. (2.3.3).

2.3.6 Profile Power and the Blade Element Theory.

Accurate descriptions of the profile power require extensive wind tunnel tests to determine the effects of thrust coefficient, advance ratio, and angle of attack of the rotor's blades on rotor performance. However, in hover and level unaccelerated flight, a limited power series expansion of the profile drag coefficient in terms of mean blade lift coefficient and advance ratio offers a convenient although approximate description of the profile power requirement.

Following simple blade element theory, the profile power is traditionally referred to by an equivalent profile drag coefficient:

$$P_{pro} = c_{pro}\,\rho\,\pi R^2\,(\Omega R)^3 \tag{17}$$

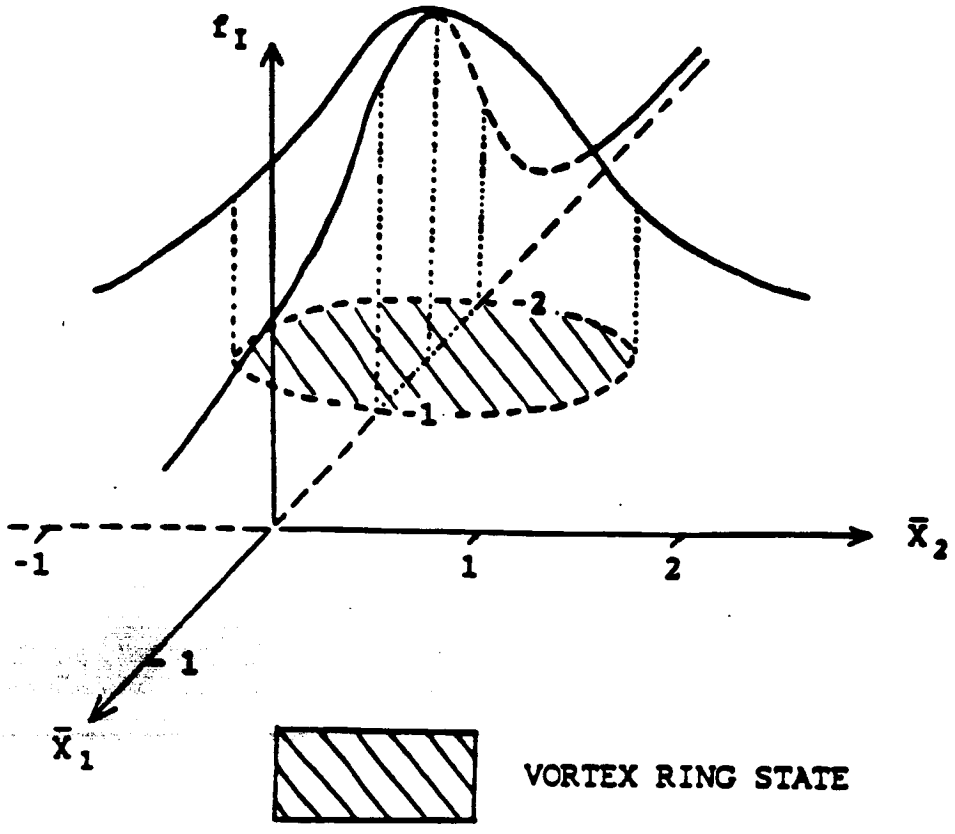

Figure 2.3.3 Variation of induced velocity parameter f_I with $\bar{x}_1$ and $\bar{x}_2$

The factor c_{pro} is the equivalent profile drag coefficient which may be approximated by [24]:

$$c_{pro} = \frac{1}{8}\sigma\,\bar{c}_d\,(1 + (\frac{6C_T}{\sigma})^2)(1 - 4.6\mu^2) \tag{18}$$

where $\bar{c}_d$ is the mean profile coefficient of the rotor's blades. With the assumed use of the NACA 0012 Airfoil on the main rotor's blades of an OH-58A helicopter, the value of $\bar{c}_d$ may be taken as 0.0087 [24]. With values of μ and $\frac{C_T}{\sigma}$ of the order of 0.15 and 0.06 respectively, both squared terms in equation (18) have been neglected. This is acceptable, as the profile power usually represents a small part of the total power requirement for helicopters.

2.3.7 The Energy Equation.

The total power required on the main rotor shaft is obtained by adding the momentum and profile powers together:

$$\begin{aligned} P_R &= P_M + P_{pro} \\ &= \vec{T}\cdot\vec{V} - K_{ind}\vec{T}\cdot\vec{v} + P_{pro} \end{aligned} \tag{19}$$

We next consider the force balance equation of the helicopter in accelerated forward flight (see Fig. (2.3.4)):

$$m\dot{\vec{V}} = \vec{T} + m\vec{g} + \vec{D} \tag{20}$$

therefore

$$m\vec{V}\cdot\dot{\vec{V}} = \vec{T}\cdot\vec{V} + m\vec{g}\cdot\vec{V} + \vec{D}\cdot\vec{V} \tag{21}$$

note that:

$$m\vec{V}\,\dot{\vec{V}} = \frac{d}{dt}(\frac{1}{2}mV^2) \tag{22}$$

and

$$m\,\vec{g}\cdot\vec{V} = -\frac{d}{dt}(mgH) \tag{23}$$

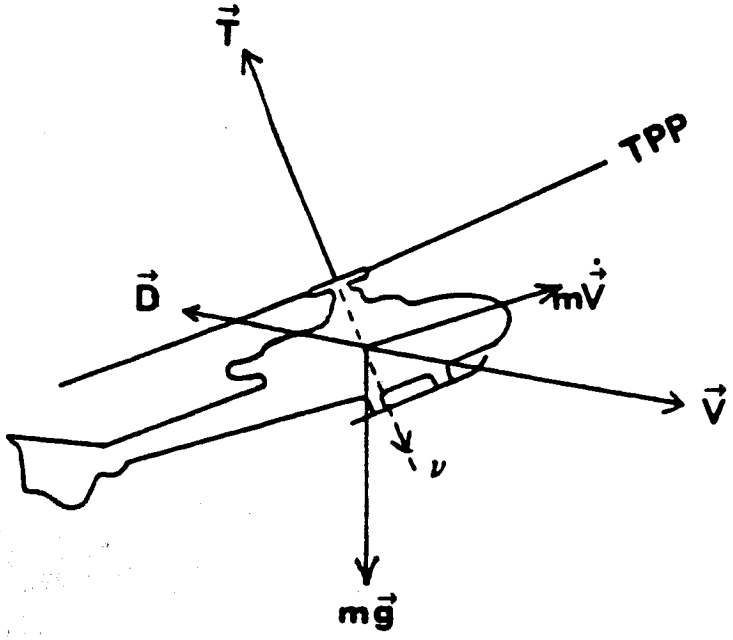

Figure 2.3.4 Force balance diagram

where H is the height of the helicopter measured in a direction opposite to that of $\bar{g}$ from an arbitrary datum.

By suitably combining equations (7). (19). (21). (22) and (23) and introducing the fuselage parasite power as :

$$\begin{aligned} P_{para} &= -\bar{D} \cdot \bar{V} \\ &= \frac{1}{2} \rho V^3 f_e \end{aligned} \tag{24}$$

(where f_e is defined in equation (4)), the time rate of change of the total energy is obtained :

$$\frac{d}{dt}(mgH + \frac{1}{2}mV^2 + \frac{1}{2}I_R\Omega^2) = P_S - (P_i + P_{pro} + P_{para}). \tag{25}$$

and the corresponding torque balance equation is :

$$\begin{aligned} I_R \dot{\Omega} &= -Q, \\ &= -\frac{1}{2}\rho(\pi R^2)(\Omega R)^2 R C_P. \end{aligned} \tag{25a}$$

where C_P is given by:

$$C_P = \frac{1}{8}\sigma \bar{c}_d + C_T \lambda, \tag{25b}$$

This energy conservation equation corresponds to the principle that any excess power supplied by the engines that is not dissipated by the helicopter is stored as internal potential, kinetic or rotational energy. Obviously, the internal energy level of the helicopter can only increase if the engine power supplied on the main rotor shaft exceeds the total power required. This excess power may be used to climb, to accelerate, or to increase rotor speed.

Conversely, in the event of engine failure, the total power or energy will decrease at a rate which depends on the helicopter's airspeed, main rotor thrust, angle of

attack and rotor RPM. The pilot's task during autorotative flight is mainly one of **Energy Management**. This can be achieved through control of the thrust vector during descent with the desired result that the aircraft can be landed at a desired (achievable) location with small vertical and forward speeds. At the same time, during the deceleration phase, the pilot must prevent the main rotor from overspeeding which would lead to unacceptable blade centrifugal stresses. This task is by no means easy.

2.3.8 Kinematical Relations.

The kinematical relations needed in the formulation of the optimal control problem are given simply by :

$$\dot{h} = w \tag{26}$$

$$\dot{x} = u \tag{27}$$

Note that these relations are coupled only one way to the dynamical relations. Since $h = h_0$ is a hard terminal constraint on the optimal control problem, equation (26) **is always needed in its formulation. Equation (27) may however be removed, unless** there is also a hard constraint on the terminal horizontal distance (as in the case where the helicopter is forced to land at a particular spot, perhaps due to terrain considerations). The removal of equation (27) will reduce the order of the problem and will facilitate the numerical solution. Information on the horizontal distance travelled may be obtained through the forward integration of equation (27) after the optimal time history of the forward speed has been found.

§2.4 Non-dimensionalization and Scaling

The efficiency and rate of convergence of numerical optimization methods depends critically on the scales used for the variables involved. This is especially true in nonlinear problems [26]. A "well scaled" problem is one in which similar changes in the variables lead to similar changes in the cost function. Now consider a typical situation where the engine of the helicopter fails while it is cruising at a forward speed of 40 *Knots* and at an altitude of 400 *ft* . The magnitude of the thrust coefficient C_T used just before engine failure is of the order of 0.003. Rotor speed before engine failure is 354 *rpm* . The different units used by the state/control variables, and the range of magnitude that these variables will assume in subsequent autorotative descent flight, clearly indicates the need to normalize and to scale.

The equations of motion may be non-dimensionalized using the quantities Ω_0 and R. Here Ω_0 is the nominal angular speed of the rotor before engine failure and R is the radius of the helicopter's rotor. Scaling factors of 10, 100 etc. are used for convenience. Non-dimensionalized and scaled quantities for the time, states, and controls used in the analysis are defined as follow:

(a) Normalized time:

$$\tau = (\frac{\Omega_0 t}{100}) \tag{28}$$

Hence, one unit of τ corresponds to about 16 rotations of the rotor.

From here onward, the notation $(\,)'$ will be used to represent differentiation with respect to the normalized time τ, where:

$$(\,)' = \frac{d}{d\tau} = \frac{100}{\Omega_0}\frac{d}{dt} \tag{28a}$$

(b) Normalized states:

$$x_1 = (\frac{w}{0.01\Omega_0 R}), \tag{29}$$

$$x_2 = (\frac{u}{0.01\Omega_0 R}), \tag{30}$$

$$x_3 = (\frac{\Omega}{\Omega_0}), \tag{31}$$

$$x_4 = (\frac{h}{10R}), \tag{32}$$

and $$x_5 = (\frac{x}{10R}). \tag{33}$$

(c) Normalized controls:

$$u_1 = 10^3 C_{T_x}, \tag{34}$$

$$u_2 = 10^3 C_{T_x}, \tag{35}$$

therefore : $$10^3 C_T = ({u_1}^2 + {u_2}^2)^{\frac{1}{2}}. \tag{36}$$

The effects of these normalizations are first to convert the time, state and control variables into dimensionless quantities, and second to scale them so that they all have order of magnitude one.

If in addition, we also define the following dimensionless constants for the system:

$$\begin{aligned} g_0 &= \frac{10^4 g}{{\Omega_0}^2 R} \\ m_0 &= \frac{10\rho\pi R^3}{m} \\ \bar{f} &= \frac{f_e}{20\pi R^2} \\ i_0 &= \frac{\rho\pi R^5}{10 I_R} \\ c_0 &= \frac{1}{8}\sigma\bar{c}_d(10^3) \\ k_0 &= \frac{K_{ind}}{\sqrt{2000}} \\ p_0 &= 0.01(\sqrt{2000}) \end{aligned} \tag{37}$$

The resultant dimensionless equations of motion are then given by:

(a) Dynamical relations (see equations (3) and (7)):

$$x_1' = g_0 - m_0(u_1 x_3^2 + \bar{f} x_1 \sqrt{x_1^2 - x_2^2}), \tag{39}$$

$$x_2' = m_0(u_2 x_3^2 - \bar{f} x_2 \sqrt{x_1^2 - x_2^2}). \tag{40}$$

$$x_3' = -i_0 x_3^2 (c_0 + \lambda \sqrt{u_1^2 + u_2^2}). \tag{40}$$

(b) Kinematical relations (see equations (26) and (27)):

$$x_4' = 0.1 x_1, \tag{41}$$

$$x_5' = 0.1 x_2. \tag{42}$$

(c) Supporting expressions:

(c1) the inflow and advance ratios are (see equations (2a)):

$$\begin{aligned} \lambda &= \frac{u \sin\alpha - w \cos\alpha}{R\Omega} + \frac{\nu}{R\Omega}, \\ &= 0.01 \frac{x_2 u_2 - x_1 u_1}{x_3 \sqrt{u_1^2 + u_2^2}} + k_0 f_I (u_1^2 + u_2^2)^{\frac{1}{4}}. \end{aligned} \tag{43}$$

$$\begin{aligned} \mu &= \frac{u \cos\alpha + w \sin\alpha}{R\Omega}, \\ &= 0.01 \frac{x_2 u_1 + x_1 u_2}{x_3 \sqrt{u_1^2 + u_2^2}}. \end{aligned} \tag{44}$$

(c2) the induced velocity parameter f_I (see equations (14)-(16)):

$$\bar{x}_1 = p_0 \frac{x_2 u_2 - x_1 u_1}{x_3 (u_1^2 + u_2^2)^{\frac{5}{4}}}, \tag{45}$$

$$\bar{x}_2 = p_0 \frac{x_2 u_1 + x_1 u_2}{x_3 (u_1^2 + u_2^2)^{\frac{5}{4}}}. \tag{46}$$

where once again, the value of the induced velocity parameter f_I, is determined from the expressions given in equation (14):

$$f_I = \begin{cases} 1.0/\sqrt{(\bar{x}_2^2 + (\bar{x}_1 + f_I)^2)}, & \text{if } (2\bar{x}_1 + 3)^2 + \bar{x}_2^2 \geq 1.0; \\ \bar{x}_1(0.373\bar{x}_1^2 + 0.598\bar{x}_2^2 - 1.991). & \text{otherwise.} \end{cases}$$

§2.5 Cost Function

The optimization problem is to arrive at the ground with small vertical and horizontal velocities subject to maintaining acceptable conditions during tha autorotative descent. The cost function, or performance criterion of the problem can therefore be taken as the weighted sum of the squared normalized sink rate and forward speed at the time of touch down:

$$I = \frac{1}{2}({x_1}_f{}^2 + W_x {x_2}_f{}^2) \tag{47}$$

Here W_x is the weighting function of normalized horizontal speed relative to vertical sink rate. Acceptable vertical sink rate at touch down that is compatible with the shock absorption capability of typical landing gear design is of the order of 8 fps [11]. A reasonable value for forward speed at touch down is 3 $knots$ (this is the average horizontal airspeed at touch down for a series of autorotative descent tests on the HERS helicopter [11]). A suitable value of W_x is therefore:

$$\begin{aligned} W_x &= (\frac{8}{3 \times 1.688})^2, \\ &= 2.5 \ . \end{aligned} \tag{48}$$

§2.6 Terminal Constraints and Initial Conditions

The helicopter is assumed to be in equilibrium level flight at the time of engine failure, with rotor speed Ω_0, forward speed u_0, and height of h_0. The position of the helicopter after engine failure is defined with respect to the point at which the

engine failure occurred. The coordinate system used is defined in Fig. (2.3.2) where h is measured in the downward direction. Therefore, the initial conditions of the state variables are:

$$\begin{aligned} x_{10} &= 0, \\ x_{20} &= \bar{u}_0, \\ x_{30} &= 1, \\ x_{40} &= 0, \\ \text{and} \quad x_{50} &= 0 \end{aligned} \tag{49}$$

where $\bar{u}_0$ is defined to be $(\frac{u_0}{0.01R\Omega_0})$.

The terminal constraints of the optimization problem include:

$$\begin{aligned} x_{4f} &= \bar{h}_f, \\ x_{5f} &= \bar{d}_f. \end{aligned} \tag{50}$$

where:

$$\begin{aligned} \bar{h}_f &= \frac{h_0}{10R}, \\ \bar{d}_f &= \frac{d_f}{10R}. \end{aligned} \tag{51}$$

Note that, while the first equation of (50) is always needed, the second equation is used only when there is a hard constraint on the terminal horizontal distance (to land at a horizontal distance of d_f ft away from the point at which engine failure occurred).

§2.7 Path Constraints

The equivalent profile drag coefficient of the rotor (c_{pro}, as defined in equation (18)) increases sharply when the thrust coefficient exceeds the rotor stall limit $(\frac{C_T}{\sigma})_{stall}$. The immediate effect of this increase in profile drag is a drop in the rotor speed. This

drop in *rpm* causes an increase in the angle of attack on the rotor's blades and will ultimately lead to rotor stall and the instability associated with it. This limitation on the thrust coefficient requires a path inequality constraint in the optimal control problem.

A typical value of $(\frac{C_T}{\sigma})_{stall}$ for the OH-58A helicopter is 0.15. This value is used in the present study. The path inequality constraint, and its non-dimensionalized form are:

$$(\frac{C_T}{\sigma})_{stall} \geq (\frac{C_T}{\sigma})$$

$$\text{or} \qquad 7.2 \geq \sqrt{u_1{}^2 + u_2{}^2} \tag{52}$$

where:

$$\begin{aligned}(10^3 C_T)_{stall} &= 10^3(\frac{C_T}{\sigma})_{stall} \times \sigma, \\ &= 10^3 \times 0.15 \times 0.048, \\ &= 7.2.\end{aligned} \tag{53}$$

This inequality constraint can be converted to a path equality constraint as shown below:

$$\text{Since} \qquad (\bar{C}_{T_s})^2 \geq (u_1{}^2 + u_2{}^2) \quad .$$

where $\bar{C}_{T_s}$ is equal to 7.2.

$$\text{therefore} \qquad \bar{C}_{T_s}^2 - (u_1{}^2 + u_2{}^2) - u_3{}^2 = 0. \tag{54}$$

where u_3 is a "slack variable" or artificial control that has been introduced to convert the inequality constraint into an equality constraint.

The upper bound on the vertical sink rate as an additional path inequality constraint will be discussed in Section (3.3).

§2.8 Further Time Normalization

The optimal control problem that has been posed thus far is one with an unspecified terminal time τ_f. The problem may be converted into one with specified terminal time through the following (further) normalization of the dimensionless time τ:

$$\xi = \frac{\tau}{\tau_f} \tag{55}$$

The transformation (55) converts the independent variable from τ to ξ where ξ now varies from 0 to 1. This transformation introduces into the problem an additional unknown parameter τ_f that has to be optimally selected. We shall from here onward denote the differentiation with respect to ξ by:

$$\begin{aligned} (\quad)^{\nabla} &= \frac{d}{d\xi}, \\ &= \tau_f(\frac{d}{d\tau}), \\ &= \tau_f(\quad)'. \end{aligned} \tag{56}$$

§2.9 Final Form of Helicopter Optimization Problem

We are now in a position to write down the final form of the helicopter optimization problem, Let:

$$\vec{X} = (x_1\ x_2\ x_3\ x_4\ x_5)^T, \tag{57}$$

$$\vec{U} = (u_1\ u_2\ u_3)^T, \tag{58}$$

$$\vec{\pi} = (\tau_f). \tag{59}$$

denote the state, control, and unknown parameter vectors of the problem.

The problem is to find $\bar{U}(\xi)$ and $\bar{\pi}$ to minimize:

$$I = \frac{1}{2}({x_{1f}}^2 + W_x {x_{2f}}^2) = \phi(\bar{X}_f), \tag{60}$$

subject to :

(1) equations of motion ($\bar{X}^{\nabla} = \bar{f}$):

$$\begin{aligned}
{x_1}^{\nabla} &= \tau_f(g_0 - m_0(u_1 {x_3}^2 - \bar{f} x_1 \sqrt{{x_1}^2 + {x_2}^2})), \\
{x_2}^{\nabla} &= \tau_f m_0(u_2 {x_3}^2 - \bar{f} x_2 \sqrt{{x_1}^2 + {x_2}^2}), \\
{x_3}^{\nabla} &= -\tau_f i_0 {x_3}^2(c_0 + \lambda\sqrt{{u_1}^2 + {u_2}^2}), \\
{x_4}^{\nabla} &= 0.1\tau_f x_1, \\
{x_5}^{\nabla} &= 0.1\tau_f x_2.
\end{aligned} \tag{61}$$

(2) the initial condition of $\bar{X}$ is given by:

$$\bar{X}_0 = (0, \bar{u}_0, 1, 0, 0)^T. \tag{62}$$

(3) path equality constraint ($\bar{S}(\bar{X}, \bar{U}, \bar{\pi}) = 0$):

$$({u_1}^2 + {u_2}^2) - (\frac{({u_1}^2 + {u_2}^2)}{\bar{C}_{T_s}})^2 - {u_3}^2 = 0. \tag{63}$$

(4) terminal constraints ($\bar{\psi}(\bar{X}_f, \bar{\pi}) = 0$):

$$\begin{aligned}
x_{4f} - \bar{h}_f &= 0, \\
x_{5f} - \bar{d}_f &= 0.
\end{aligned} \tag{64}$$

In the next chapter, a gradient-type numerical optimization technique that can be used to solve this problem is described in detail. It requires the calculation of $\frac{\partial \bar{f}}{\partial \bar{U}}$

(5×3 matrix), $\frac{\partial \bar{f}}{\partial \bar{X}}$ (5×5 matrix), $\frac{\partial \bar{f}}{\partial \bar{\pi}}$ (5×1 matrix), $\frac{\partial \bar{S}}{\partial \bar{U}}$ (1×3 matrix), $\frac{\partial o}{\partial \bar{X}_f}$ (1×5 matrix) and $\frac{\partial \bar{v}}{\partial \bar{X}_f}$ (2×5 matrix). Detailed expressions of these matrices are given in Appendix (B).

Chapter 3

Numerical Optimization Techniques

In the previous chapter, the landing of a helicopter after engine failure was formulated as a nonlinear optimal control problem with path equality constraints. Numerical optimization algorithms that can be used to solve this problem are described in this chapter.

This chapter begins with a review of algorithms for solving optimal programming problems with bounded controls and/or states. A combined function and parameter optimization algorithm is then described. It is an extension of the ordinary gradient-type numerical algorithm (FCNOPT) [16], to handle the presence of an unknown parameter vector. In Section (3.3), we describe the Sequential Gradient Restoration algorithm which can be used to solve optimization problems with nondifferential path equality constraints. Several transformation techniques are then presented that convert problems with path inequality constraints to problem with equality constraints. The chapter ends with a description of an algorithm that can be used to compute neighboring feedback control laws for optimization problems with path equality constraints.

§3.1 Algorithms for Problems with Bounded Controls and/or States

One of the earliest attempts at numerical solution of optimal programming problems with control or state inequality constraints was made by Bryson et al [27-28, see also chapter 3 of 29]. Necessary conditions for extremal solutions to programming problems with an inequality constraint on a function of the control or state variables were given. It was shown that, in general, certain terms must be added to the Hamiltonian function during the interval in which the solution curve lies on the constraint boundary. Furthermore, for inequality constraint functions not explicitly involving the control variable, one or more functions of the state and time must satisfy equality constraints at the beginning (the *entry* corner) of a constraint boundary interval. The Lagrange multiplier functions are not uniquely defined on state constraints. In the work reported in Reference 28, a modified version of the steepest-ascent technique was used in the numerical solution of two atmospheric entry trajectory problems. An advantage of the method is that improvements in the control program are not required for the period on the constraint boundary, making possible a more rapid convergence towards the optimal program. However, the method requires prior assumptions concerning the number and location of the junction points.

Inequality constraints on functions of control and/or state variables have also been treated by several investigators through the use of integral penalty functions [31-33]. One such scheme [31-32] uses an auxiliary state variable which is the integral of a quadratic measure of the violation of the inequality constraint, which is brought as close to zero as is necessary to provide a satisfactorily small violation of inequality constraint. Rate of convergence to a satisfactory solution is usually slow [29].

McGill [33] developed a generalized Newton-Raphson algorithm based upon essen-

tially the same idea of reducing the constraint problem to an unconstrained one by the introduction of an additional state. His approach does not require assumptions as to the number and location of junction points. Computational experience with one example problem (a modified version of the classical brachistochrone problem) suggests that it may be useful for obtaining solutions to the class of nonlinear problems with bounds on the state space.

In an extension of the work given in references [27-28], Speyer and Bryson [34] gave a new set of necessary conditions for solution of an optimal programming problem with a state variable inequality constraint. It was shown that unconstrained arcs must satisfy certain "tangency" constraints; namely, these arcs must have zero values of the state variable constraint function and all of its time derivatives that do not involve the control function, at both the entry and exit corners of the constrained arc. These conditions are satisfied automatically if the necessary conditions of reference [27] are used. However, if one uses the "direct-adjoining" approach of reference [35], explicit use must be made of the tangency constraints at both corners.

In reference [36], Mehra et al showed that some of the difficulties associated with nonlinear programming problems with state variable inequality constraints and singular arcs arise due to the exclusive use of control variables as the independent variables in the search procedure. They proposed a conjugate-gradient algorithm which based its choice of independent variables on the problem constraints. This choice could result in different combinations of state and control variables as independent variables along different parts of the trajectory. Four numerical examples were successfully solved using this approach. Two of the solved problems had a state variable inequality constraint and the other two had singular arcs. The inequality constraint and singular arcs were handled in a regular fashion without explicit use

of extra necessary conditions of optimality. This is considered to be a special feature and an advantage of the method.

In reference [37], Maurer et al distinguish between two main cases of optimal programming problems with bounded state variables, depending on whether the control variable appears nonlinearly or linearly. The distinction arises naturally from the fact that a nonlinear optimal control in the first class must be continuous at the junctions between the interior arcs and boundary arcs, whereas any linear optimal control in the second class is discontinuous in general. Maurer et al exploited the fact that the optimal control in the first case must be continuous and satisfy a suitable augmented Two-Point Boundary-Value Problem (TPBVP). This consists of the basic two-point boundary-value problem of the Maximum principle, and of additional differential equations and boundary conditions constructed in such a way that all the necessary conditions are automatically fulfilled by the solution. The TPBVP's encountered were solved using the method of multiple shooting [38]. Three numerical examples were solved to illustrate the efficiency of the algorithm. Once again, predetermination of the number and sequence of subarcs of the optimal solution has to be made prior to the initialization of the algorithm.

Most of the above mentioned methods suffer from the following disadvantages:

(1) it is not known a priori, whether there will be more than one joining of unconstrained and constrained arcs, and where in time these joining will occur;

(2) the discontinuities in the Lagrange variables at the junctions of the unconstrained and constrained arcs are, a priori, unknown, and have to be guessed and iterated upon.

To overcome these difficulties, Jacobson et al [39] suggested the use of a different approach. A device suggested by Valentine was used to transform a control problem with a state variable inequality constraint into an unconstrained one of increased dimension. With a p^{th} order state variable inequality constraint, it can be shown that in the transformed unconstrained problem, the p^{th} time derivative of the slack variable becomes the new control variable. One feature of the transformed problem is that any guessed nominal control results in a feasible state trajectory, i.e., the inequality constraint is automatically satisfied. A second feature is that the transformed problem exhibits singular arcs which correspond, in the original state constrained problem, to arcs lying along the state constraint boundary.

However, a major difficulty arises with Jacobson's approach when the number of state bounds (r) does not equal the dimension of the control vector (m). In particular, if $m < r$, then one cannot express u as functions of the r slack variables unless some of these variables are dependent upon each other. Thus one cannot use the appropriate time derivative of the r slack variables as independent new controls. Two numerical examples without the above difficulty were given in [39].

Instead of replacing the control u in the original problem formulation by appropriate slack variables and its time derivatives, one can enforce the state/control bound by the addition of path equality constraints to the original problem. These path equality constraints are again obtained by the use of Valentine's device on path inequality constraints. In this way, nonlinear optimal programming problems with path inequality constraints can be transformed into ones with nondifferential path equality constraints.

The solution to this class of problems with path equality constraints differs from the solution without the constraints. The usual approach of backward integration of

the adjoint-equations and forward integration of the equations of motion cannot be employed here. This is due to the fact that the computation of the Lagrange multiplier $\bar{\rho}(t)$ (associated with the path constraints $\bar{S}$) over the time interval requires the simultaneous solution of both the adjoint-equations and the equations of motion. Because of the coupling, the total system must be integrated simultaneously in either the forward or backward direction. One way of solving the coupled, nonlinear, two-point boundary-value problem is by the Method of Particular Solutions given in references [40-41]

Miele et al [42], at about the same time as Jacobson, developed a Sequential Gradient Restoration algorithm for the solution of optimal control problems with path equality constraints. The algorithm made use of the method of particular solutions of [40]-[41]. Both the feasibility as well as the efficiency of the algorithm were illustrated through the solutions of example problems given in [42] and other related papers [43-45]. The approach taken in the present work on the optimal autorotation trajectory of a helicopter is to combine these two mathematical tools (the Valentine's device and the Method of Particular Solutions for the solution of a nonlinear TPBVP) for the solution of the constrained optimization problem posed in Section (2.9). The Sequential Gradient Restoration method is described in greater detail in Section (3.3).

§3.2 Combined Function and Parameter Optimization Algorithm

Direct analytical solutions of dynamical optimization problems are only possible when the system equations, the performance index, and the constraints of the problem are very simple. One of the more reliable methods for the numerical solution of the dynamical optimization problem is the steepest-descent gradient method [30]. The method is characterized by iterative steps for improving estimates of the con-

trol history, $u(t)$, so as to come closer to satisfying the optimality conditions and the boundary conditions. First-order gradient methods usually show great improvements in the first few iterations but have poor convergence characteristics as the optimal solution is approached. Second-order gradient methods have excellent convergence characteristics as the optimal solution is approached but may have starting difficulties associated with picking a "convex" nominal solution [29]. Variable Step-size Gradient methods can improve the convergence characteristics of the first-order gradient methods through the optimal selection of step-size at each iteration step. Further information on the variable step-size gradient algorithm can be obtained from [26].

In this section, we wish to extend the gradient algorithm for function optimization problems [16] so that it is capable of solving optimal control problems that also have an unknown parameter vector. We assume that there are no inequality constraints, that the initial time and state are fixed, and that functions of some of the state variables and unknown parameters are specified at a given or an unspecified terminal time. Thus we wish to consider the following optimization problem:

$$\begin{aligned} \min_{\vec{u},\vec{\pi}} I &= \phi_1(\vec{x}_f, \vec{\pi}) + \int_0^{t_f} \bar{L}(\vec{x}, \vec{u}, \vec{\pi}, t)\, dt, \\ \dot{\vec{x}} &= \bar{f}(\vec{x}, \vec{u}, \vec{\pi}, t), \\ \vec{x}(0) &= given, \\ \text{and} \qquad \vec{\psi}(\vec{x}_f, \vec{\pi}) &= 0. \end{aligned} \tag{1}$$

Here $\vec{x}(n \times 1)$, $\vec{u}(m \times 1)$, and $\vec{\pi}(p \times 1)$ are the state, control and the unknown parameter vectors. $\vec{\psi}(q \times 1)$ are the terminal constraints of the problem. If the end-time t_f of the problem is unspecified, the problem may be converted to one with a specified end-time through the use of the following transformation:

$$\tau = \frac{t}{t_f}. \tag{1a}$$

The independent variable is now τ which varies from 0 to 1 (therefore the subscript "1" in equation (1) denotes terminal condition). The final time t_f is included as one of the components of $\bar{\pi}$. $\bar{L}$ and $\bar{f}$ are replaced by $L = t_f \bar{L}$ and $f = t_f \bar{f}$.

If we adjoin the system differential equations and the terminal constraints to the performance index I with multiplier function $\lambda(t)(n \times 1)$ and multiplier $\mu(q \times 1)$ respectively, we get:

$$J = (\phi + \mu^T \psi)_1 + \int_0^1 [L + \lambda^T (f - \dot{x})] d\tau . \tag{2}$$

Now consider the variation in J due to variations in both the control and parameter vectors:

$$\begin{aligned} \delta J = (-\lambda^T + \Phi_x)_1 \delta x_1 + [\int_0^1 H_\pi d\tau + (\Phi_\pi)_1] \delta \bar{\pi} \\ + \int_0^1 [H_u \delta \bar{u} + (H_x + \dot{\lambda}^T) \delta \bar{x}] d\tau , \end{aligned} \tag{3}$$

where for convenience, we have defined scalar functions H (the Hamiltonian function) and Φ as given below:

$$\begin{aligned} H &= L + \lambda^T f , \\ \Phi &= \phi + \mu^T \psi . \end{aligned} \tag{4}$$

Therefore, first-order necessary conditions for the extremal solution are given by the following relations:

$$\begin{aligned} \dot{\lambda}^T &= - H_x , \\ \lambda_1{}^T &= (\Phi_x)_1 , \\ H_u &= 0 , \\ \text{and} \quad \int_0^1 H_\pi d\tau + (\Phi_\pi)_1 &= 0 . \end{aligned} \tag{5}$$

In the special case when the unknown parameter $\bar{\pi}$ contains the unspecified terminal time, the corresponding component in the last equation in (5) becomes the transversality condition of the classical literature (cf. Appendix D).

Equations (1) and (5) contain all the conditions needed in the solutions of $\bar{x}(\tau)$ $(n \times 1)$, $\bar{u}(\tau)$ $(m \times 1)$, $\bar{\lambda}(\tau)$ $(n \times 1)$, $\bar{\pi}$ $(p \times 1)$ and $\bar{\mu}$ $(q \times 1)$.

Various methods have been suggested for the solution of this two-point boundary-value problem. The method used here may be termed the Impulse Response method [29].

The method involves making initial guesses for both the control time history $\bar{u}(\tau)$ and the unknown parameter $\bar{\pi}$. The dynamic equations are integrated forward using the given initial conditions. In general, the terminal conditions are not satisfied. To make improvements in the feasibility condition, we consider the following (q+1) impulse response functions $H_u{}^{(i)}$, where $i = 0, 1, \cdots, q$. Note that $H_u{}^{(0)}(\tau)$ represents the variation in the cost function due to a unit impulse (Dirac Function) in $\delta\bar{u}$ at time τ, while holding $\bar{x}(0)$ and $\bar{\pi}$ constant and satisfying the dynamic equations. Similarly, $H_u{}^{(i)}(\tau)$ where i = 1,...,q corresponds to variations in the terminal constraints $\bar{\psi}$ due to a unit impulse in $\delta\bar{u}$ at time τ. These impulse response functions are given by the following expression:

$$H_u{}^{(i)}(\tau) = r^{(i)} L_u(\tau) + [\lambda^{(i)}]^T f_u(\tau), \tag{6}$$

where

$$r^{(i)} = \begin{cases} 1 & \text{if } i = 0; \\ 0 & \text{if } i \neq 0. \end{cases} \tag{6a}$$

for i = 0,1,...,q. The influence functions $\lambda^{(i)}(\tau)$ are determined from the backward integrations of the following adjoint equations using the time histories of $\bar{x}(\tau)$, $\bar{u}(\tau)$ and the value of $\bar{\pi}$ from the forward integrations:

$$\dot{\lambda}^{(i)} = -r^{(i)} L_x(\tau) - [\lambda^{(i)}]^T f_x(\tau), \tag{7}$$

$$[\lambda^{(i)}]_1 = (\psi_i)_x{}^T, \tag{8}$$

where

$$\psi_0 = \phi(\bar{x}_f, \bar{\pi}). \tag{9}$$

In this way, the (q−1) impulse response functions $H_u^{(i)}$, where i = 0,1,...,q, for the current iteration, can be computed.

The quantities $[\int_0^1 H_\pi^{(j)}(\tau)d\tau + (\psi_j)_\pi]$, where j = 0,1,....q represent the variations in either the performance index or terminal constraints due to a unit changes in the elements of $\bar{\pi}$, while holding $\bar{x}(0)$ and $\bar{u}$ constant and satisfying the dynamic equation.

Therefore variations in the cost function and the terminal constraints due to small variations in the control histories $\delta\bar{u}(\tau)$ and the parameters $\delta\bar{\pi}$ are given by the following relations:

$$\delta J = \int_0^1 H_u^{(0)}\delta\bar{u}(\tau)\,d\tau + [\int_0^1 H_\pi^{(0)}(\tau)\,d\tau + (\psi_0)_\pi]\delta\bar{\pi}, \tag{10}$$

and

$$\delta\psi_j = \int_0^1 H_u^{(j)}(\tau)\delta\bar{u}\,d\tau + [\int_0^1 H_\pi^{(j)}(\tau)d\tau + (\psi_j)_\pi]\delta\bar{\pi}, \tag{11}$$

where j = 1,....q

If we adjoin equation (11) to (10) with q Lagrange multipliers μ_i, where i = 1,...,q, we have:

$$\begin{aligned}\delta\bar{J} &= \delta J + \sum_{i=1}^{q}\mu_i\delta\psi_i,\\ &= \int_0^1 [H_u^{(0)} + \sum_{i=1}^{q}\mu_i H_u^{(i)}]\delta\bar{u}\,d\tau \\ &\quad + [\int_0^1 H_\pi^{(0)}\,d\tau + (\psi_0)_\pi + \sum_{i=1}^{q}\mu_i\int_0^1 H_\pi^{(i)}d\tau + \sum_{i=1}^{q}\mu_i(\psi_i)_\pi]\delta\bar{\pi}.\end{aligned} \tag{12}$$

If we wish to obtain the largest change in $\delta\bar{J}$, we would calculate the gradients $H_u^{(i)}$ and $[\int_0^1 H_\pi^{(i)}(\tau)d\tau + (\psi_i)_\pi]$ (i = 0,1,...,q) and then direct $\delta\bar{\pi}$ and $\delta\bar{u}$ opposite to their respective gradients as follow:

$$\delta\bar{\pi} = -K_\pi\Big[\int_0^1 H_\pi^{(0)}d\tau + (\psi_0)_\pi + \sum_{i=1}^{q}\mu_i\Big(\int_0^1 H_\pi^{(i)}d\tau + (\psi_i)_\pi\Big)\Big]^T,$$

$$= -K_\pi\Big[\int_0^1 (H_\pi^{(0)})^T d\tau + (\psi_0)_\pi{}^T + \sum_{i=1}^{q}\mu_i\Big(\int_0^1 (H_\pi^{(i)})^T d\tau + (\psi_i)_\pi{}^T\Big)\Big], \quad (13)$$

where K_π is a $(p \times p)$ diagonal gain matrix that controls the stepsize of $\delta\bar{\pi}$.

Similarly,

$$\delta\bar{u} = -K_u\Big[(H_u^{(0)})^T + \sum_{i=1}^{q}\mu_i(H_u^{(i)})^T\Big], \quad (14)$$

where K_u is an $(m \times m)$ diagonal gain matrix that controls the stepsize of $\delta\bar{u}$.

When we make these choices in $\delta\bar{\pi}$ and $\delta\bar{u}$, the predicted variation in the augmented performance index $\bar{J} \triangleq J - \sum_{i=1}^{q}\mu_i\psi_i$ is:

$$\delta\bar{J} = -N_{K_\pi}\Big[\int_0^1 (H_\pi^{(0)})^T d\tau + (\psi_0)_\pi{}^T + \sum_{i=1}^{q}\mu_i\Big(\int_0^1 (H_\pi^{(i)})^T d\tau + (\psi_i)_\pi{}^T\Big)\Big]$$

$$- \int_0^1 N_{K_u}\Big[(H_u^{(0)})^T + \sum_{i=1}^{q}\mu_i(H_u^{(i)})^T\Big]d\tau \le 0. \quad (15)$$

Here the weighted norm-function $N_K(\ )$ is defined as:

$$N_{K_y}[\bar{Y}] = \bar{Y}^T K_y \bar{Y}. \quad (15a)$$

Similarly, the substitutions of equations (13) and (14) into (11) give the following changes in the terminal constraints:

$$\delta\psi_j = -\int_0^1 (H_u^{(j)})K_u(H_u^{(0)})^T d\tau - \sum_{i=1}^{q}\mu_i\int_0^1 (H_u^{(j)})K_u(H_u^{(i)})^T d\tau$$

$$- \Big[\int_0^1 H_\pi^{(j)}d\tau + (\psi_j)_\pi\Big](K_\pi)\Big[\int_0^1 (H_\pi^{(0)})^T d\tau + (\psi_0)_\pi{}^T\Big] \quad (16)$$

$$- \sum_{i=1}^{q}\mu_i\Big[\int_0^1 H_\pi^{(j)}d\tau + (\psi_j)_\pi\Big](K_\pi)\Big[\int_0^1 (H_\pi^{(i)})^T d\tau + (\psi_i)_\pi{}^T\Big],$$

where j = 1,...,q

One way to simplify expressions (16) and (17) is to "absorb" K_u into $H_u^{(j)}$ and K_π into $H_\pi^{(j)}$. To do this, we first note that both K_u and K_π, being positive definite matrices, can be expressed as products of their respective "square-roots":

$$\begin{aligned} K_\pi &= S_\pi S_\pi{}^T , \\ K_u &= S_u S_u{}^T . \end{aligned} \tag{17}$$

Let us define the following quantities:

$$\begin{aligned} \bar{H}_u^{(0)}(\tau) &= H_u{}^{(0)}(\tau) S_u , \\ \bar{H}_u^{(i)}(\tau) &= H_u{}^{(i)}(\tau) S_u . \end{aligned} \tag{18a}$$

where i = 1,...,q.

Therefore an expression for $\bar{H}_u(\tau)$ is given by

$$\begin{aligned} H_u(\tau) &= H_u{}^{(0)}(\tau) - \sum_{i=1}^{q} \mu_i H_u{}^{(i)}(\tau) , \\ \bar{H}_u(\tau) = H_u(\tau) S_u &= \bar{H}_u^{(0)}(\tau) - \sum_{i=1}^{q} \mu_i \bar{H}_u^{(i)}(\tau) . \end{aligned} \tag{18b}$$

Similarly, $\bar{H}_\pi^{(\,)}$ and $(\bar{\psi}_{(\,)})_\pi$ are defined as

$$\begin{aligned} \bar{H}_\pi^{(0)}(\tau) &= H_\pi{}^{(0)}(\tau) S_\pi , \\ \bar{H}_\pi^{(i)}(\tau) &= H_\pi{}^{(i)}(\tau) S_\pi , \\ (\bar{\psi}_0)_\pi &= (\psi_0)_\pi S_\pi , \\ (\bar{\psi}_j)_\pi &= (\psi_j)_\pi S_\pi . \end{aligned} \tag{19}$$

where $i = 1,...,q$ and $j = 1,...,q$

Substitutions of (17)-(19) into (15)-(16) give

$$\delta \bar{J} = -N \int_0^1 (\bar{H}_\pi^{(0)})^T d\tau + (\bar{\psi}_0)_\pi{}^T + \sum_{i=1}^{q} \mu_i \left(\int_0^1 (\bar{H}_\pi^{(i)})^T d\tau + (\bar{\psi}_i)_\pi{}^T \right) \Big] - N \left[(\bar{H}_u^{(0)})^T + \sum_{i=1}^{q} \mu_i (\bar{H}_u^{(i)})^T \right], \tag{20}$$

$$\begin{aligned} \delta \psi_j = & - \int_0^1 \bar{H}_u^{(j)} (\bar{H}_u^{(0)})^T d\tau - \sum_{i=1}^{q} \mu_i \int_0^1 \bar{H}_u^{(j)} (\bar{H}_u^{(i)})^T d\tau \\ & - \left[\int_0^1 \bar{H}_\pi^{(j)} d\tau + (\bar{\psi}_j)_\pi \right] \left[\int_0^1 (\bar{H}_\pi^{(0)})^T d\tau + (\bar{\psi}_0)_\pi{}^T \right] \\ & - \sum_{i=1}^{q} \mu_i \left[\int_0^1 \bar{H}_\pi^{(j)} d\tau + (\bar{\psi}_j)_\pi \right] \left[\int_0^1 (\bar{H}_\pi^{(i)})^T d\tau + (\bar{\psi}_i)_\pi{}^T \right]. \end{aligned} \tag{21}$$

where j = 1,...,q

Equation (21) can be rewritten in a vector-matrix form after the introduction of the following notation:

$$\begin{aligned} \delta\vec{\psi}\,(q \times 1) &= (\delta\psi_1, ..., \delta\psi_q)^T, \\ \vec{\mu}\,(q \times 1) &= (\mu_1, ..., \mu_q)^T, \\ \text{and} \qquad \vec{g}\,(q \times 1) &= (g_1, ..., g_q)^T. \end{aligned} \tag{22}$$

The j^{th} component of $\vec{g}$ is given by:

$$g_j = - \int_0^1 \bar{H}_u^{(j)} (\bar{H}_u^{(0)})^T d\tau - \left[\int_0^1 \bar{H}_\pi^{(j)} d\tau + (\bar{\psi}_j)_\pi \right] \left[\int_0^1 (\bar{H}_\pi^{(0)})^T d\tau + (\bar{\psi}_0)_\pi{}^T \right] \tag{23}$$

where j = 0,1,...,q

Furthermore, let us define a $(q \times q)$ symmetrical matrix Q whose components are

$$\begin{aligned} Q_{ij} &= Q_{ji}, \\ &= - \int_0^1 \bar{H}_u^{(j)} (\bar{H}_u^{(i)})^T d\tau - \left[\int_0^1 \bar{H}_\pi^{(j)} d\tau + (\bar{\psi}_j)_\pi \right] \left[\int_0^1 (\bar{H}_\pi^{(i)})^T d\tau + (\bar{\psi}_i)_\pi{}^T \right]. \end{aligned} \tag{24}$$

where $(i, j) = 1, \cdots, q$

Using equations (22)-(24), equation (21) can be written in a more compact form:

$$\delta\bar{\psi} = \bar{g} - Q\bar{\mu}\,. \tag{25}$$

If we choose $\delta\bar{\psi} = -\epsilon\bar{\psi}$, where $0< \epsilon \leq 1$, the Lagrange multiplier $\bar{\mu}$ can be evaluated as:

$$\bar{\mu} = -Q^{-1}(\bar{g} + \epsilon\bar{\psi})\,. \tag{26}$$

If Q^{-1} exists (the controllability condition, see also Chapter 2 of [29]), we can substitute the value of $\bar{\mu}$ found in equation (26) into both equations (13) and (14) and express both $\delta\bar{\pi}$ and $\delta\bar{u}$ only as functions of the impulse response functions $H_u^{(i)}(\tau)$ and $H_\pi^{(i)}(\tau)$ (that have been computed and stored during backward integrations):

$$\begin{aligned}
\delta\bar{\pi} &= -S_\pi\Big[\int_0^1 (\bar{H}_\pi^{(0)})^T d\tau - (\bar{\psi}_0)_\pi{}^T + \sum_{i=1}^{q}\mu_i\int_0^1 (\bar{H}_\pi^{(i)})^T d\tau + (\bar{\psi}_i)_\pi{}^T\Big]\,,\\
\delta\bar{u} &= -S_u\Big[(\bar{H}_u^{(0)})^T + \sum_{i=1}^{q}\mu_i(\bar{H}_u^{(i)})^T\Big]\,.
\end{aligned} \tag{27}$$

For the next iteration, the uses of new trial values

$$\begin{aligned}
\bar{u}_{N+1}(\tau) &= \bar{u}_N(\tau) + \delta\bar{u}_N(\tau)\,,\\
\bar{\pi}_{N+1} &= \bar{\pi}_N + \delta\bar{\pi}_N\,,
\end{aligned} \tag{28}$$

(where N is the current iteration number)

will reduce the value of the performance index and bring the system closer to satisfying the terminal constraints.

After many iterations of the above procedure, all the terminal constraints are satisfied to a prescribed accuracy:

$$|\,\psi_j(\bar{x}_f, \bar{\pi})\,| \leq \epsilon_\psi\,, \tag{29}$$

for j = 1,...,q, where ϵ_{ψ_j} denotes the feasibility condition (e.g. $\epsilon_{\psi_j} = 10^{-4}$).

Using this procedure, a feasible path satisfying the constraints is determined. However, the performance index can still be decreased further. The procedure now concentrates on minimizing the value of the performance index while keeping ψ_j within the accuracy of (29). The procedure is repeated until

$$\int_0^1 N\left|(\bar{H}_u^{(0)})^T + \sum_{i=1}^{q} \mu_i (\bar{H}_u^{(i)})^T\right| d\tau \leq \epsilon_u \tag{30}$$

and

$$N\left|\int_0^1 (\bar{H}_\pi^{(0)})^T d\tau + (\bar{\psi}_0)_\pi^T + \sum_{i=1}^{q} \mu_i \left(\int_0^1 (\bar{H}_\pi^{(i)})^T d\tau + (\bar{\psi}_i)_\pi^T\right)\right| \leq \epsilon_\pi \tag{31}$$

where ϵ_u and ϵ_π represent the optimality conditions (e.g. $\epsilon_u = \epsilon_\pi = 10^{-8}$).

A numerical algorithm that implements the above procedures has been written. The procedure is basically an extension of the program FCNOPT by Bryson [16].

Example Problems

Two example applications of the Combined Function and Parameter Optimization Algorithm are given here. The first example involves a nonlinear first order system with a specified control law. The second example considers the optimal landing of a helicopter that is initially in hover.

(1) Specified Control Law Problem [46]

Consider the following optimization problem:

$$\min_u I = \frac{1}{2}\int_0^1 (x^2 + u^2)\, dt$$

subject to the scalar nonlinear differential relation

$$\dot{x} = -x^2 + u\,.$$

The initial condition is

$$x(0) = 10.$$

There is no terminal condition.

In order to exercise the parameter optimizatiobn capability, the control law is specified to have the following form

$$u = a\,x,$$

where a is an unknown parameter whose value is to be optimally selected. The *transformed* problem becomes

$$\min_a I = \frac{1}{2}\int_0^1 [x^2 + a^2\,x^2]dt,$$

with the following equation of motion

$$\dot{x} = -x^2 + a\,x,$$

while the initial condition of $x(0)$ remains unchanged.

The transformed problem now becomes a problem with an unknown parameter a but without any control. The problem can be solved using the combined function and parameter algorithm and the optimum value of a found is:

$$a = \text{-}0.10334.$$

The minimum value of the cost function is:

$$I = 4.5218.$$

The value of I is slightly larger than the minimum value when $u(t)$ is open:

$$I_{min} = 4.5108.$$

Time histories of both the state and control of the system, using either $u(t) = a\,x(t)$ or the open-loop optimal solution are given in Figure (3.2.1).

(2) Optimal Landing of a Helicopter in Hover

In reference [15], Johnson formulated an optimal, autorotative landing problem for a helicopter initially in hover close to the ground. He showed that the optimal descent is purely vertical. Under these conditions, the general landing problem posed in Chapter 2 can be simplified.

Imposing a purely vertical descent, the horizontal distance component x, velocity component u, and control component C_{T_x} are omitted. The remaining states of the problem are the vertical height h, vertical sink rate V and the angular speed of the rotor Ω. In addition, the induced velocity parameter f_I in the vortex-ring state and the momentum theory states is given by the following one-parameter family of equations:

$$f_I = \begin{cases} \frac{1}{2}\bar{V} + \sqrt{1 + (\frac{\bar{V}}{2})^2}\,, & \text{for } 0 \le \bar{V} \le 1 \\ -\bar{V}(0.373\bar{V}^2 - 1.991)\,, & \text{for } 1 < \bar{V} \le 2 \\ \frac{1}{2}\bar{V} - \sqrt{(\frac{\bar{V}}{2})^2 - 1}\,. & \text{for } 2 < \bar{V} \end{cases} \tag{32}$$

Note that the first and third expressions of equation (32) are solutions of the momentum quartic, while the second is an empirical expression given by Johnson [15] for the vortex-ring state. The dimensionless parameter $\bar{V}$ is defined as the ratio of the vertical sink rate and the induced velocity in hover ν_h:

$$\begin{aligned} \bar{V} &= \frac{V}{\nu_h}\,, \\ &= \frac{V}{\Omega R\sqrt{\frac{C_T}{2}}}\,. \end{aligned} \tag{33}$$

Figure (3.2.2) shows the variation of f_I with the parameter $\bar{V}$.

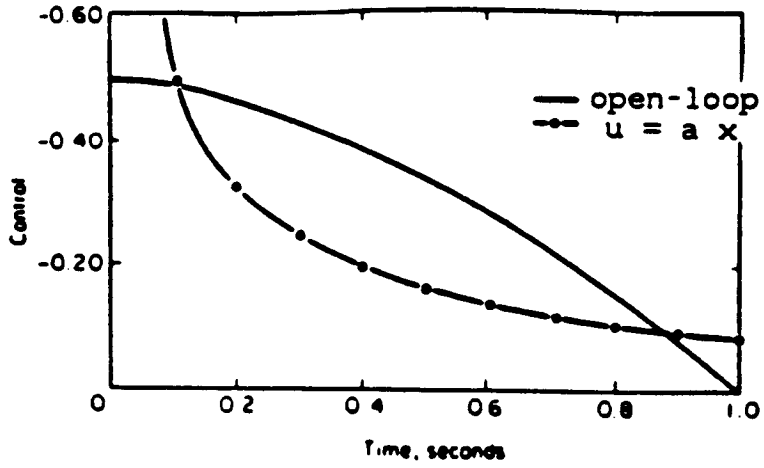

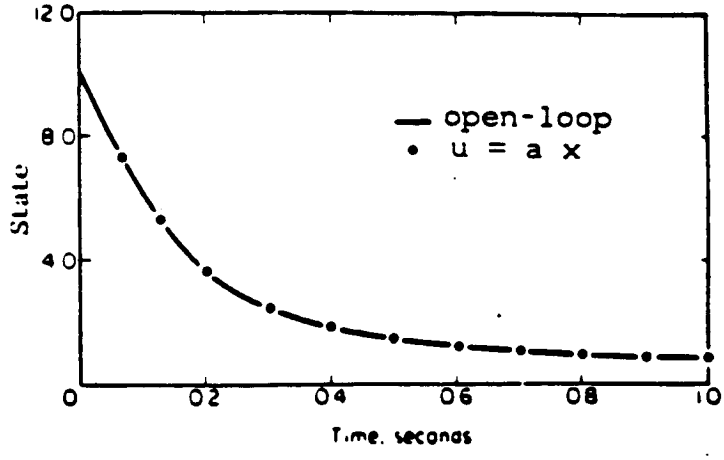

Figure 3.2.1 Example Optimal Control Problem

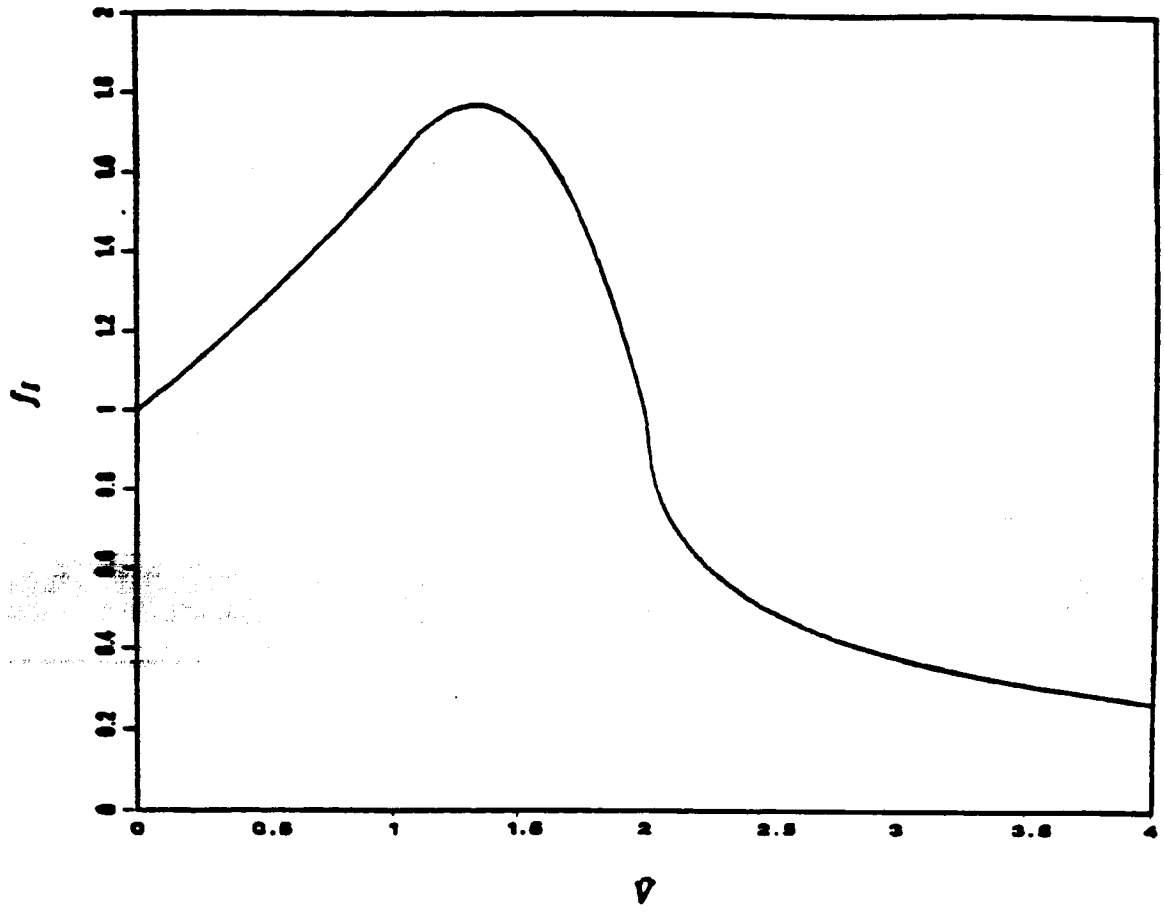

Figure 3.2.2 Variation of Induced Velocity Parameter f_I with $\bar{V}$

If we go through the normalization and scaling processes of Section (2.4), the non-dimensionalized and scaled time, states and control of the problem are given by the following relations:

$$\begin{aligned} \bar{\tau} &= (\frac{\Omega_0 t}{100}), \\ x_1 &= (\frac{V}{0.01\Omega_0 R}), \\ x_2 &= (\frac{\Omega}{\Omega_0}), \\ x_3 &= (\frac{h}{R}), \\ u_1 &= 10^3 C_{T_z}. \end{aligned} \tag{34}$$

In terms of these normalized quantities, the optimal autorotation from hover is formulated as the minimization of the cost function I, where

$$I = \frac{1}{2} x_{1f}{}^2 .$$

The equations of motion are given by

$$\begin{aligned} x_1' &= g_0 - m_0 x_2^2 u_1 - f_0 x_1^2 , \\ x_2' &= -i_0 x_2^2 c_0 - u_1(-0.01\frac{x_1}{x_2} - k_0\sqrt{u_1} f_I), \\ x_3' &= x_1 . \end{aligned} \tag{35}$$

Here $(\,)'$ denotes time differentiation with respect to $\bar{\tau}$ and the dimensionless quantities g_0, m_0, f_0, c_0, and k_0 are as defined in Section (2.4) (see equation (37)). The induced velocity parameter f_I is a function of $\bar{V}$, which is now given by the following normalized expression:

$$\bar{V} = p_0 \frac{x_1}{x_2\sqrt{u_1}}, \tag{35a}$$

where p_0 is also defined in Section (2.4).

The optimization problem is constrained at the end-time by the "stopping" condition:

$$x_{3f} - \bar{h}_f = 0, \tag{36}$$

and the following one-sided path inequality constraint:

$$u_1 \leq \bar{C}_{T_e} . \tag{37}$$

Further Time Normalization

Since the end-time of the problem is unspecified. further normalization of the independent variable $\bar{\tau}$ is needed. The problem is converted to one with fixed end-time by the following change of independent variable:

$$\xi = \frac{\bar{\tau}}{\bar{\tau}_f} , \tag{38}$$

The transformation (38) converts the independent variable from $\bar{\tau}$ to ξ where ξ now varies from 0 to 1. This transformation introduces into the problem an additional unknown parameter $\bar{\tau}_f$ that must be optimally determined. From here on we shall denote differentiation with respect to ξ by:

$$\begin{aligned} (\,)^{\Gamma} &= \frac{d}{d\xi} , \\ &= \bar{\tau}_f \left(\frac{d}{d\bar{\tau}}\right) , \\ &= \bar{\tau}_f (\,)' . \end{aligned} \tag{39}$$

Substitution Technique

The path inequality constraint (37) can be eliminated if we substitute for u_1 the new control variable u_2, where u_2 is defined as :

$$u_1 = \bar{C}_{T_e} \cos^2 u_2 . \tag{40a}$$

Final Form of Optimal Autorotation Problem

The state, control, and unknown parameter vectors of the problem are:

$$\bar{X} = (x_1\ x_2\ x_3)^T, \tag{41}$$

$$\bar{U} = (u_2), \tag{42}$$

$$\bar{\pi} = (\tau_f). \tag{43}$$

denote the state, control, and unknown parameter vectors of the problem.

The problem is to find $\bar{U}(\xi)$ and $\bar{\pi}$ to minimize:

$$I = \frac{1}{2}[x_{1f}]^2 = \phi(\bar{X}_f), \tag{44}$$

subject to:

(1) equations of motion ($\bar{X}^\nabla = \bar{f}$):

$$\begin{aligned} x_1{}^\nabla &= \tau_f[g_0 - m_0 x_2{}^2(\bar{C}_{T_*}\cos^2 u_2) - f_0 x_1{}^2], \\ x_2{}^\nabla &= -\tau_f i_0 x_2{}^2[c_0 + (\bar{C}_{T_*}\cos^2 u_2)(-0.01\frac{x_1}{x_2} + k_0\sqrt{\bar{C}_{T_*}}\cos u_2 f_1)], \\ x_3{}^\nabla &= \tau_f x_1 . \end{aligned} \tag{45}$$

(2) the initial condition of $\bar{X}$ is given by:

$$\bar{X}_0 = (0,1,0)^T. \tag{46}$$

(3) terminal constraint ($\bar{\psi}(\bar{X}_f, \bar{\pi}) = 0$):

$$x_{3f} - \bar{h}_f = 0 \tag{47}$$

The optimization problem (41)-(47) is now in a form that can be solved using the combined function and parameter gradient algorithm. Several other example applications of the algorithm are given in Appendix C.

§3.3 Sequential Gradient Restoration Technique [42]

This section explains the Sequential Gradient Restoration (SGR) method given in [42]. The SGR technique is one way that problems with bounded control may be solved. The technique is employed in the solution of the optimal helicopter landing problem posed in Section (2.9).

The problem is similar to the one in Section (3.2) except that here we consider more general path constraints. Specifically, we consider the following problem with unknown parameter vector $\bar{\pi}$ and path equality constraints $\vec{S}$:

$$\begin{aligned} \min_{\vec{u},\bar{\pi}} I &= \phi(\vec{x}_f, \bar{\pi}) + \int_0^1 L(\vec{x}, \vec{u}, \bar{\pi}, \tau) d\tau, \\ \dot{\vec{x}} &= f(\vec{x}, \vec{u}, \bar{\pi}, \tau), \\ \vec{x}(0) &= \text{given}, \\ \vec{S}(\vec{x}, \vec{u}, \bar{\pi}, \tau) &= 0, \\ \text{and} \qquad \vec{\psi}(\vec{x}_f, \bar{\pi}) &= 0. \end{aligned} \tag{1}$$

Where $\vec{S}(r \times 1)$ are the path equality constraints of the problem. The motivations for this formulation are:

(1) Many optimization problems arise directly in the form considered here. i.e. with path equality constraints.

(2) Problems involving inequality constraints can be converted to the present scheme through suitable transformations. This statement applies, for instance, to the following situations:

(a) Problems with bounded controls.

(b) Problem with bounded states.

(c) Problems with bounded time rate of change of state.

(d) Problems where some bound is imposed on an arbitrarily prescribed function of the parameters, the control and the time rate of change of the state.

The transformation techniques employed are of the Valentine-type [41]. The transformation is performed by augmenting the dimension of the control space, with or without augmentation of the state space. In the process, non-differential path equality constraints relating the original control and the slack control are produced that must be satisfied by the solution of the original optimization problem. Four example problems with bounded control, state or time rate of change of state are presented in Appendix (G).

3.3.1 First Order Conditions

If we adjoin the system differential equations, the path equality constraints and the terminal constraints to the performance index I with multiplier functions $\bar{\lambda}(\tau)(n \times 1)$ and $\bar{\rho}(\tau)(r \times 1)$, and multiplier $\bar{\mu}(q \times 1)$ respectively, we obtain the following augmented performance index J

$$J = (\phi + \mu^T \psi)_1 + \int_0^1 [L + \lambda^T (f - \dot{x}) + \rho^T S] d\tau \,, \tag{2}$$

$$= (\lambda^T x)_0 + (\Phi - \lambda^T x)_1 + \int_0^1 (\dot{\lambda}^T x + H) d\tau \,, \tag{3}$$

where, for convenience, we have defined scalar functions H (the Hamiltonian function) and Φ as given below:

$$H(\vec{x}, \vec{u}, \vec{\pi}, \vec{\lambda}, \vec{\rho}, \tau) = L(\vec{x}, \vec{u}, \vec{\pi}, \tau) + \lambda^T f(\vec{x}, \vec{u}, \vec{\pi}, \tau) + \rho^T S(\vec{x}, \vec{u}, \vec{\pi}, \tau) \,, \tag{5}$$

$$\Phi(\vec{x}_f, \vec{\pi}, \vec{\mu}) = \phi(\vec{x}_f, \vec{\pi}) + \mu^T \psi(\vec{x}_f, \vec{\pi}) \,. \tag{6}$$

Now consider the variation in J due to variations in both the control and the parameter vectors

$$\delta J = (\lambda^T \delta x)_0 + (-\lambda^T + \Phi_x)_1 \delta x_1 + \left[\int_0^1 H_\pi d\tau + (\Phi_\pi)_1\right]\delta\bar{\pi} + \int_0^1 [H_u \delta\bar{u} + (H_x + \dot{\lambda}^T)\delta\bar{x}]d\tau .$$

Therefore, first-order necessary conditions of the problem are given by the following relations:

$$\begin{aligned} \dot{\bar{x}} &= f(\bar{x}, \bar{u}, \bar{\pi}, \tau), \\ \bar{S}(\bar{x}, \bar{u}, \bar{\pi}, \tau) &= 0, \\ \dot{\bar{\lambda}}^T &= -H_x, \\ H_u &= 0, \\ \bar{x}(0) &= \text{given}, \\ (\bar{\lambda}^T)_1 &= (\Phi_x)_1, \\ \bar{\psi}(\bar{x}_f, \bar{\pi}) &= 0, \\ \text{and} \quad (\Phi_\pi)_1 + \int_0^1 H_\pi d\tau &= 0. \end{aligned} \tag{4}$$

Summarizing, we seek functions $\bar{x}(\tau)$, $\bar{u}(\tau)$, $\bar{\pi}$ and multipliers $\bar{\lambda}(\tau)$, $\bar{\rho}(\tau)$ and μ which satisfy the first order necessary conditions (4).

3.3.2 Approximate Methods

In general, the problem posed in Section (3.3.1) is nonlinear and can only be solved iteratively. In this connection, we define two scalar functionals

$$P = \int_0^1 N[\dot{x} - f]d\tau + \int_0^1 N[S]d\tau + N[(\psi)_1], \tag{7}$$

and

$$Q = \int_0^1 N[\dot{\lambda} + H_x^T]d\tau + \int_0^1 N[H_u^T]d\tau + N[(\Phi_\pi^T)_1 + \int_0^1 H_\pi^T d\tau] + N[(\lambda - \Phi_x^T)_1], \tag{8}$$

where the norm-function N[ ] was defined in equation (15a) of Section (3.2).

P and Q are measures of the errors in the constraints and the optimality conditions, respectively. For the exact optimal solution, one must have

$$\begin{aligned} P &= 0, \\ Q &= 0. \end{aligned} \tag{9}$$

For an approximation to the optimal solution, one must have

$$P \leq \epsilon_1 . \tag{10a}$$

$$Q \leq \epsilon_2 , \tag{10b}$$

where ϵ_1 and ϵ_2 are small pre-selected numbers.

3.3.3 The Sequential Gradient Restoration Algorithm

The Sequential Gradient Restoration algorithm involves a sequence of cycles, where each cycle has a gradient phase and may or may not have a restoration phase.

The restoration phase is iterative and is started when the inequality (10a) is violated. In each restoration step, the norm of the variations of the control and the parameter is minimized, while the constraints are satisfied to first order; this has the effect of reducing P, i.e. more closely satisfying the feasibility conditions. The restoration phase is terminated when the inequality (10a) is satisfied.

The gradient phase is started when the inequality (10a) is satisfied. It involves a single step, which reduces the functional I, while the constraints are satisfied to first order; this has the effect of reducing Q, i.e. more closely satisfying the optimality conditions.

The algorithm ends when both inequality (10a) and (10b) are satisfied.

Notation

For steps in the gradient phase or the restoration phase, the following notation is used: $x(\tau)$, $u(\tau)$, π denote the nominal functions; $\tilde{x}(\tau)$, $\tilde{u}(\tau)$, $\tilde{\pi}$ denote the varied functions, and $\Delta x(\tau)$, $\Delta u(\tau)$, and $\Delta\pi$ denote perturbations of $x(\tau)$, $u(\tau)$ and π about the nominal values, i.e.

$$\begin{aligned} \tilde{x}(\tau) &= x(\tau) + \Delta x(\tau)\,, \\ \tilde{u}(\tau) &= u(\tau) + \Delta u(\tau)\,, \\ \tilde{\pi} &= \pi + \Delta\pi\,. \end{aligned} \tag{11}$$

(Note the removal of the arrow on top of the symbols for the vectors $\vec{x}$, $\vec{u}$ and $\vec{\pi}$ in (11).)

Concerning the functionals I, J and P , the following terminology is used: I, J and P denote the values associated with the nominal functions; $\tilde{I}$, $\tilde{J}$, and $\tilde{P}$ denote the values associated with the varied functions; and ΔI, ΔJ, and ΔP denote the total variations of these functionals caused by the perturbations $\Delta x(\tau)$, $\Delta u(\tau)$, and $\Delta\pi$, i.e.

$$\begin{aligned} \tilde{I} &\triangleq I + \Delta I\,, \\ \tilde{J} &\triangleq J + \Delta J\,, \\ \tilde{P} &\triangleq P + \Delta P\,. \end{aligned} \tag{12}$$

If the variations appearing in (11) are linear in the stepsize α , (where $\alpha > 0$), they take the forms

$$\Delta x(\tau) \triangleq \alpha\, A(\tau)\,,$$

$$\Delta u(\tau) \triangleq \alpha\, B(\tau)\,, \tag{13}$$

$$\Delta\pi \triangleq \alpha\, C\,. \tag{14}$$

3.3.4 Desired Properties in the SGR Process

The functions $A(\tau)$, $B(\tau)$, and C are determined so as to decrease the functional I, and/or J, and/or P. (Alternatively, the condition (10b) on the value of Q can also be used.) Thus, the following properties are required.

$$\begin{aligned} &\Delta I < 0, \\ \text{and/or} \quad &\Delta J < 0. \\ \text{and/or} \quad &\Delta P < 0. \end{aligned} \tag{15}$$

In turn, relations (15) can be enforced at every iteration providing the stepsize α is sufficiently small and the functions $A(\tau)$, $B(\tau)$, and C are chosen so that

$$\delta I < 0, \tag{16a}$$

$$\text{and/or} \quad \delta J < 0, \tag{16b}$$

$$\text{and/or} \quad \delta P < 0, \tag{17}$$

where $\delta(...)$ denotes the first variation. Inequalities (16a) and (16b) characterize the gradient phase, and inequality (17) characterizes the restoration phase.

3.3.5 The First Variations

The first variations of the functionals I, J, and P are

$$\begin{aligned} \delta I &= \int_0^1 [L_x \Delta x + L_u \Delta u + L_\pi \Delta \pi] d\tau + (\phi_x \Delta x + \phi_\pi \Delta \pi)_1 , \\ \delta J &= \int_0^1 [\dot{\lambda}^T + H_x] \Delta x d\tau + \int_0^1 H_u \Delta u d\tau + [(\Phi_\pi)_1 + \int_0^1 H_\pi d\tau] \Delta \pi \\ &\quad + [(\Phi_x - \lambda^T) \Delta x]_1 , \\ \delta P &= 2 \int_0^1 (\dot{x} - f)^T (\Delta \dot{x} - f_x \Delta x - f_u \Delta u - f_\pi \Delta \pi) d\tau \\ &\quad + 2 \int_0^1 S^T (S_x \Delta x + S_u \Delta u + S_\pi \Delta \pi) d\tau \\ &\quad + 2 [\psi^T (\psi_x \Delta x + \psi_\pi \Delta \pi)]_1 , \end{aligned} \tag{18}$$

where $(\delta x)_0$ has been assumed zero in the expression for δJ.

3.3.6 Gradient Phase

Suppose that nominal functions $x(\tau)$, $u(\tau)$, and π satisfying (1) are available (a feasible solution). Let $\tilde{x}(\tau)$, $\tilde{u}(\tau)$, and $\tilde{\pi}$ denote varied functions also satisfying (1). The varied functions are related to the nominal functions by (11), where $\Delta x(\tau)$, $\Delta u(\tau)$, and $\Delta\pi$ denote the perturbations of $x(\tau)$, $u(\tau)$, and π about the nominal values.

To first order, the perturbations $\Delta x(\tau)$, $\Delta u(\tau)$, and $\Delta\pi$ must satisfy linearized constraint relations

$$\begin{aligned} \Delta\dot{x} - f_x\Delta x - f_u\Delta u - f_\pi\Delta\pi &= 0\,, \\ S_x\Delta x + S_u\Delta u + S_\pi\Delta\pi &= 0\,, \end{aligned} \tag{19}$$

with the following linearized boundary conditions

$$\begin{aligned} [\Delta x]_0 &= 0\,, \\ [\psi_x\Delta x + \psi_\pi\Delta\pi]_1 &= 0\,. \end{aligned} \tag{20}$$

An inspection of equation (18) reveals that δJ can be made negative through the following choice of variations of the control u and the parameter vector π.

$$\begin{aligned} \Delta u &= -\alpha H_u^T\,, \\ \Delta\pi &= -\alpha\,[(\Phi_\pi)_1 + \int_0^1 H_\pi d\tau]^T\,. \end{aligned} \tag{21}$$

where α denotes a scaling factor (gradient stepsize). The multipliers $\lambda(\tau)$, $\rho(\tau)$, and μ appearing in equation (21) must be consistent with the differential relation

$$\dot{\lambda}^T = -H_x\,. \tag{22a}$$

and the final conditions

$$(\lambda^T)_1 = (\Phi_x)_1\,. \tag{22b}$$

With the variations defined by (21), the first variation of the augmented functional (18) becomes

$$\delta J = -\alpha Q . \tag{23}$$

where Q is the error in the optimality conditions (8), which, with (22), reduces to

$$Q = \int_0^1 N[H_u^T]d\tau + N[(\Phi_\pi^T)_1 + \int_0^1 H_\pi^T d\tau] . \tag{24}$$

Since $Q > 0$, (23) shows that $\delta J < 0$. Hence, for sufficiently small α, the decrease in the augmented functional J is guaranteed.

To simplify the problem, we can make use of the auxiliary variables $A(\tau)$, $B(\tau)$ and C introduced in (13). Using these variables, the linearized relations (19)-(23) become

$$\begin{aligned} \dot{A} - f_x A - f_u B - f_\pi C &= 0 , \\ S_x A + S_u B + S_\pi C &= 0 , \end{aligned} \tag{25}$$

with the following boundary conditions

$$\begin{aligned} (A)_0 &= 0 , \\ [\psi_x A + \psi_\pi C]_1 &= 0 . \end{aligned} \tag{26}$$

The special variations are

$$\begin{aligned} B &= -H_u^T , \\ C &= -[(\Phi_\pi)_1 + \int_0^1 H_\pi d\tau]^T . \end{aligned} \tag{27}$$

where once again the multipliers $\lambda(\tau)$, $\rho(\tau)$, and μ satisfy the following differential relation

$$\dot{\lambda}^T = -H_x , \tag{28a}$$

and the terminal conditions

$$(\lambda^T)_1 = (\Phi_x)_1 . \tag{28b}$$

The descent property of the augmented functional (18) is

$$\delta J = -\alpha Q,$$

where Q is the error in the optimality condition (24), which reduces to

$$Q = \int_0^1 B^T B d\tau - C^T C \tag{29}$$

We note that the differential system (25)-(28) is linear and nonhomogeneous in the functions $A(\tau)$, $B(\tau)$, and C and the multipliers $\lambda(\tau)$, $\rho(\tau)$, and μ and can be solved without assigning a value to the gradient stepsize α. The selection of α is done *a posteriori* in such a way that the descent requirement (15-2) (second equation of equation (15)) is enforced.

3.3.7 Solution Technique in the Gradient Phase

The usual approach of backward integration of the λ-equations and forward integration of the A-equations cannot be employed with this class of problems since the computation of $\rho(\tau)$ over the interval $0 \leq \tau \leq 1$ requires the simultaneous solution of both the λ and A equations. Because of this coupling, the total system must be integrated simultaneously either forward or backward. Forward integration is chosen here.

Using the *Method of Particular Solutions* [39-40], the differential system consisting of equations (25), (26-1), (27-1) and (28) may be integrated forward $n + p + 1$ times. Given

$$\dot{A} = f_x A + f_u B + f_\pi C, \tag{a}$$

$$0 = S_x A + S_u B + S_\pi C, \tag{b}$$

$$(A)_0 = 0, \tag{c}$$

$$B = -H_u^T,$$

$$= -(L_u^T + f_u^T \lambda + S_u^T \rho)\,, \qquad (d)$$

$$\dot{\lambda}^T = -(L_x + \lambda^T f_x + \rho^T S_x)\,. \qquad (e)$$

Substituting equation (d) into (b) and solving for ρ, we get

$$\rho = [S_u S_u^T]^{-1}(S_x A - S_u L_u^T - S_u f_u^T \lambda - S_\pi C)\,, \qquad (f)$$

which is unique provided

$$\det[S_u S_u^T] \neq 0\,.$$

Therefore a necessary (but not sufficient) condition for the existence of a solution is that all the components of the path equality constraint vector $\bar{S}$ must involve some components of the control vector $\bar{u}$. If this is not true, time derivative(s) of some of the constraints have to be taken to involve the control $\bar{u}$ in $\bar{S}$. In principle, ρ may be eliminated by substituting (f) into (d), and (e) and B may then be eliminated by substituting (d) into (a).

The initial conditions for the i^{th} forward integration are

$$(A)_0 = 0\,,$$

$$\lambda_i(0) = [\delta_{i1}, \delta_{i2}, \ldots, \delta_{in}]^T\,, \qquad (g)$$

$$C_i = [\delta_{i(n+1)}, \delta_{i(n+2)}, \ldots, \delta_{i(n+p)}]^T\,, \qquad (h)$$

where $i = 1,2,\ldots,[n+p+1]$ and δ_{ij} is the usual *Kronecker delta function*. Values of ρ and B can be computed using equations (f) and (g) respectively. The differential system:

$$\begin{aligned} \dot{A} &= f_x A + f_u B + f_\pi C\,, \\ \dot{\lambda} &= -L_x^T - f_x^T \lambda - S_x^T \rho\,, \end{aligned} \qquad (i)$$

can then be integrated forward.

The solution of the system is given by

$$\begin{aligned} A(\tau) &= \sum_{i=1}^{n-p-1} k_i A_i(\tau)\,, \\ B(\tau) &= \sum_{i=1}^{n-p-1} k_i B_i(\tau)\,. \\ C &= \sum_{i=1}^{n-p-1} k_i C_i\,, \\ \lambda(\tau) &= \sum_{i=1}^{n-p-1} k_i \lambda_i(\tau)\,. \\ \rho(\tau) &= \sum_{i=1}^{n-p-1} k_i \rho_i(\tau)\,. \end{aligned} \tag{30}$$

Here $(...)_i$ is the value of $(...)$ obtained from the i^{th} iteration. The k_i are unknown coefficients determined from the simultaneous solution of the following equations:

$$\begin{aligned} &\sum_{i=1}^{n-p-1} k_i = 1\,, \\ &\sum_{i=1}^{n-p-1} k_i (\psi_x A_i - \psi_\pi C_i)_1 = 0\,, \\ &\sum_{i=1}^{n-p-1} k_i (\lambda_i)_1 = (\Phi_x^T)_1\,, \\ &\sum_{i=1}^{n-p+1} k_i \left[\int_0^1 (f_\pi^T \lambda_i + S_\pi^T \rho_i) d\tau + C_i\right] = -\left[(\Phi_\pi^T)_1 + \int_0^1 L_\pi^T d\tau\right]. \end{aligned} \tag{31}$$

where we have made use of the function

$$\Phi = \phi + \mu^T \psi\,,$$

defined earlier in equation (5).

Equation (31) is equivalent to $[1 + q + n + p]$ scalar equations for the solution of the $[n + p + 1]$ unknowns k_i and the q components of the multiplier μ. Using these

C - 2

coefficients from equation (31), the solution (30) satisfies the end constraints of (26-2), (27-2) and (28b). After the constants k_i and the components of the multiplier μ are known, the functions $A(\tau)$, $B(\tau)$, and C as well as the multipliers $\lambda(\tau)$ and $\rho(\tau)$ are computed according to equation (30). In this way, the linear TPBVP is solved.

3.3.8 Gradient Stepsize

The gradient stepsize α is selected in such a way that the following inequality is satisfied.

$$\tilde{J}(\alpha) < \tilde{J}(0)\,, \tag{32}$$

subject to

$$\tilde{P}(\alpha) \leq \epsilon_3\,, \tag{33a}$$

and

$$t_f > 0\,. \tag{33b}$$

The last equation in (33b) expresses the need to have the unspecified end-time t_f greater than zero.

Here ϵ_3 is a small, preselected number (e.g. $\epsilon_3 = 1$). Satisfaction of (32) is guaranteed by the descent property of the gradient phase. Satisfaction of (33a) is desirable in order to limit the constraint violation which is due to the use of the linearized constraint equations (25)-(26). Satisfaction of (33b) is automatic for problems with fixed terminal time, and is required in problems where the final time is free.

3.3.9 Restoration Phase

At the end of the gradient phase, the varied functions $\tilde{x}(\tau)$, $\tilde{u}(\tau)$, and $\tilde{\pi}$ are known, and the varied constraint error $\tilde{P}$ can be computed with equation (7). In this connection, two possibilities arise: either (i) Inequality (10a) is satisfied or (ii) Inequality (10a) is violated.

Case (i) occurs if the equations (1) are linear or if they are nonlinear and the gradient stepsize is sufficiently small. In this case, the gradient phase is repeated by employing as nominal functions $x(\tau)$, $u(\tau)$, and π the varied functions $\tilde{x}(\tau)$, $\tilde{u}(\tau)$, and $\tilde{\pi}$ of the previous gradient phase.

Case (ii) occurs if the equations (1) are nonlinear and the stepsize is not small. In this case, prior to repeating the gradient phase, a restoration phase is inserted in such a way that (a) the constraint error is reduced to a level compatible with inequality (10a) and (b) the descent property of the augmented functional J is preserved.

While the gradient phase involves a single step, the restoration is iterative and hence may involve several steps. This is due to the fact that the constraint equations (1) are considered only in their linearized form in the restoration phase. For the first restoration phase, we employ as the nominal functions the varied functions $\tilde{x}(\tau)$, $\tilde{u}(\tau)$, $\tilde{\pi}$ of the previous gradient phase. For any subsequent restoration iteration, we employ as nominal functions the varied functions $\tilde{x}(\tau)$, $\tilde{u}(\tau)$, $\tilde{\pi}$ of the previous restoration iteration.

Now consider the generic restoration iteration. Let $x(\tau)$, $u(\tau)$, π denote nominal functions satisfying the initial condition $x(0) = \text{given}$, and let $\tilde{x}(\tau)$, $\tilde{u}(\tau)$, $\tilde{\pi}$ denote the varied functions also satisfy the initial condition. The varied functions are related to the nominal functions by (11). To first order, the perturbations $\Delta x(\tau)$, $\Delta u(\tau)$, and $\Delta\pi$ must satisfy the linearized constraint equations

$$\begin{aligned} \Delta\dot{x} - f_x\Delta x - f_u\Delta u - f_\pi\Delta\pi + \alpha(\dot{x} - f) = 0\,, \\ S_x\Delta x + S_u\Delta u + S_\pi\Delta\pi + \alpha S = 0\,, \end{aligned} \tag{34}$$

with the following linearized boundary conditions

$$\begin{aligned} [\Delta x]_0 = 0\,, \\ [\psi_x\Delta x + \psi_\pi\Delta\pi + \alpha\psi]_1 = 0\,, \end{aligned} \tag{35}$$

where α denotes a scaling factor (restoration stepsize) in the range $0 \leq \alpha \leq 1$. Its function is to prevent the forcing terms in (34) -(35) from generating variations too large for the linearized assumptions to hold.

When the variations defined by (34)-(35) are employed, the first variation of the constraint error (7) becomes (use equation (18-3))

$$\delta P = -2\alpha P , \tag{36}$$

where P is as defined in (7). Since $P > 0$, equation (36) shows that $\delta P < 0$. Hence, for a sufficiently small α, the decrease in the constraint error P is guaranteed.

Since equations (34)-(35) admit an infinite number of solutions, the restoration iteration is not uniquely defined, unless some additional requirement is introduced. This added requirement is that the restoration be accomplished with the least square change in the controls and the parameters. Hence we seek the minimum of the following function

$$K = \int_0^1 [\Delta u^T \Delta u] d\tau + \Delta \pi^T \Delta \pi , \tag{37}$$

that also satisfies the linearized constraints (34)-(35).

3.3.10 Special Variations

The problem formulated in Section (3.3.9) is a linear-quadratic Bolza problem in the calculus of variations. The Δu and $\Delta \pi$ that minimize (37) subject to the constraints (34)-(35) are:

$$\begin{aligned} \Delta u &= -\alpha(\lambda^T f_u + \rho^T S_u)^T , \\ \Delta \pi &= -\alpha[\int_0^1 (\lambda^T f_\pi + \rho^T S_\pi) d\tau + (\mu_-^T \psi_\pi)_1]^T . \end{aligned} \tag{38}$$

The multipliers $\lambda(\tau)$, $\rho(\tau)$, and μ appearing in equation (38) must be consistent with the following differential relation

$$\dot{\lambda}^T = -(\lambda^T f_x + \rho^T S_x) , \tag{39a}$$

and the final conditions

$$(\lambda^T)_1 = (\mu^T \psi_x)_1 \,. \tag{39b}$$

To simplify, we make use of the auxiliary variables $A(\tau)$, $B(\tau)$ and C defined in (13). Using these variables, the linearized relations (34)-(35) become

$$\begin{aligned} \dot{A} - f_x A - f_u B - f_\pi C - (\dot{x} - f) = 0\,, \\ S_x A + S_u B - S_\pi C + S = 0\,. \end{aligned} \tag{40}$$

with the following boundary conditions

$$\begin{aligned} (A)_0 = 0\,, \\ [\psi_x A + \psi_\pi C + \psi]_1 = 0\,. \end{aligned} \tag{41}$$

The special variations are

$$\begin{aligned} B &= -(\lambda^T f_u - \rho^T S_u)^T\,, \\ C &= -[\int_0^1 (\lambda^T f_\pi + \rho^T S_\pi) d\tau + (\mu^T \psi_\pi)_1]^T\,. \end{aligned} \tag{42}$$

where once again the multipliers $\lambda(\tau)$, $\rho(\tau)$, and μ satisfy the following differential relation

$$\dot{\lambda}^T = -(\lambda^T f_x - \rho^T S_x)\,, \tag{43a}$$

and the terminal conditions

$$(\lambda^T)_1 = (\mu^T \psi_x)_1\,. \tag{43b}$$

We note that the differential system (40)-(43) is linear and nonhomogeneous in the functions $A(\tau)$, $B(\tau)$, and C and the multipliers $\lambda(\tau)$, $\rho(\tau)$, and μ and can be solved without assigning a value to the gradient stepsize α. The selection of α is done *a posteriori* in such a way that the descent requirement (15-2) is enforced. This property is the same as in the gradient phase.

3.3.11 Solution Technique in the Restoration Phase

Once again, because of the coupling due to the presence of ρ, the total system must be integrated simultaneously either forward or backward. Using the method of particular solutions, the differential system consisting of equations (40), (41-1), (42-1) and (43a) may be integrated forward $[n - p + 1]$ times. Given

$$\dot{A} = f_x A - f_u B - f_\pi C - (\dot{x} - f)\,, \tag{a}$$

$$0 = S_x A + S_u B - S_\pi C + S\,, \tag{b}$$

$$(A)_0 = 0\,. \tag{c}$$

$$B = -(f_u^T \lambda + S_u^T \rho)\,. \tag{d}$$

$$\dot{\lambda}^T = -(\lambda^T f_x + \rho^T S_x)\,. \tag{e}$$

Substitution of equation (d) into (b) and solve for ρ, we get

$$\rho = [S_u S_u^T]^{-1}(S_x A - S_u f_u^T \lambda + S_\pi C + S)\,. \tag{f}$$

Note as in the gradient case that the above admits an unique solution providing:

$$\det[S_u S_u^T] \neq 0\,.$$

Back substitution of (f) into (d) give

$$B = -(f_u^T \lambda + S_u^T \rho)\,, \tag{g}$$

where ρ is determined from equation (f).

The initial conditions for the i^{th} forward integration are as given before (by equation (h) in the gradient phase). The differential system

$$\dot{A} = f_x A + f_u B + f_\pi C - (\dot{x} - f)\,, \tag{h}$$

$$\dot{\lambda} = -(f_x^T \lambda + S_x^T \rho)\,, \tag{i}$$

can then be integrated forward. The solution of the system is given by equation (30). The unknown coefficients k_i, which differ from those in the gradient phase, are determined from the simultaneous solution of the following equations:

$$\begin{aligned}
\sum_{i=1}^{n+p-1} k_i &= 1 , \\
\sum_{i=1}^{n+p-1} k_i (\psi_x A_i + \psi_\pi C_i)_1 &= -(\psi)_1 , \\
\sum_{i=1}^{n-p-1} k_i (\lambda_i)_1 &= [\mu^T (\psi_x)]_1 , \\
\sum_{i=1}^{n+p-1} k_i \left[\int_0^1 (f_\pi^T \lambda_i + S_\pi^T \rho_i) d\tau + C_i \right] &= -[(\mu^T (\psi_\pi)_1]^T ,
\end{aligned} \tag{44}$$

Equation (44) is equivalent to $[1 + q + n + p]$ scalar equations for the solution of the $[n + p - 1]$ unknown k_i and the q components of the multiplier μ. Using these coefficients from equation (31), the solution (30) satisfies the end constraints of (41-2), (42-2) and (43b). After the constants k_i and the components of the multiplier μ are known, the functions $A(\tau)$, $B(\tau)$, and C as well as the multipliers $\lambda(\tau)$ and $\rho(\tau)$ are computed according to equation (30). In this way, the linear TPBVP is solved.

3.3.12 Restoration Stepsize

The restoration stepsize is selected in such a way that the following inequality is satisfied.

$$\tilde{P}(\alpha) < \tilde{P}(0) , \tag{45}$$

subject to

$$t_f(\alpha) \geq 0 . \tag{46}$$

In summary, the restoration stepsize must be chosen so that the above inequality constraints are satisfied. Should any violation occur, then a smaller value of α must

be employed and can be obtained, for example, with a *bisection* process, starting with $\alpha = 1$.

3.3.13 Summary of the SGR algorithm

The SGR algorithm has cycles, composed of a gradient phase and (possibly) a restoration phase. The objective of each cycle is to decrease the functional I, while the differential and nondifferential constraints are satisfied to the predetermined accuracy required by (10).

The gradient phase involves a single step, which reduces the functional J. It starts with nominal functions $x(\tau)$, $u(\tau)$, π which satisfy the constraints (1) within the preselected accuracy (10a). Using these nominal functions, the matrices f_x, f_u, f_π; S_x, S_u, S_π etc. are evaluated at the integration intervals. The TPBVP (25)-(28) is then solved using the method of particular solutions. The functions $A(\tau)$, $B(\tau)$, C and the multipliers $\lambda(\tau)$, $\rho(\tau)$, μ, are used in turn to compute the corrections $\Delta x(\tau)$, $\Delta u(\tau)$ and $\Delta\pi$ after a suitable value of the stepsize α is found. The varied functions $\tilde{x}(\tau)$, $\tilde{u}(\tau)$, $\tilde{\pi}$ are given by equation (11).

The restoration phase is iterative, hence involves one or more steps, and reduces the constraint errors to a level required by (10a). The nominal functions $x(\tau)$, $u(\tau)$, π are those from the previous gradient phase in the first restoration iteration, or those from the previous restoration iteration for any subsequent restoration iterations. In either case, they satisfy the given initial condition $x(0)$.

Using these nominal functions, the matrices f_x, f_u, f_π; S_x, S_u, S_π, as well as the vectors $\bar{S}$ and $[\dot{x} - f]$, are evaluated at the integration intervals. The TPBVP (40)-(43) is then solved using the method of particular solutions, obtaining the functions $A(\tau)$, $B(\tau)$, C and the multipliers $\lambda(\tau)$, $\rho(\tau)$, and μ, which are used in turn to compute the corrections $\Delta x(\tau)$, $\Delta u(\tau)$, $\Delta\pi$ after a suitable stepsize α has been

found. The varied functions $\tilde{x}(\tau)$, $\tilde{u}(\tau)$, $\tilde{\pi}$ can then be computed using equation (11).

The satisfaction of the condition (10b) signals the termination of the process and the converged solution is given by the varied function $\tilde{x}(\tau)$, $\tilde{u}(\tau)$, $\tilde{\pi}$ at the end of the *restoration* phase.

A flow chart of the SGR algorithm is given in Figure (3.3.3).

3.3.14 Example Problem

The example given here is a modification of the autorotation problem that was formulated in Section (2.9). Here we add an upper bound on the vertical sink rate. Experience gained from the study on the optimal landing of a helicopter after engine failure indicates that the optimal control program usually results in an unacceptably high maximum sink rate. This upper bound on sink rate appears as a state variable inequality constraint:

$$v_{descent} \leq (v_{descent})_{maximum} , \tag{47}$$

which can be transformed to a path equality constraint by the use of a Valentine-type slack variable. Since x_1 denotes the normalized vertical sink rate, we have

$$x_1 - x_{1m} + x_6^2 = 0 , \tag{48}$$

where x_6 is an auxiliary state variable created to convert (47) to (48). Note that the initial condition of x_6 is given by

$$x_6(0) = \pm\sqrt{[x_{1m} - x_1(0)]} , \tag{48a}$$

where either the "+" or "−" sign can be used.

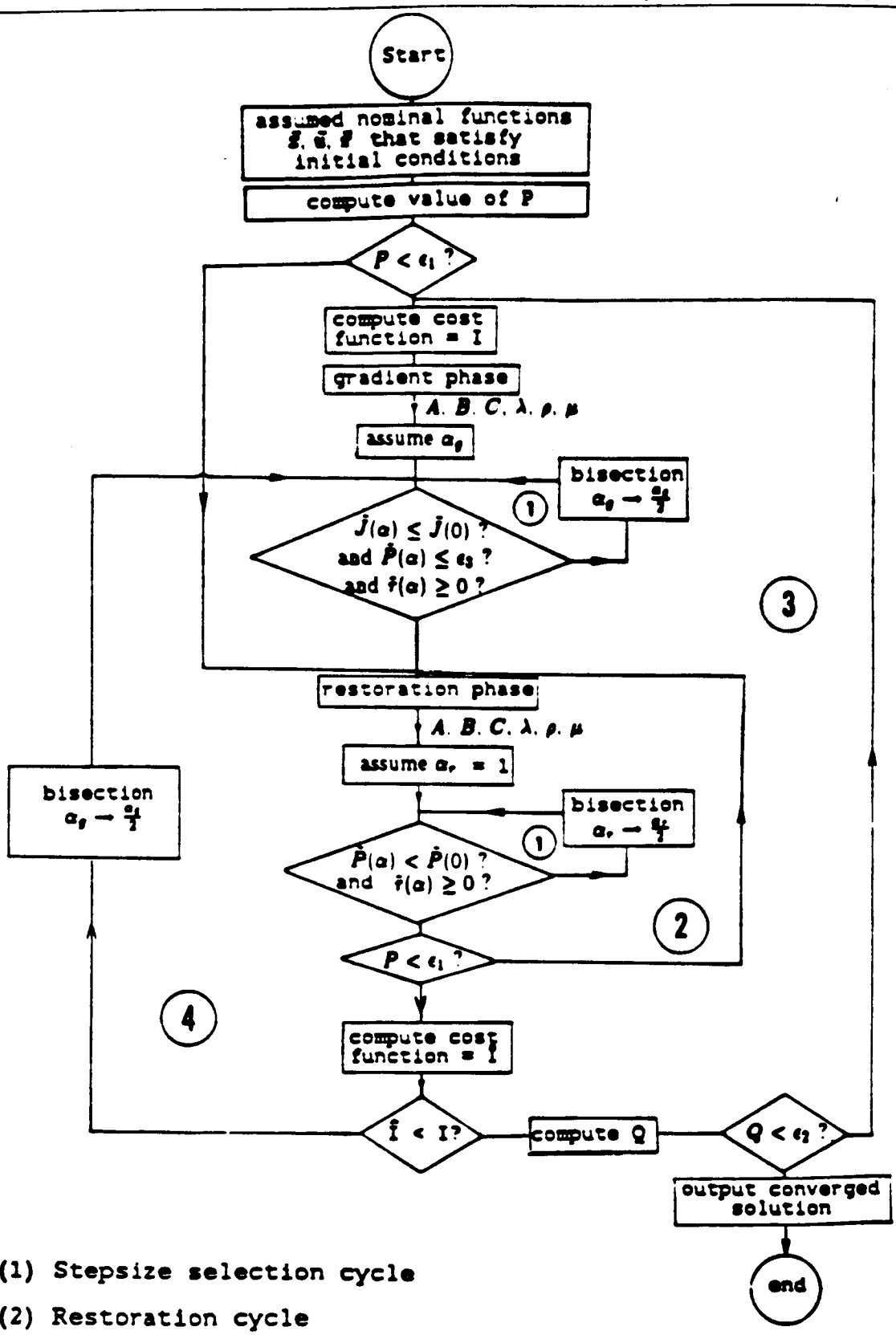

(1) Stepsize selection cycle

(2) Restoration cycle

(3) Gradient restoration cycle

(4) Stability cycle

Figure 3.3.3 Flow Chart of the Sequential Gradient Restoration Technique

The first time derivative of (48) is

$$x_1' + 2x_6u_4 = 0, \tag{49}$$

where $(\,)'$ denotes time differentiation with respect to the normalized time τ. and u_4 is an auxiliary control variable defined as

$$u_4 = x_6'. \tag{50}$$

Since

$$x_1' = g_0 - m_0(u_1x_3^2 + \bar{f}x_1\sqrt{x_1^2 + x_2^2}), \tag{51}$$

we can substitute (51) into (49) and convert it into the following path equality constraint that involves the two controls u_1 and u_4:

$$g_0 - m_0(u_1x_3^2 + \bar{f}x_1\sqrt{x_1^2 + x_2^2}) + 2x_6u_4 = 0. \tag{52}$$

The new form of the autorotation optimization problem with vertical sink rate bound is as given below. Let

$$\vec{X} = (x_1\ x_2\ x_3\ x_4\ x_5\ x_6)^T, \tag{53}$$

$$\vec{U} = (u_1\ u_2\ u_3\ u_4)^T, \tag{54}$$

$$\vec{\pi} = (\tau_f). \tag{55}$$

denote the augmented state, control, and unknown parameter vectors.

The problem is to find $\vec{U}(\xi)$ and $\vec{\pi}$ to minimize:

$$I = \frac{1}{2}({x_1}_f^2 + W_z{x_2}_f^2) = \phi(\vec{X}_f), \tag{56}$$

subject to :

(1) equations of motion ($\dot{\vec{X}} = \vec{f}$):

$$\begin{aligned}
\dot{x_1} &= \tau_f(g_0 - m_0(u_1 x_3^2 + \bar{f} x_1 \sqrt{x_1^2 - x_2^2})), \\
\dot{x_2} &= \tau_f m_0(u_2 x_3^2 - \bar{f} x_2 \sqrt{x_1^2 + x_2^2}), \\
\dot{x_3} &= -\tau_f i_0 x_3^2(c_0 + \lambda\sqrt{u_1^2 - u_2^2}), \\
\dot{x_4} &= 0.1\tau_f x_1, \\
\dot{x_5} &= 0.1\tau_f x_2, \\
\dot{x_6} &= \tau_f u_4.
\end{aligned} \tag{57}$$

(2) the initial condition:

$$\vec{X}_0 = (0, \bar{u}_0, 1, 0, 0, \sqrt{x_{1m}})^T. \tag{58}$$

(3) path equality constraints ($\vec{S}(\vec{X}, \vec{U}, \vec{\pi}) = 0$) are:

$$\begin{aligned}
(u_1^2 + u_2^2) - (\frac{(u_1^2 + u_2^2)}{\bar{C}_{T_e}})^2 - u_3^2 = 0., \\
g_0 - m_0(u_1 x_3^2 + \bar{f} x_1 \sqrt{x_1^2 + x_2^2}) + 2x_6 u_4 = 0.
\end{aligned} \tag{59}$$

(4) terminal constraints ($\vec{\psi}(\vec{X}_f, \vec{\pi}) = 0$) are:

$$\begin{aligned}
x_{4f} - \bar{h}_f = 0, \\
x_{5f} - \bar{d}_f = 0.
\end{aligned} \tag{60}$$

Simplification

Since the computational effort involved in obtaining the optimal control solution using the SGR algorithm is approximately proportional to the square of the dimension of the state vector, the optimal landing problem in its "reduced" form is much preferred.

Since equation (48) is linear in the state x_1, we can find x_1 in terms of the other state variables and eliminate it from equations (53)-(60). We first note from (48) that

$$x_1 = x_{1m} - x_6^2 . \tag{61}$$

Substituting (61) into equations (53)-(60) gives the following reduced problem. Let:

$$\vec{X} = (x_2\ x_3\ x_4\ x_5\ x_6)^T, \tag{62}$$

$$\vec{U} = (u_1\ u_2\ u_3\ u_4)^T. \tag{63}$$

$$\vec{\pi} = (\tau_f). \tag{64}$$

denote the reduced state, control, and unknown parameter vectors of the problem.

The problem is to find $\vec{U}(\xi)$ and $\vec{\pi}$ to minimize:

$$I = \frac{1}{2}[(x_{1m} - x_{6_f}^2)^2 + W_x {x_{2_f}}^2] = \phi(\vec{X}_f), \tag{65}$$

subject to :

(1) equations of motion ($\vec{X}^{\nabla} = \vec{f}$):

$$\begin{aligned}
{x_2}^{\nabla} &= \tau_f m_0 (u_2 {x_3}^2 - \bar{f} x_2 \sqrt{(x_{1m} - x_6^2)^2 + x_2^2}), \\
{x_3}^{\nabla} &= -\tau_f i_0 {x_3}^2 (c_0 + \lambda \sqrt{{u_1}^2 + {u_2}^2}), \\
{x_4}^{\nabla} &= 0.1 \tau_f (x_{1m} - x_6^2), \\
{x_5}^{\nabla} &= 0.1 \tau_f x_2, \\
{x_6}^{\nabla} &= \tau_f u_4 .
\end{aligned} \tag{66}$$

The equation of motion for x_1, which is not needed in the reduced formulation has been removed. Note also that the inflow ratio λ used in (66) is given by a modified version of equation (43) (cf. Chapter 2) given below:

$$\lambda = 0.01[\frac{x_2 u_2 - (x_{1m} - x_6^2) u_1}{x_3 \sqrt{{u_1}^2 + {u_2}^2}}] + k_0 f_l ({u_1}^2 + {u_2}^2)^{\frac{1}{4}} . \tag{67}$$

(2) the initial condition is:

$$\vec{X}_0 = (\bar{u}_0, 1, 0.0, \sqrt{x_{1m}})^T. \tag{68}$$

(3) path equality constraint ($\vec{S}(\vec{X}, \vec{U}, \vec{\pi}) = 0$)

$$\begin{aligned} (u_1{}^2 + u_2{}^2) - (\frac{(u_1{}^2 - u_2{}^2)}{\bar{C}_{T_e}})^2 - u_3{}^2 = 0., \\ g_0 - m_0 u_1 x_3^2 - \bar{f}(x_{1m} - x_6^2)\sqrt{(x_{1m} - x_6^2)^2 + x_2^2)} - 2x_6 u_4 = 0. \end{aligned} \tag{69}$$

(4) terminal constraints ($\vec{\psi}(\vec{X}_f, \vec{\pi}) = 0$) are:

$$\begin{aligned} x_{4f} - \bar{h}_f = 0, \\ x_{5f} - \bar{d}_f = 0. \end{aligned} \tag{70}$$

On completion of the optimization process, $x_1(\tau)$ can be recovered from:

$$x_1(\tau) = x_{1m} - x_6^2(\tau). \tag{71}$$

Results obtained for this problem are given in Chapter 4.

§3.4 Neighboring Extremal with Path Constraints

The necessary conditions for optimal control problems with path equality constraints are given by equations (4)-(6) of the last section. The SGR algorithm described in that section is one way that such a problem can be solved. However, this solution is open-loop and even slight changes in the initial or final conditions require a new computation of the entire control program.

A linear neighboring optimal feedback control scheme was developed by Breakwell, Speyer, and Bryson for optimal control problems in which the state variables are subjected to initial and terminal constraints [50]. Their approach minimizes the

second variation of the performance index. Kelley developed a similar feedback control scheme using the second variation in an accessory minimization formation [51]. Bryson and Ho [29] utilized a Riccati transformation with a backward sweep method to obtain the feedback gains needed to approximate neighboring optimal solution.

In this sub-section, we extend these earlier works to problems which include path equality constraints, and specifically to problems with both path equality constraints $\vec{S}$ and an unknown parameter vector $\vec{\pi}$. The necessary conditions for this class of problems are given by equations (4)-(6) of Section (3.3). These necessary conditions are repeated here for easy reference:

$$\dot{\vec{x}} = f(\vec{x}, \vec{u}, \vec{\pi}, \tau)\,. \tag{1}$$

$$\begin{aligned} \vec{S}(\vec{x}, \vec{u}, \vec{\pi}, \tau) &= 0\,, \\ \dot{\vec{\lambda}}^T &= -H_x\,, \\ H_u &= 0\,, \\ \vec{x}(0) &= \text{given}\,, \\ (\vec{\lambda}^T)_1 &= (\Phi_x)_1\,, \\ \vec{\psi}(\vec{x}_f, \vec{\pi}) &= 0\,, \end{aligned} \tag{2}$$

$$\text{and} \qquad (\Phi_\pi)_1 + \int_0^1 H_\pi d\tau = 0\,.$$

Now consider small perturbations from the nominal optimal path produced by small perturbations in both $\delta\vec{x}(0)$ and $\delta\vec{\psi}$. These perturbations give rise to perturbations $\delta\vec{x}(\tau)$, $\delta\vec{\lambda}(\tau)$, $\delta\vec{u}(\tau)$, $\delta\vec{\rho}(\tau)$, $\delta\vec{\mu}$ and $\delta\vec{\pi}$. The relationships among these perturbed quantities are given by

(1) Perturbed differential relations:

$$\begin{pmatrix} \delta\dot{\bar{x}} \\ \delta\dot{\bar{\lambda}} \end{pmatrix} = \begin{pmatrix} f_x & f_u & f_\pi & 0 & 0 \\ -H_{xx} & -H_{xu} & -H_{x\pi} & -f_x{}^T & -S_x{}^T \end{pmatrix} \begin{pmatrix} \delta\bar{x} \\ \delta\bar{u} \\ \delta\bar{\pi} \\ \delta\bar{\lambda} \\ \delta\bar{\rho} \end{pmatrix}. \tag{3}$$

(2) Perturbed path equality relations:

$$\begin{pmatrix} S_x & S_u & S_\pi & 0 & 0 \\ H_{ux} & H_{uu} & H_{u\pi} & f_u{}^T & S_u{}^T \end{pmatrix} \begin{pmatrix} \delta\bar{x} \\ \delta\bar{u} \\ \delta\bar{\pi} \\ \delta\bar{\lambda} \\ \delta\bar{\rho} \end{pmatrix} = \begin{pmatrix} 0 \\ 0 \end{pmatrix}. \tag{4}$$

and

$$\begin{aligned} 0 = (\Phi_{\pi x})_1(\delta\bar{x})_1 + (\psi_\pi{}^T)_1(\delta\bar{\mu}) + \left[(\Phi_{\pi\pi})_1 + \int_0^1 H_{\pi\pi}\,d\tau\right]\delta\bar{\pi} \\ - \left(\int_0^1 H_{\pi x}\delta\bar{x}\,d\tau\right) + \left(\int_0^1 H_{\pi u}\delta\bar{u}\,d\tau\right) - \left(\int_0^1 f_\pi{}^T\delta\bar{\lambda}\,d\tau\right) - \left(\int_0^1 S_\pi{}^T\delta\bar{\rho}\,d\tau\right). \end{aligned} \tag{5}$$

(3) End conditions

$$\begin{aligned} \delta\bar{x}(0) &= \text{specified}, \\ (\delta\bar{v})_1 &= (\psi_x)_1(\delta\bar{x})_1 - (\psi_\pi)_1\delta\bar{\pi} = \text{specified}. \\ (\delta\bar{\lambda})_1 &= (\Phi_{xx})_1(\delta\bar{x})_1 + (\Phi_{x\pi})_1\delta\bar{\pi} + (\psi_x{}^T)_1\delta\bar{\mu}. \end{aligned} \tag{6}$$

Note that these relations have been simplified using the following identities:

$$H_{x\lambda} = f_x{}^T,$$

$$H_{x\rho} = S_x{}^T,$$

$$H_{ux} = f_u{}^T,$$

$$H_{u\rho} = S_u{}^T,$$

$$(\Phi_{\pi\mu})_1 = (\psi_\pi{}^T)_1,$$

$$H_{\pi\lambda} = f_\pi{}^T,$$

and $$H_{\pi\rho} = S_\pi{}^T.$$

From equation (4), we can solve $\delta\bar{u}$ and $\delta\bar{\rho}$ in terms of $\delta\bar{x}$, $\delta\bar{\lambda}$, and $\delta\bar{\pi}$ as follows:

$$\begin{pmatrix} \delta\bar{u} \\ \delta\bar{\rho} \end{pmatrix} = \begin{pmatrix} A_{11} & A_{12} & A_{13} \\ A_{21} & A_{22} & A_{23} \end{pmatrix} \begin{pmatrix} \delta\bar{x} \\ \delta\bar{\lambda} \\ \delta\bar{\pi} \end{pmatrix} \tag{7}$$

Equation (7) can be substituted into equations (3) and (5) and the result is the following linear, time-varying differential equation

$$\begin{pmatrix} \delta\dot{x} \\ \delta\dot{\lambda} \end{pmatrix} = \begin{pmatrix} C_{11} & C_{12} & C_{13} \\ C_{21} & C_{22} & C_{23} \end{pmatrix} \begin{pmatrix} \delta\bar{x} \\ \delta\bar{\lambda} \\ \delta\bar{\pi} \end{pmatrix} \tag{8}$$

with the integral path constraint

$$S_{10} + S_{11}\delta\bar{\pi} + \int_0^1 (S_{12}\,\delta\bar{x} + S_{13}\,\delta\bar{\lambda})d\tau = 0. \tag{9}$$

Here A_{ij}, C_{ij} ($i = 1,2$ and $j = 1,2,3$) and S_{10}-S_{13} (not to be confused with the path equality constraints $\bar{S}$) are time-varying matrices evaluated on the nominal optimal path. Detailed expressions of these matrices, as well as those of H_{uu}, $H_{u\pi}$, H_{xx}, H_{ux}, $H_{\pi x}$ and $H_{\pi u}$ are given in Appendix (E). Using the results given in Appendix (E), we can easily establish that $-C_{11}{}^T = C_{22}$ and that both C_{12} and C_{21} are symmetrical matrices.

Note that the system of equations (3)-(6) admits an unique solution providing: (1) H_{uu} is non-singular; and (2) S_4 ($r \times r$) ($= S_u\,H_{uu}{}^{-1}S_u{}^T$) is also non-singular.

The first requirement is the usual convexity condition (or strengthened Legendre-Clebsch condition). The condition is easily understood from the fact that $\bar{u}(\tau)$ is determined by minimizing the Hamiltonian function (H) with respect to $\bar{u}$ while holding $\bar{x}$, $\bar{\lambda}$ and $\bar{\pi}$ fixed. For a smooth H-function with no constraint on $\bar{u}(\tau)$, it requires that

$$H_u = 0, \quad \text{and} \quad H_{uu} > 0.$$

The second requirement (*i.e.* $S_4 > 0$) can thus be interpreted as a modified form of the convexity condition for problems with path equality constraints $\bar{S}$. Note that if any of the path equality constraints does not involve some components of the control vector $\bar{u}$, the determinant of $\left| S_u H_{uu}^{-1} S_u^T \right|$ is zero. A necessary (but not sufficient) condition for the non-singularity of the S_4 matrix is hence the involvment of the control $\bar{u}$ in $\bar{S}$.

Simplifications

If ϕ, $\bar{\psi}$, $\bar{S}$ and f_π are not functions of $\bar{\pi}$, some simplifications are possible. These include:

(1) Simplified expressions for some of the S-matrices (cf. Appendix (E)):

$$S_2 = S_u H_{uu}^{-1} H_{u\pi} ,$$

$$S_5 = S_{10} = 0 ,$$

$$S_{11} = \int_0^1 (H_{u\pi} S_8) d\tau ,$$

$$S_{12} = H_{\pi x} + H_{\pi u} S_6 ,$$

$$\text{and} \quad S_{13} = H_{\pi u} S_7 - f_\pi^T .$$

(2) Simplified end-conditions:

$$\delta\bar{x}(0) = given ,$$

$$(\delta\bar{\psi})_1 = (\psi_x)_1 (\delta\bar{x})_1 = given ,$$

$$(\delta\bar{\lambda})_1 = (\Phi_{xx})_1 (\delta\bar{x})_1 + (\psi_x^T)_1 (\delta\bar{\mu}) .$$

(3) Simplified expressions for $H_{(\,)}$:

$$\text{Since} \quad H(\bar{x}, \bar{u}, \bar{\pi}, \bar{\lambda}, \bar{\rho}, \tau) = L(\bar{x}, \bar{u}, \bar{\pi}, \tau) + \lambda^T f(\bar{x}, \bar{u}, \bar{\pi}, \tau) + \rho^T S(\bar{x}, \bar{u}, \tau) ,$$

$$\text{therefore} \quad H_u = L_u + \lambda^T f_u + \rho^T S_u ,$$

$$H_x = L_x + \lambda^T f_x + \rho^T S_x ,$$

$$H_\pi = L_\pi + \lambda^T f_\pi .$$

General expressions of $H_{(.)}$ are given by

$$
\begin{aligned}
H_{xx} &= \frac{\partial}{\partial x}(H_x^T) = \frac{\partial}{\partial x}(L_x^T + f_x^T\lambda + S_x^T\rho)\,,\\
H_{uu} &= \frac{\partial}{\partial u}(H_u^T) = \frac{\partial}{\partial u}(L_u^T + f_u^T\lambda - S_u^T\rho)\,,\\
H_{u\pi} &= \frac{\partial}{\partial \pi}(H_u^T) = \frac{\partial}{\partial \pi}(L_u^T + f_u^T\lambda)\,,\\
H_{ux} &= \frac{\partial}{\partial x}(H_u^T) = \frac{\partial}{\partial x}(L_u^T + f_u^T\lambda + S_u^T\rho)\,,\\
H_{\pi x} &= \frac{\partial}{\partial x}(H_\pi^T) = \frac{\partial}{\partial x}(L_\pi^T + f_\pi^T\lambda)\,.\\
\text{and}\quad H_{\pi u} &= \frac{\partial}{\partial u}(H_\pi^T) = \frac{\partial}{\partial u}(L_\pi^T + f_\pi^T\lambda)\,.
\end{aligned}
$$

With these simplifications, the linear TPBVP (given by equations (6)-(9)) is given in Section (3.4.1).

3.4.1 Problem Formulation

$$
\begin{pmatrix} \delta\dot{x} \\ \delta\dot{\lambda} \end{pmatrix} = \begin{pmatrix} C_{11} & C_{12} & C_{13} \\ C_{21} & -C_{11}{}^T & C_{23} \end{pmatrix} \begin{pmatrix} \delta\bar{x} \\ \delta\bar{\lambda} \\ \delta\bar{\pi} \end{pmatrix} \tag{10}
$$

with the following integral path constraints

$$
S_{11}\delta\bar{\pi} + \int_0^1 (S_{12}\delta\bar{x} + S_{13}\delta\bar{\lambda})\,d\tau = 0\,,
$$

and subjected to the following end conditions

$$
\begin{aligned}
&\delta\bar{x}(0) = given\,,\\
&(\delta\bar{\psi})_1 = (\psi_x)_1(\delta\bar{x})_1 = given\,,\\
&(\delta\bar{\lambda})_1 = (\Phi_{xx})_1(\delta\bar{x})_1 + (\psi_x{}^T)_1\delta\bar{\mu}\,.
\end{aligned}
$$

3.4.2 Solution by the Backward Sweep Method

$\delta\bar{\lambda}$ and $\delta\bar{\psi}$ can be expressed in terms of $\delta\bar{x}$, $\delta\bar{\mu}$ and $\delta\bar{\pi}$ in the following form (cf. Chapter (6) of reference [29])

$$
\begin{aligned}
\delta\bar{\lambda} &= \bar{T}\,\delta\bar{x} + \bar{R}\,\delta\bar{\mu} + \bar{P}\,\delta\bar{\pi}\,,\\
\delta\bar{\psi} &= R^T\,\delta\bar{x} + Q\,\delta\bar{\mu} + H\,\delta\bar{\pi}\,.
\end{aligned} \tag{11}
$$

Here $T(n \times n)$, $R(n \times q)$, $P(n \times p)$, $Q(q \times q)$ and $H(q \times p)$ are matrices that satisfy the following differential equations:

$$\begin{aligned}
\dot{T} &= -TC_{11} - C_{11}^T T - TC_{12}T + C_{21}\,, \\
\dot{R} &= -(C_{11}^T + TC_{12})R\,, \\
\dot{P} &= C_{23} - C_{11}^T P - T(C_{12}P + C_{13})\,, \qquad (12) \\
\dot{Q} &= -R^T C_{12} R\,, \\
\text{and } \dot{H} &= -R^T(C_{12}P + C_{13})\,.
\end{aligned}$$

The first three relations in equation (12) can be obtained as follows. We first take the time differentiation of $\delta\bar{\lambda}$ in equation (11) and substitute into the resultant equation expressions of $\delta\dot{x}$ and $\delta\dot{\lambda}$ from equation (10) (noting that both $\delta\bar{\mu}$ and $\delta\bar{\pi}$ are constant). The final equation has the form

$$[\ ]\delta\bar{x} + [\ ]\delta\bar{\mu} + [\ ]\delta\bar{\pi} = 0\,.$$

If the above equation is to be identically true for all $\delta\bar{x}$, $\delta\bar{\mu}$ and $\delta\bar{\pi}$, all the $[\ ]$ terms must be zero. Thus, we obtain the first three relations of equation (12).

The last two relations in equation (12) are obtained in a similar way. Here we note that $\delta\bar{\psi}$ is a constant when we take the time derivative of the second equation in (11). Substitution into the resultant equation expression for $\delta\dot{x}$ from equation (10) and the expression for $\delta\bar{\lambda}$ from equation (11) give the differential relations for Q and H.

The terminal conditions of the T, R, P, Q and H matrices are obtained in this

manner and are given by the following relations:

$$\begin{aligned} T(1) &= (\Phi_{xx})_1 , \\ R(1) &= (\nu_x^T)_1 , \\ P(1) &= (\Phi_{x\pi})_1 = 0 , \\ Q(1) &= 0 , \\ \text{and } H(1) &= (\psi_\pi)_1 = 0 . \end{aligned} \tag{13}$$

Finally, to obtain the neighboring optimal feedback law, we can substitute equation (11) into equation (7), yielding the following relation:

$$\delta\bar{u} = -\Lambda_1\delta\bar{x} - \Lambda_2\delta\bar{\psi} - \Lambda_3\delta\bar{\pi} , \tag{14}$$

The time-varying neighboring optimal feedback gains, Λ_i ($i = 1$, 2 and 3) are given by the following relations:

$$\begin{aligned} \Lambda_1(m \times n) &= -[A_{11} + A_{12}(T - R\,Q^{-1}R^T)] , \\ \Lambda_2(m \times q) &= -A_{12}R\,Q^{-1} , \\ \text{and } \Lambda_3(m \times p) &= -[A_{13} + A_{12}(P - R\,Q^{-1}H)] . \end{aligned} \tag{15}$$

Equation (14) is a continuous linear feedback law that will produce the desired small changes in the terminal conditions $\delta\bar{\psi}$ starting from the revised initial conditions of $\bar{x}(0) + \delta\bar{x}(0)$. These end-conditions are met in such a way that the performance index I (and hence J) is minimized. This method constitutes the Neighboring Optimal Feedback Law.

In addition to our earlier mention of the non-singularities of the H_{uu} and $S_u H_{uu}^{-1} S_u^T$ matrices, we now note from equation (15) other necessary conditions for a local minimum in J. These additional necessary conditions are that both

$$[T - RQ^{-1}R^T]$$

and $|P - RQ^{-1}H|$

be finite for $0 \leq \tau \leq 1$. This is similar to the classical Jacobi condition, or the condition that no conjugate points exist on the path. If either of these conditions is violated, for example, $|T - RQ^{-1}R^T|$ approaches infinity at time τ' (where $0 < \tau' \leq 1$), it is necessary that certain combinations of the components of $\delta\vec{x}$ at time τ' be zero. The set of all possible perturbations is now restricted to a dimension less than n (the dimension of $\vec{x}$). In fact, the path is not a minimum path if it continues beyond τ'.

Note from equation (13) that the matrix Q is identically zero at the terminal time. All the gain matrices given by equation (13) approach infinity as the end-time nears. This mathematical singularity can be bypassed if we adopt the strategy of "switching-off" the feedback law as the end-time is approached.

The value of $\delta\vec{\pi}$ is needed in the neighboring optimal feedback law. This value must be determined by the simultaneous solution of both the linear TPBVP and path equality constraints. Appendix (F) gives an iterative procedure that can be used to find $\delta\vec{\pi}$ by taking advantage of the fact that $\delta\vec{\pi}$ enters both the differential equation (10) and its initial condition linearly. A schematic diagram of the neighboring feedback control is given in Figure (3.4.4).

3.4.3 Example Problems

Two example problems are given here to demonstrate the concept. The first is for a dynamic optimization problem constrained by a path equality constraint S, but without the variable parameter vector $\vec{\pi}$. The second example includes both $\vec{S}$ and $\vec{\pi}$. The computer code that is used in the following computation is called Program "SECOND". Furhter information about the computer program can be found in Appendix (F).

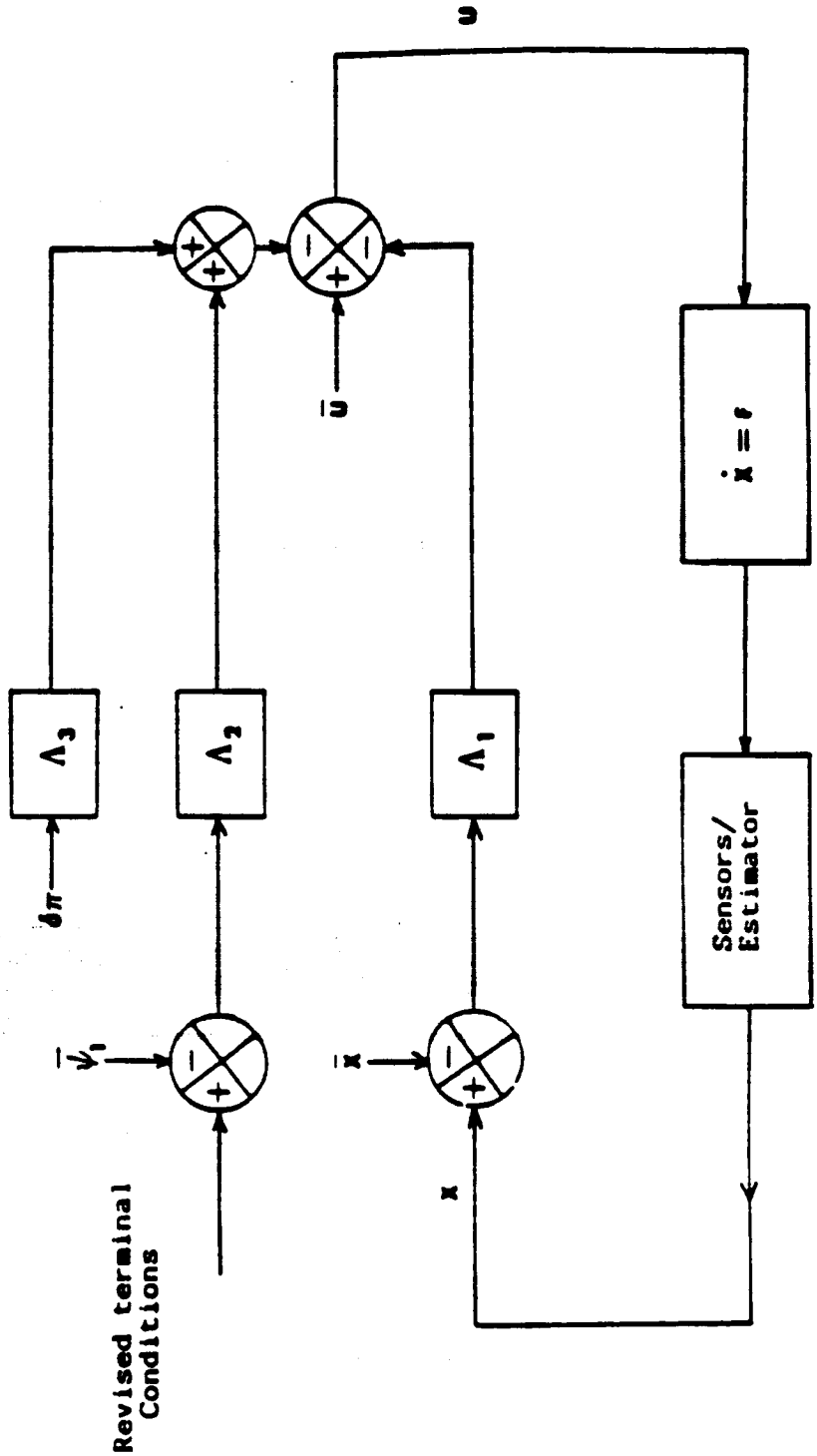

Figure 3.4.4 Neighboring Optimal Feedback Law

Example Problem (1)

Problem Statement

$$\min_{\theta} I = -y_f$$

$$\dot{x} = V\cos\theta\,,$$

$$\dot{y} = V\sin\theta\,.$$

The initial conditions of the problem are

$$x(0) = 0\,,$$

$$y(0) = 0\,,$$

and the terminal constraint

$$x(t_f) = x_f\,.$$

The end-time of the problem t_f is fixed.

This is a simple two-dimensional problem of transferring between the initial and final states of a vehicle with a constant velocity V. The objective is to control the velocity orientation angle θ in such a way as to maximize $y(t_f)$. The problem is simple enough that analytical solutions for both the optimal control problem and its neighboring optimal feedback law can be determined as shown below.

(A) Optimal Control Solution

Using standard optimal control techniques (cf. Chapter (2) of [29]), the optimal solution is given by the following relations:

$$\sin\theta^* = (1 - (\frac{x_f}{Vt_f})^2)^{\frac{1}{2}},$$
$$\cos\theta^* = (\frac{x_f}{Vt_f})$$
$$x^*(t) = (\frac{x_f t}{t_f})$$
$$y^*(t) = V(1 - (\frac{x_f}{Vt_f})^2)^{\frac{1}{2}}t.$$

Therefore the optimal orientation of the velocity vector θ^* is fixed and is given by the above expression. The optimal trajectory in space is a straight line and the problem is well posed only when

$$|x_f| \leq Vt_f.$$

(B) Neighboring Optimal Feedback Control

The neighboring optimal feedback control law can also be determined in the usual way (cf. Chapter (6) of [29]). The optimal feedback law is given by the following equation:

$$\delta\theta^* = -\Lambda_1\delta\bar{x} - \Lambda_2\delta\psi.$$

Here $\Lambda_1(1 \times 2)$ and $\Lambda_2(1 \times 1)$ are the feedback gain matrices associated with the state and the terminal constraints respectively. These gain matrices are given by the following relations:

$$\Lambda_1 = \left(\frac{1}{V(t_f - t)\sin\theta^*} \quad 0\right),$$
$$\Lambda_2 = \left(-\frac{1}{V(t_f - t)\sin\theta^*}\right).$$

Substitutions of these gain matrices into the feedback law give

$$\delta\theta^* = -\left(\frac{\delta\bar{x}}{V^*(t_f - t)\sin\theta^*}\right) + \left(\frac{\delta\psi}{V^*(t_f - t)\sin\theta^*}\right).$$

These "exact" analytical results are used as references for comparison with numerical results.

The above problem can be re-formulated into one with path equality constraint as follow

Alternative Problem Formulation

$$\min_{\bar{u}} I = -x_2(t_f)$$

$$\dot{x}_1 = 2u_1,$$

$$\dot{x}_2 = 2u_2.$$

The initial conditions of the reformulated problem are the same as those given before

$$x_1(0) = 0,$$

$$x_2(0) = 0,$$

The terminal constraint is

$$x(t_f) = 1.$$

The new problem is the same as the original one with $V = 2$, $t_f = 1$ and $x_f = 1$. Instead of using the orientation angle θ as the control, we choose to use the sine

and cosine of the same angle as the controls of the problem. That is,

$$u_1 = \cos\theta,$$

$$u_2 = \sin\theta.$$

Because of these control definitions, the problem is now constrained by a path equality constraint

$$u_1^2 + u_2^2 = 1.$$

The neighboring optimal feedback law of the problem in its alternative form is solved using the numerical technique described earlier. The procedure is started with the solution of the nominal optimization problem and followed by the computations of the neighboring feedback gain matrices Λ_1 and Λ_2. The non-zero components of these matrices are given in Figure (3.4.5).

These numerically obtained gain matrices should now be compared with those determined analytically. With $x_f = 1$, $V = 2$, and $t_f = 1$, we have from the analytical results

$$\sin\theta^* = \sqrt{\frac{3}{4}},$$

$$\text{or} \quad \cos\theta^* = \left(\frac{1}{2}\right),$$

$$\text{and} \quad \delta\theta^* = -\left(\frac{\delta x}{\sqrt{3}(1-t)}\right) + \left(\frac{\delta x_f}{\sqrt{3}(1-t)}\right).$$

But since

$$u_1 = \cos\theta,$$

$$u_2 = \sin\theta.$$

therefore we have

$$\begin{pmatrix} \delta u_1 \\ \delta u_2 \end{pmatrix} = \begin{pmatrix} -\sqrt{\frac{3}{4}} \\ \frac{1}{2} \end{pmatrix} \delta\theta^*.$$

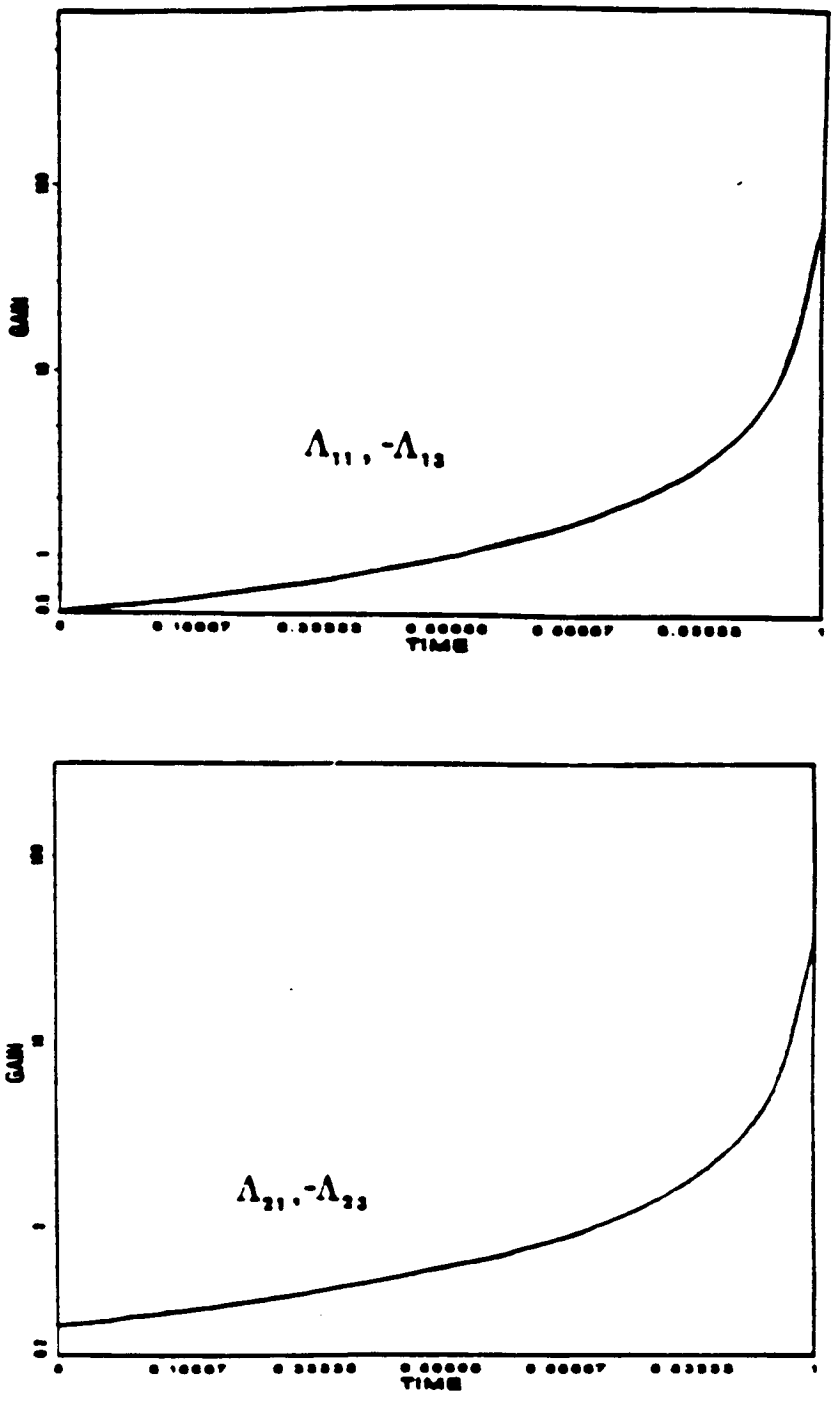

Figure 3.4.5 Feedback Gains in Example (1)

Substitution into the last equation expression for $\delta\theta^*$ gives us the neighboring optimal feedback law, $(\delta u_1\ ,\ \delta u_2)^T$

$$\begin{pmatrix}\delta u_1\\ \delta u_2\end{pmatrix} = -\begin{pmatrix}-\frac{1}{2(1-t)} & 0\\ \frac{1}{2\sqrt{3}(1-t)} & 0\end{pmatrix}\begin{pmatrix}\delta x_1\\ \delta x_2\end{pmatrix} - \begin{pmatrix}\frac{1}{2(1-t)}\\ -\frac{1}{2\sqrt{3}(1-t)}\end{pmatrix}\delta\nu.$$

These results agree with those obtained numerically (see also Figure (3.4.5)). Note that the magnitudes of these gains approach infinity at the terminal time.

The usefulness of the neighboring optimal feedback law can be confirmed in several ways. For example, the initial and terminal conditions of the nominal control problem may be "perturbed" simultaneously as follow

$$x_1(0) = 0.0 \rightarrow +0.1\ ;\ \delta x_1(0) = +0.1\,,$$

$$x_2(0) = 0.0 \rightarrow -0.1\ ;\ \delta x_2(0) = -0.1\,,$$

$$x_1(1) = 1.0 \rightarrow +0.9\ ;\ \delta x_1(1) = -0.1\,.$$

The optimal solution to this perturbed problem can be obtained numerically using SECOND. The solution may also be determined analytically using the revised end-conditions.

Figure (3.4.6) shows the results obtained numerically for both the nominal and the perturbed problems. The former is obtained using the sequential gradient restoration (SGR) technique while the later by SECOND. It can be seen from these figures that the neighboring optimal feedback law has predicted substantial changes in both u_1 and u_2, resulting in large changes in the time history of $x_1(t)$ and $x_2(t)$.

Both the analytical and numerically computed results for the perturbed problem are given in Figure (3.4.7). The figure shown indicates excellent agreement.

Example Problem (2)

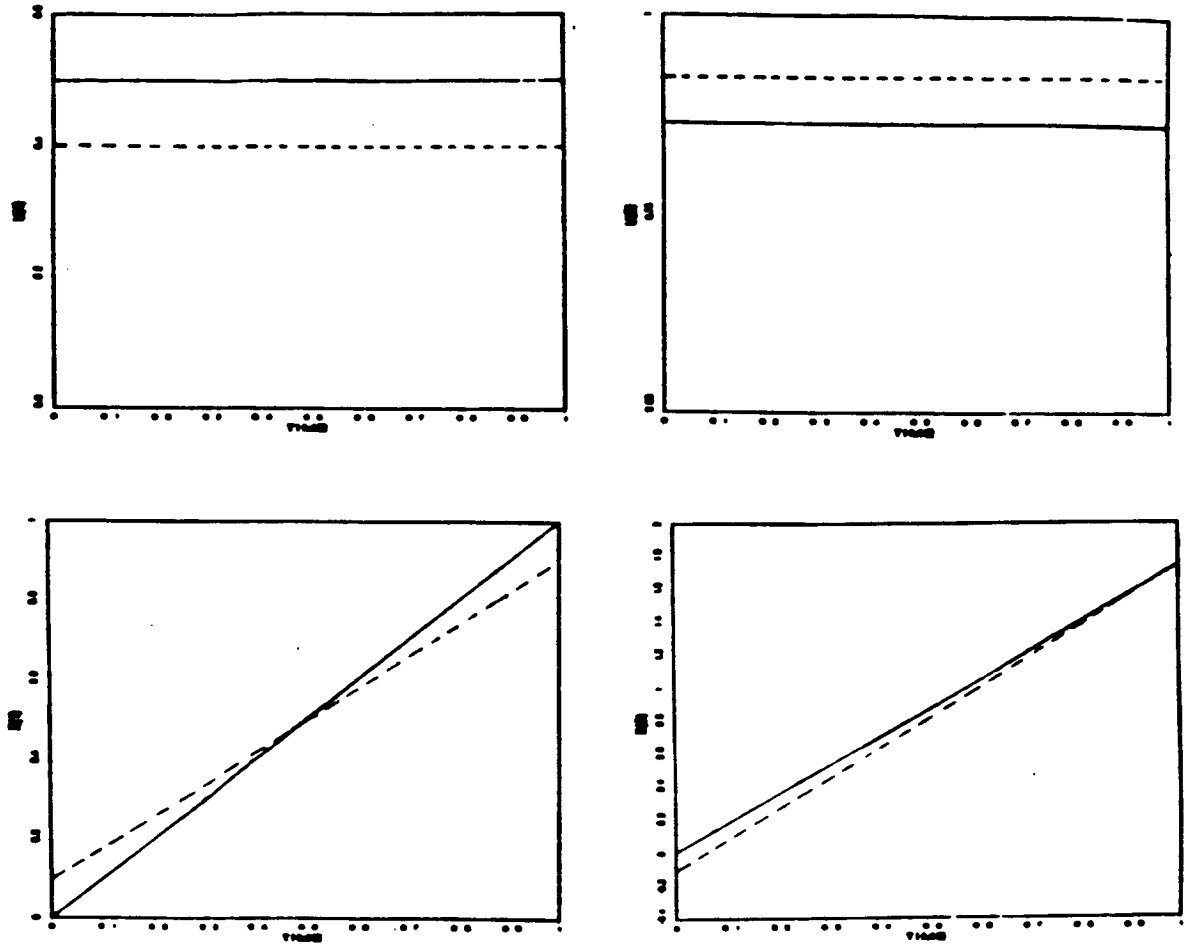

Figure 3.4.6 Nominal and Perturbed Results in Example (1)

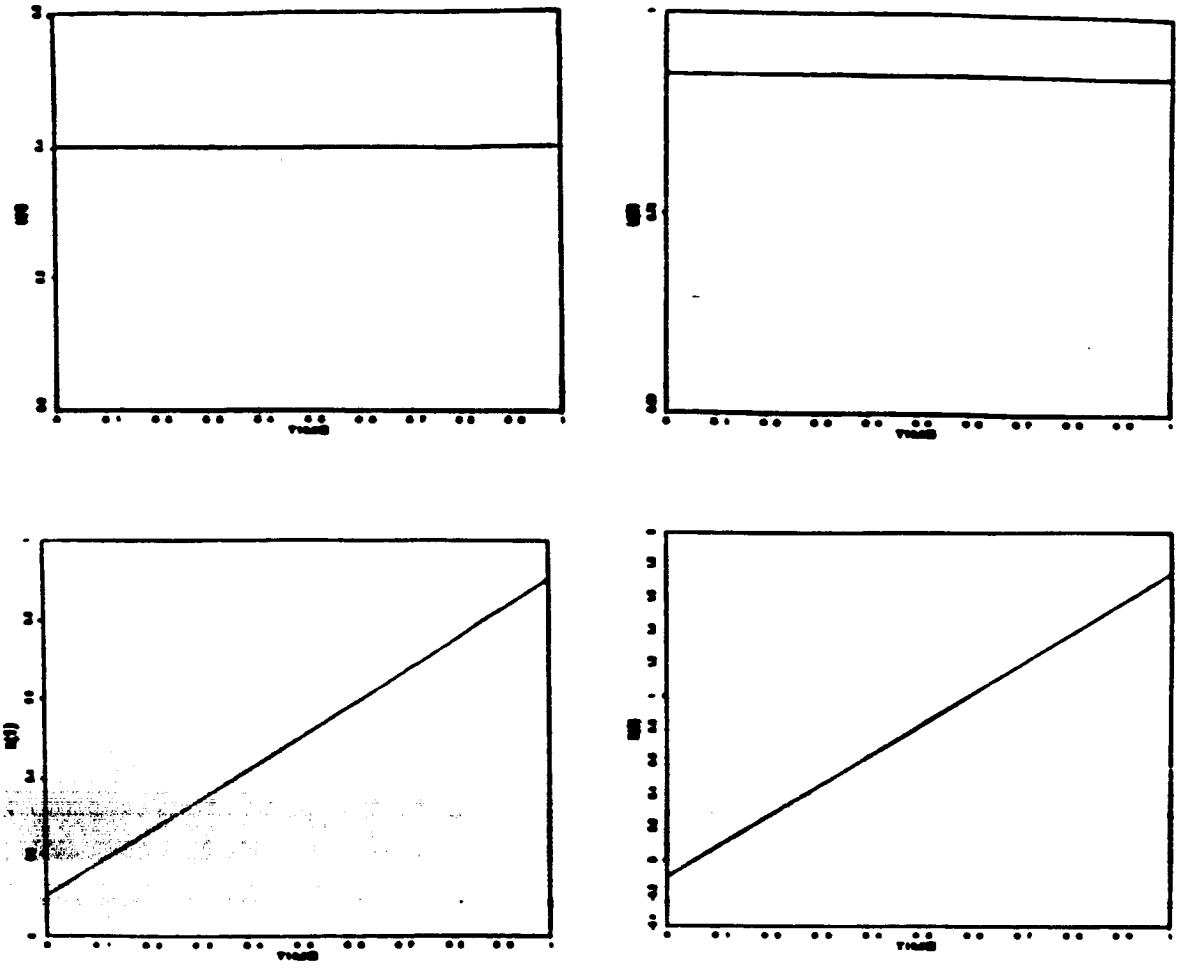

——— : Direct Optimization Technique with revised end-conditions

- - - - - - - - : Predictions of Neighboring Optimal Feedback Laws

Figure 3.4.7 Comparison of Exact Results with those from Feedback Law in Example (i)

The second example is one with the terminal time unspecified. The problem statement is

$$\min_{\bar{u}} I = \int_0^{t_f} [u_1^2 + x_2^2\, dt$$

$$\dot{x_1} = u_1\,,$$

$$\dot{x_2} = (u_2 - x_1)\,.$$

The initial conditions of the problem are

$$x_1(0) = 0\,, \qquad x_2(0) = 0\,.$$

The path constraint is given by the following equation

$$u_2^2 + x_1^2 = 1\,.$$

and the terminal constraints are

$$x_1(t_f) = 0.5\,, \qquad x_2(t_f) = 0.5\,.$$

Note that the problem is linear except for the path constraint. The problem is designed in such a way that both H_{uu} and $[S_u H_u^{-1} S_u^T]$ do not vanish for $0 \leq t \leq t_f$. $\bar{x}(2 \times 1)$, $\bar{u}(2 \times 1)$, $\bar{\nu}(2 \times 1)$ and $\bar{S}(1 \times 1)$ are respectively the state, control, terminal, and path equality constraint vectors of the problem.

The above problem can be transformed into one with fixed end-time with the following change of independent variable

$$\tau = \frac{t}{t_f}$$

The independent variable of the problem is now τ which varies from 0 to 1.

The transformed problem is

$$\min_{\bar{u}} I = \int_0^1 t_f [u_1^2 + x_2^2] d\tau$$

$$x_1' = t_f u_1 ,$$

$$x_2' = t_f (u_2 - x_1) .$$

The initial conditions of the problem are

$$x_1(0) = 0 , \qquad x_2(0) = 0 .$$

Here $( )'$ denotes differentiation with respect to the new independent variable τ.

The path constraint is given by the following equation

$$u_2^2 + x_1^2 = 1 ,$$

and the terminal constraints are

$$x_1(1) = 0.5 , \qquad x_2(1) = 0.5 .$$

We have introduced in the above process an unknown parameter t_f into the problem. The only component of the vector $\bar{\pi}$ is hence the unspecified end-time of the problem t_f.

The nominal optimization problem is first solved and the neighboring optimal feedback gain matrices (A_1 , A_2 , A_3) in the following feedback law are computed.

$$\delta \bar{u}(\tau) = -A_1(\tau)\delta \bar{x} - A(\tau)\delta \bar{\psi} - A_3(\tau)\delta \bar{\pi} .$$

Here A_1, A_2 and A_3 are (2×2), (2×2) and (2×1) matrices respectively. The non-zero components of these matrices are given in Figure (3.4.8). Note that (once again) these gain components approach infinity near the end-time of the problem.

The nominal optimal control problem is being perturbed in the following ways

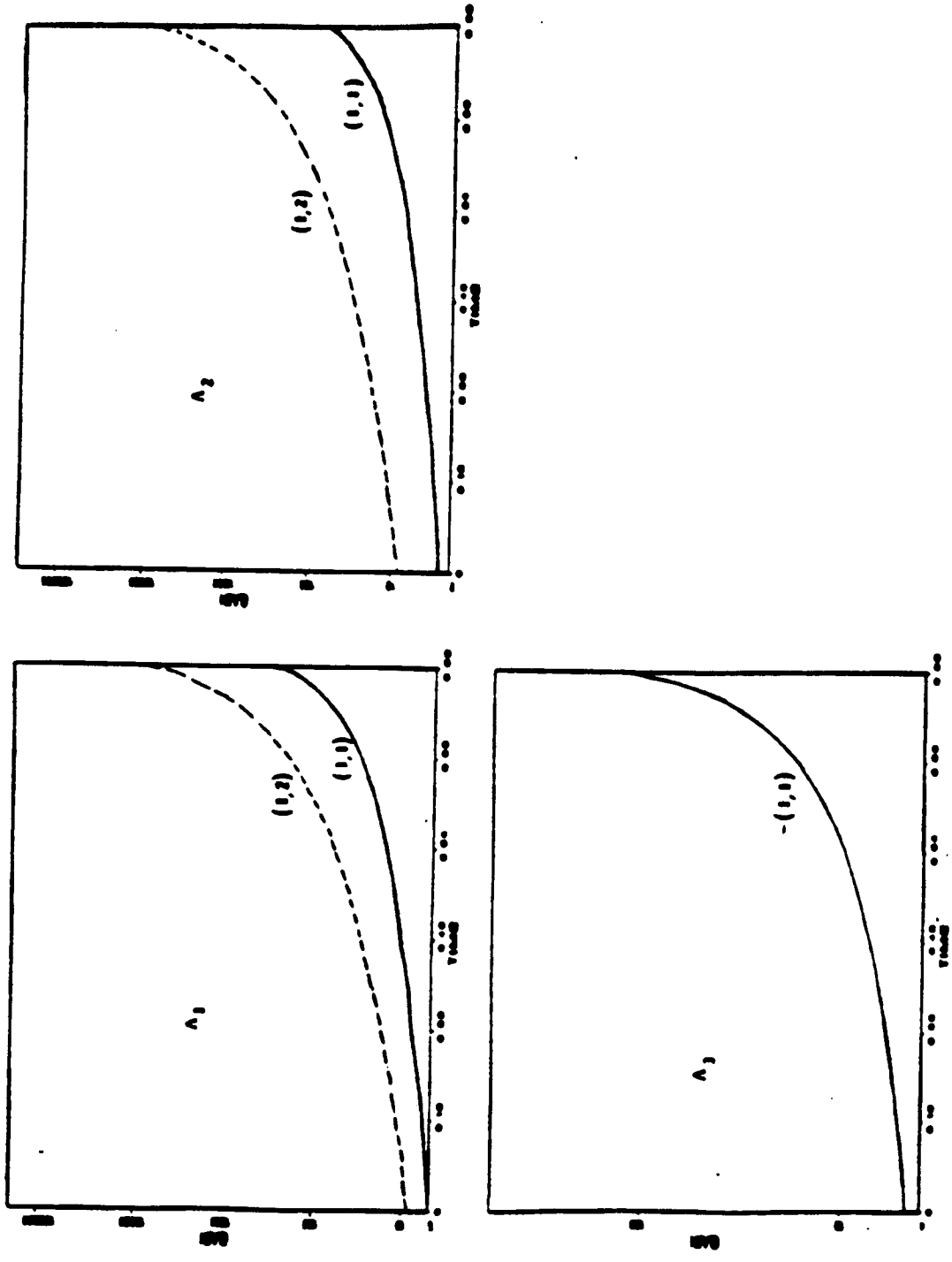

Figure 3.4.8 Feedback Gains in Example (2)

(1) Perturbed initial conditions

$$\delta\bar{x}(0) = (0.05\,,\,0.05)^T$$

(2) Perturbed terminal conditions

$$\delta\bar{\psi}(1) = (0.05\,,\,-0.05)^T$$

(3) Perturbed initial and terminal conditions

$$\delta\bar{x}(0) = (-0.03, 0.03)^T\,, \qquad \delta\bar{\psi}(1) = (0,03, -0.03)^T\,.$$

Since analytical solution of the problem cannot be easily obtained, these problems with revised end-conditions must be solved by using the SGR technique. The results obtained in this way are considered to be "exact". The neighboring optimal feedback law is then used to solve the same problems. In this way, the accuracy of the results obtained by using the feedback law can be gauged by a comparison with the "exact" results.

(1) Perturbed initial conditions

The time history of both $\bar{x}(\tau)$ and $\bar{u}(\tau)$ in the nominal control problem are given in Figure (3.4.9). Those for the perturbed problem with revised initial conditions, as predicted by the feedback law are given in the same plots. The purpose of showing these figures is to give some indication of the percentage changes in the state/control vectors that have occurred due to the revision of the initial conditions.

By using the SGR technique, the end-times of the nominal and perturbed problems are found to be 0.728 and 0.681 respectively. Therefore the change in the terminal time t_f is

$$\delta t_f = 0.681 - 0.728 = -0.047$$

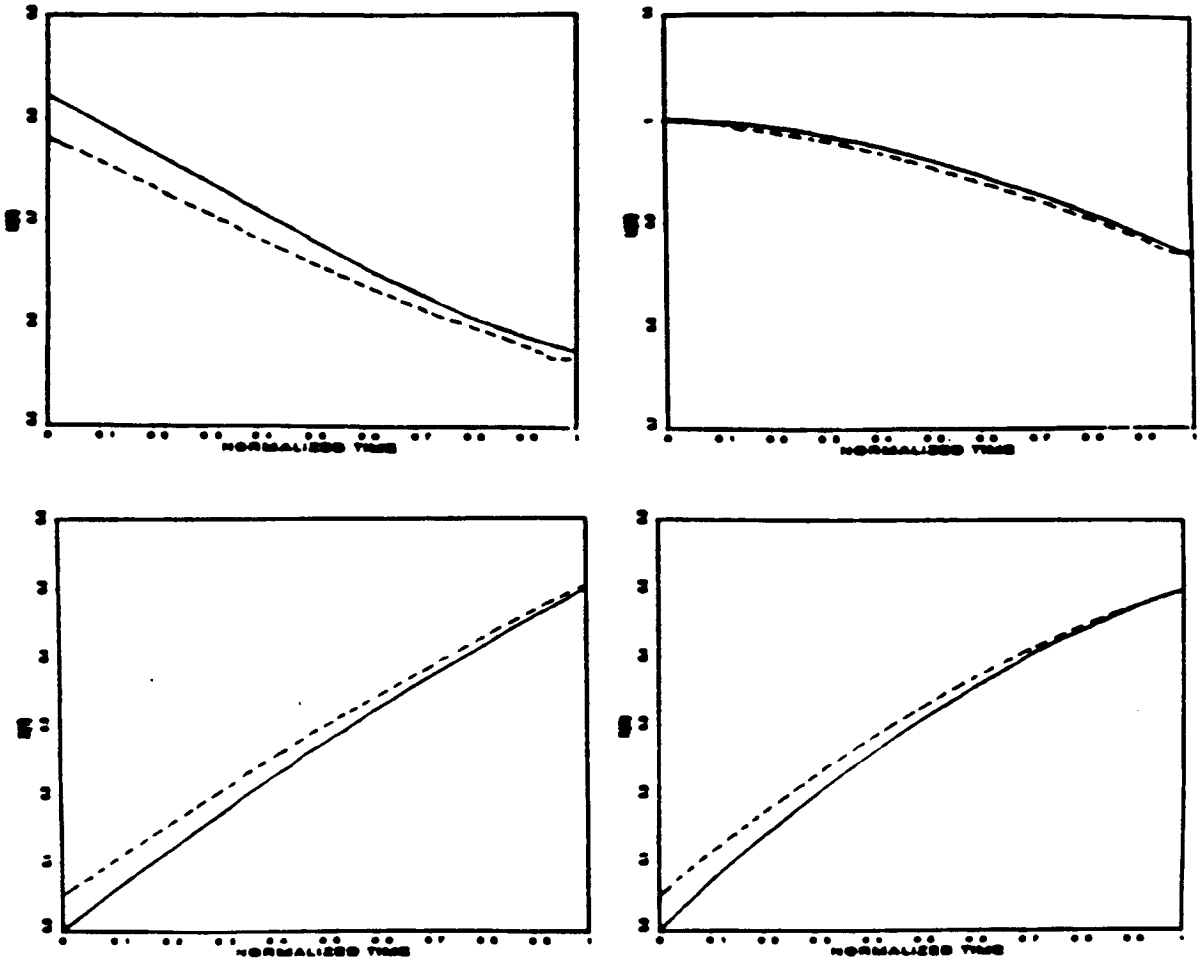

——— : Nominal Path

- - - - - - - - : Predictions of Neighboring Optimal Feedback Laws

Figure 3.4.9 Nominal and Perturbed (initial condition) Results in Example (2)

Using the iterative procedure described in Appendix (F), the value of δt_f is found to be -0.045 (with $\epsilon = 10^{-6}$, see Appendix (F) for definition of ϵ). The computed δt_f is in good agreeement with the "exact" value. Error between these values of δt_f is mainly due to the computational error incurred in the backward integration of equation (12) and also due to the early termination of the iterative procedure at $\epsilon = 10^{-6}$.

The solutions to the perturbed problem obtained by using the neighboring optimal feedback law and those obtained directly by using the SGR tecnnique are plotted together in Figure (3.4.10). These plots shown excellent agreement between results obtained from the two approaches.

(2) Perturbed terminal conditions

The perturbations of the terminal conditions are $\delta\bar{\psi} = (0.05\,,\,-0.05)^T$. The neighboring optimal feedback law is once again used to compute the revised optimal control program. By using the SGR technique, the end-times of the nominal and perturbed problems are found to be 0.728 and 0.700 respectively. Therefore the value of δt_f is given by

$$\delta t_f = 0.700 - 0.728 = -0.028\,.$$

Once again the iterative procedure of Appendix (F) is used to estimate the change in the end-time δt_f and the value computed is -0.0278 (with $\epsilon = 10^{-6}$). This value agrees well with the "true" value of -0.028.

Since Λ_1, Λ_2 and Λ_3 approach infinity near the end-time, we adopt the strategy that whenever $\delta\bar{u}(\tau)$ is larger than a pre-determined amount, the neighboring op-

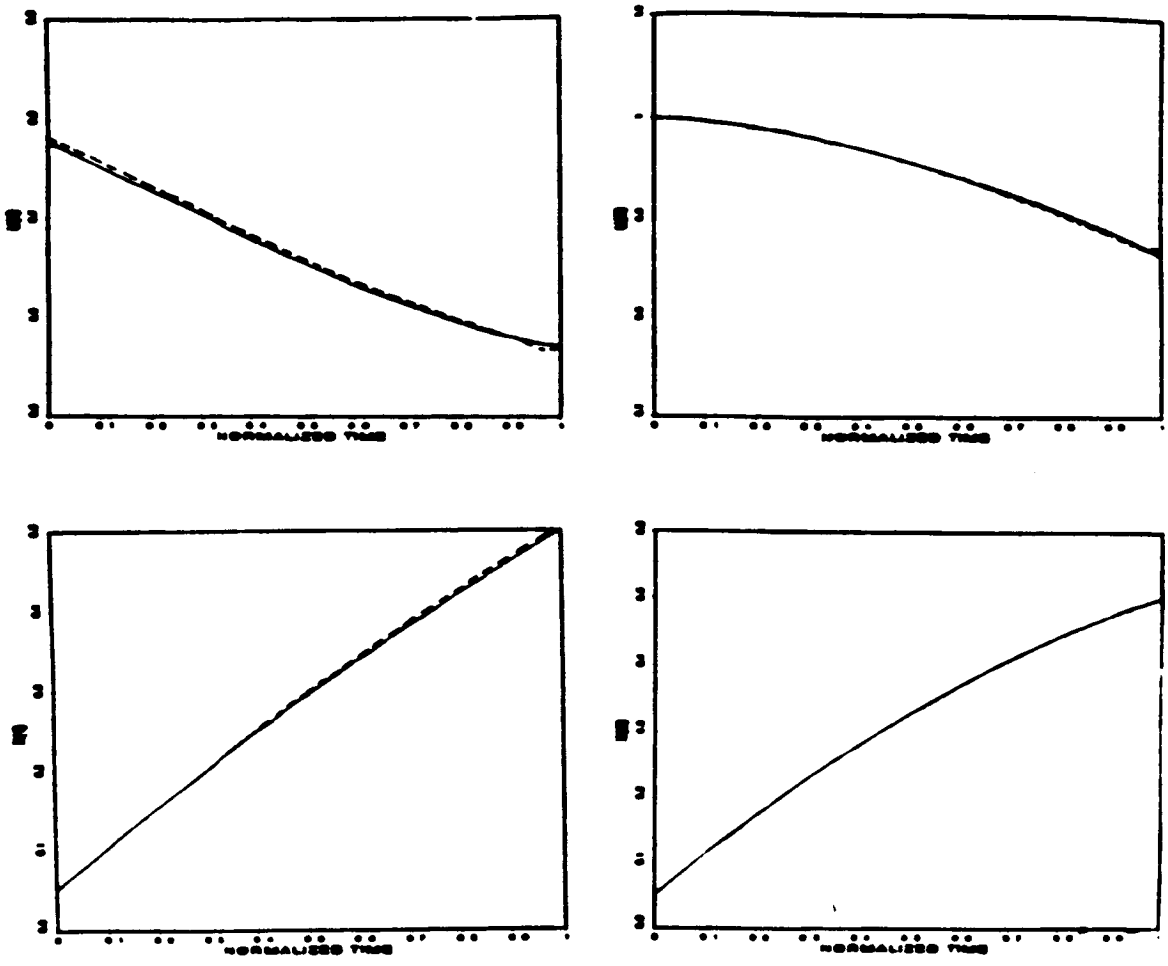

——— : Direct Optimization Technique with revised end-conditions

- - - - - - - - : Predictions of Neighboring Optimal Feedback Laws

δt_f (Direct) = -0.047

δt_f (Predicted) = -0.045

Figure 3.4.10 Comparison of Exact Results with those from Feedback Law in Example (2)

timal feedback law should be turned "off". Figure (3.4.11) shows the time history of $\bar{x}(\tau)$ and $\bar{u}(\tau)$ of the nominal control problem and those of the perturbed problem as predicted by the neighboring optimal feedback law. The usefulness of the neighboring optimal feedback law can once again be confirmed by comparison of the results obtained by these different approaches. Such a comparison is given in Figure (3.4.12).

Other than the time history of $u_1(\tau)$, the results given in Figure (3.4.12) show good overall agreement with the "exact" results. The prediction for $\delta u_1(\tau)$ is very good initially but deteriorates as the end-time is near. This error near the end-time is quite common among neighboring extremal problems with revised terminal conditions. In the present case, the difficulty is compounded by the the fact that δt_f has been "inaccurately" determined (δt_f(estimated) $= -0.0278$ as compare with -0.0280). This small error (-0.0002) in the determination of δt_f is being amplified by the magnitude of $\Lambda_3(u_1\ component)$ which becomes very large as the end-time is approached. Therefore the neighboring optimal feedback law over-estimates the value of u_1 by a substantial amount near the end-time. Since $\Lambda_3(u_2\ component)$ is identically zero, the estimation of u_2 is not being affected by this error in δt_f.

(3) Problem with perturbed initial and terminal conditions

Here the initial conditions are perturbed by $\delta\bar{x}(0) = (-0.03, 0.03)^T$ while the terminal conditions are perturbed by $\delta\bar{\psi} = (0.03\,,\, -0.03)^T$. The neighboring optimal feedback law is used to obtain the optimal program for the perturbed problem. Using the SGR tecnhique, the end-times of the nominal and perturbed problems are found to be 0.728 and 0.650 respectively. Therefore the value of δt_f is given by

$$\delta t_f = 0.650 - 0.728 = -0.078\,.$$

Using the iterative procedure of Appendix (F), the change in the end-times of

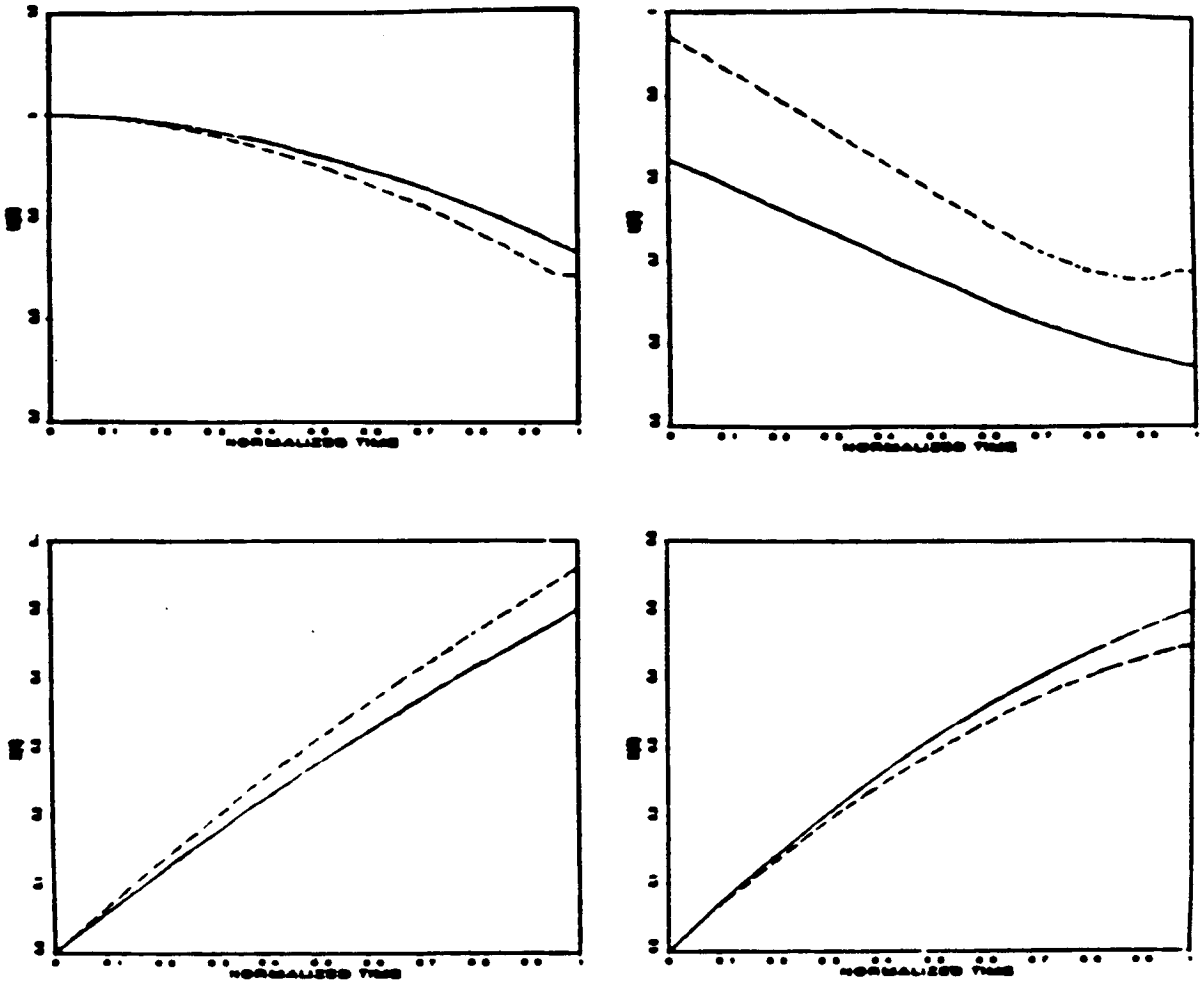

——— : Nominal Path

- - - - - - - - : Predictions of Neighboring Optimal Feedback Laws

Figure 3.4.11 Nominal and Perturbed (terminal condition) Results in Example (2)

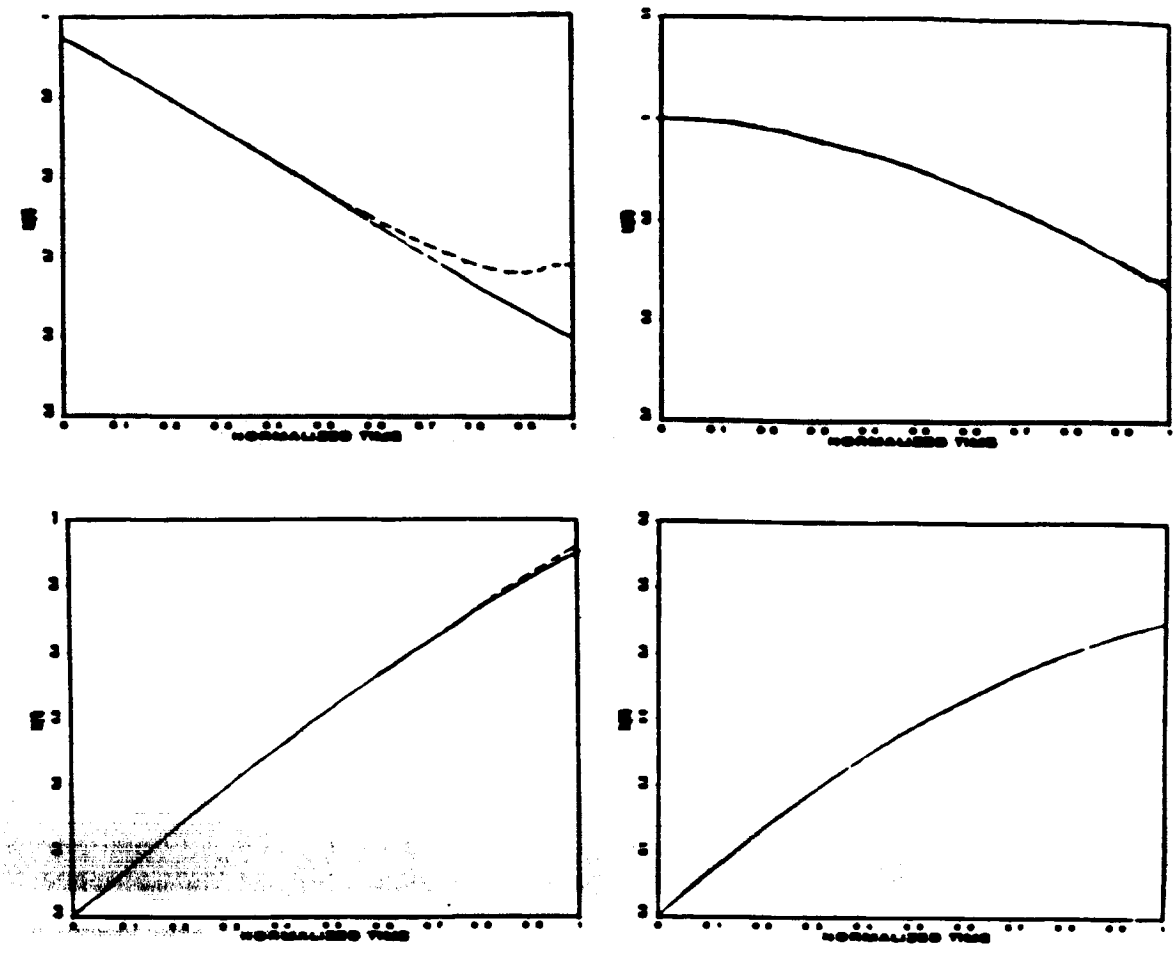

——— : Direct Optimization Technique with revised end-conditions

- - - - - - - - : Predictions of Neighboring Optimal Feedback Laws

δt_f (Direct) = -0.0280

δt_f (Predicted) = -0.0278

Figure 3.4.12 Comparison of Exact Results with those from Feedback Law in Example (2)

the nominal and perturbed problems is computed to be -0.077 (with $\epsilon = 10^{-6}$). The estimation of δt_f is once again good. Figure (3.4.13) shows the time history for both the nominal control problem and the solution to the perturbed problem obtained using the neighboring optimal feedback law. Figure (3.4.14) shows the results obtained for the perturbed problem using either the neighboring optimal feedback law or the SGR technique. The overall agreement between these results is good. The cause of the discrepancy found in the time history of $u_1(\tau)$ was given before.

3.4.4 Conclusions

Neighboring extremal paths for dynamic optimization problems with path equality constraints and unknown parameter vector were considered in this section. With certain simplifications, the problem can be reduced to one of solving a linear TPBVP with integral path equality constraints. The solution technique employed is an extension of the backward sweep method given in Bryson and Ho (cf. reference [29]).

Two example problems are solved using a numerical algorithm called SECOND. Excellent agreement with the "exact" results can be obtained for problems with small changes in the initial conditions. For cases with changes in the terminal conditions, the agreement deteriorates when the end-time is approached. This problem near the end-time is compounded by the multiplication of the small error involved in the determination of $\delta\bar{\pi}$ and the large feedback gain (Λ_π) near the end-time. One probable way of overcoming this problem is to switch from problems with hard terminal constraints into problems with only soft constraints as the end-time is near. This idea has not been investigated in depth and is recommended for future research.

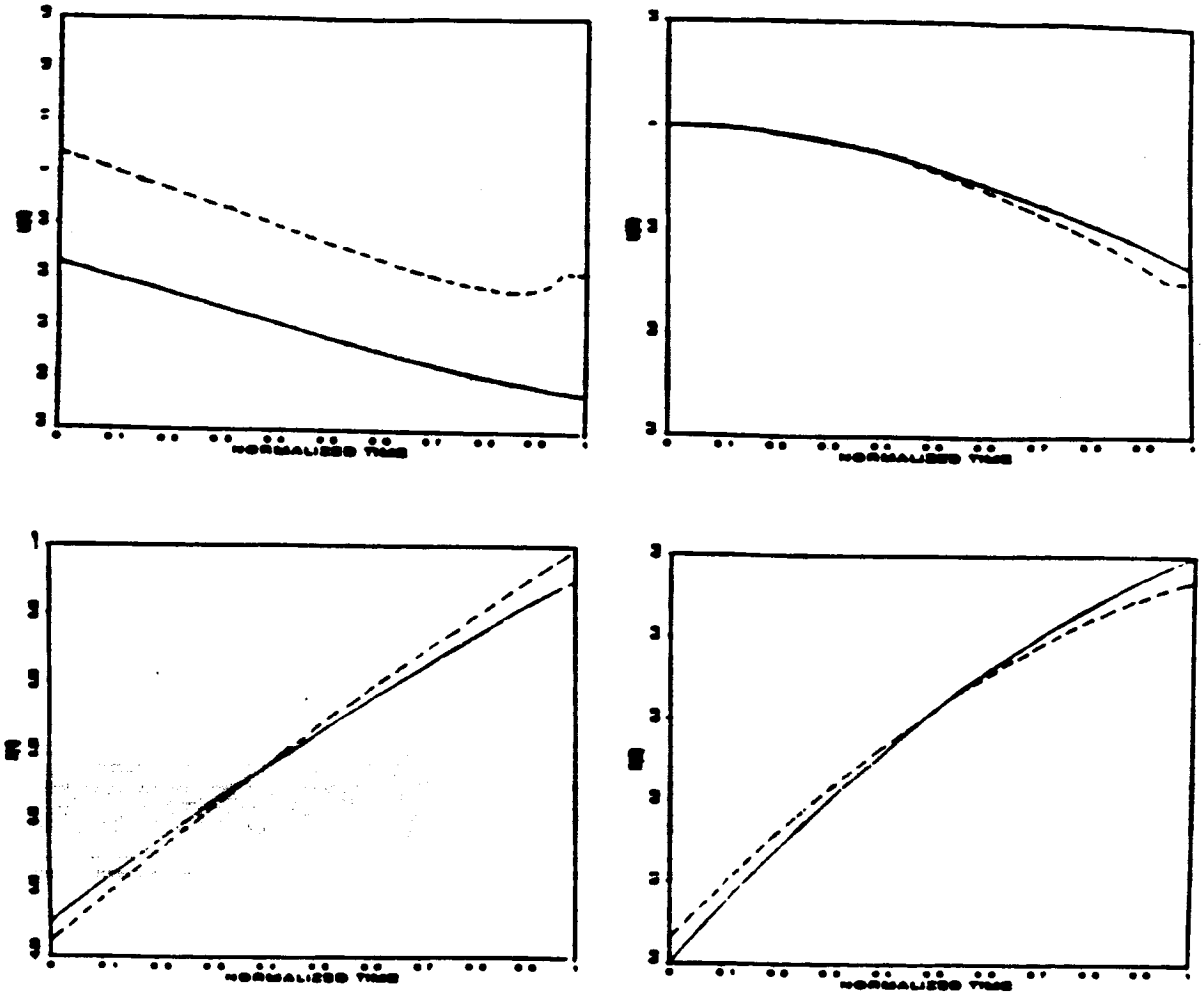

——— : Nominal Path

- - - - - - - - : Predictions of Neighboring Optimal Feedback Laws

Figure 3.4.13 Nominal and Perturbed (initial and terminal conditions) Results in Example (2)

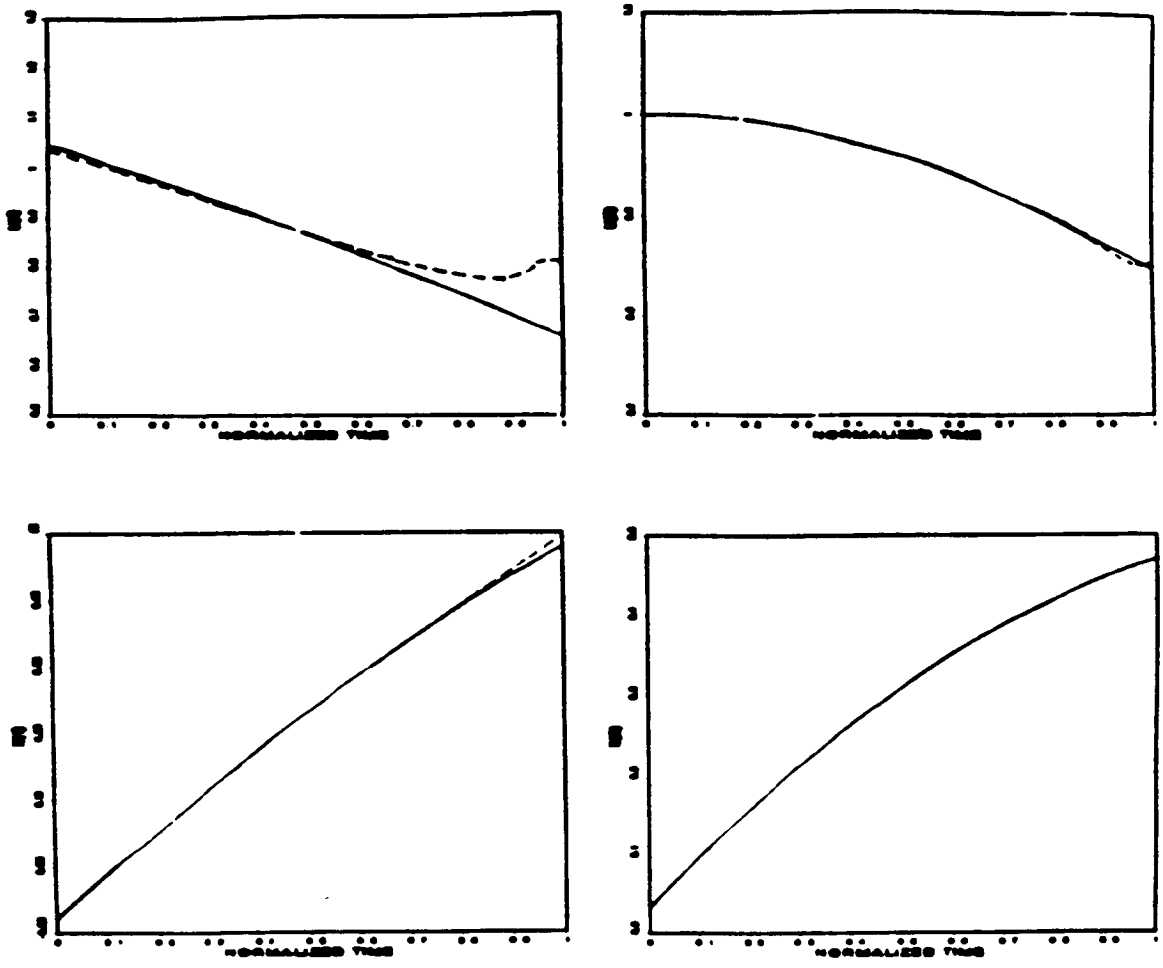

——— : Direct Optimization Technique with revised end-conditions

- - - - - - - - : Predictions of Neighboring Optimal Feedback Laws

δt_f (Direct) = -0.077

δt_f (Predicted) = -0.076

Figure 3.4.14 Comparison of Exact Results with those from Feedback Law in Example (2)

Chapter 4

Optimal Solutions and their Interpretations

In this chapter, optimal solutions are obtained for the the helicopter autorotation problem without and with the descent velocity bound (cf. Sections (2.9) and (3.3)) using the algorithm developed in Chapter 3.

We begin with a description of an OH-58A helicopter modified with a High Energy Rotor System (HERS). An autorotation flight test program [12] was conducted by the Bell Helicopter Company using this helicopter in 1976/77. The data from this program are suitable for comparison with analytical results of this research. Sections (4.2) and (4.3) describe the energy management considerations during autorotation, and the piloting techniques that were employed during the autorotation maneuver. These techniques are compared with those associated with the optimal control schemes.

Optimal solutions obtained for autorotation landings from hover, from forward flight, and from forward flight with a descent velocity bound are given in Sections (4.4), (4.5), and (4.6) respectively. These results are presented using plots of the time histories of the thrust coefficient, collective pitch, and states of the helicopter. In each case, the optimal results are interpreted physically and the ad-

vantages and disadvantages of the optimal control scheme are discussed. We end with some general comments on the effectiveness of the algorithms used in solving dynamic optimization problems with path inequality constraints.

§4.1 Description of Test Vehicle

The helicopter model used in our study of autorotative landings is a point-mass model of a modified OH-58A, shown in Figure (4.1.1). This helicopter was equipped with an experimental High Energy Rotor System (HERS), and was constructed by the Bell Helicopter Textron Company (BHT) as a concept demonstrator. The inertia of the rotor system was increased by the addition of tip weights in the spar cavity of the blades (hence the name "High Energy Rotor"). Flight evaluations [12] indicated that the high energy rotor could eliminate the usual height-velocity (H-V) restriction, and that the rotor kinetic energy could be used to provide transient power for better maneuverability. This model is used in our study because flight test data of the helicopter in autorotation are available in references [11], [12] and [57].

The HERS consists of a two-bladed rotor with a diameter of 35.3 feet which operates at 354 rpm. The rotor blades have 16 inch chords and were designed so that the rotational inertia of the rotor system could be varied from the standard OH-58A inertia to over twice this value. Four external steel doublers were added to carry the increased centrifugal force. Lock numbers, γ, of 5.43, 3.19, and 2.61, which correspond to blade inertias I_b of 323, 550, and 672 $slug\text{-}ft^2$ respectively, were used in flight tests. The Lock number, γ, of the rotor is defined as

$$\gamma = \frac{\rho a c R^4}{I_b}, \tag{1}$$

which is a measure of the ratio of aerodynamic and inertia forces on the blade.

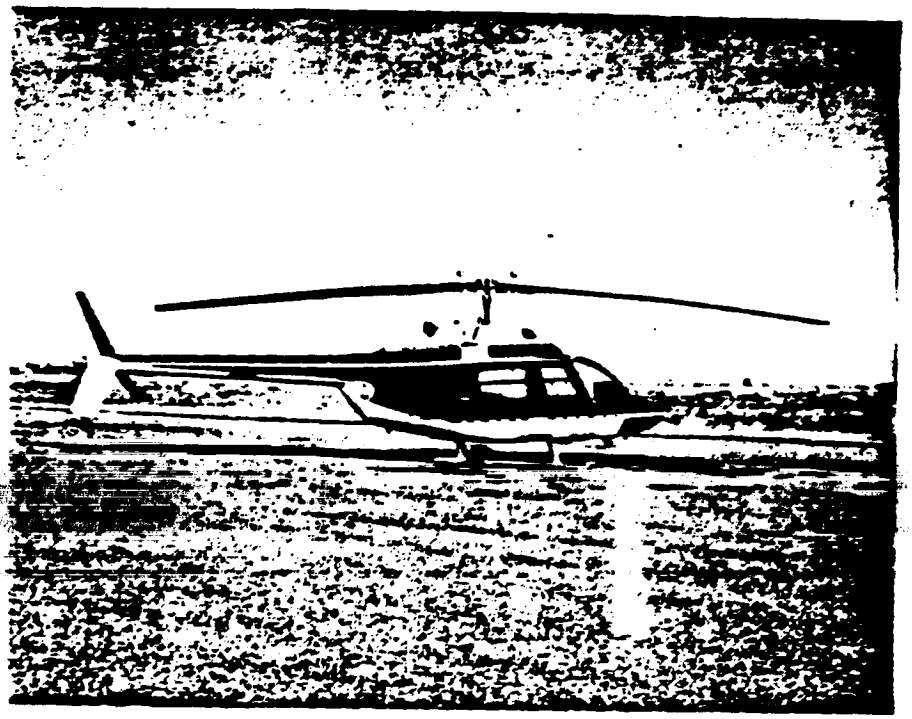

Figure 4.1.1 Experimental High Energy Rotor System (HERS)

Here

$$\begin{aligned} \rho &= \text{density of air (slug/ft}^3\text{)}, \\ a &= \text{lift curve slope of rotor airfoil (rad}^{-1}\text{)}, \\ c &= \text{chord of blades (ft)}, \\ R &= \text{rotor radius (ft)}, \\ I_b &= \text{rotational inertia of one blade and hub (slug ft}^2\text{)}. \end{aligned} \tag{2}$$

Another quantity, the rotor solidity σ, is of importance to the autorotational performance of helicopter. The rotor solidity is defined as the ratio of the total blade area (NcR for constant chord blades) to the total disk area (πR^2). Therefore, the rotor solidity is given by the following expression:

$$\sigma = \frac{Nc}{\pi R}, \tag{3}$$

where N is the total number of blades per rotor. The solidity of the HERS rotor is 0.048.

A detailed description of the helicopter is given in reference [56]. Table (4.4.1) gives the values of the model parameters used in the point-mass model of this vehicle that was developed in Chapter 2.

4.1.1 Height-Velocity Restriction Curves

Most helicopters have a region of operation from which a safe autorotational landing cannot be executed. This area of limited autorotational capability exists for both single and multiple engine helicopters and is described by the altitude above the ground and the airspeed. It is commonly illustrated with a height-velocity restriction diagram (sometimes refered to as a deadman's curve). The height velocity restriction curves for the standard OH-58A helicopter, as determined by flight tests and reported in reference [57], are given in Figure (4.1.2). The two restriction regions indicated in Figure (4.1.2) are typical for conventional helicopters. The low

S/NO.	SYSTEM PARAMETER	VALUE USED
1	f_e, equivalent flat plate area (ft^2)	24.0
2	g, acceleration due to gravity (ft/sec^2)	32.17
3	ρ, air density ($slug/ft^3$)	0.002378
4	m, mass of helicopter (slug) (lb.wt.)	93.16 (3000.0)
5	σ, rotor solidity	0.048
6	K , induced velocity correction factor	1.13
7	a, $\frac{\partial}{\partial\alpha}(C_\ell)$	5.73
8	R, radius of main rotor (ft)	17.63
9	ω, nominal rotor speed (rpm)	354.0
10	δ_e, profile drag coefficient (NACA 0012 airfoil assumed)	0.0087
11	γ, rotor system Lock number	2.6

Table 4.1.1 System Parameters Used in Optimal Control Study

speed region is usually described by three points: the high hover point, the low hover point, and the knee or the highest speed point. The low speed region of the H-V restriction curve indicates that autorotation from hovering is the most critical case.

In the restricted high speed region there is insufficient clearance between the tail of the helicopter and the ground to allow flare to decelerate and control rotor RPM prior to ground contact. Since we model the helicopter as a point mass, we cannot study the high speed region. The restricted low speed region is of primary interest in this work.

The restricted regions of the H-V diagram are traditionally determined by flight test. Using a build-up technique, the pilot performs a series of simulated engine failures starting at entry conditions expected to be well outside the restriction regions. Subsequent entries are made at more critical conditions until the pilot feels a safe landing could not be performed from conditions more critical than the last. These tests are performed to establish limits at enough altitude and airspeed combinations to allow construction of the H-V diagram. A pilot reaction time of two seconds following engine failure is usually employed, along with landing at groundspeeds of 15 Knots or less.

Another important factor affecting the H-V restriction is the effect of wind. The published restriction areas are shown for zero wind conditions. The presence of a headwind when performing an autorotational landing will significantly reduce the difficulty of the task. Optimal descents of a helicopter from power loss in hover, as well as those with initial forward speed, are given in subsequent sections of this chapter for cases with negligible wind effect.

Another factor that affects the restriction region is the technique used to perform the

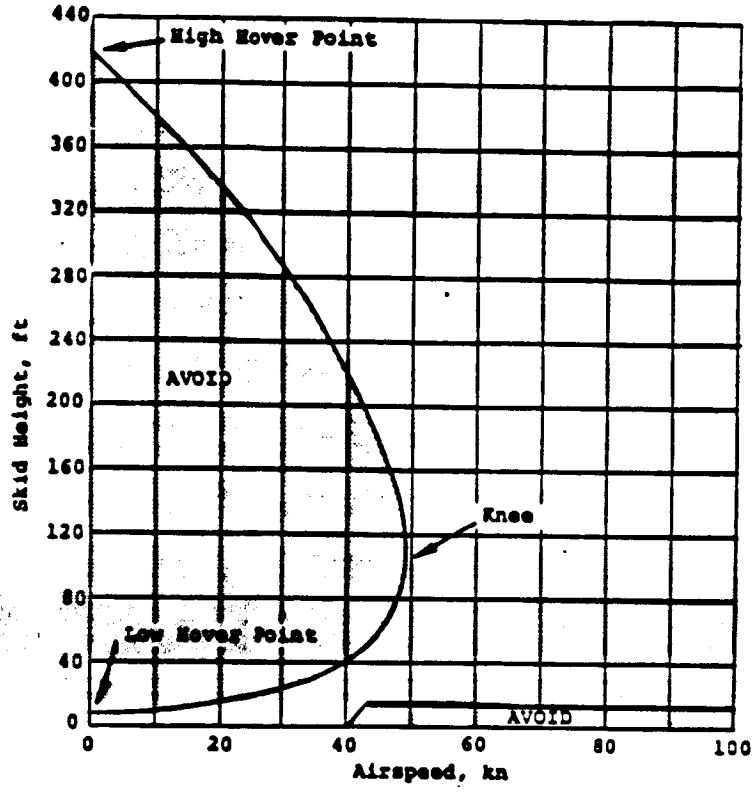

Figure 4.1.2 OH-58A Maximum Performance Height-Velocity Restriction Curves

landings. For the tests reported in reference [12], the pilot's primary objective was to attain zero rate-of-sink and a safe horizontal speed at touchdown. The technique was to level the helicopter 1 or 2 feet off the ground with no rate-of-descent and then gradually sink to the ground as RPM continued to decrease. During this phase of the maneuver, small amounts of aft cyclic were applied to reduce the horizontal velocity. This technique yielded consistent zero rate-of-descent touchdowns while the horizontal velocity varied somewhat.

§4.2 Energy considerations

Consideration of the helicopter energy state aids in understanding the pilot techniques required during an autorotational landing, and also the optimal control solutions given in subsequent sections. After an engine failure, the helicopter has three sources of energy: (1) the potential energy of altitude, mgH, (2) the kinetic energy of the flight path velocity, $\frac{1}{2}mV^2$, and (3) the rotational energy of the main rotor $\frac{1}{2}I_R\Omega_t{}^2$. Here we have neglected the small contribution of the tail rotor. Therefore the total energy (TE) of the helicopter after engine failure is approximately given by

$$\begin{aligned} \text{TE} &= \text{PE} + \text{KE} + \text{RE}, \\ &= mgH + \frac{1}{2}mV^2 + \frac{1}{2}I_R\Omega_t{}^2 . \end{aligned} \tag{1}$$

Not all the energy given in the above equation is available to the pilot. While it is true that we can make "complete" use of the potential and kinetic energy, the amount of rotational energy available to the pilot executing an autorotational landing is limited. This is due to the fact that the rotor must at all times maintain an angular speed above some minimum value Ω_{min}. Any drop in rotor speed causes an increase in the angle of attack on the rotor's blades. If not checked, this increase

in the angle of attack will ultimately lead to stall (first on the retreating blades) of the rotor and the instability associated with it. The minimum rotor speed Ω_{min} defines a bound on the maximum usable rotor energy. The maximum amount of energy available to the pilot after engine failure is thus given by

$$\text{Maximum Usable Energy} = mgH + \frac{1}{2}mV^2 + \frac{1}{2}I_R(\Omega_i^2 - \Omega_{min}^2)\,. \tag{2}$$

The importance of the various energy terms in equation (2) varies with both the (H,V) combination at the time of engine failure and the physical configuration of the vehicle as represented by the parameters m and I_R. For example, the importance of the potential energy term increases with the altitude H at which power failure occurs. Similarly, the rotational energy term becomes more important either when the rotational inertia of the rotor system is increased (such as in the HERS case) or when the altitude and airspeed at the time of failure decrease. For a given helicopter model (i.e. (m, I_R) = fixed), one can expect the use of different pilot techniques with different (H,V) entry conditions. Similarly, under the same entry condition, pilots will use somewhat different autorotational landing techniques with different helicopter models having different (m, I_R) values.

The time rate of change of the total energy of the helicopter in a typical flight situation is given by equation (25) of Section (2.3):

$$\frac{d}{dt}\left(mgH + \frac{1}{2}mV^2 + \frac{1}{2}I_R\Omega^2\right) = P_S - (P_i + P_{pro} + P_{para})\,. \tag{3}$$

where

$$\begin{aligned} P_S &= \text{power supplied to rotor shaft}\,, \\ P_i &= \text{induced power loss}\,, \\ P_{pro} &= \text{profile power loss}\,, \\ P_{para} &= \text{parasite power loss}\,, \end{aligned} \tag{4}$$

where the various power terms are defined in Section (2.3).

Equation (3) expresses the energy conservation principle according to which any excess power supplied by the engines that is not dissipated by the helicopter is stored as internal potential, kinetic or rotational energy.

In the event of engine failure (i.e. $P_S = 0$), the total power or energy will decrease at a rate which depends on the helicopter configuration as defined by airspeed, main rotor thrust, angle of attack and rotor RPM. The pilot's task when entering power-off autorotative flight is mainly one of "Energy Management". He has to control the energy losses such that the total amount of energy used from the time of engine failure to the final touchdown does not exceed the maximum usable energy (MUE) of equation (2). This can be achieved through control of the thrust vector during descent in order to land the aircraft at the correct level attitude with small vertical and forward speeds. At the same time, during the deceleration phase, the pilot must prevent the main rotor from overspeeding which would lead to unacceptable blade centrifugal stresses. This task requires considerable pilot skill.

§4.3 Autorotation Landing Techniques used by Pilots

For the standard OH-58A helicopter, the autorotation technique depends on the flight condition before engine failure. At low altitude and airspeed, below the knee of the curve, the pilot technique required for a safe landing is to use increased collective to reduce the sink rate as the helicopter approaches 10 to 15 feet above the ground. At about 10 feet above the ground, the fuselage is leveled and collective is increased as the helicopter settles. At higher airspeeds (still below the airspeed at the knee) the collective may be reduced somewhat to regain or maintain rotor RPM while the helicopter is decelerated using a cyclic flare. In these conditions, the rotor does not enter into a true condition of "autorotation".

For higher altitude entries (above the altitude at the knee of the curve), the collective is reduced and the cyclic moved forward to pitch the nose down in order to gain some forward airspeed. The objective is to increase airspeed to that required to build rotor speed during a decelerating flare, usually close to the speed defined by the knee of the curve. An additional objective of attaining a higher airspeed is to establish an operating point at the airspeed corresponding to minimum drag. thereby maximizing the amount of time the pilot has to select and maneuver to a desired landing area. As the speed increases, altitude rapidly decreases until the pilot initiates a flare. The purpose of this flare is to first reduce the rate of sink, second, to reduce the forward airspeed before touchdown; and third, to maintain or increase rotor RPM. As the helicopter slows down, forward cyclic is applied to level the fuselage at the proper landing attitude and, simultaneously, the collective is raised to cushion the landing. The techniques described above are taught to Army pilots and are described in the OH-58A Flight Manual [59].

From an energy point of view, the maneuver of the helicopter, from pilot recognition of engine failure to touchdown, can be divided into three phases; entry, descent, and flare. The entry phase consists primarily of arresting the RPM decay of the main rotor by lowering the collective pitch angle. This reduces the induced power loss P_i and established an angle of attack distribution along the blade that results in aerodynamic autorotative forces that maintain RPM within the desired range. This is especially critical for entry conditions with large induced power loss such as when the helicopter is in hover. However, if in hover very near the ground, the collective can not be lowered and the rotor RPM will decay immediately. Under these conditions, there will not be a steady-state descent phase, and the pilot must rely on judicious timing to extract the last available rotor energy to arrest the sink rate as ground impact approaches.

During the steady-state descent phase, air flows upward through the rotor disk. The increase in angle of attack on the rotor blades offsets the drop in the collective pitch angle. Total aerodynamic force is increased and inclined forward to establish equilibrium. The maneuver in this phase typically consists of a longitudinal cyclic "push over" to a nose down attitude, followed by acceleration to a desired steady descent speed (usually from 50 to 75 knots depending on the helicopter and its gross weight). Given enough altitude, steady-state autorotation at this speed can be established. Angle of descent is normally 17 to 20 degrees from the horizontal (compare to 2 or 3 degrees used in powered descent). The center of attention of the pilot in the steady state phase is on maintaining the equilibrium flight through uses of the collective and cyclic pitch. In the steady descent phase, some of the potential energy of the vehicle has been converted into kinetic energy of the helicopter fuselage. In effect, the pilot gives up altitude at a controlled rate in return for energy to maintain the rotor at a constant RPM.

During the flare phase, the pilot must reduce airspeed and sink rate just before touchdown. Both of these actions can be accomplished by moving the cyclic control to the rear. The rearward oriented rotor disk (or TPP) allows a larger volume of air to flow through it, resulting in an increase in the total lifting force. The larger, rearward pointing thrust will reduce both the airspeed and sink rate. At the same time, an in-plane force component is created which causes the rotor to accelerate so that some of the lost RPM can be regained. In this phase, kinetic energy of the vehicle is converted into rotor energy which, in turn, is used to generate lift. During the flare, collective control application may be necessary to prevent rotor overspeed or to slow the vertical descent rate even further. Finally, the collective is raised to convert the stored rotor energy into lift which further cushions the landing. The center of attention of the pilot in the touchdown phase is split between the raising

of the collective to cushion the landing and the leveling of the fuselage. The latter is performed to avoid striking the tail rotor just prior to touchdown.

The approximate variations of the various energy terms in the entry, steady descent, and deceleration/touchdown phases are illustrated in Figure (4.3.3).

§4.4 Optimal landing of a Helicopter Initially in Hover

The optimal descent of a helicopter after power loss in hover was considered by Johnson [15]. Instead of having a hard bound on the thrust coefficient C_T, Johnson chose to reflect this limitation on the thrust coefficient in another way. The profile power loss of the rotor was modified to include a "penalty" term which increases sharply as the loading is raised above the stall limit:

$$c_{pro} = \frac{1}{8}\sigma\bar{c}_d\left[1 + \left(\frac{6C_T}{\sigma}\right)^2 + \left(\frac{\frac{C_T}{\sigma}}{\left(\frac{C_T}{\sigma}\right)_{stall}}\right)^{N_s}\right](1 + 4.6\mu^2) \qquad (4)$$

where $\left(\frac{C_T}{\sigma}\right)_{stall}$ is the rotor stall limit and N_s is an arbitarily selected large number (e.g. $N_s = 20$).

The last term in the square bracket of (4) is the "penalty" term. Its function is to increase the profile power loss manyfold when the loading is above the stall limit. Its contribution to the profile power loss is insignificant when the rotor operates below the stall limit.

The main advantage of Johnson's approach is that it avoids the use of path equality constraints from the constrained optimization problem of Section (2.9). As a result, an ordinary gradient-type, steepest descent algorithm can be used to solve the

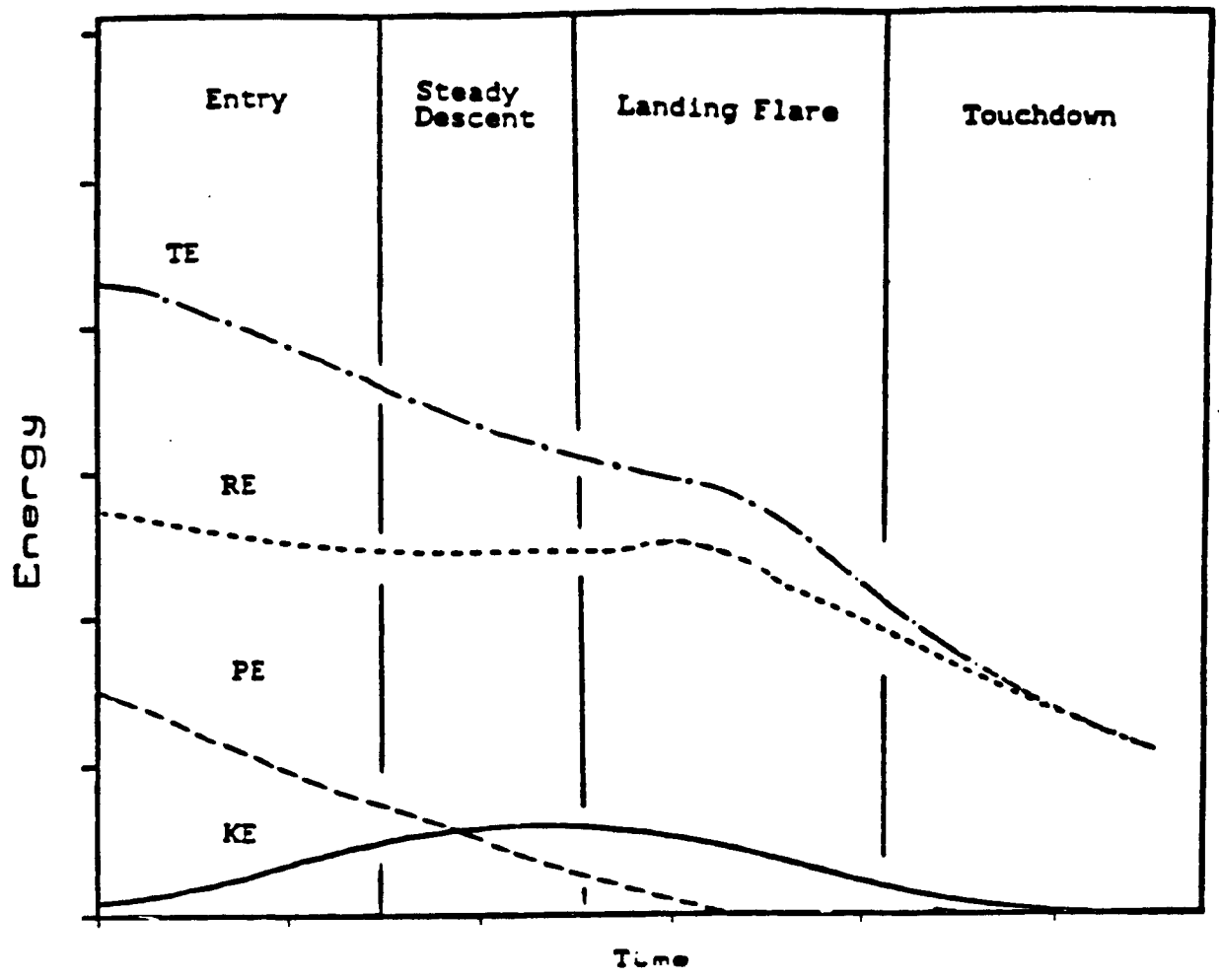

TE : Total Energy of the Helicopter

PE : Potential Energy of the Helicopter

KE : Kinetic Energy of the Helicopter

RE : Rotational Energy of the Helicopter's Rotor

Figure 4.3.3 Variations of Energy Terms in Phases of an Autorotational Landing of a Helicopter

resultant TPBVP. The disadvantage of the penalty function approach is that the $(\frac{C_T}{\sigma})_{\text{stall}}$ limit is usually exceeded (by as much as 13 percent) over the last 20 percent of the trajectory as "ground contact" is approached [15].

4.4.1 A Pure Vertical Descent Path

This section establishes the fact that a pure vertical flight path from power failure in hover satisfies the first order necessary conditions. (However, the possible existence of a non-vertical flight path with high entry height is suggested by Figure (4.5.27) of Section (4.5).) We define a Hamiltonian function H based upon the problem formulation of Section (2.9).

$$\begin{aligned}\frac{1}{\tau_f}H = {} & \lambda_1[g_0 - m_0 u_1 x_3^2 - m_0 \bar{f} x_1 \sqrt{x_1{}^2 + x_2{}^2}] \\ & + \lambda_2[m_0 u_2 x_3^2 - m_0 \bar{f} x_2 \sqrt{x_1{}^2 + x_2{}^2}] \\ & + \lambda_3[-i_0 x_3^2 (c_0 + \bar{\lambda}\sqrt{u_1{}^2 + u_2{}^2})] + \lambda_4[0.1 x_1]\end{aligned} \tag{5}$$

Since neither the Hamiltonian function nor the terminal payoff ϕ are functions of x_4 (vertical height), we can easily establish the fact that λ_4 is a constant (this is not true if ground effect has been included in the formulation; in which case H will be a function of height). Knowing this, the Hamiltonian function defined in equation (5) can be simplified to

$$\begin{aligned}\frac{1}{\tau_f}H = {} & \lambda_1[g_0 - m_0 u_1 x_3^2 - m_0 \bar{f} x_1 \sqrt{x_1{}^2 + x_2{}^2}] \\ & + \lambda_2[m_0 u_2 x_3^2 - m_0 \bar{f} x_2 \sqrt{x_1{}^2 + x_2{}^2}] \\ & + \lambda_3[-i_0 x_3^2 (c_0 + \sqrt{u_1{}^2 + u_2{}^2}\bar{\lambda})] + \lambda_4[0.1 x_1]\,.\end{aligned} \tag{6}$$

The optimal controls u_1 and u_2 are obtained from the optimality conditions of

$$H_{u_1} = 0, \qquad H_{u_2} = 0. \tag{7}$$

Using equation (6), these optimality conditions become:

$$\begin{aligned}\lambda_1 m_0 x_3^2 - i_0 \lambda_3 x_3^2 \left[\frac{u_1}{\sqrt{u_1^2 + u_2^2}} \bar{\lambda} + \bar{\lambda}_{u_1} \sqrt{u_1^2 + u_2^2}\right] = 0\,,\\ \lambda_2 m_0 x_3^2 + i_0 \lambda_3 x_3^2 \left[\frac{u_2}{\sqrt{u_1^2 + u_2^2}} \bar{\lambda} + \bar{\lambda}_{u_2} \sqrt{u_1^2 + u_2^2}\right] = 0\,.\end{aligned} \tag{8}$$

From the Euler-Lagrange equations, the partial differential equation of λ_2 is given by

$$\begin{aligned}\lambda_2^{\nabla} &= -H_{x_2}\,,\\ -\frac{1}{\tau_f}\lambda_2^{\nabla} &= -\lambda_1 m_0 \bar{f}\left(\frac{x_1 x_2}{\sqrt{x_1^2 - x_2^2}}\right) - \lambda_2 m_0 \bar{f}\left[\sqrt{x_1^2 - x_2^2} - \frac{x_2^2}{\sqrt{x_1^2 + x_2^2}}\right]\\ &\quad - \lambda_3 i_0 x_3^2 \left[\bar{\lambda}_{x_2} \sqrt{u_1^2 + u_2^2}\right].\end{aligned} \tag{9}$$

Using the optimality condition of (7), and the Euler-Lagrange equations, the optimal controls u_1 and u_2 can be solved for simultaneously with the Lagrange multipliers λ_i where i = 1,...,3. The analytical solution of the problem cannot be easily obtained. However, if we guess that the u_2 component (i.e. the horizontal component) of the optimal control $\bar{U}(\xi)$ is zero,

$$u_2 = 0\,, \tag{10}$$

we can proceed to show that the resultant solution of the Lagrange multiplier λ_2 satisfies the optimality condition of (8-2).

Substitution of (10) into the equation of motion of the normalized forward speed x_2 gives

$$x_2^{\nabla} = \tau_f m_0 \bar{f} x_2 \sqrt{x_1^2 + x_2^2}\,. \tag{11}$$

If we integrate this equation forward (in time ξ), using the initial condition of $x_2(0) = 0$ (i.e. hover condition), the result is

$$x_2(\xi) = 0\,, \quad \text{for} \quad 0 \le \xi \le 1\,. \tag{12}$$

Knowing that both $u_2(\xi)$ and $x_2(\xi)$ are zero, the inflow ratio $\bar{\lambda}$ defined by equation (43) of Section (2.4) can be simplified to

$$\bar{\lambda} = -0.01\frac{x_1}{x_3} + k_0 f_I \sqrt{u_1}\,, \tag{13}$$

which is neither a function of u_2 nor x_2. Also, depending on whether it lies within the vortex-ring state or the momentum theory state, the induced velocity parameter f_I is given by equation (14) of Section (2.3). Under assumptions (10) and (12), f_I is now only a function of $\bar{x}_1$, since $\bar{x}_2$ is identically zero:

$$\begin{aligned} \bar{x}_1 &= -\frac{p_0 x_1}{x_2\sqrt{u_1}}\,, \\ \bar{x}_2 &= 0\,. \end{aligned} \tag{14}$$

Using equation (14), we can easily prove that both $(f_I)_{u_2}$ and $(f_I)_{x_2}$ are zero. Therefore, we have from equation (13) that the inflow ratio $\bar{\lambda}$ is not a function of either u_2 or x_2:

$$\begin{aligned} \bar{\lambda}_{u_2}(\xi) &= 0\,, \\ \bar{\lambda}_{x_2}(\xi) &= 0\,. \end{aligned} \tag{15}$$

Making use of the fact that both $x_2(\xi)$ and $\bar{\lambda}_{x_2}(\xi)$ are identically zero in equation (9) gives the following homogeneous differential equation in λ_2:

$$\lambda_2^{\nabla} = [\tau_f m_0 \bar{f} x_1(\xi)]\lambda_2\,. \tag{16}$$

Since the terminal payoff ϕ is not a function of x_2 (because $x_2(\xi) = 0$ for $0 \le \xi \le 1$), the terminal value of λ_2 is zero. The solution of the homogeneous equation (16) is therefore

$$\lambda_2(\xi) = 0, \quad \text{for} \quad 0 \le \xi \le 1. \tag{17}$$

Finally, back substitution of equations (10), (15-1), and (17) into (8-2) establish the fact that $H_{u_2} = 0$. Therefore the original assumption of $u_2 = 0$ produces conditions

that satisfy the optimality condition of $H_{u_2} = 0$. Optimal descent of a helicopter after power loss in hover as formulated in this section is thus a pure vertical flight path. The same conclusion was reached by Johnson in [15].

In practice, a small amount of forward speed is usually required, both to avoid a vertical descent into the helicopter's own rotor wake, and also to keep the landing point in sight.

4.4.2 Interpretations of Optimal Control Results

Both flight tests and analysis indicate that an initial forward velocity greatly improves the autorotational characteristics of the helicopter. Therefore optimal control results are first given for the most critical case of descent from power loss in hover. This case was found in Section (4.4.1) to involve only a pure vertical descent. With this knowledge, we can eliminate the states x_2 (forward speed) and x_5 (horizontal distance), and the control u_2 (horizontal component of the thrust coefficient, C_{T_x}) from the problem formulated in Section (2.9). The simplified problem is given in Section (3.2) and consists of only three state variables (vertical sink rate, vertical height, and angular speed of rotor), and one control variable C_{T_z} $(= C_T)$.

The simplified problem was solved here using the Sequential Gradient Restoration Algorithm. The Lock number of the OH-58A helicopter considered is 2.61, which corresponds to the heaviest blade inertia of 672 $slug\text{-}ft^2$. The entry heights of the helicopter at the time of power loss, given in Figure (4.4.4), vary from 25 to 250 feet above ground level (AGL).

Figures (4.4.5) to (4.4.8) present in detail the optimal solution of power-off descent from hover from an initial altitude of $h_0 = 100$ feet (Case (3) in Figure (4.4.4)). The flight time for this case is 4.9 seconds. Figure (4.4.5) gives the collective pitch control and the thrust coefficient required as functions of time. Note that the initial

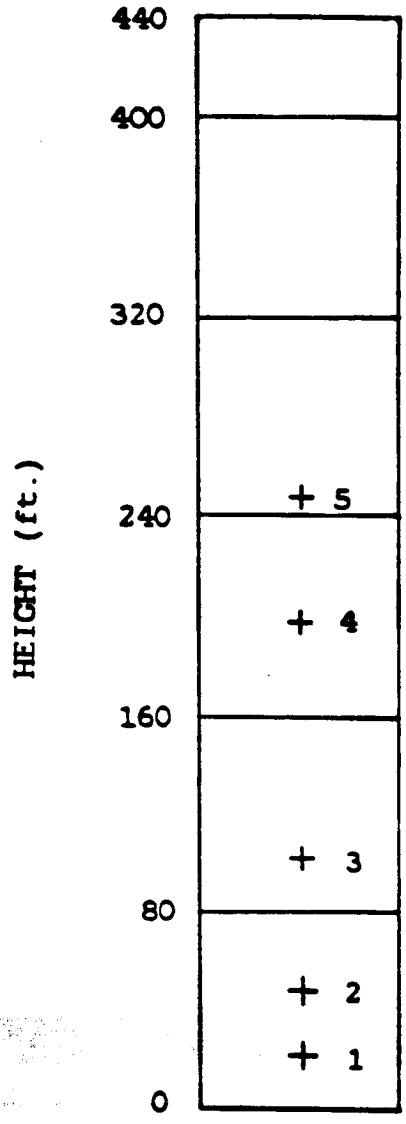

ENTRY CONDITION	1	2	3	4	5
ENTRY HEIGHT (ft.)	25	50	100	200	250

Figure 4.4.4 Entry Heights of a Helicopter with Power Loss in Hover

value of the thrust coefficient just before engine failure is given by

$$\begin{aligned} C_T &= \frac{T}{\rho\pi R^2(\Omega R)^2}\,, \\ &= \frac{W}{\rho\pi R^2(\Omega R)^2}\,, \\ &= \frac{3000}{0.002378\,\pi\,(17.65)^2\,(37\times 17.65)^2}\,, \\ &= 3.0226\times 10^{-3}\,. \end{aligned} \tag{18}$$

Therefore the initial values of $\frac{C_T}{\sigma}$, the inflow ratio λ, and the collective pitch angle (at 75 percent chord) θ_{75} are given by

$$\frac{C_T}{\sigma} = 0.063\,, \tag{19}$$

$$\begin{aligned} \lambda &= \sqrt{\frac{C_T}{2}} \\ &= 0.0389\,. \end{aligned} \tag{20}$$

$$\begin{aligned} \theta_{75} &= \frac{6C_T}{a\sigma} - \frac{3}{2}\lambda \\ &= 7.12 \quad \text{degrees}\,. \end{aligned} \tag{21}$$

The results given in Figure (4.4.5) agree generally with those from reference [12]. The initial drop in the collective is followed by a gradual increase for flare. In Figure (4.4.5), the collective flare begins at about one second after engine failure, when the helicopter is about 80 feet above the ground. Thereafter, the collective pitch starts to increase, and its rate of change reaches a maximum of 6 degrees per second when the helicopter is at about the mid-point (in time) of its travel. Because of the hard bound on the thrust coefficient at $(\frac{C_T}{\sigma})_{stall} = 0.15$, the increase in collective pitch (or the thrust coefficient) levels off towards the end when touchdown is imminent. The thrust coefficient is on the bound during the last one second of travel when the helicopter is at about 4 feet above ground level. The results also demonstrate

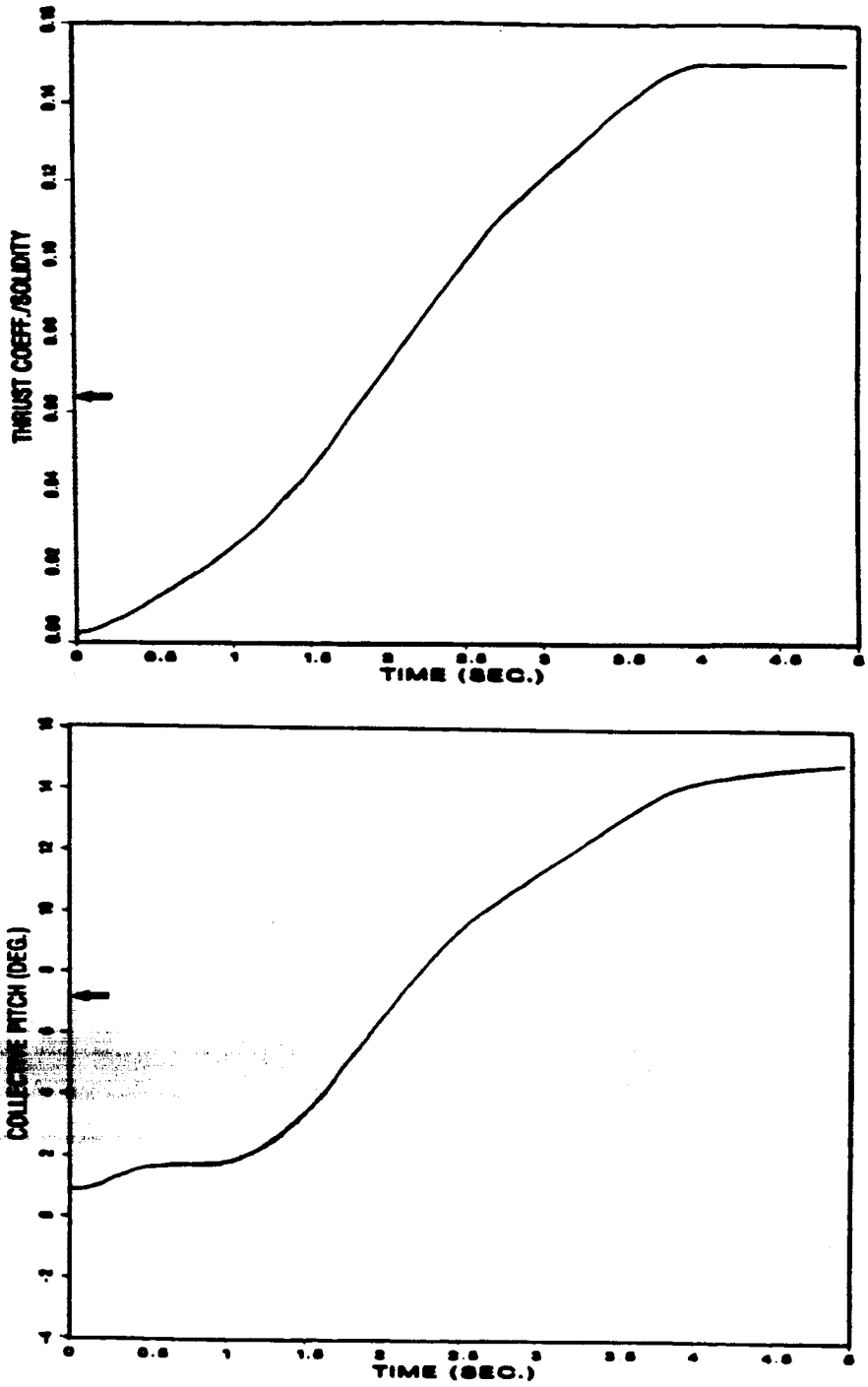

Figure 4.4.5 Optimal Time Variations of Thrust Coefficient and Collective Pitch Control, $h_0 = 100$ feet

the effectiveness of the numerical algorithm used in the enforcement of the path inequality constraint on the thrust coefficient.

Figures (4.4.6) and (4.4.7) show the variations of the vertical height, vertical sink rate, and the angular speed of the rotor as functions of flight time.

When the rotor starts to descend, the flows inside and outside the slipstream (created when the helicopter was in the hovering state) are in opposite directions. Therefore, from hover to any subsequent windmill brake state, the flow has to first go through the vortex-ring state. Figure (4.4.8) shows the variation of the induced velocity with the rate of descent in the various states of the rotor in vertical descent.

The normal hover state and the windmill brake state are well described using momentum theory because a definite slipstream exists in these states. By convention (see pp. 99 of reference [54]), the vortex-ring state is defined by $P = T(V - \nu) > 0$ (velocity terms are defined positive in the upward direction), so that the power extracted from the airstream is less than the induced power loss. The vortex-ring state is also characterized by large recirculation and high turbulence. The region with $P = T(V + \nu) < 0$ is called the turbulent wake state. Here, there is a net extraction of energy from the airstream. The rotor in this state experiences some roughness due to turbulence, but nothing like the high vibration in the vortex-ring state. Note that the empirical fairing in Figure (4.4.7) intersects the ideal autorotation line $V + \nu = 0$ at $V/\nu_h = 1.6$ (see also Figure (3.2.2)).

In the optimal descent of the helicopter, the rotor is operating in the windmill state when the vertical sink rate is increasing (except for a brief period immediately after engine failure). It then operates in the vortex-ring state when the velocity is decreasing. Maximum rate of descent is of the order of 2200 fpm and occurs when the helicopter is at about 50 feet above ground level. The touchdown sink rate is

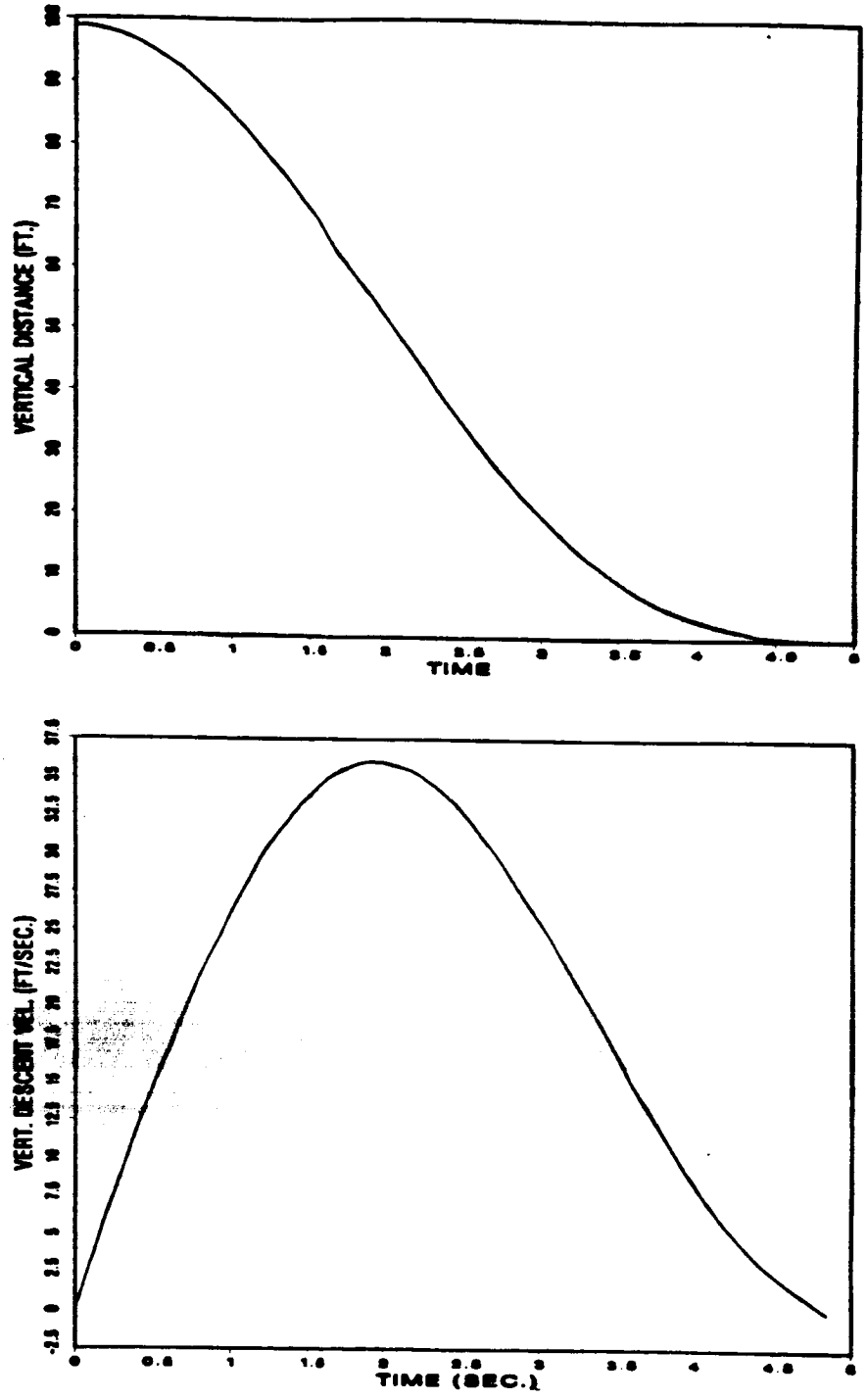

Figure 4.4.6 Optimal Time Variations of Vertical Height and Vertical Sink Rate [Case (3),h_0 = 100 feet]

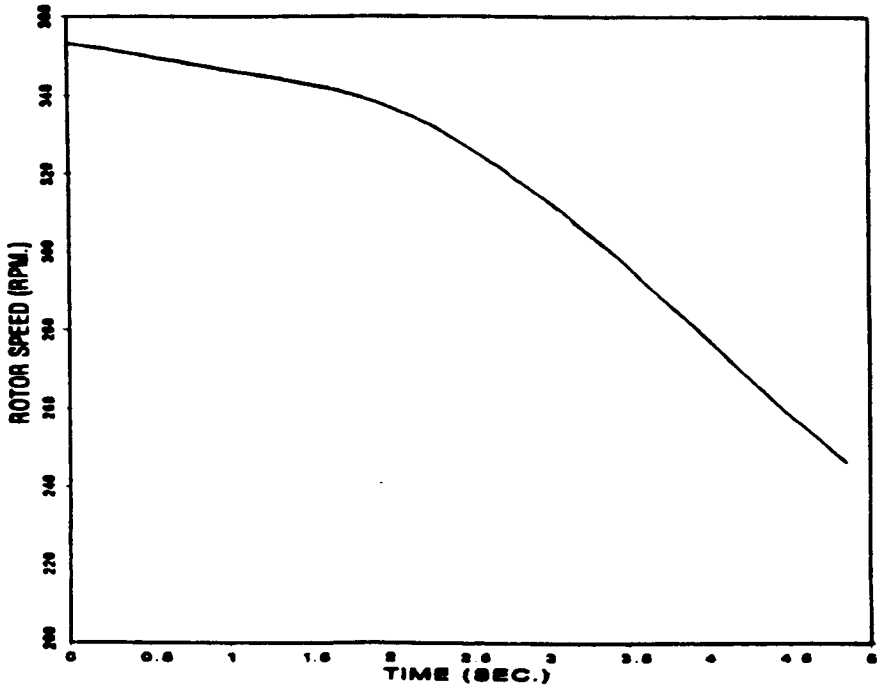

Figure 4.4.7 Optimal Time Variation of Rotor RPM

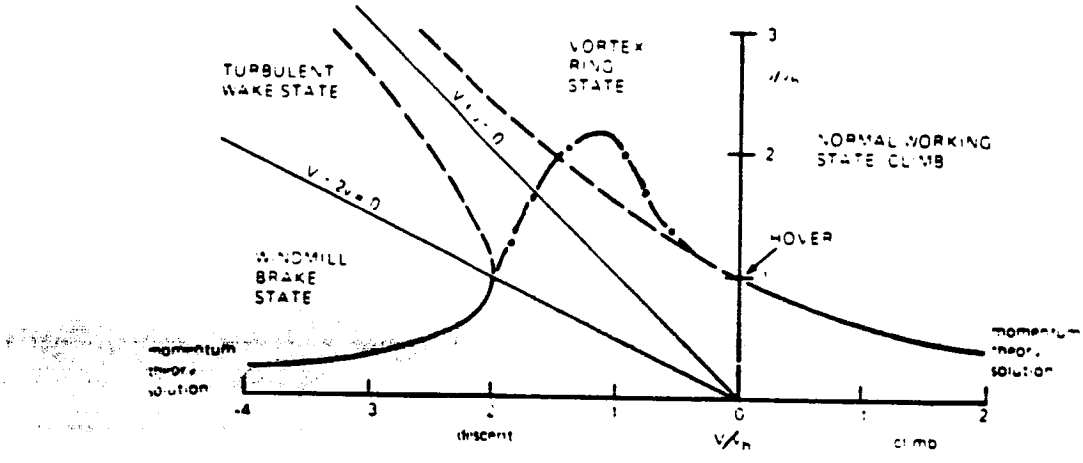

Figure 4.4.8 Variation of Induced Velocity with Rate of Descent [54]

of the order of a few feet per second.

Figure (4.4.8) shows the variation of the rotor RPM with the flight time. The initial rate of the RPM decay is about 7 *rpm* per second. This low rate is due to the drop in the collective pitch immediately after power loss. The rate of RPM decay gradually increases and reaches a rate of 36 *rpm* per second at touchdown, when rotational energy stored in the rotor is being traded for more lift to cushion the impact. The RPM at touchdown is 247, which is about 70 percent of the nominal angular speed.

4.4.3 Comparison with Flight Data

To investigate the effect of rotor inertia on autorotational landing performance, a flight test program with more than 100 autorotational entries and landings was conducted during the HERS flight test programs (cf. [12,57]). Results obtained for autorotation landings of HERS from power loss in hover are given in Section (2.4) of reference [12]. An optimal flight path was not flown in these tests, of course, and in practice, in order to avoid a vertical descent into the rotor's own wake, some forward speed and cyclic flare were involved. Nevertheless, a comparison of flight data with results calculated by the optimal programs will shed some light on the differences in the piloting techniques involved.

However, there are difficulties associated with these comparisons. First, it is found that the engine torque involved in these flight tests does not decrease to zero immediately after the throttle is closed to simulate the engine failure. Instead, the engine torque pressure decays exponentially with a time constant of approximately one second. Second, the grid camera that was used to record the time history of the vertical height during these flights covered only up to about 100 feet above the ground. The initial portion of the maneuver for a simulated engine failure for a hover at 300 feet altitude was therefore out of the range of the camera. We are

forced to use results from the only other case, which is a low altitude autorotation from an initial height of 50 feet AGL. Third, there is no record of the vertical sink rate over time. Finally, for flight tests reported in [12], the pilot's primary objective was to attain a zero rate of sink at touchdown and to accept any safe horizontal velocity. The technique used is to level the aircraft 1 or 2 feet off the ground with no rate of descent. The helicopter then gradually sinks to the ground while small amounts of aft cyclic are applied to reduce the horizontal velocity. The technique consistently yields a zero rate of descent at touchdown but the flight time is usually much longer than that calculated from the optimal program.

Because of the second difficulty mentioned above, we only compare results from a simulated engine failure for a hover at 50 feet AGL. The difference in flight times obtained from flight data and from calculation make direct comparisons of time histories of the rotor speed and the collective pitch control meanningless. The problem can be overcome if we instead use height as the independent variable and compare plots of rotor speed and collective pitch versus height. Figures (4.4.9) and (4.4.10) present the results of these comparisons. Table (4.4.2) summarizes the conditions under which the comparisons are made.

Figure (4.4.9) compares time histories of the collective pitch calculated by the optimal program (we shall from here onward call it the computed result) and recorded from flight. The comparison is qualitatively good. Two distinct features emerged from the comparison. First, relative to the smooth (with an almost uniform increase in the collective pitch) computed result, the flight data are wavy. Over two intervals in height, first from 5 to 20 and then from 35 to 45 feet, the recorded collective pitch remains practically unchanged. The pilot has, perhaps subconsciously divided the autorotational landing into phases within each of which his center of attention changes. In the interval from 5 to 20 feet, his concentration is on stopping RPM

	Optimal Program	Flight Data [12]
Gross Weight (lb.)	3000	3048
Rotational Inertia per blade (slug-ft^2)	672	672
Wind Condition (Knots)	0	<3
Entry Height (ft.)	50	50
Collective Time Delay (sec.)	0	0
Flight Time (sec.)	3.8	8.1
Use of Cyclic Pitch	No	Yes
Engine Condition	Engine Seizure	Exponential Decay with one second time constant

Table 4.4.2 Conditions Used in Comparison of Calculated Results with Flight Data [12]

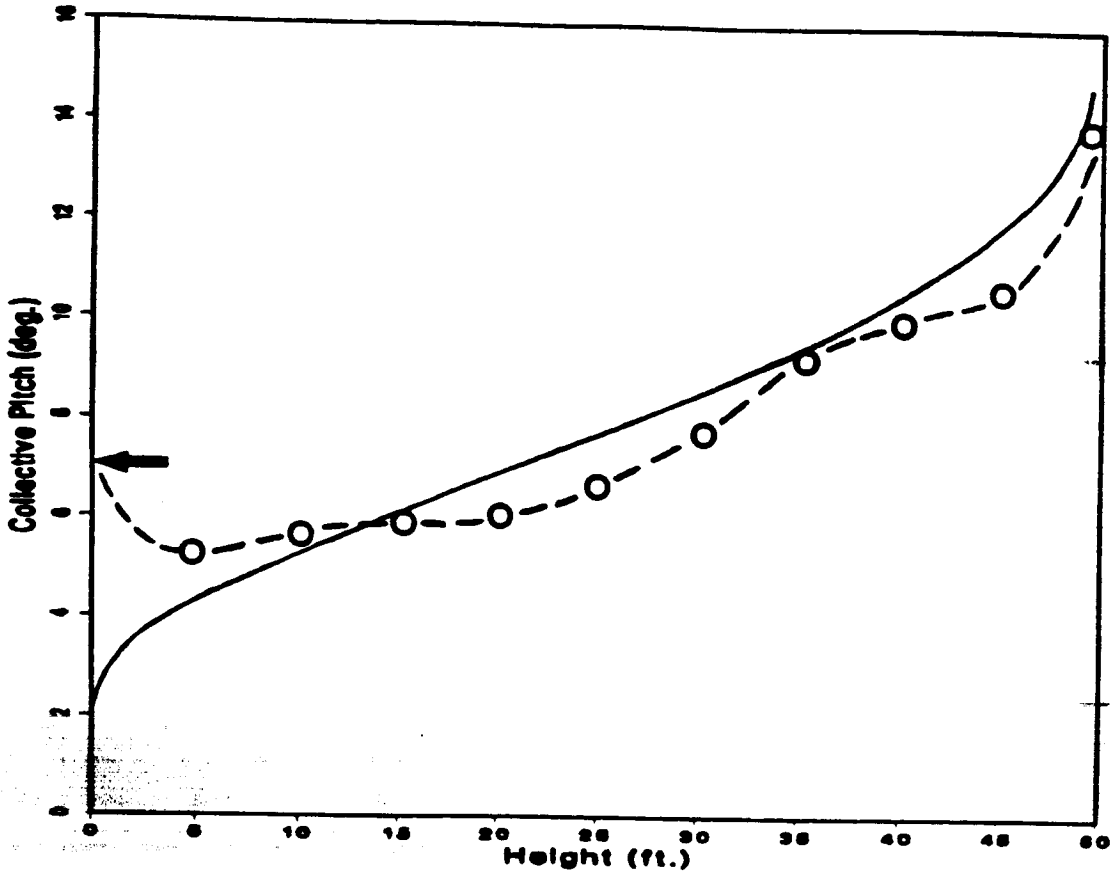

O : Flight Data [12]

Figure 4.4.9 Comparison of Flight Data with Optimal Results : Collective Pitch Control

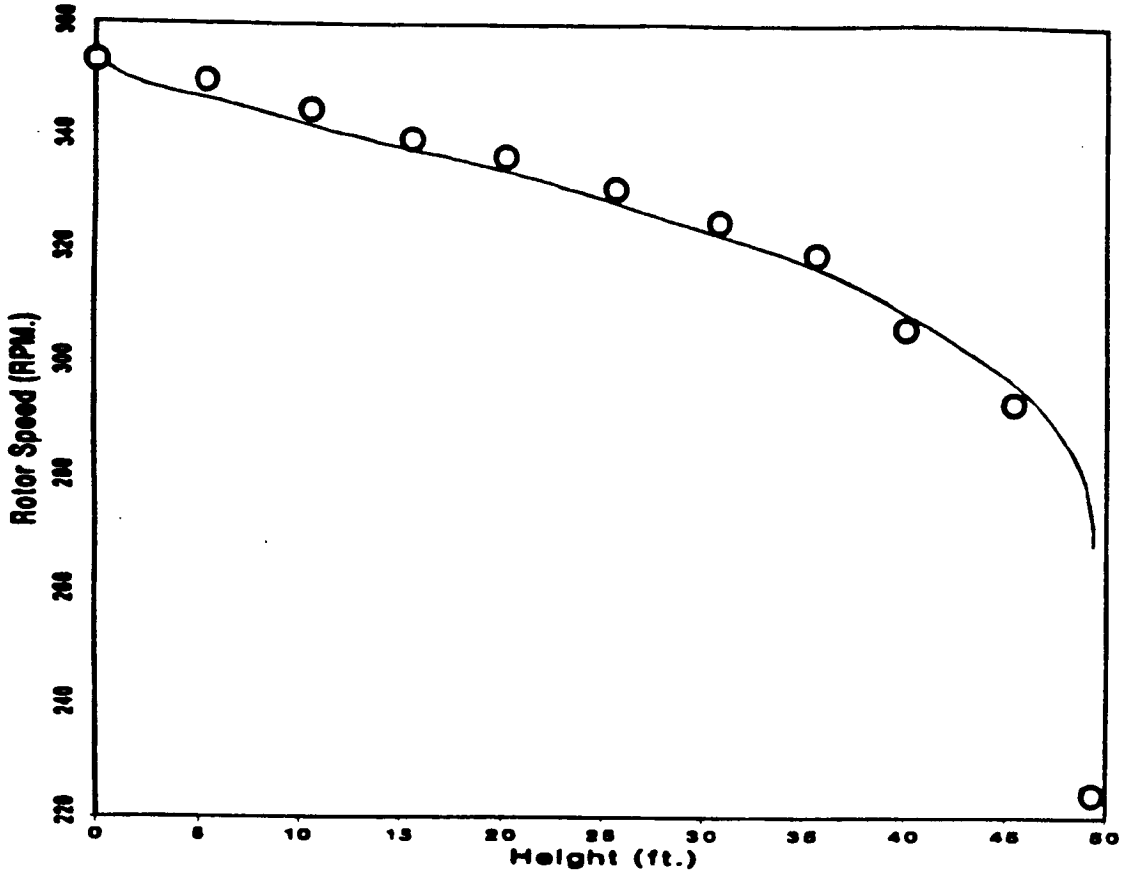

O : Flight Data [12]

Figure 4.4.10 Comparison of Flight Data with Optimal Results : Rotor RPM

decay by reducing the collective pitch control. When the helicopter is at about 10 feet above the ground (interval from 35 to 45 feet), his attention has shifted to the use of aft cyclic to reduce both the forward speed and vertical sink rate. Preparation is made at this stage for the subsequent raising of collective control to cushion the touchdown. It is in such a rapidly changing, often confusing situation that an automated control program, which pays attention to "all" aspects of the landing maneuver, from the begining till the final touchdown, could be of assistance to inexperienced pilots.

Second, the initial drop in the collective pitch recorded in flight data is only about two degrees. This is substantially less than the computed result of five degrees. Thereafter the time history of the collective pitch lies consistently below the computed result. These observations might be explained as follows. In flight tests, the engine torque does not drop to zero immediately after engine failure. Instead, it decays exponentially with a 1-second time constant to a level which is 10-15 percent of the full power output torque. Therefore the residual power available on the rotor shaft at the begining of the autorotational descent is significant. This may explain why the initial drop in collective pitch is not as much as the computed result. After the initial lowering of the collective pitch, the pilot applies a small amount of forward cyclic to pitch the helicopter nose down and attain about 5 knots ground speed. This forward motion reduces the induced power consumption of the helicopter which explains why recorded data lie consistently below computed results. The gain obtainable with the use of forward cyclic is of course not without a price. Aft cyclic must be applied in the landing flare phase of the descent to reduce the forward speed of the helicopter to zero ground speed at touchdown. In addition to the increased induced power loss associated with the use of aft cyclic, the total flight time of the autorotation descent is lengthened.

Figure (4.4.10) compares the recorded time history of rotor speed with that calculated by the optimal program. While one should not look for too much correlation here, the comparison is surprisingly good. The rotor speed at touchdown is 220 *rpm*. This value is somewhat lower than the computed result of 268 *rpm* (see also Table (4.4.3)). The total amount of energy spent in the optimal program is

$$\begin{aligned} \text{Energy Used (Optimal Program)} &= mgH + \frac{1}{2} I_R(\Omega_i^2 - \Omega_f^2) \\ &= 3000 \times 50 + \frac{1}{2}(672 \times 2)(37^2 - 28^2) \\ &= 54.3 \times 10^4 \text{ ft.} - \text{lb.wt.} \end{aligned} \tag{22}$$

This amount is about 24 percent less than that used by the pilot in achieving the same zero rate of sink at touchdown from a 50 feet hovering throttle chop:

$$\begin{aligned} \text{Energy Used (Pilot)} &= 3000 \times 50 + \frac{1}{2}(672 \times 2)(37^2 - 23^2), \\ &= 71.4 \times 10^4 \text{ ft.} - \text{lb.wt.} \end{aligned} \tag{23}$$

4.4.4 Effects of Entry Height

Figure (4.4.11) compares the time history of the collective pitch control calculated by the optimal program at three different entry heights of 50, 100, and 200 feet. Since the computed optimal flight time varies with the entry height, we change the independent variable from time to the normalized time (ξ), where ξ is defined as

$$\xi = \frac{t}{t_f}, \tag{24}$$

where t_f is the flight time. Computed time histories of the thrust coefficient are compared in Figure (4.4.12)

Figure (4.4.11) shows that the optimal collective pitch control program changes with the entry height. From the 7.2-degree collective pitch used before engine failure, the initial collective pitch reduction is in the range of 5-6 degrees for all the entry

	Flight Data [12]	Optimal Program
Time of Touchdown (sec.)	8.1	3.8
Max. Rate of Descent (fps.)	15	20
Touchdown vertical speed (fps.)	0	0
Rotor Speed at Touchdown (rpm)	221	268
Minimum Collective Pitch (degrees)	2.0	5.2
Collective Pitch at Touchdown (degrees)	14.2	14.8

Table 4.4.3 Comparison of Optimal Results with Flight Data, $h_0 = 50$ feet [12]

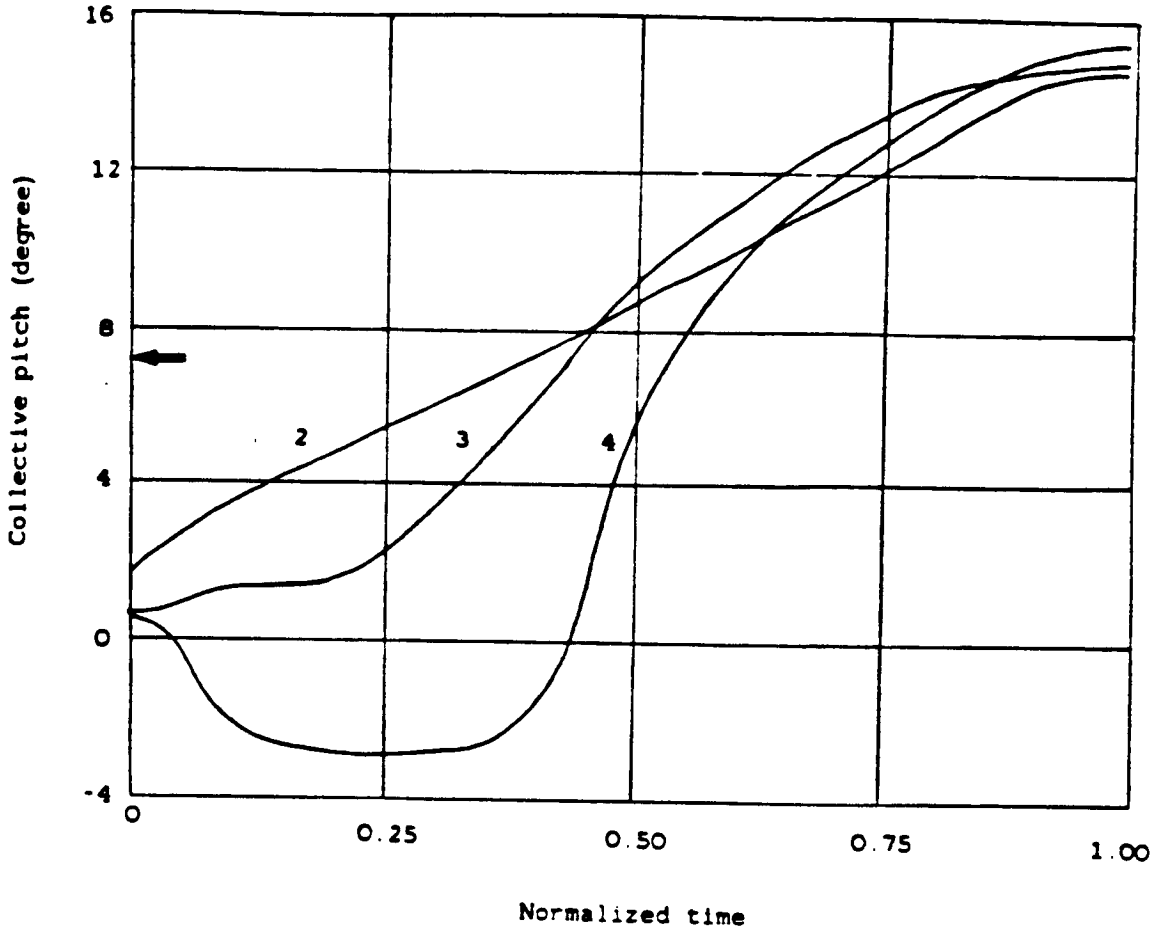

ENTRY CONDITION	2	3	4
ENTRY HEIGHT (ft.)	50	100	200
FLIGHT TIME (sec.)	3.8	4.9	6.1

Figure 4.4.11 Time Variations of Collective Pitch Control from Different Entry Heights

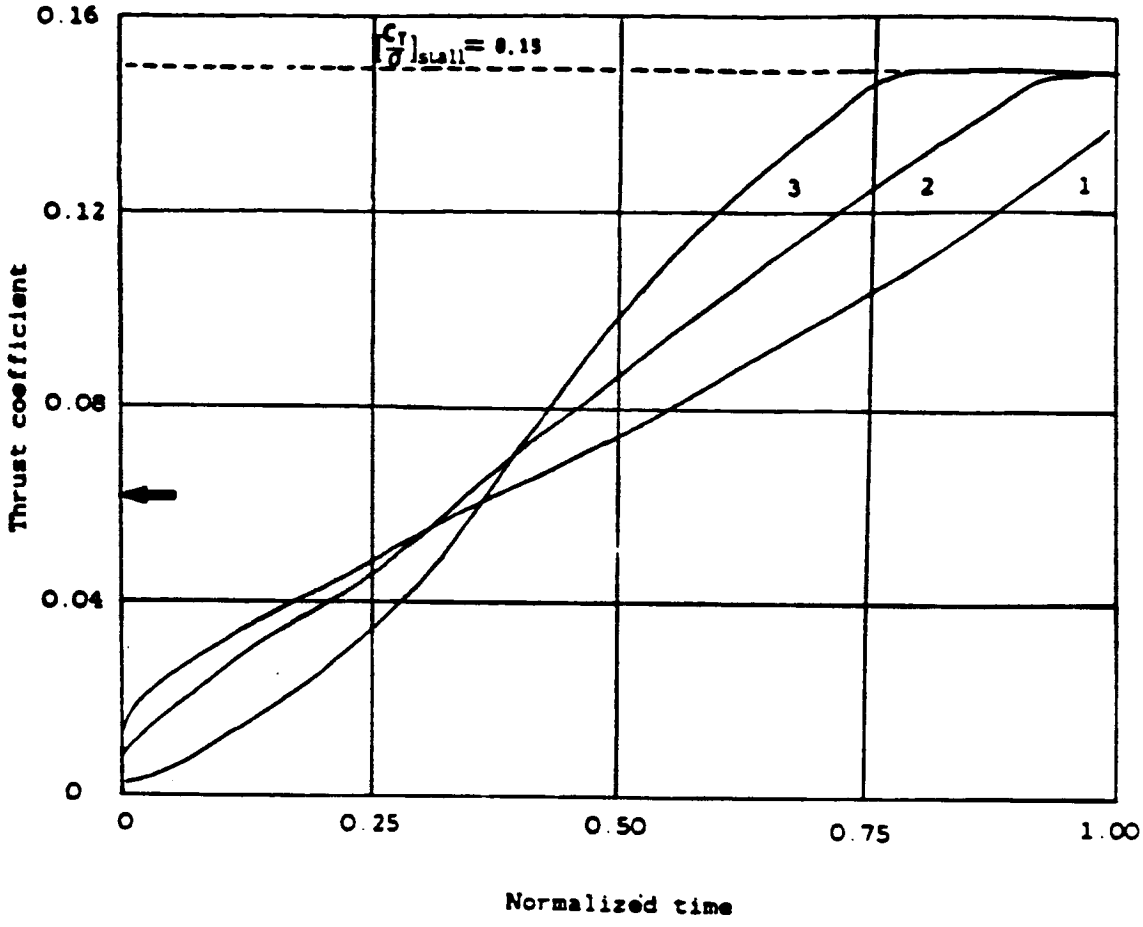

ENTRY CONDITION	1	2	3
ENTRY HEIGHT (ft.)	25	50	100
FLIGHT TIME (sec.)	2.7	3.8	4.9

Figure 4.4.12 Time Variation of Thrust Coefficient from Different Entry Heights

heights considered. The collective is lowered to minimize RPM decay. At the lowest entry height of 50 feet, the collective is immediately raised again after the initial drop in collective. At the higher entry heights of 100 and 200 feet, the lowered collective pitch is maintained for some time before it is raised to reduce the rate of descent. This delay allows a build-up in the rate of descent of the helicopter, but with the high rotor inertia, subsequent collective increase provides a sufficient deceleration to allow a safe landing.

4.4.5 Most Critical Entry Height

Figure (4.4.12) shows the time history of the thrust coefficient calculated by the optimal program at three different entry heights of 25, 50, and 100 feet. The curve for case (4) (with entry height of 200 feet) lies slightly to the right of that for case (3) and has been omitted in the interest of clarity.

As the entry height is increased, Figure (4.4.12) shows a corresponding increase in the amount of (normalized) time that the thrust coefficient spends on its stall limit. This trend continues till the entry height of 100 feet is reached. Beyond the "critical" height of 100 feet, any further increase in entry height reduces the time that the thrust coefficient is on its stall limit. Since prolonged usage of the maximum available thrust is an indication of an irrevocable extraction of the rotational energy from the rotor system during the autorotational landing maneuver, the observed results suggest the existence of a "Most Critical Entry Height" (MCEH). Above or below this critical height, which in the present case is around 100 feet, the autorotational landing procedure becomes progressively easier to execute.

Further confirmation of this hypothesis can be found in the time history of the rotor angular speed in Figure (4.4.13). Since the rates of descent at touchdown for all entry heights considered are practically zero, we cannot use them to compare

the criticality of the landings. However, we have learned from Section (4.4.3) that the lower the rotor RPM at touchdown, the larger is the amount of energy (of the helicopter) used in the landing maneuver. One easy way to show the existence of the MCEH is to plot the rotor speed at touchdown against the corresponding entry height of the autorotational descent. Such a plot is given in Figure (4.4.14).

Figure (4.4.14) shows that the MCEH (denoted by h_{cr}) is at around 100 feet where the rotor speed at touchdown is a minimum. Therefore the "Most Critical Entry Condition" is one with engine failure in hover at h_{cr}. This conclusion agrees with flight test results recorded in reference [11].

§4.5 Optimal Landing of a Helicopter in Forward Flight

The autorotational landing of a helicopter in forward flight has been formulated as an optimal control problem in Section (3.3). Unlike the case when power loss occurs in hover, the present case involves more than a pure vertical descent. As such, we have to consider the "full state" problem with five states

$$\begin{aligned} x_1 &= \text{normalized vertical velocity}, \\ x_2 &= \text{normalized horizontal speed}. \\ x_3 &= \text{normalized rotor speed}, \\ x_4 &= \text{normalized vertical height}, \\ x_5 &= \text{normalized horizontal distance}. \end{aligned} \tag{24a}$$

and two controls

$$\begin{aligned} u_1 &= \text{vertical component of thrust}, \\ u_2 &= \text{horizontal component of thrust}. \end{aligned} \tag{25}$$

If the helicopter is not constrained to land at a particular spot on the ground, the state x_5 may be removed from the list in (24). Optimization is then performed on a

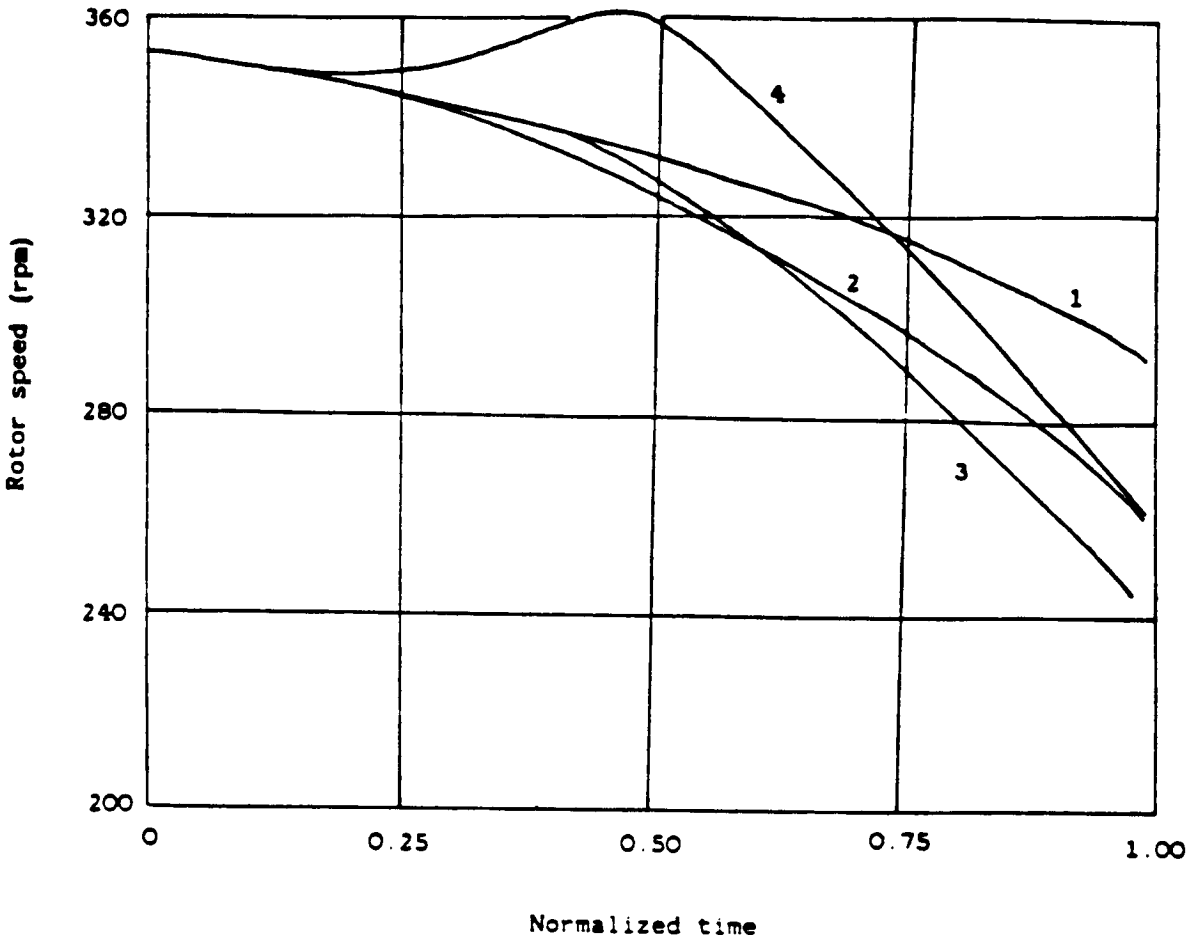

ENTRY CONDITION	1	2	3	4
ENTRY HEIGHT (ft.)	25	50	100	200
FLIGHT TIME (sec.)	2.7	3.8	4.9	6.1

Figure 4.4.13 Time Variations of Rotor Speed at Different Entry Heights

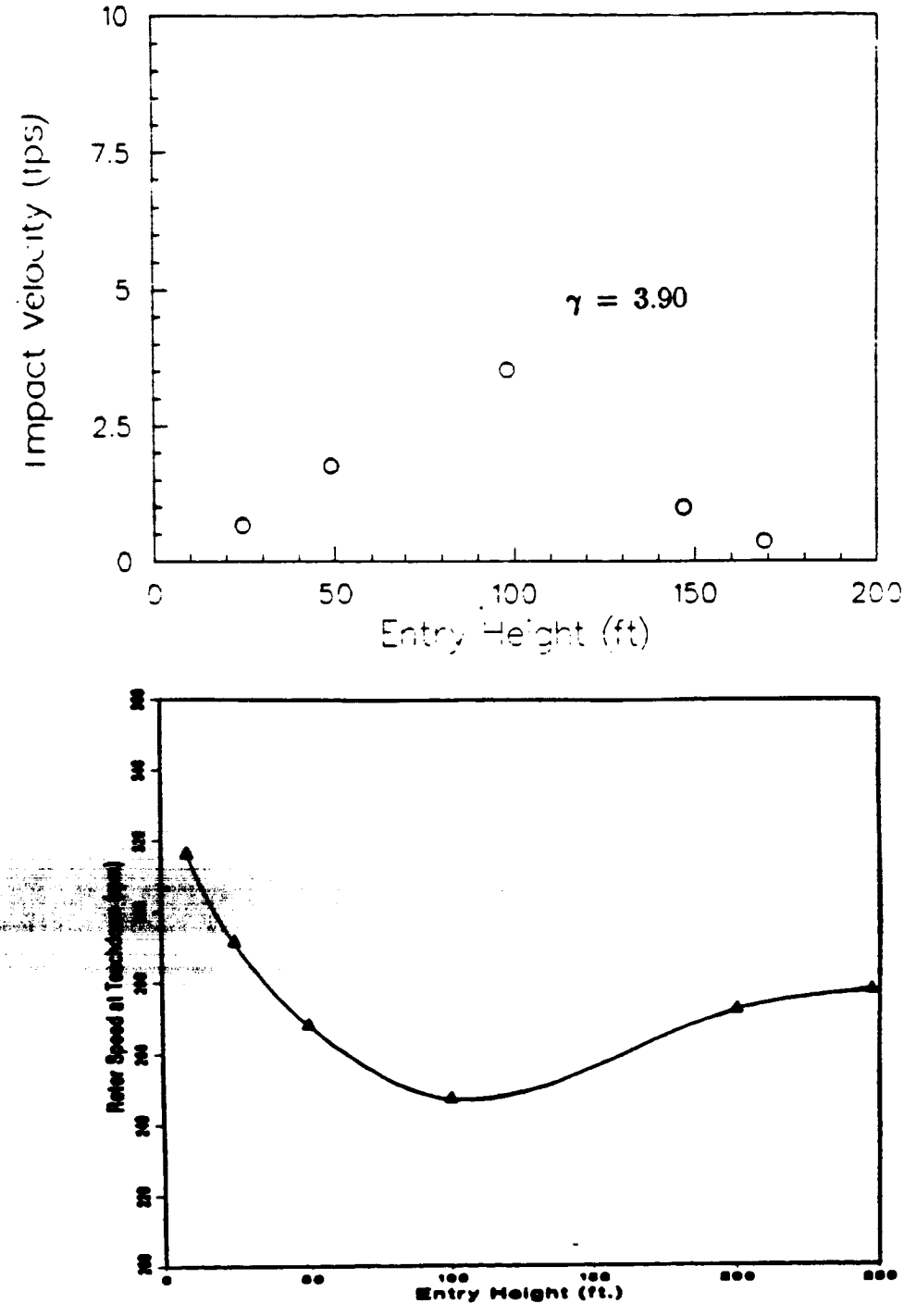

Figure 4.4.14 Variations of Terminal Descent Velocity and Rotor Speed with Entry Height

problem with only four states and two controls. After the optimal solution has been computed, information on the horizontal distance (x_5) may be recovered through the forward integration of the kinematical relation:

$$x_5(\xi) = \int_0^1 [0.1\tau_f x_2(\xi)]\, d\xi . \tag{26}$$

where ξ is the normalized flight time.

4.5.1 Flight Program

Once again, the High Energy Rotor System (HERS) described in Section (4.1) is used as the basis for the analytical model. However, we note in reference [12] that the highest inertia rotor (with $\gamma = 2.61$) allows complete elimination of the height-velocity restriction curves. For the mid-inertia rotor (with $\gamma = 3.19$), only a small restricted region remains between 75 to 125 feet altitude with airspeed less than 5 knots. Therefore it is more interesting to investigate optimal landings of the HERS with its lowest inertia rotor. We have chosen, rather arbitarily, a rotor with Lock Number γ of 4.38 which corresponds to a rotor inertia (per blade) of 400 $slug\text{-}ft^2$. The low-speed height-velocity restrictions for the HERS with rotor inertia at three different levels are given in Figure (4.5.15) along with the diagram for the standard OH-58A helicopter.

Entry conditions studied are summarized in Figure (4.5.16). We have chosen to analyse entry conditions that are within or close to the height-velocity restriction curve of the HERS with its low-inertia rotor. Note also that entry conditions 1, 2 and 6 are at the same altitude of 100 feet but with different forward speeds. Similarly, entry conditions 1, 5 and 4 have (approximately) the same forward speed of 8 knots but are at different entry heights. In this way, effects of both the forward speed and altitude at entry can be studied. Optimal landings of the HERS studied at these

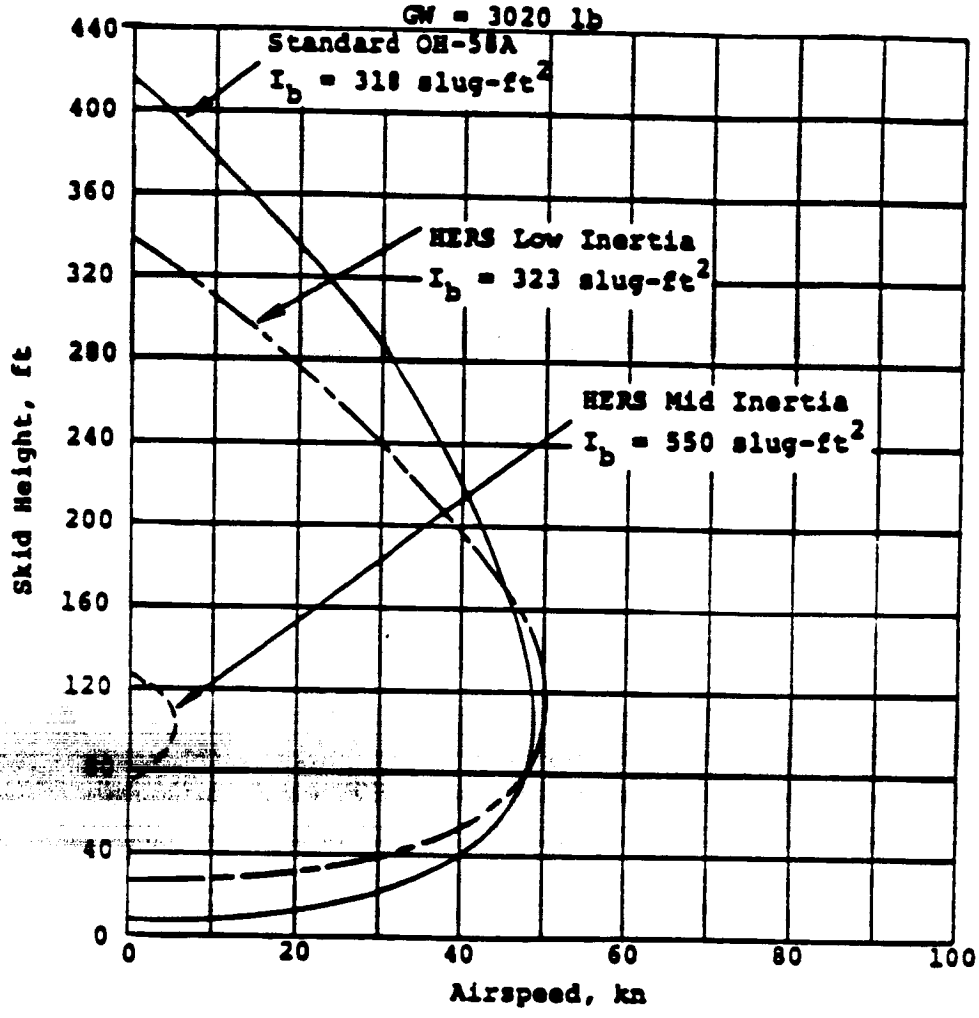

Figure 4.5.15 Comparison of HERS Test Results with Standard OH-58A [12]

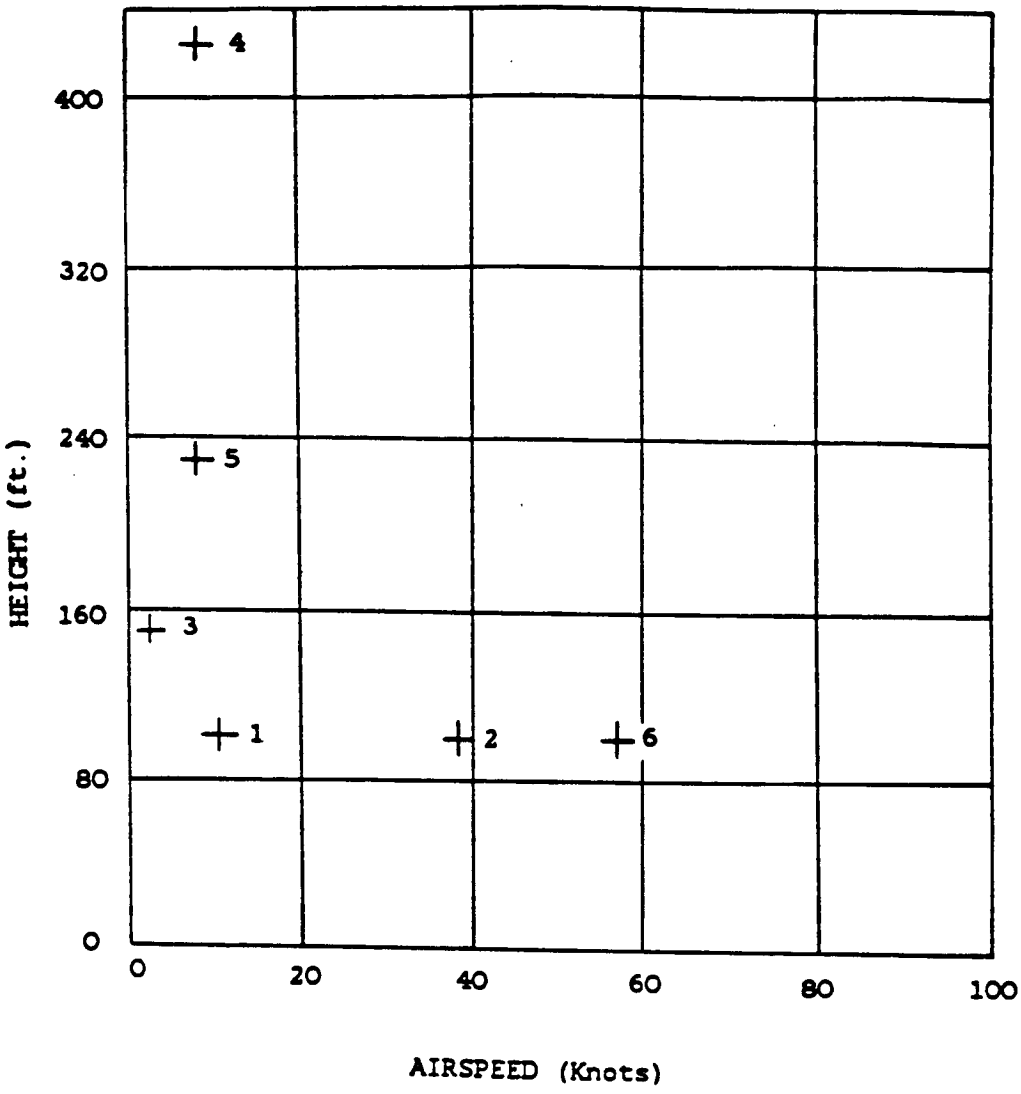

ENTRY CONDITION	1	2	3	4	5	6
HEIGHT (ft.)	100	100	150	420	230	100
AIRSPEED (Knots)	12	38	4	8	8	57

Figure 4.5.16 (H-V) Entry Conditions

entry conditions are without any terminal constraint on the horizontal distance. The only exception is entry condition 5, where the helicopter is constrained to land at various horizontal distances from the point of engine failure.

4.5.2 Interpretation of Results

Figures (4.5.17) to (4.5.19) present in detail the optimal solution of power-off descent from an altitude of 100 feet and at 12-knots forward speed (entry condition 1 in Figure (4.5.16)). Figure (4.5.17) gives the collective pitch control and the thrust coefficient as functions of time. Since the parasite drag on the fuselage of the helicopter in level flight is small compared with the weight of the vehicle, equation (18) is still approximately true and the value of the thrust coefficient divided by the rotor solidity before engine failure is given (approximately) by 0.063.

The induced velocity in level flight can be found from the momentum quartic:

$$\bar{v}^4 - 2\bar{V}\bar{v}^3 \sin\alpha + \bar{V}^2\bar{v}^2 - (\frac{T}{W})^2 = 0. \tag{27}$$

where the normalized induced velocity ($\bar{v}$) and the normalized flight path velocity ($\bar{V}$) are given by

$$\begin{aligned} \bar{v} &= \frac{v}{\sqrt{\frac{W}{2\rho A}}}, \\ \bar{V} &= \frac{V}{\sqrt{\frac{W}{2\rho A}}}. \end{aligned} \tag{28}$$

In level flight, the angle which the flight path velocity V makes with the TPP, α, is approximately zero. Equation (27) can thus be simplified and the value of $\bar{v}$ is given by the following equation

$$\bar{v} = \sqrt{-\frac{\bar{V}^2}{2} + \sqrt{(\frac{\bar{V}^2}{2})^2 + 1}}. \tag{29}$$

The value of the induced velocity at hover, ν_h, is given by

$$\begin{aligned} \nu_h &= \sqrt{\frac{W}{2\rho A}}, \\ &= 25.38 \quad \text{fps}. \end{aligned} \tag{30}$$

Values of $\bar{\Gamma}$ and $\bar{\nu}$ can then be computed from equations (28-2) and (29) respectively. Their values are

$$\begin{aligned} \bar{\Gamma} &= 0.798, \\ \bar{\nu} &= 0.855. \end{aligned} \tag{31}$$

Therefore the inflow and advance ratios are given by

$$\begin{aligned} \mu &= 0.031, \\ \lambda &= 0.0332. \end{aligned} \tag{32}$$

The collective pitch used before engine failure can then be computed from the following relation

$$\begin{aligned} \theta_{75} &= \frac{(1+\frac{3}{2}\mu^2)(\frac{6C_T}{a\sigma})+\frac{3}{2}\lambda(1-\frac{1}{2}\mu^2)}{(1-\mu^2+\frac{9}{4}\mu^4)}, \\ &\doteq \frac{6C_T}{a\sigma}+\frac{3}{2}\lambda, \\ &\doteq 6.63 \quad \text{degrees}. \end{aligned} \tag{33}$$

As expected, this value is smaller than the value used in the hover case (7.72 degrees).

The optimal solution is similar to that found in the hover case. Initially the collective is lowered to maintain rotor speed, and nose-down cyclic is used to maintain airspeed. The results of these control actions are an initial build-up of the vertical sink-rate as well as an increase in the forward airspeed. However, the rate of RPM decay is being curtailed. In fact, the angular speed of the rotor stabilizes at around 332 *rpm* until a rearward, nose-up cyclic flare is used to slow both the rate of descent and forward airspeed.

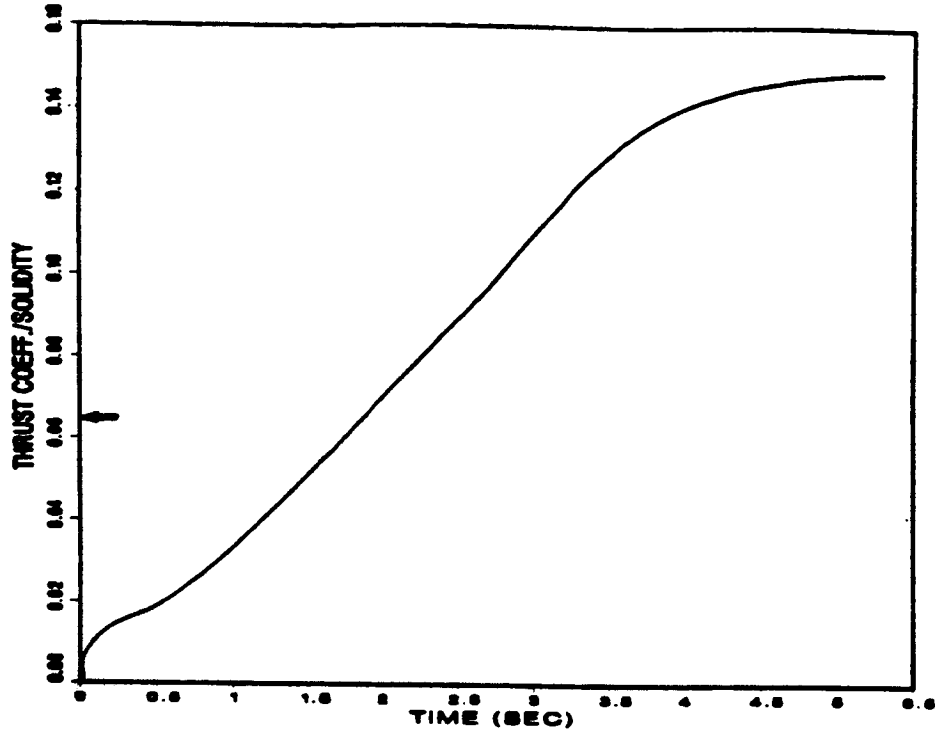

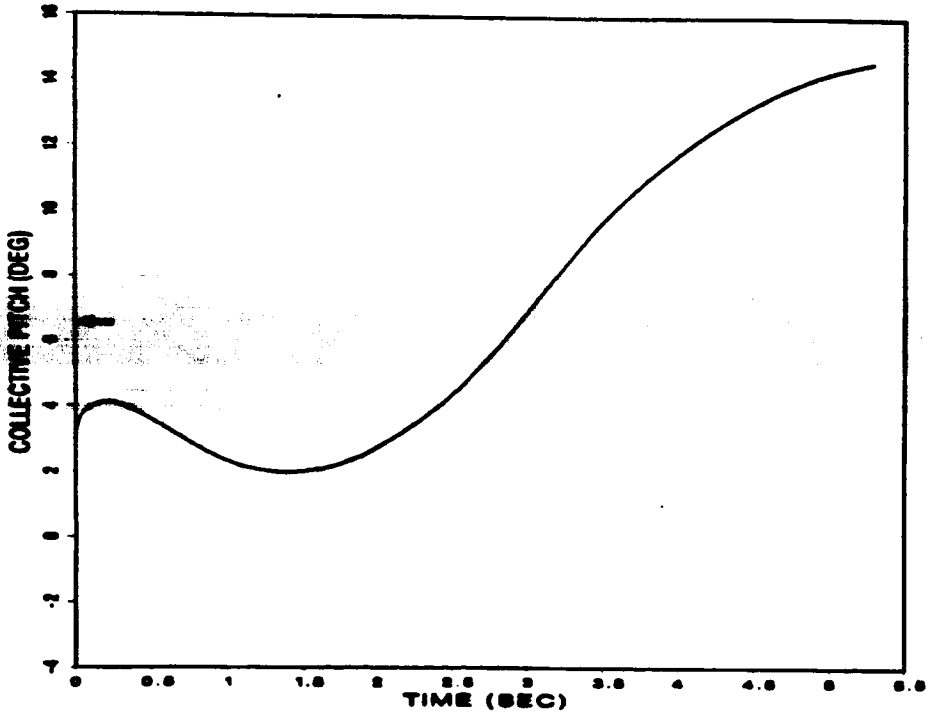

Figure 4.5.17 Optimal Time Variations of Thrust Coefficient and Collective Pitch Control

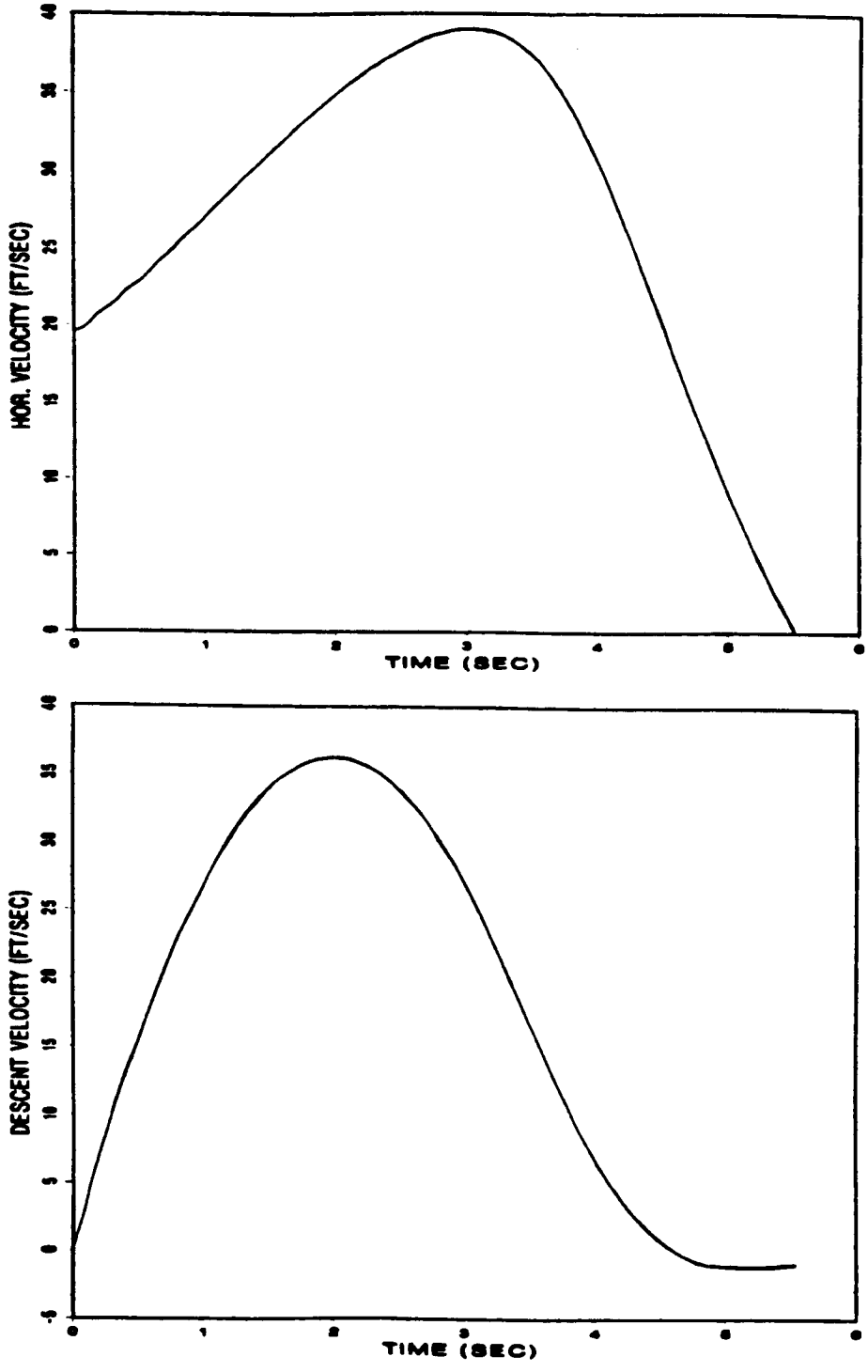

Figure 4.5.18 Optimal Time Variations of Horizontal and Vertical Velocity

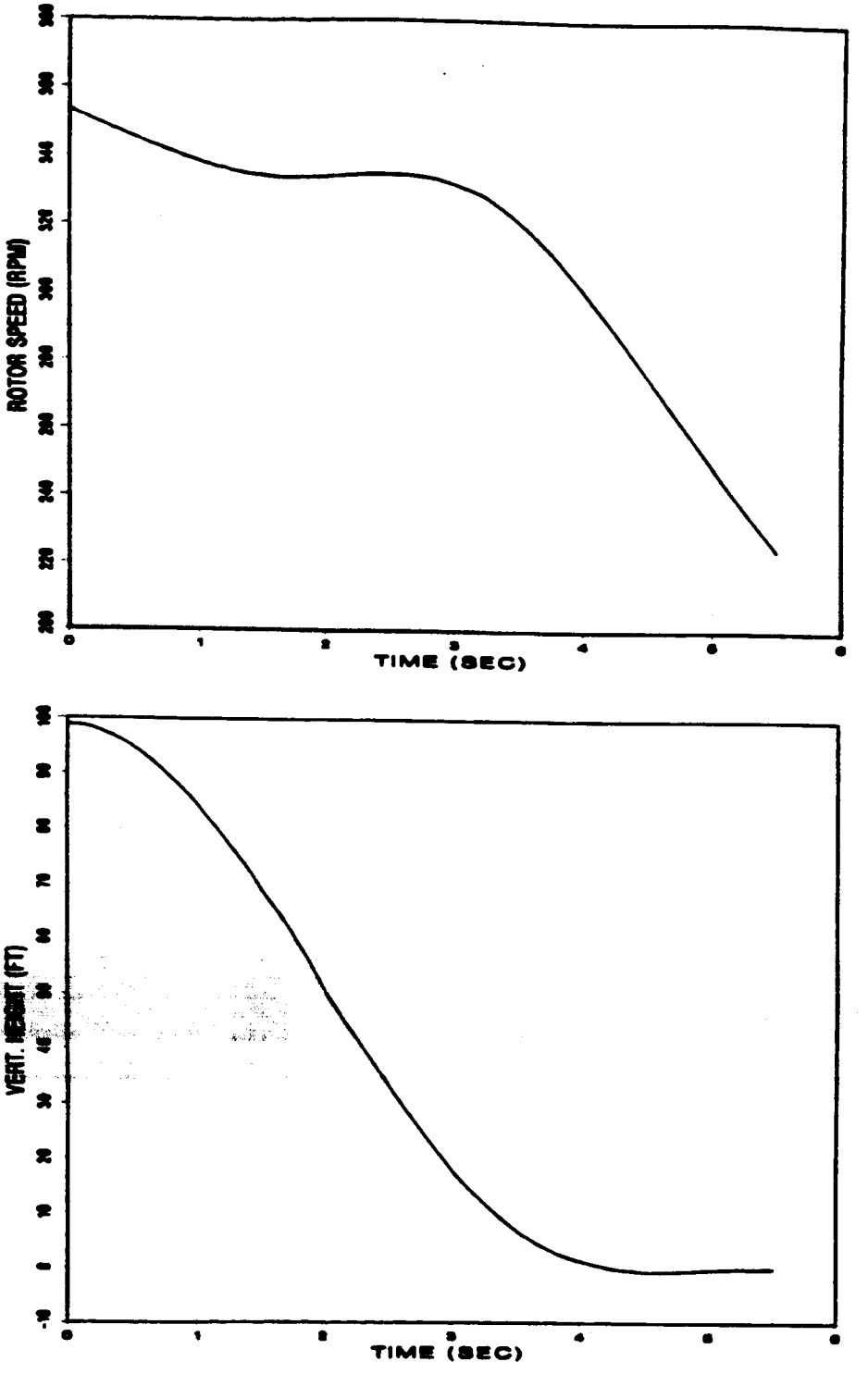

Figure 4.5.19 Optimal Time Variations of Rotor RPM and Helicopter's Altitude

Because of the bound on thrust coefficient at $(\frac{C_T}{\sigma}) = 0.15$, the steady increase in the collective pitch levels off towards the end when touchdown is imminent. The thrust coefficient stays on its bound during the last second of the travel when the helicopter is very near to the ground. Once again, the path inequality constraint on the thrust coefficient has been effectively enforced by the optimization algorithm.

Nose-up cyclic is initiated 2 seconds after the engine failure when the helicopter is at about 50 feet above the ground. This occurs later than was the case for hover, yet there will be sufficient kinetic energy available for the landing flare on account of the initial forward speed. With a rearward tilt of the TPP, the projected area of the TPP in the direction perpendicular to the air flow has increased. More air now flows through the rotor disk. The resultant increase in the angle of attack of the rotor blades increases the thrust. This effect, together with the steady increase in the collective pitch, bring about the desired reductions in the forward speed and rate of descent approaching touchdown.

The time variation of rotor speed is given in Figure (4.5.19). The figure clearly shows that some of the lost RPM can be regained if a nose-up cyclic flare is initiated with sufficiently high helicopter forward speed. Effects produced by a rearward (nose-up)cyclic flare are illustrated in Figure (4.5.20). Because of the increased lift force (i.e. L >> D in Figure (4.5.20)), the resultant thrust vector R is tilted forward and produces a net force component in the plane of the rotor's blades. This force component generates a torque that accelerates the rotor. During the touchdown phase, the collective is raised to cushion the impact. The rotor speed is reduced to 225 *rpm* at touchdown, indicative of extracting most of the available rotor energy. The touchdown is made at a near zero horizontal speed.

4.5.3 Comparison with Flight Data

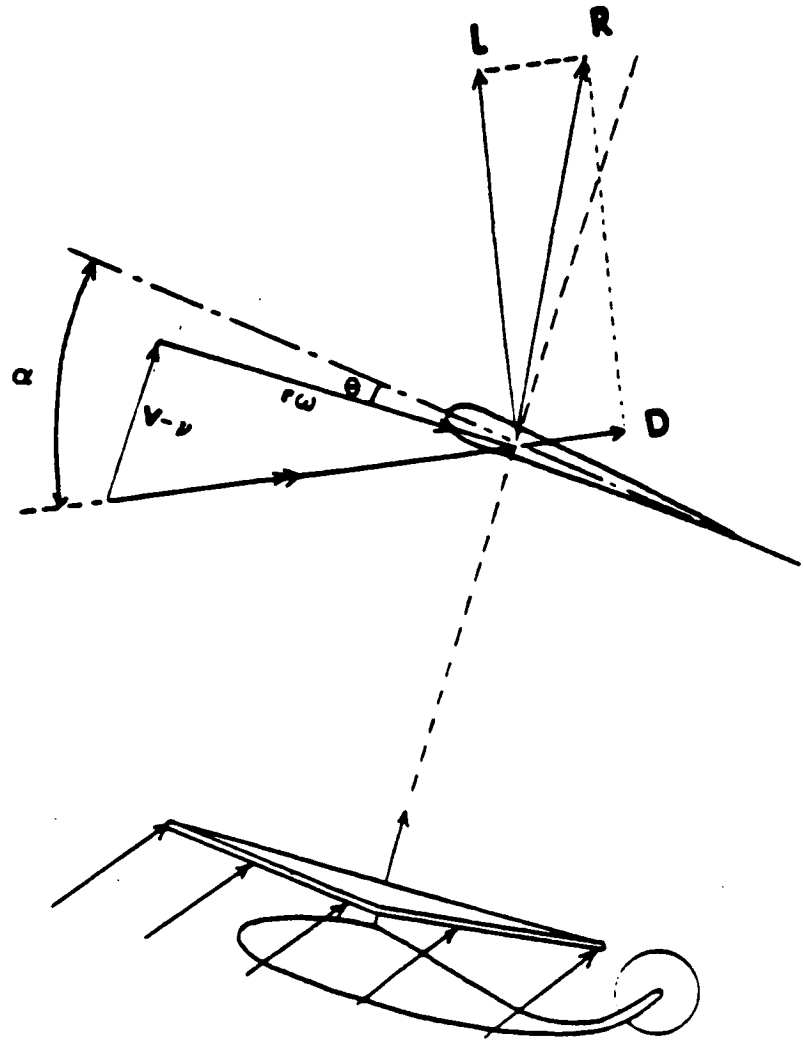

L : LIFT, D : DRAG, R : RESULTANT FORCE

ν : INDUCED VELOCITY, V: DESCENT VELOCITY

θ : PITCH ANGLE, α : ANGLE OF ATTACK, ω : ROTOR RPM

Figure 4.5.20 Effects of Rearward (Nose-Up) Cyclic Flare

In this sub-section, techniques used by pilots are compared with those computed from the optimal program. We use flight data obtained from a simulated engine failure of the low-inertia version of the HERS at the "knee" of the height velocity restriction curve [12]. Flight data obtained from this entry condition (with 115 feet altitude and 45 knots forward speed) are compared with those computed by the optimal program for the entry condition at 100 feet altitude and 38 knots forward speed. Therefore, one must note the small differences in both the entry height and speed when making comparisons. Additionally, because of the strong emphasis on a zero vertical sink-rate at touchdown, pilots tend to neglect the horizontal component of the velocity in their landing maneuver (both military and civil criteria permit this). In this particular case, the touchdown horizontal speed of the helicopter is 20 *fps*. This pilot priority is quite different from the cost function used in the formulation of the optimal control problem. Other differences in flight conditions are summarized in Table (4.5.4).

Because of the difference in flight times obtained from flight data and that from calculation, direct comparisons of the time histories of the collective pitch and the rotor angular speed are not meaningful. The previously used technique of converting the independent variable from time to height is not applicable here because of the difference in entry heights. Therefore we choose to use the normalized time (ξ, see equation (24)) as the independent variable in making comparisons. Figures (4.5.21), (4.5.22) and (4.5.23) present results of these comparisons.

Figure (4.5.21) compares time histories of the collective pitch calculated by the optimal program and from flight data. The comparison is qualitatively good. The most obvious differences in these time histories are the undulating nature of the flight data, as well as the fact that the collective pitch control used in flight tests is lower than that calculated. One of the reasons for the observed difference in

	Optimal Program	Flight Data [12]
Gross Weight (lb.)	3000	3040
Rotational Inertia per Blade (slug-ft^2)	400	323
Wind Condition (Knots)	0	<3
Entry Height (ft.)	100	115
Entry Speed (Knots)	38	45
Collective Time Delay (sec.)	0	0
Touchdown Vertical Speed (fps.)	0	0
Touchdown Horizontal Speed (fps.)	0	20
Rotor Speed at Touchdown (rpm)	224	280
Flight Time (sec.)	8.7	10.8
Engine Condition	Engine Seizure	Exponential Decay with 1-second time constant

Table 4.5.4 Flight Test Conditions

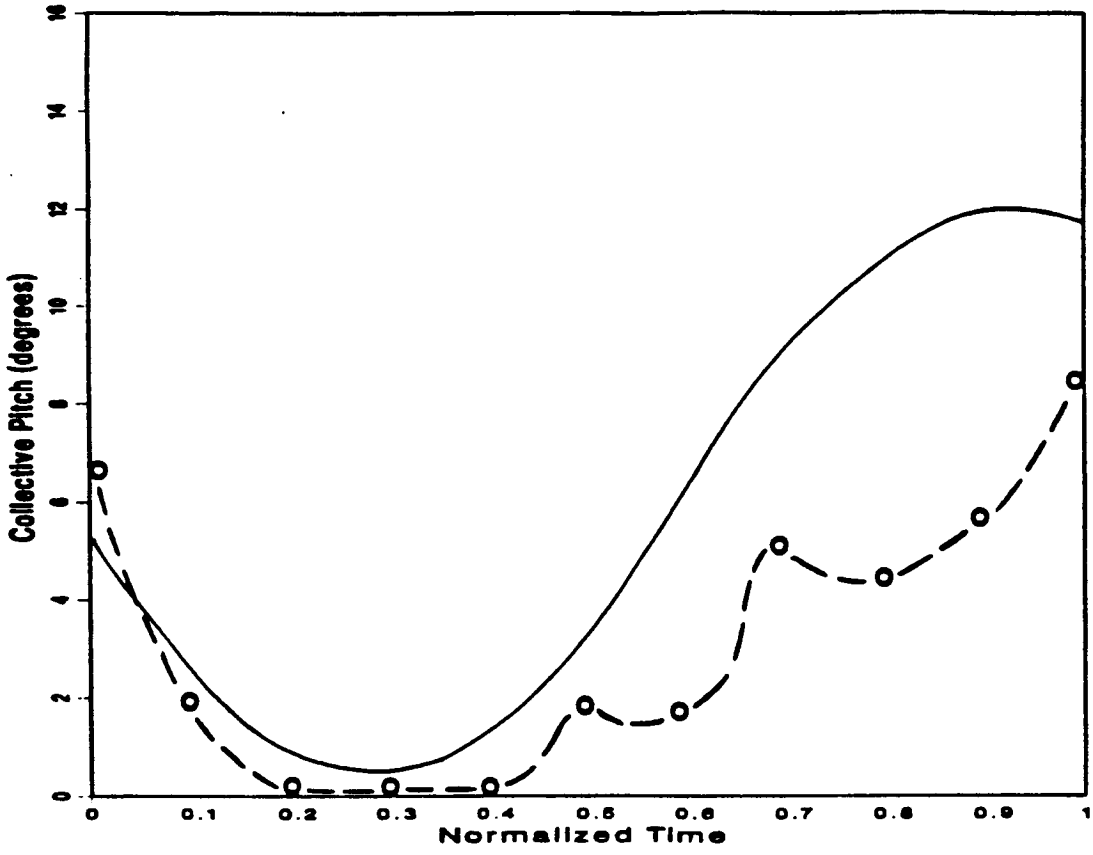

O Flight Data [12]

Figure 4.5.21 Comparison of Flight Data with Optimal Results : Collective Pitch Control

collective pitch controls is the availability of the residual power to the helicopter in flight tests. The difference is also partly due to the fact that the touchdown horizontal speed of the helicopter in the flight test is 20 *fps* (as compared with the near zero value in the optimal result). With reference to Figure (4.5.18), we can see that the calculated vertical sink-rate of the helicopter over the last 1/3 of the flight time is practically zero. Over the same period of time, the forward speed of the helicopter is being steadily reduced to its near zero value at touchdown. Therefore the touchdown condition of the flight test (zero rate of descent and 20 *fps* forward speed) has been achieved in the optimal program at around 2/3 of the flight time. If we now compare the value of the computed collective pitch at around 2/3 of the flight time with that from flight data at touchdown, their values become comparable. Unlike the flight test, the optimal program will not land the helicopter with high forward speed. Instead it will try to reduce the forward speed to as near to zero as possible. This is done over the last 1/3 of the flight time where both the collective pitch and rear cyclic are used to further decelerate the helicopter. The above reasoning helps to explain the difference in collective pitch controls shown in Figure (4.5.18).

Figure (4.5.22) compares the recorded time history of the rotor speed with that calculated by the optimal program. The comparison is again qualitatively good. Notice that the pilot had placed much greater emphasis on maintaining a constant rotor RPM than that reflected in the optimal results. Consequently, the collective pitch is maintained at a minimum for as long as possible. This helps to explain the discrepancy found in Figure (4.5.22). Since the optimal program decelerates the forward speed of the vehicle to near zero while flight test to 20 *fps*, the computed rotor RPM at touchdown (about 230 *rpm*) is lower than that found in the actual flight test (280 *rpm*).

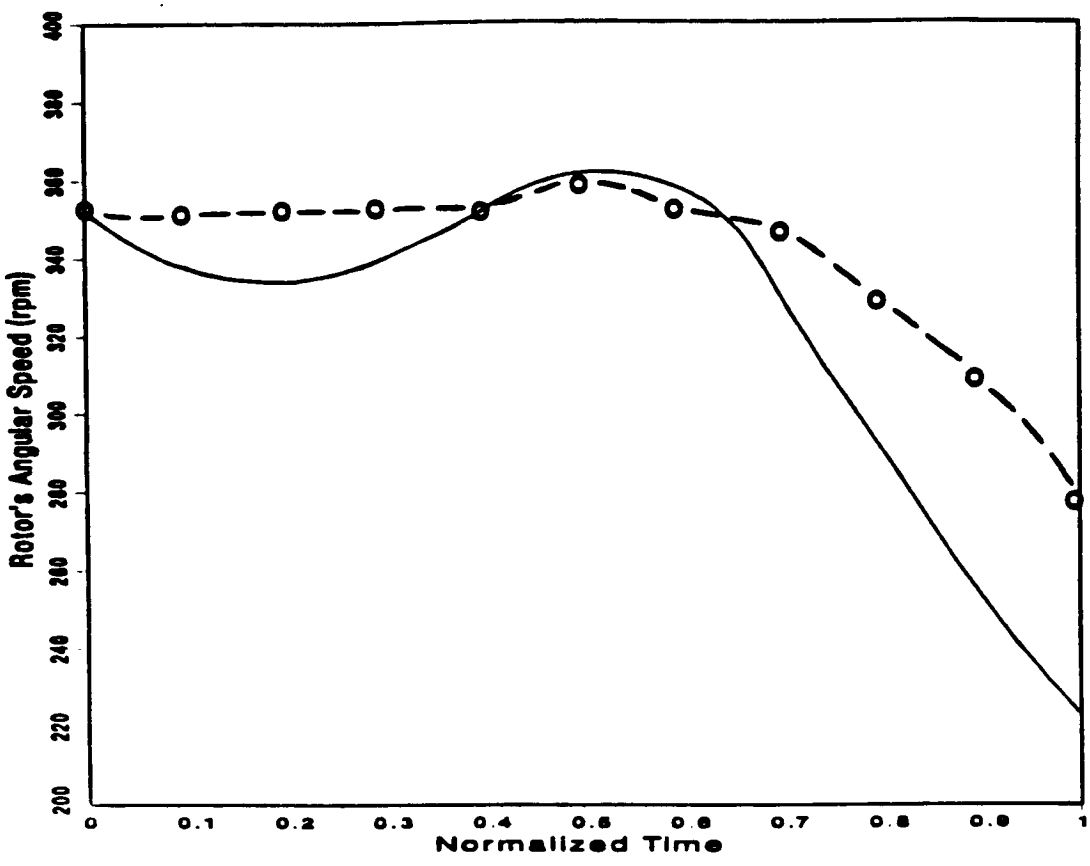

Figure 4.5.22 Comparison of Flight Data with Optimal Results : Rotor RPM

C-2

A comparison of the optimal trajectory with that found in flight tests is shown in Figure (4.5.23). Flight data show a 535 ft horizontal distance at touchdown, which is larger than that from the optimal program (400 ft). The extra distance was used by the pilot in the reduction of forward speed through the use of cyclic control. In order to maintain the helicopter at its level attitude for the final touchdown, only small amount of rearward cyclic was used in the deceleration of the vehicle. This pilot actions results in a prolonged touchdown and a longer horizontal distance travelled.

Landing Techniques

The most critical phase of the autorotation descent of a helicopter is the final approach to a landing flare. Figures (4.5.24) and (4.5.25) show the pilot control motions and flight profiles from the flight data, and those obtained by the optimal program, respectively. Both records are for an autorotation entry condition of about 40 to 45 knots airspeed, and level flight at around 100 feet altitude. Superimposed on the flight profile are reference lines indicating the orientation of the helicopter's pitch attitude at one-second intervals. Close spacing of the reference lines indicates a slow maneuver while larger spacing indicates a faster maneuver. As the helicopter is modelled as a point mass, pitch attitude of the vehicle is not available from the optimal program. In Figure (4.5.25), we have substituted for it the orientation of the TPP in space. Also, since the longitudinal cyclic cannot be determined from the optimal program, it is not shown in Figure (4.5.25).

As can be seen from the flight data, a cyclic flare is initiated just below 100 feet and held to about 20 feet above the ground. This results in a nose-up attitude of 18 degrees. The collective is increased slightly during the flare to prevent rotor overspeed. Only after reaching about 15 feet does the final collective pull begin. In

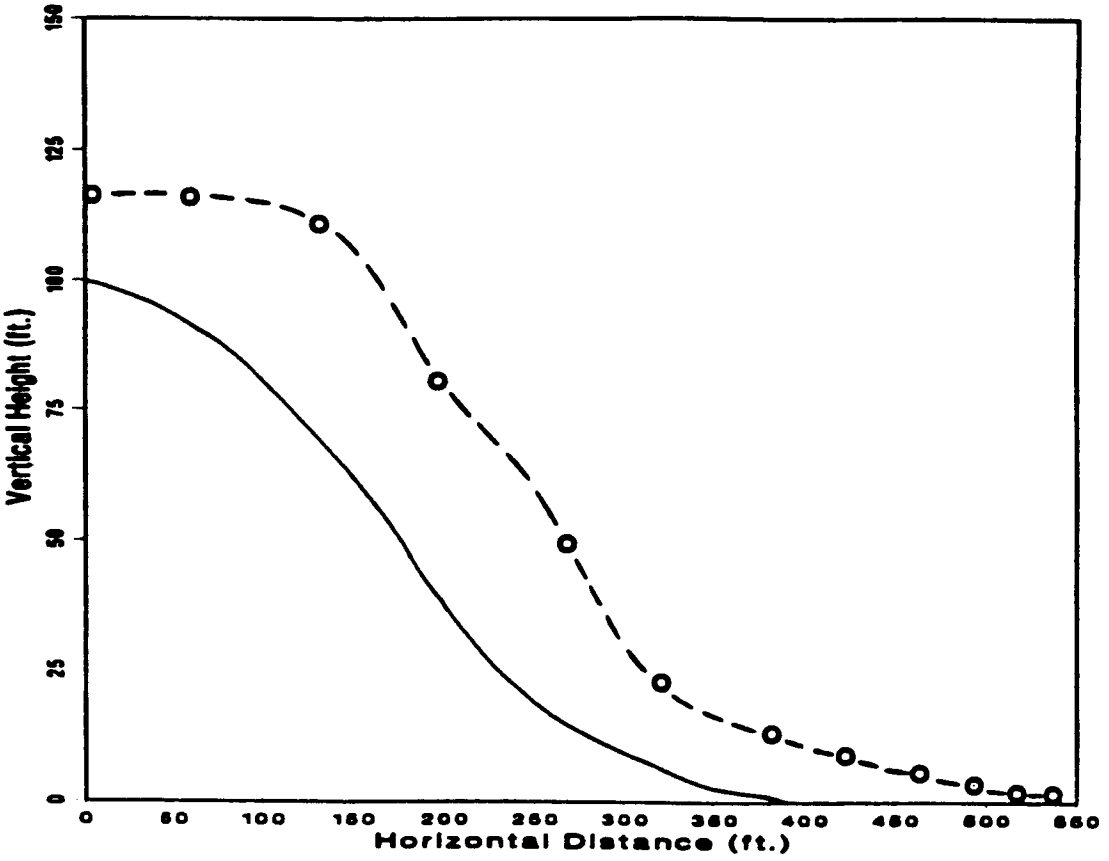

Figure 4.5.23 Comparison of Flight Data with Optimal Results Flight Trajectory

contrast, the computed results given in Figure (4.5.25) show that the collective is pulled earlier at an altitude of about 30 feet and is raised almost continuously until touchdown. Rear cyclic is applied at about 70 feet altitude to reduce the horizontal velocity. The maximum deviation of the TPP from horizontal during the descent is 24 degrees (in the nose-up direction). This angle is reduced progressively as the end-time is approached. The return of the thrust vector to the vertical is done because most of the forward speed of the vehicle has already been reduced as the end-time is approached. It also provides additional lift to cushion the touchdown. In an actual landing, the vehicle must be rotated to its landing attitude so as to provide sufficient clearance between the tail-rotor and the ground. This particular constraint is not included here because of our use of a point mass model.

4.5.4 Effects of Entry Height

Time histories of optimal thrust coefficient for entry conditions with approximately the same forward speed (8-12 knots), but at three different entry heights of 100, 230. and 420 feet, are compared in Figure (4.5.26). Since the computed flight time varies with the entry height, we change the independent variable from time t to the normalized time ξ. Figure (4.5.26) shows that the optimal thrust program changes with the entry height. In all three cases considered, $\frac{C_T}{\sigma}$ drops from its initial value of 0.063 (used before engine failure) to a lower value in order to reduce the initial RPM decay. This initial drop in $\frac{C_T}{\sigma}$ is most severe at the lower entry height of 100 feet. The reduction is relatively mild at higher entry heights of 230 and 420 feet.

After the initial reduction, the thrust coefficient then increases monotonically. The rate at which $\frac{C_T}{\sigma}$ is increased is again a function of the entry height. At the lower height of 100 feet, there is a relatively rapid increase in the thrust coefficient. Because of the upper bound on $\frac{C_T}{\sigma}$, the rate of increase levels off when the end-time

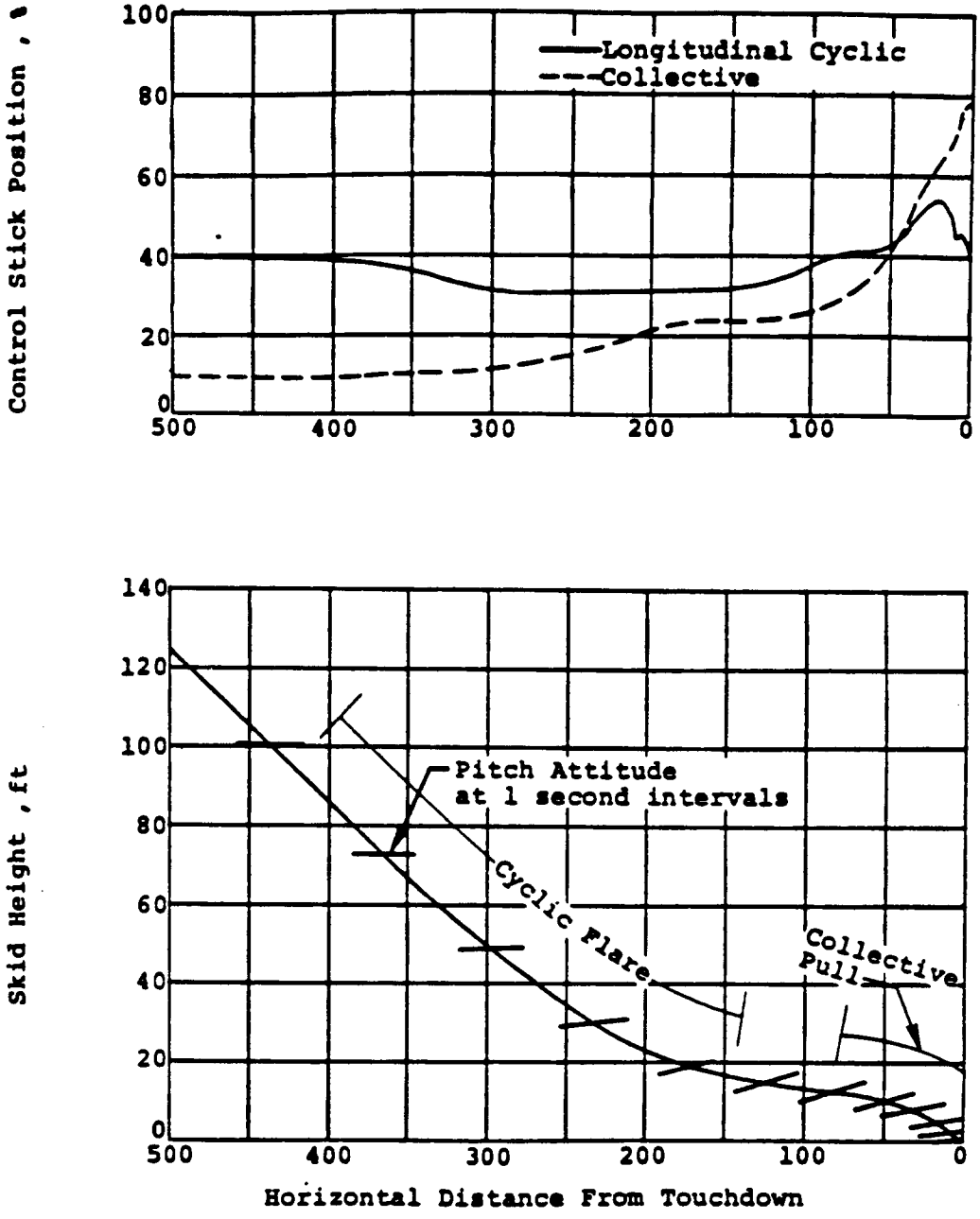

Figure 4.5.24 Flight Data for Autorotation Landing [12]
[Entry Condition : 125 feet, 45 knots]

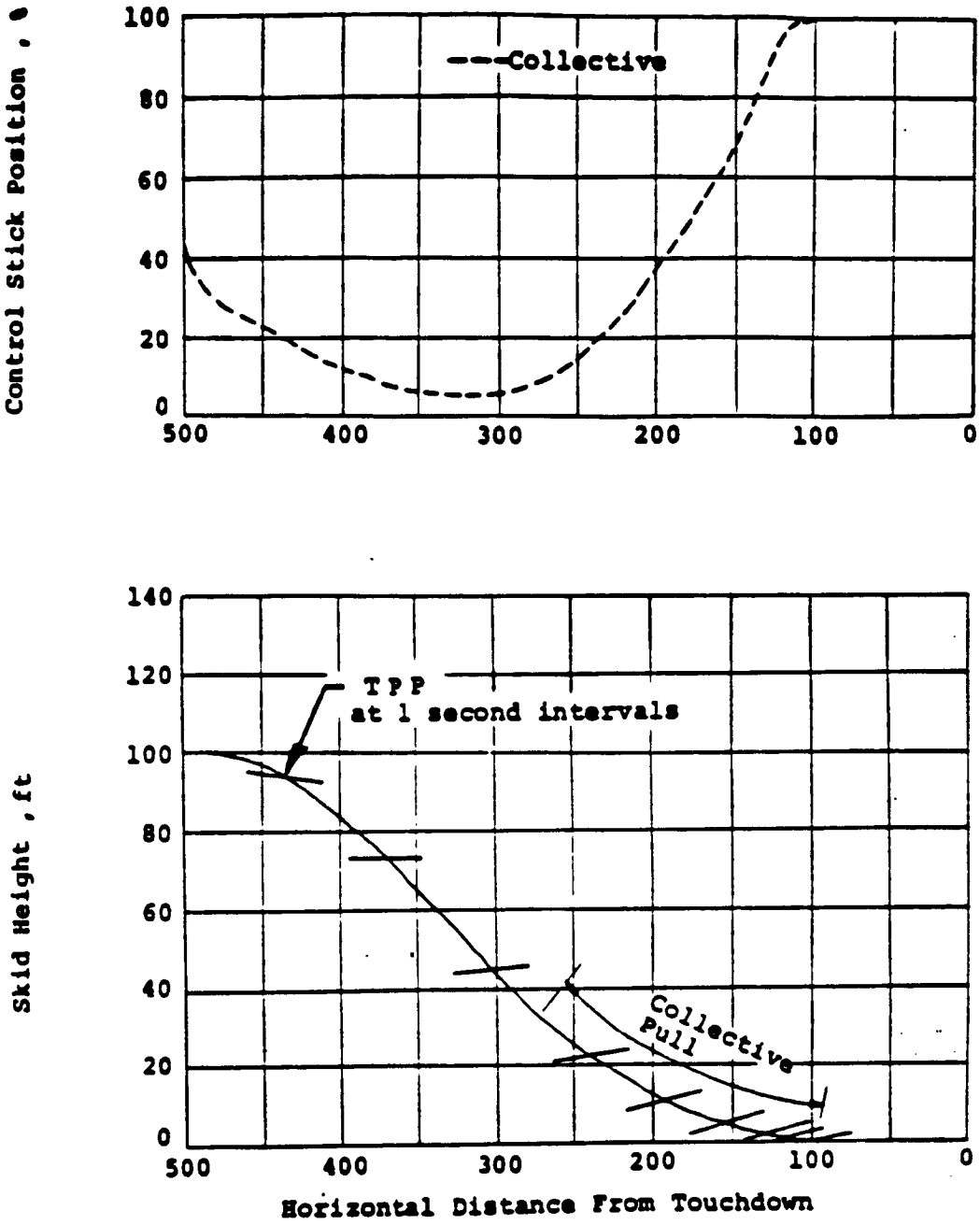

Figure 4.5.25 Computed Optimal Program for Autorotation Landing
[Entry Condition : 100 feet, 38 knots]

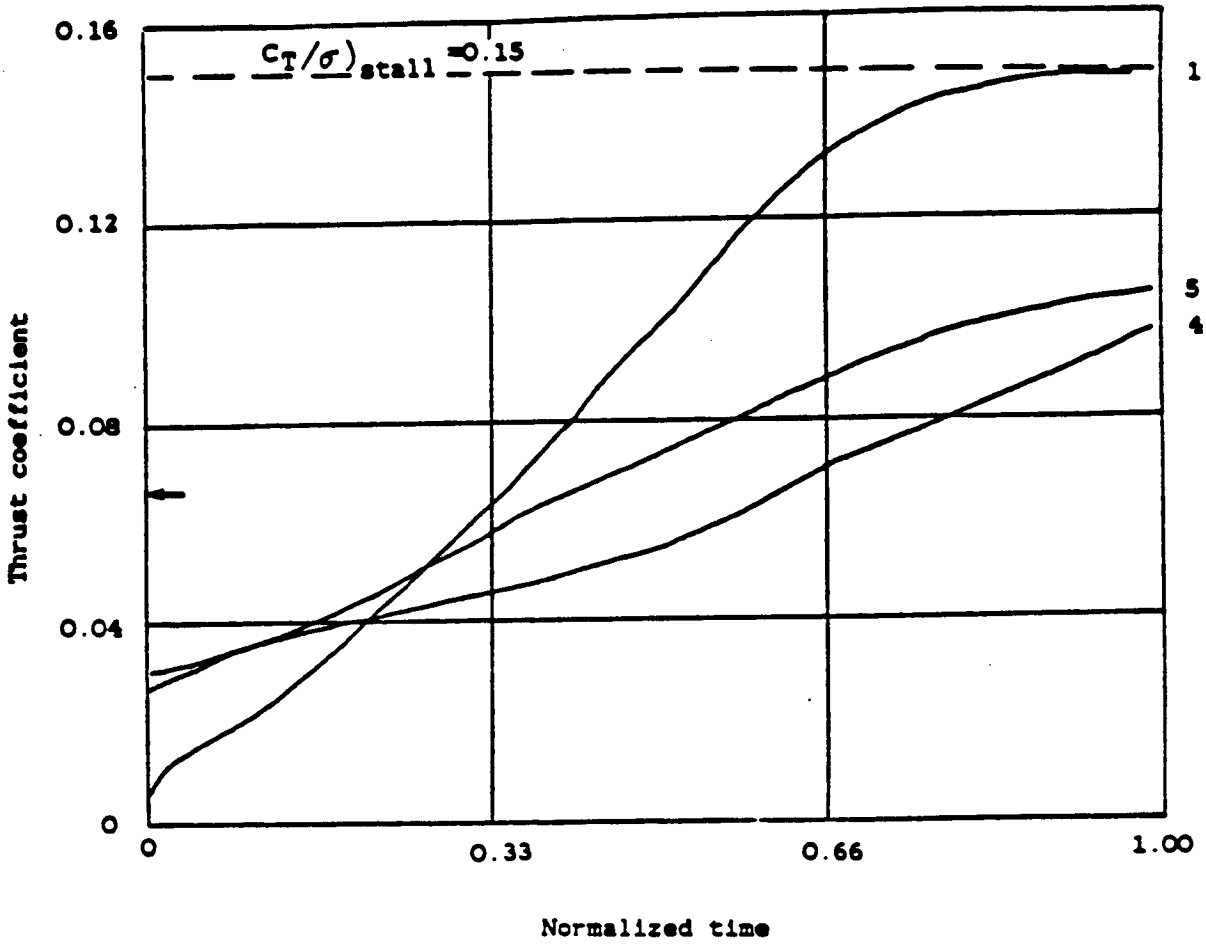

ENTRY CONDITION	1	5	4
ENTRY HEIGHT (ft.)	100	230	420
FLIGHT TIME (sec.)	5.5	9.3	11.3

Figure 4.5.26 Variations of Thrust Coefficients with Entry Height
[Entry Speed : 8-12 knots]

is approached. The thrust coefficient stays on its stall limit ($\frac{C_T}{\sigma} = 0.15$) over the last second of its travel in the optimal control program.

The same trend is followed in cases when engine failure occurs at the higher altitudes of 230 and 420 feet. However, the larger potential energy which is now available to the helicopter makes it unnecessary to have a large increase in thrust coefficient. This is because some of the potential energy of the helicopter can be traded for kinetic energy, and that the same increase in collective pitch produces a larger thrust at a higher forward speed than at a lower speed. Also. throughout the complete descent process, the stall limit is never reached. These observations agree with those found in the hover cases. In these cases, a "most critical entry height" (MCEH) exists from which the autoroational descent is more difficult to execute than from any other entry heights. This concept of MCEH can be extended to entry conditions with the same entry speed but different entry heights. As is indicated in Figure (4.5.26), with approximately the same entry speed of 8-12 knots, the autorotational landing from the entry height of 100 feet is more difficult to execute than from any other entry height.

Further insights from the optimal programs can be gained if we resolve the thrust coefficient into its horizontal and vertical components and plot these thrust components against the normalized time. Such a plot is given in Figure (4.5.27). Variation of C_{T_x} with the normalized time is qualitatively similar to that of the thrust coefficient shown in Figure (4.5.26). In all three cases considered, the horizontal component of thrust coefficient is positive for the first half (in time) of the descent, indicative of the use of forward cyclic to accelerate the helicopter to a higher speed. This forward acceleration, of course, cannot be continued for too long, and at around mid-time, rear cyclic is applied to decelerate the helicopter and prepare it for the final touchdown. Time histories of the forward speeds obtained with such

an acceleration/deceleration optimal control program are shown in Figure (4.5.28).

In Figure (4.5.28), the forward speed first increases, reaches a peak at around mid-time and then decreases to zero at touchdown: the higher the entry height, the larger the peak speed. The higher forward speed in turn increases the effectiveness of the rearward (nose-up) cyclic flare (i.e. with negative C_{T_x}). This explains why touchdown is made with progressively lower $\frac{C_T}{\sigma}$ value in Figure (4.5.26) as the entry height is increased.

4.5.5 Effects of Entry Speed

Time histories of optimal thrust coefficient with entry speeds of 12, 38, and 57 knots, all at an entry height of 100 feet, are compared in Figure (4.5.29). Entry height of 100 feet is selected because of the "criticality" of this height discussed previously. Optimal time variations of the horizontal and vertical components of the thrust vector are given in Figure (4.5.30). Time variations of forward speed for these entry conditions are given in Figure (4.5.31).

Figure (4.5.29) shows the effect that entry speed has on the thrust program. The time variation of $\frac{C_T}{\sigma}$ in entry condition 1, which is the case considered in Section (4.5.4), consists of an initial drop in $\frac{C_T}{\sigma}$, followed immediately by a steady increase that levels off as the end-time is approached. Variations in cases with higher entry speeds are qualitatively similar to that of the first case. The higher the entry speed, the larger is the kinetic energy available to the helicopter in its execution of the autorotation landing. Since the effectiveness of the rearward cyclic flare increases with flight path velocity, there is no need for a large increase in collective at the end of the maneuver for entries with high forward speed. Hover, a condition with zero forward speed, is therefore the most critical case to execute an autorotation landing for any given entry height.

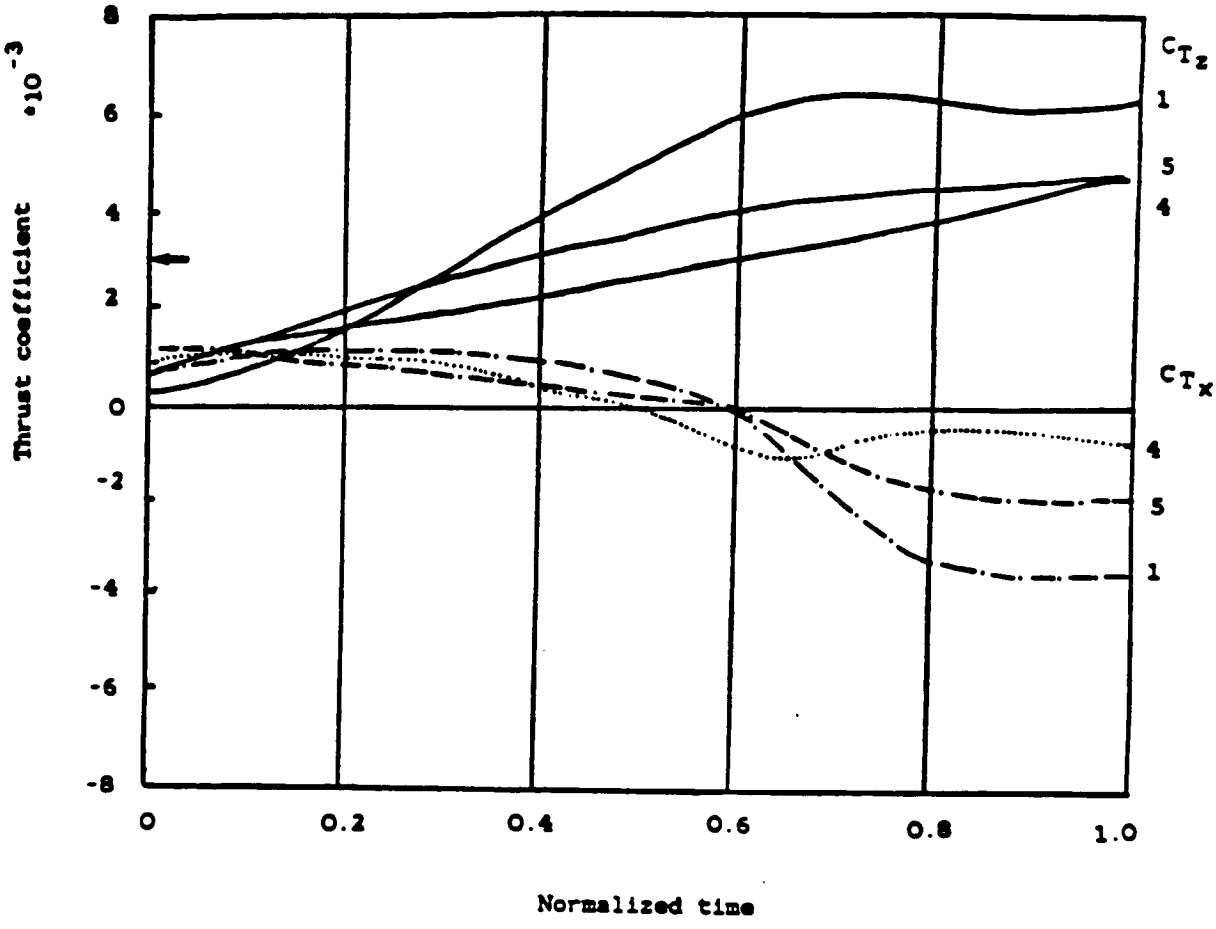

ENTRY CONDITION	1	5	4
ENTRY HEIGHT (ft.)	100	230	420
FLIGHT TIME (sec.)	5.5	9.3	11.3

Figure 4.5.27 Variations of Horizontal and Vertical Thrust Components with Entry Height [Entry Speed: 8-12 knots]

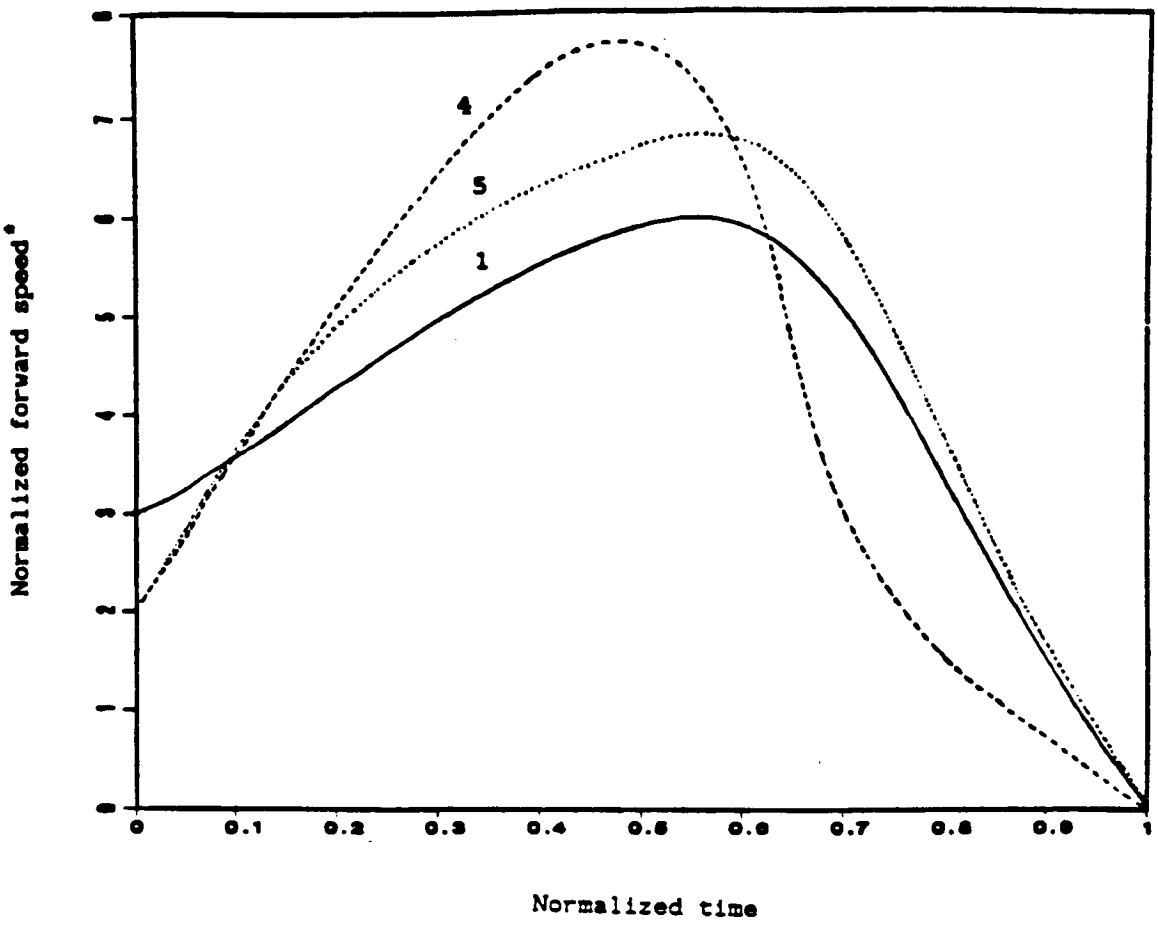

* 1 unit=3.8 Knots

ENTRY CONDITION	1	5	4
ENTRY HEIGHT (ft.)	100	230	420
FLIGHT TIME (sec.)	5.5	9.3	11.3

Figure 4.5.28 Optimal Time Histories of Forward Speed at different Entry Heights [Entry Speed : 8-12 knots]

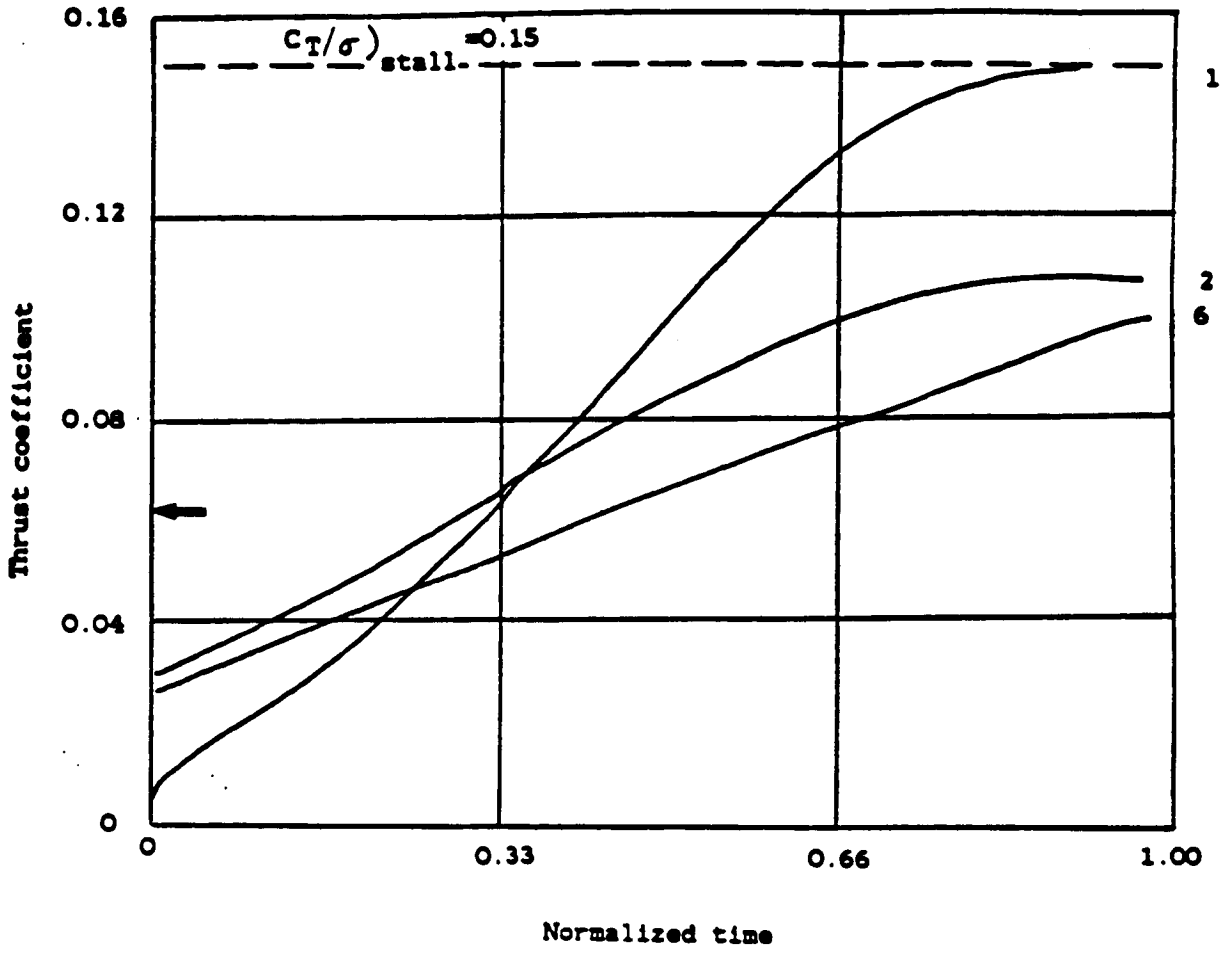

ENTRY CONDITION	1	2	6
ENTRY SPEED (Knots)	12	38	57
FLIGHT TIME (sec.)	5.5	8.7	10.4

Figure 4.5.29 Variations of Thrust Coefficients with Entry Speed [at Entry Height of 100 feet]

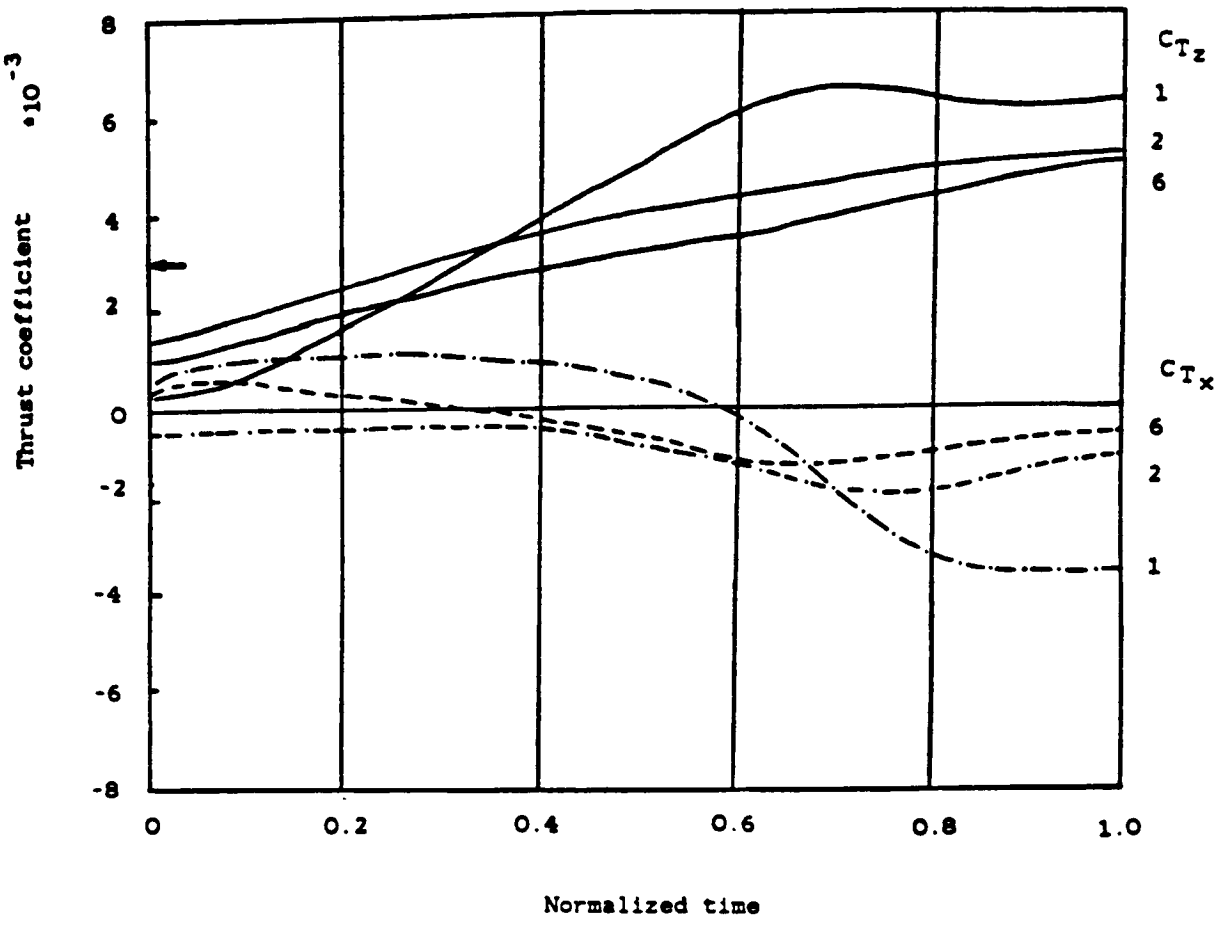

ENTRY CONDITION	1	2	6
ENTRY SPEED (Knots)	12	38	57
FLIGHT TIME (sec.)	5.5	8.7	10.4

Figure 4.5.30 Variations of Horizontal and Vertical Thrust Components with Entry Speed [at Entry Height of 100 feet]

An interesting feature of the optimal program is observed in Figure (4.5.30). With the same entry height of 100 feet, we note the change in the C_{T_z}-program with entry speed. If the forward speed at the time of power loss is relatively low (e.g. 12 knots), forward cyclic must be used to accelerate the helicopter to a higher forward speed before the aft cyclic is initiated to slow it down for the touchdown. At an intermediate speed of 38 knots, there is but a brief period of forward acceleration. At the highest forward speed considered (57 knots), aft cyclic must be applied immediately after engine failure in order to decelerate the helicopter in time for the final touchdown. Time variations of forward speeds in these three cases considered are given in Figure (4.5.31).

4.5.6 Best Endurance Speed

The need to accelerate the helicopter to a higher forward speed when engine failure occurs at low entry speeds and to decelerate it when power is lost at high speeds indicates the existence of some intermediate speed at which the helicopter is neither accelerated nor decelerated. To reduce workload, a pilot might prefer to initiate an autorotation landing from this speed.

This "preferred" speed can be better understood if we study the effect of forward speed on the energy consumption of a helicopter in level, powered flight. Total power consumption is the sum of induced power loss of the rotor, blade profile power loss, fuselage parasite power loss, and tail rotor power. Tail rotor power and blade profile power are not strong functions of the forward velocity. In contrast, induced power loss decreases drastically with increased forward velocity while the parasite power loss increases with the third power of the forward velocity. Figure (4.5.32), which shows variations of the various power terms with forward speed, has the characteristic "bucket" shape. The speed for best endurance is the speed at

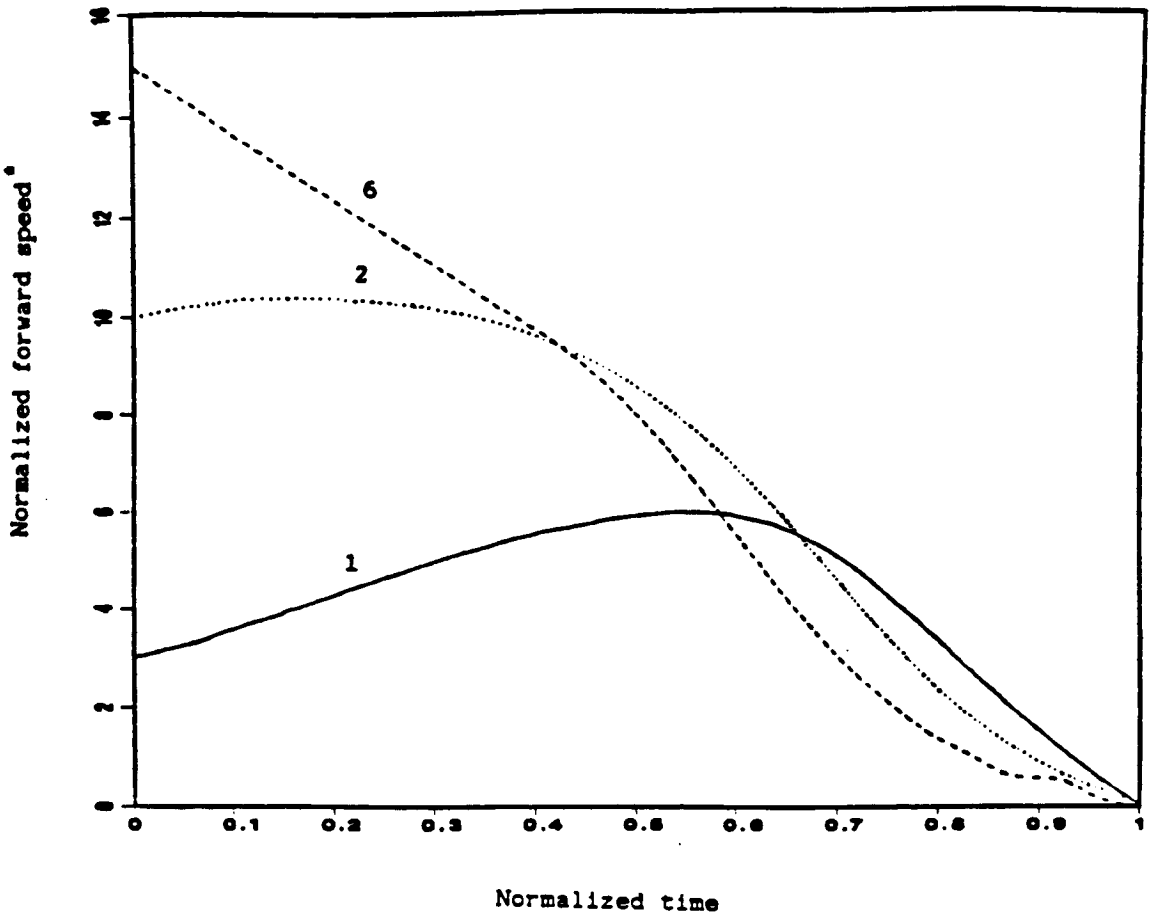

* 1 unit=3.8 Knots

ENTRY CONDITION	1	2	6
ENTRY SPEED (Knots)	12	38	57
FLIGHT TIME (sec.)	5.5	8.7	10.4

Figure 4.5.31 Variation of Forward Speed with Entry Speed at Entry Height of 100 feet

which the power-required curve is at its minimum. The speed for best range, which is usually slightly higher than the speed for best endurance, is the speed at which the power-required curve is tangent to a line drawn through the origin. This is also the point at which the ratio of speed to power (and therefore, of distance to fuel) is greatest.

In autorotation, steady flight can be achieved only by descending. The rate of steady autorotative descent is once again a strong function of the forward speed of the helicopter. Appendix (A) presents a way to compute the rate of steady descent at different forward speeds. The rate of steady descent in autorotation of the OH-58A helicopter considered here is shown in Figure (4.5.33). Again, we see the characteristic "bucket" shape, indicative of some intermediate speed at which the rate of descent is a minimum. The forward speed with the minimum rate of descent is the same as the speed for best endurance shown in Figure (4.5.32). This speed for the OH-58A helicopter is at around 45-50 knots.

From the point of view of energy mangement, the optimal control program tries to fly the helicopter at a speed which minimizes the power loss. The optimal program achieves this by accelerating or decelerating the helicopter to a higher or lower forward speed as the case may be. However, we note that results shown in both Figures (4.5.32) and (4.5.33) are obtained with the helicopter in a steady state condition. Since the optimal results are in the transient state, we cannot compare these optimal results with those shown in the figures directly. Nevertheless, it is still not too surprising to see that the optimal program has avoided both high and low forward speed with very high power consumption.

§4.6 Optimal Descent of a Helicopter with a bound on Vertical Sinkrate

In the last section, we presented and interpreted some of the results obtained from

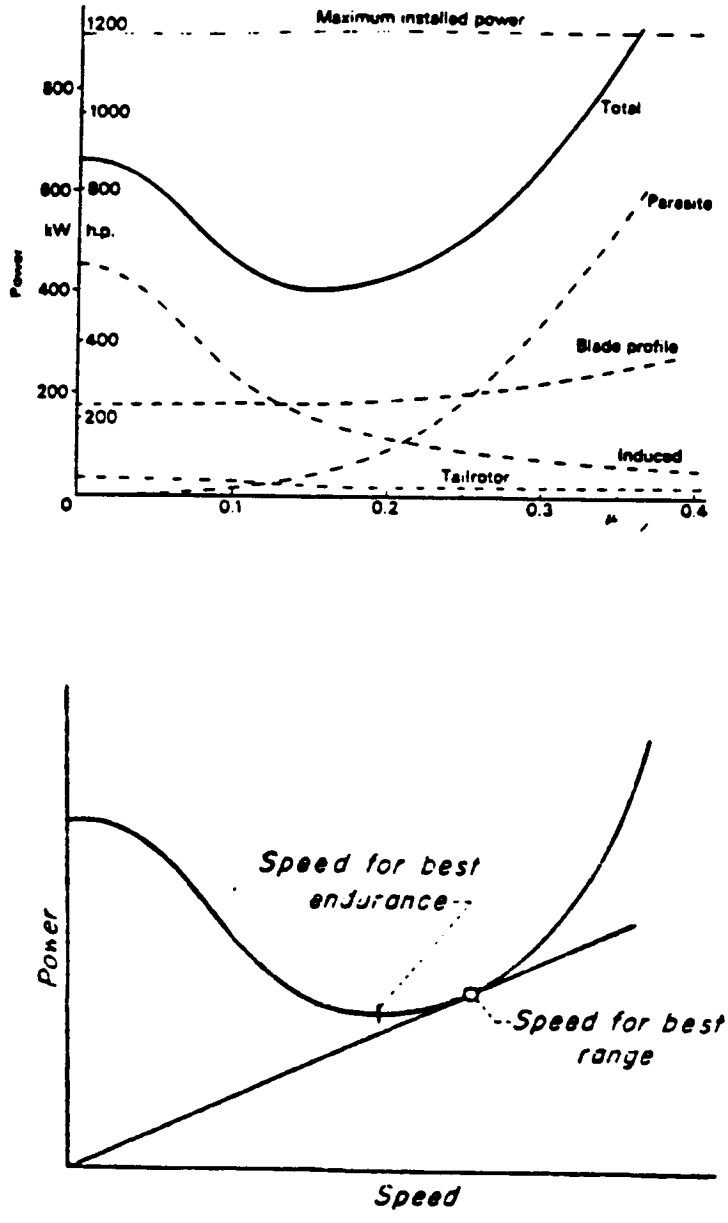

Figure 4.5.32 Variation of Power with Forward Speed

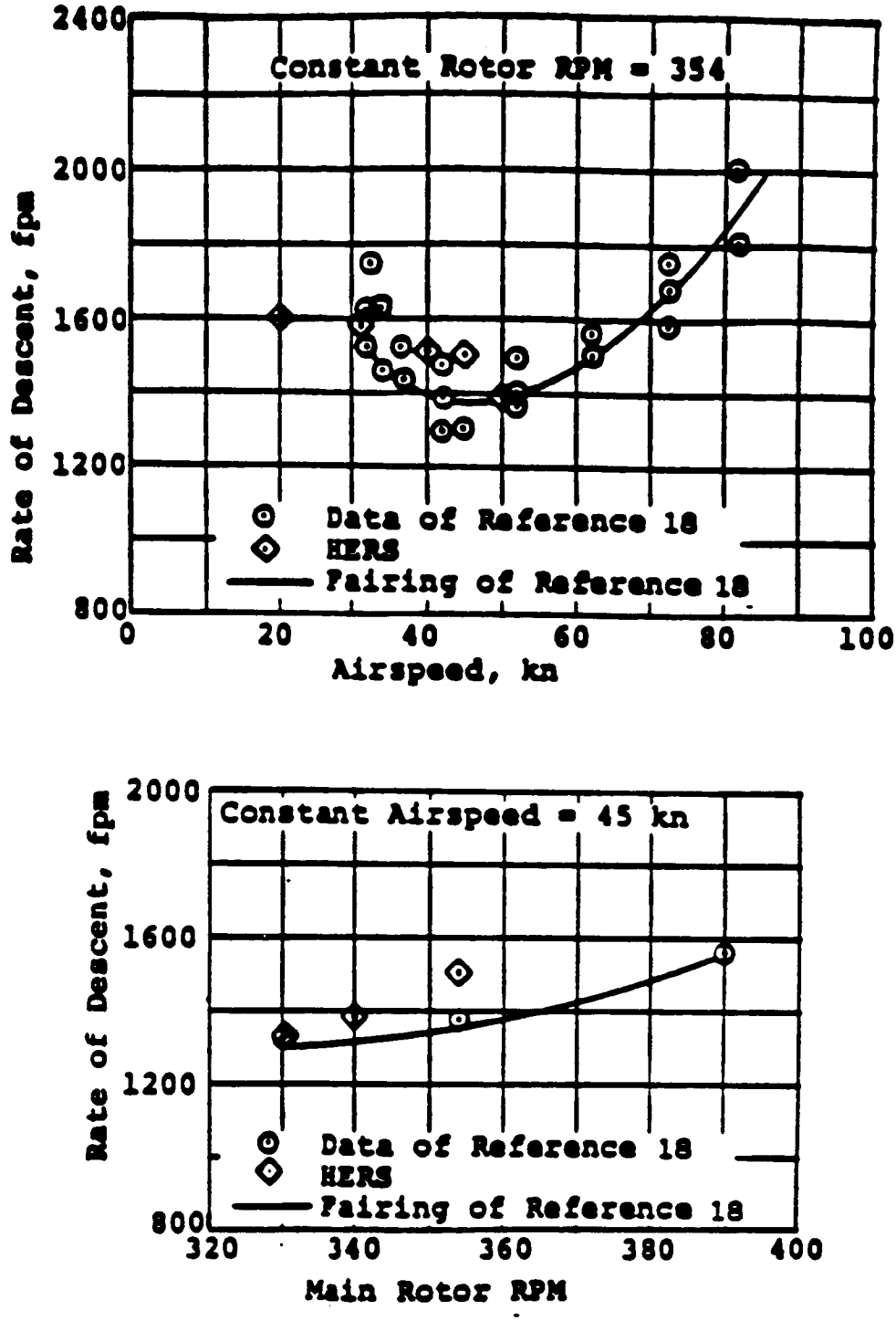

Figure 4.5.33 Variation of Steady Rate of Descent with Forward Speed of an OH-58A Helicopter

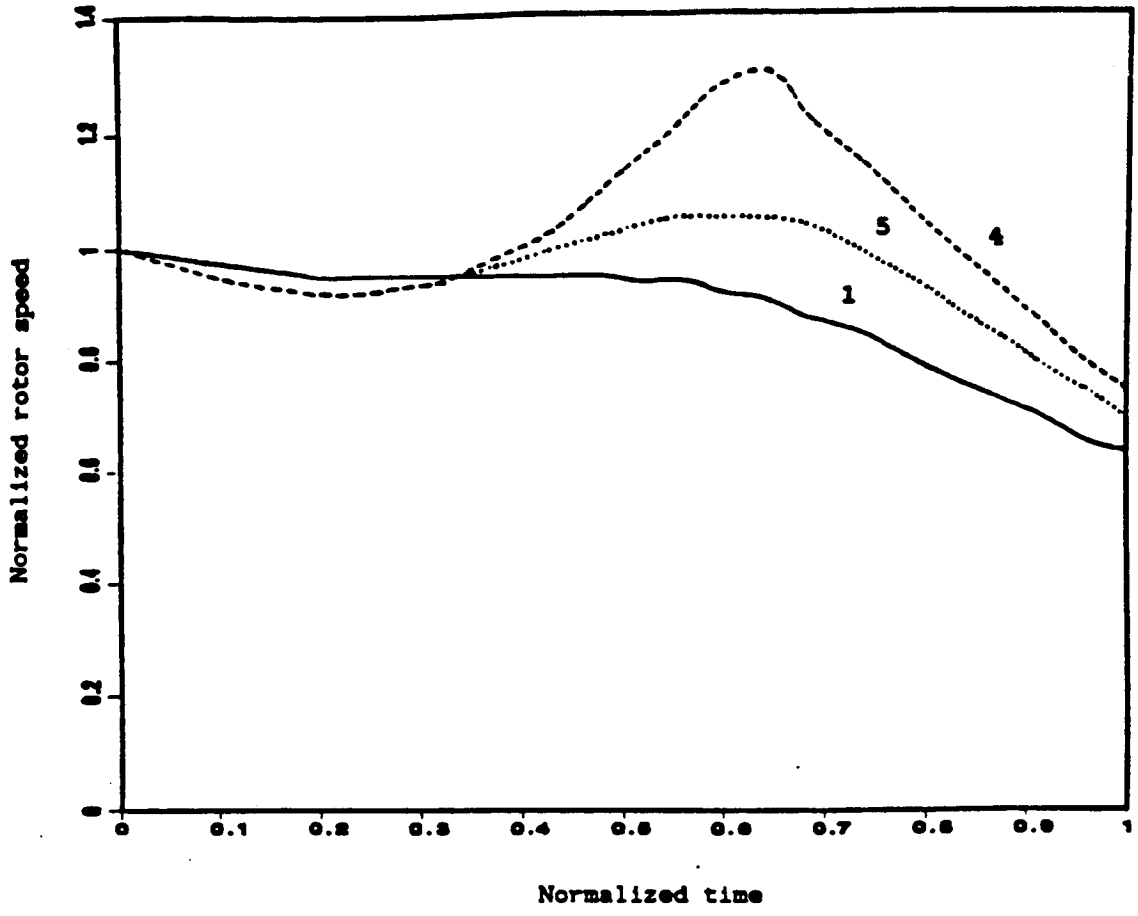

ENTRY CONDITION	1	5	4
ENTRY HEIGHT (ft.)	100	230	420
FLIGHT TIME (sec.)	5.5	9.3	11.3

Figure 4.5.34 Time Variations of Rotor Speed
[Entry Speed : 8-12 knots]

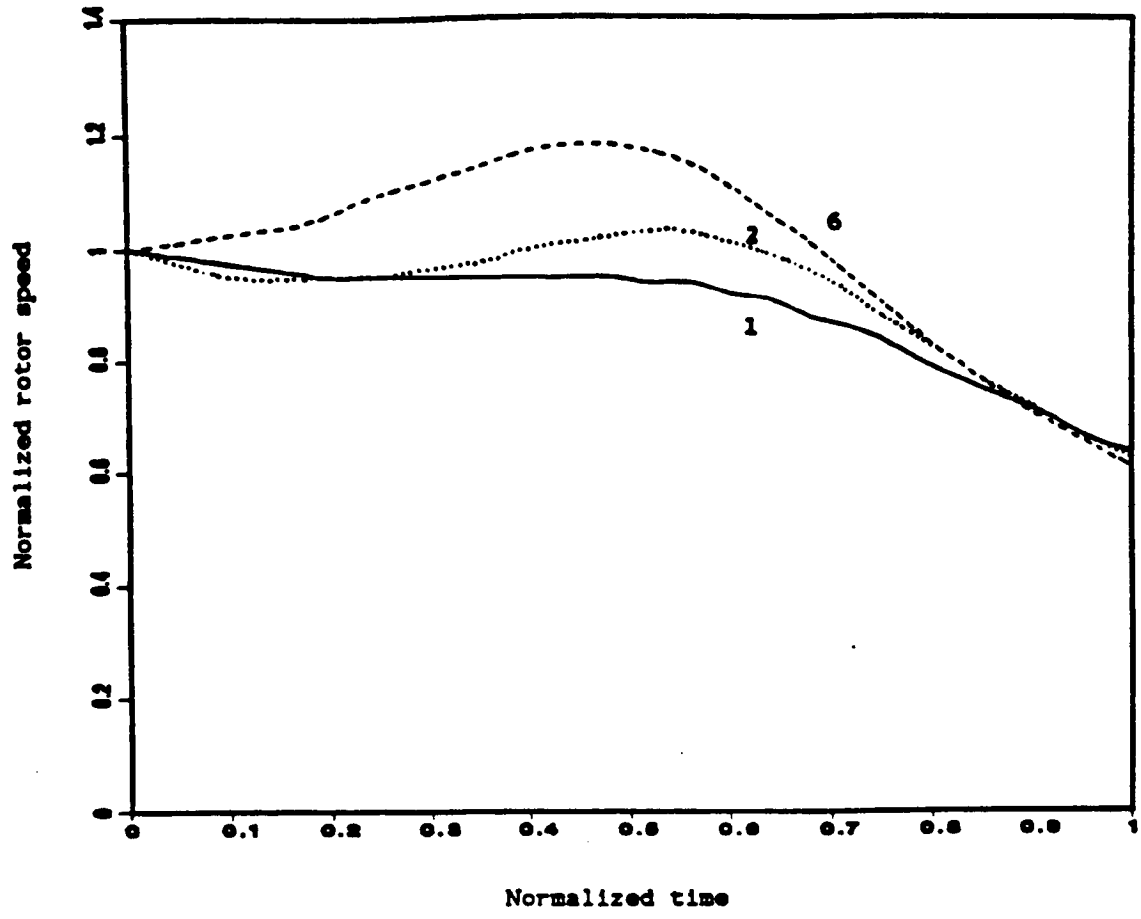

ENTRY CONDITION	1	2	6
ENTRY SPEED (Knots)	12	38	57
FLIGHT TIME (sec.)	5.5	8.7	10.4

Figure 4.5.35 Time Variations of Rotor Speed
[Entry Height : 100 feet]

computations of optimal descents of a helicopter in forward flight. The optimal descents of the HERS from entry conditions either with a high forward speed or at a high altitude result in peak rates of descent that are unacceptably high to pilot, and to overspeeding of the rotor during the rearward cyclic flare.

To remedy this problem, we add an upper bound on the vertical sink-rate of the helicopter to the optimal landing problem. The new problem, with an additional state variable inequality constraint is given in Section (3.3). An entry condition with a 7.7-knot initial speed at an initial altitude of 423 feet was selected for the present study. This entry condition was used because the optimal descent of the HERS with this particular entry condition results in unacceptably high peak descent velocity. Results obtained with the optimal descent of the HERS from this entry condition and subjected to a descent velocity bound are presented in this section.

4.6.1 Optimal Descent of a Helicopter with a Descent Velocity Bound

If the optimal rate of descent of the helicopter in the unbounded solution exceeds the upper bound, it is reasonable to assume that the optimal time variation of the descent velocity in the solution to the new problem will resemble that shown in Figure (4.6.36). The helicopter starts initially with a zero rate of descent. This rate then increases, touches and stays on its upper bound for a period of time. Finally, the rate of descent is reduced so as to allow for a soft touchdown. Typically, this time variation of the descent velocity consists of three phases. These phases of entry, steady descent, and landing flare are shown in Figure (4.6.36).

The amount of time that the helicopter spends in each of these phases depends on the magnitude of the descent velocity bound, $[V_D]_{max}$. Generally speaking, the higher the descent velocity bound, the shorter the time spent in the steady descent phase. As illustrated in Figure (4.6.37), the steady descent phase ceases to exist

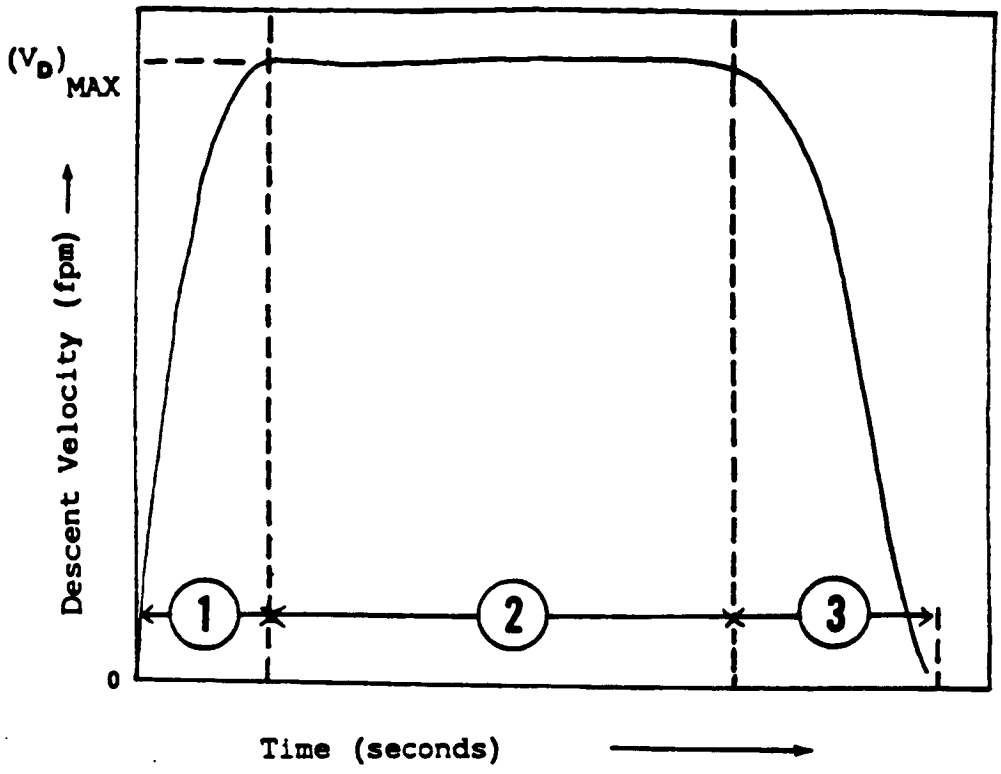

(1) Entry Phase : $\frac{dV_D}{dt}$ = positive,
[phase ends with $V_D = (V_D)_{max}$]

(2) Steady Descent Phase : $\frac{dV_D}{dt}$ = zero,
[$V_D = (V_D)_{max}$]

(3) Landing Flare Phase ; $\frac{dV_D}{dt}$ = negative,
[phase ends with $V_D \simeq 0$]

Figure 4.6.36 Time Rate of Change of Descent Velocity with a $[V_D]_{max}$ Bound

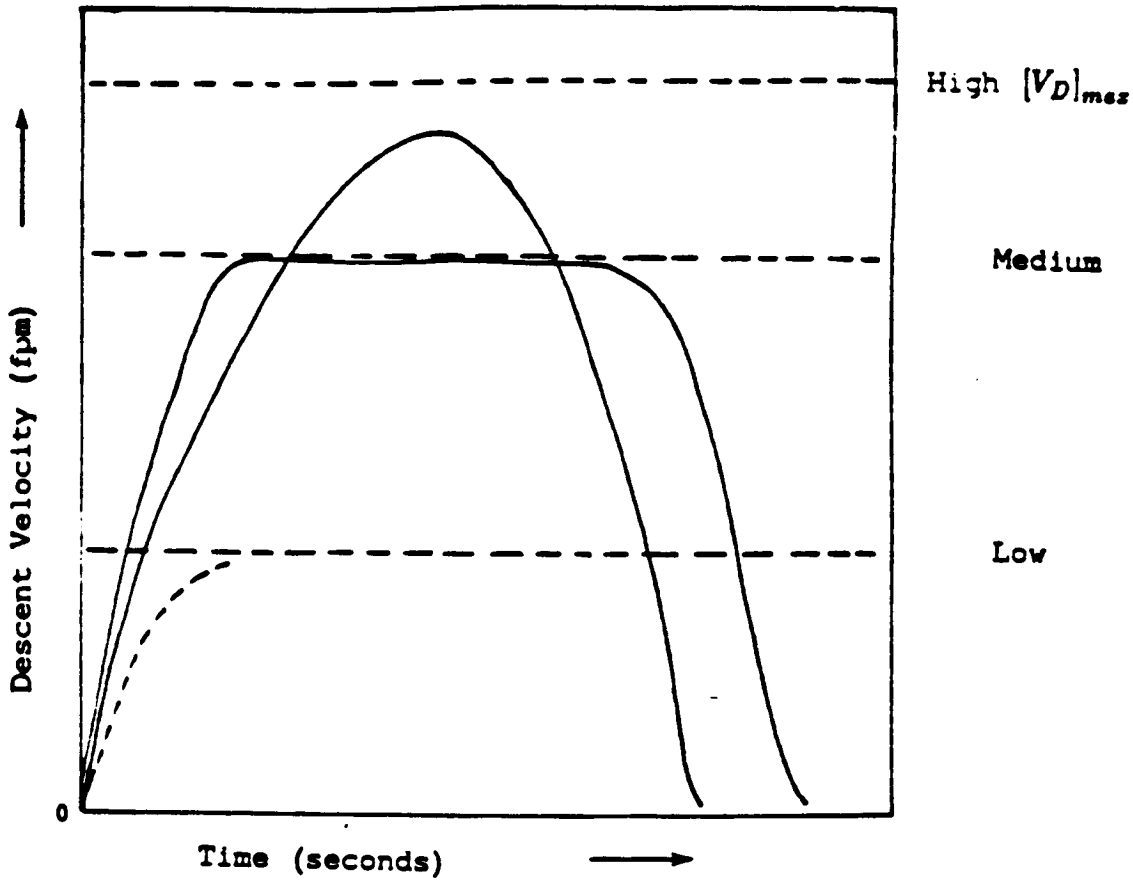

(1) High $[V_D]_{max}$: The variation is essentially that without a descent velocity bound.

(2) Medium $[V_D]_{max}$: The variation consists of the entry, steady descent and landing flare phases.

(3) Low $[V_D]_{max}$: No feasible solution exists in this case.

Figure 4.6.37 Time Variation of Descent Velocity with Different Values of $[V_D]_{max}$

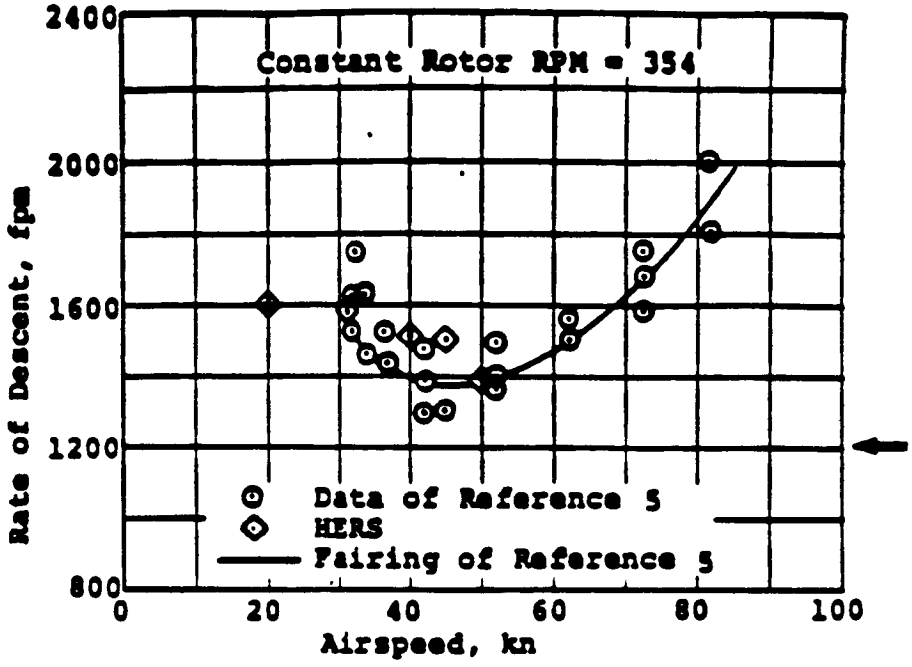

Figure 4.6.38 Variation of Steady Autorotative Sink-rate of the HERS with Forward Airspeed

when the $[V_D]_{max}$-bound is chosen too high. In this case, the variation of the descent velocity becomes essentially that without the descent velocity bound. The other extreme is when the $[V_D]_{max}$-bound selected is too low, e.g., at around 1200 fpm. As can be seen from Figure (4.6.38), the horizontal line $[V_D]_{max} = 1200\ fpm$ does not intersect the curve which shows the variation of the steady autorotative sink-rate of the HERS with its forward airspeed. Therefore, no feasible control exists that will allow the helicopter to autorotate at a steady sink-rate of 1200 fpm.

An intermediate value of 1800 fpm was selected as an upper bound on the vertical sink-rate of the helicopter in autorotative descent. From here on we shall use the term "nominal case" to represent the autorotative descent of the HERS from an entry condition with a 7.7-knots forward airspeed, at an initial altitude of 423 feet, and having a 1800 fpm bound on its vertical sink-rate.

The time variations of the C_{T_x}, C_{T_z}, $\frac{C_T}{\sigma}$, and the collective pitch for the nominal case are given in Figure (4.6.39)-(4.6.40). With reference to the C_{T_z}-curve, one can see a natural division of the autorotative landing maneuver into the three phases mentioned earlier. Similar divisions can also be observed in both the time histories of the collective pitch and the thrust coefficient.

An approximate Solution of the C_{T_z}

During the steady descent phase, when the sink-rate of the helicopter stays close to the value $[V_D]_{max}$, the vertical component of the thrust coefficient C_{T_z}, can be determined using the following approximations. During the steady descent phase, the time rate of change of the helicopter's sink-rate is near zero. By equating the

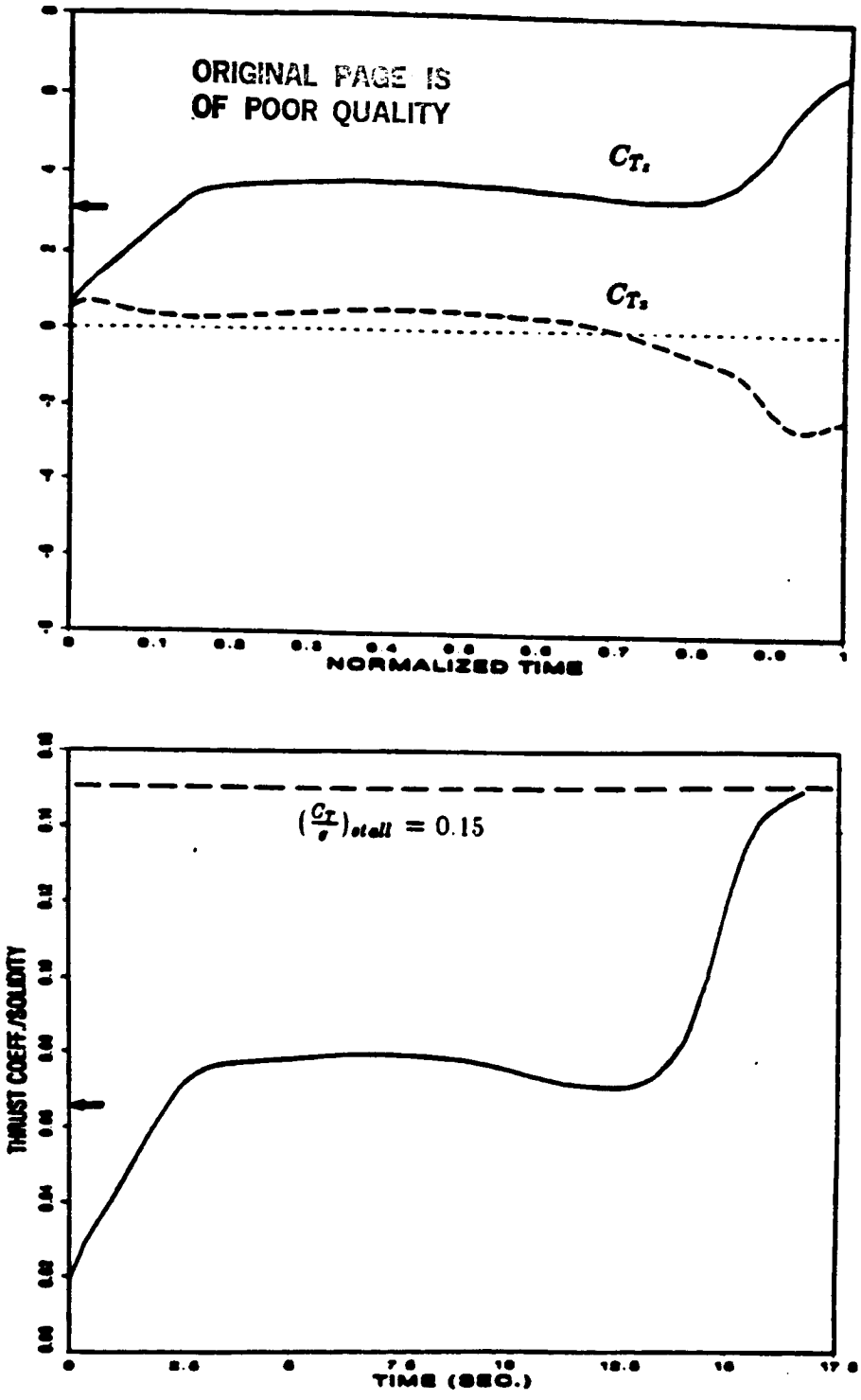

Figure 4.6.39 Time Variations of the Thrust Coefficient and its Horizontal and Vertical Components

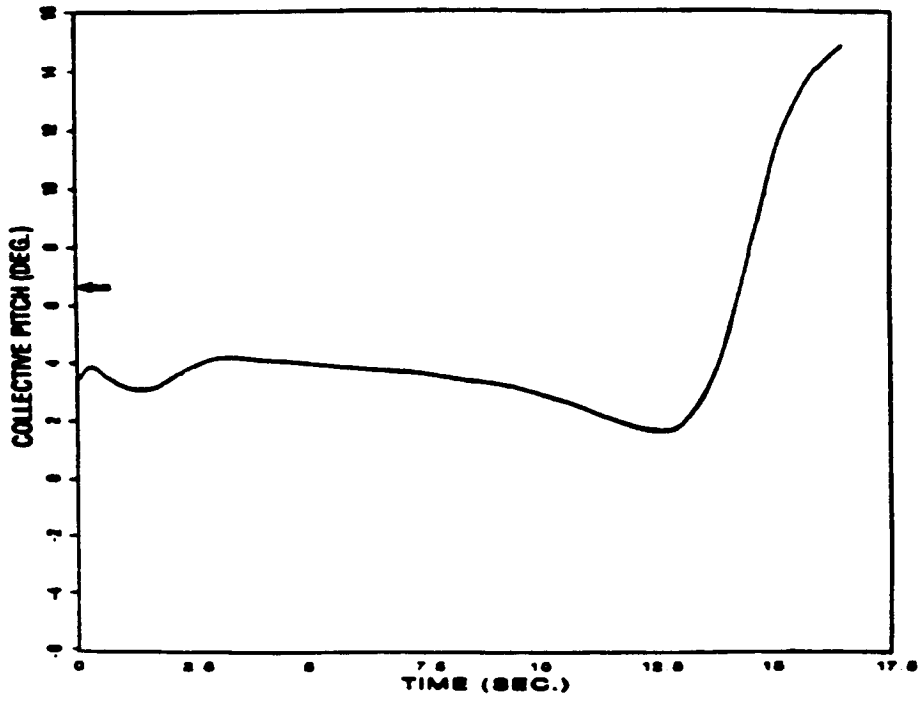

Figure 4.6.40 Time Variation of the Collective Pitch with a Descent Velocity Bound

LHS of the first equation of Appendix (A) to zero. we obtain

$$\begin{aligned} 0 &= g_0 - m_0(u_1 x_3^2 + \bar{f} x_1 \sqrt{x_1^2 + x_2^2}) , \\ \frac{g_0}{m_0} &= u_1 x_3^2 + \bar{f} x_1 \sqrt{x_1^2 - x_2^2} . \end{aligned} \tag{34}$$

Since $\frac{g_0}{m_0} = 3.02$, $\bar{f} = 0.0306$, and magnitudes of both x_1, x_2 and x_3 are of the order of 1. the second term in equation (34) (i.e., the parasite-drag term, $\bar{f} x_1 \sqrt{x_1^2 - x_2^2}$) may be neglected. Therefore, we obtain the approximate relation:

$$\begin{aligned} \frac{g_0}{m_0} &= 3.02 , \\ &= u_1 x_3^2 . \end{aligned} \tag{35}$$

which can be used to estimate the value of the normalized vertical thrust coefficient u_1.

If the angular speed of the main rotor does not vary too much during the steady descent phase. the normalized rotor speed x_3 can be approximated by its mean value $[x_3]_{mean}$. Therefore the approximate value of u_1 in the steady descent phase is given by:

$$\begin{aligned} u_1 &= \frac{g_0}{m_0 (x_3)_{mean}^2} , \\ &= \frac{3.02}{(0.95)^2} , \\ &= 3.33 . \end{aligned} \tag{36}$$

where we have used a value of 0.95 for the average normalized rotor speed ($(x_3)_{mean}$) in the steady descent phase (see also Figure (4.6.43)). The computed value of 3.33 for the vertical component of the thrust coefficient in the steady descent phase agrees well with the value 3.7 found in the optimal solution (see Figure (4.6.41)).

4.6.2 Comparisons between Results Obtained With and Without

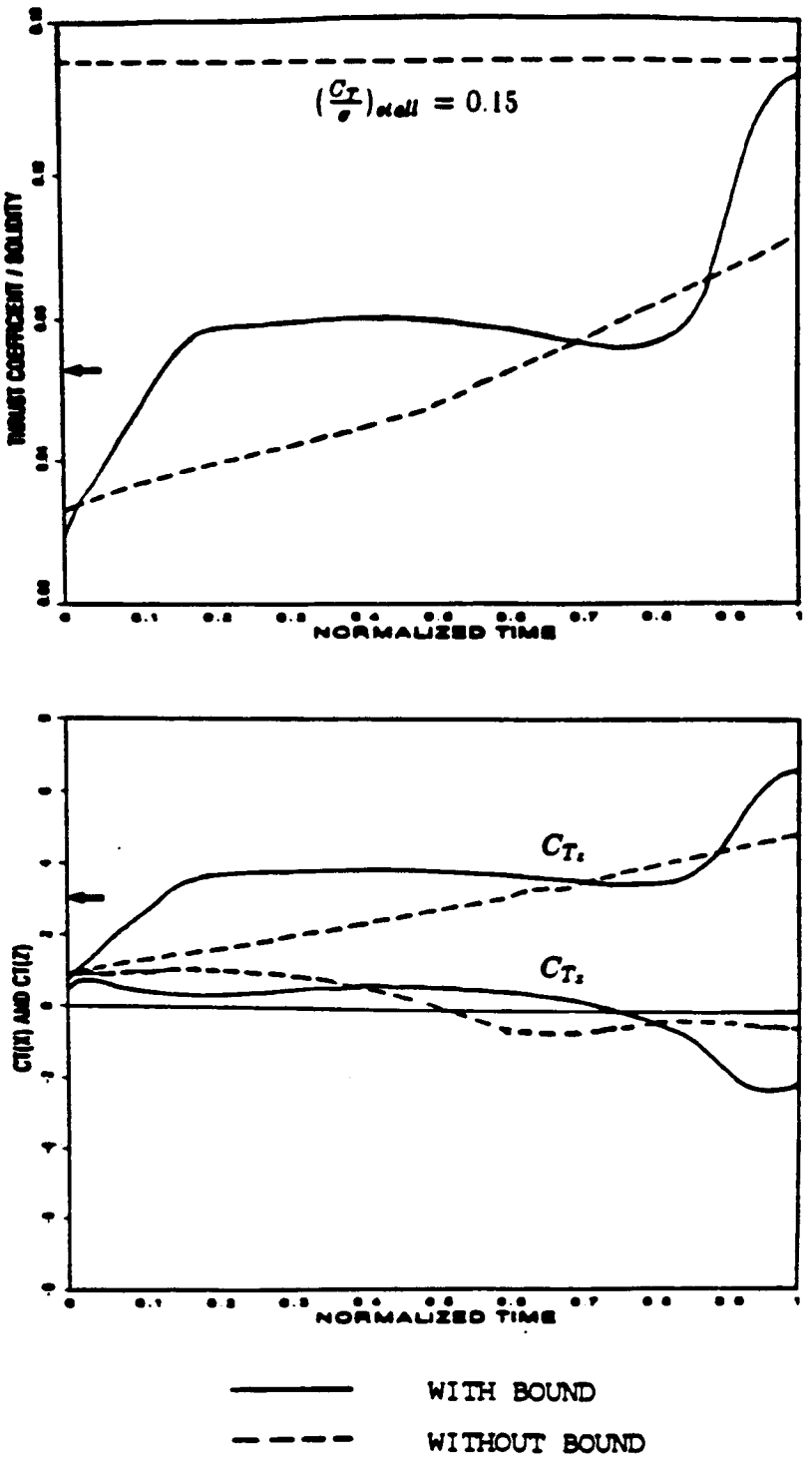

Figure 4.6.41 Time Variations of the Thrust Coefficients With and Without a $[V_D]_{max}$-Bound

the Descent Velocity Bound

Figure (4.6.41) compares the time variations of the thrust coefficient obtained from optimal control programs with and without a descent velocity bound. The latter consists of an initial drop in the collective pitch control. This is followed by a gradual, steady increase in the thrust coefficient till the final touchdown. The case with the descent velocity bound is characterized by phases:

(1) The entry phase consists of a similar sharp drop in the thrust coefficient to preserve the rotor RPM. This is followed by a steady increase in the thrust until the steady state value of 0.08 is reached.

(2) In the steady descent phase, the thrust coefficient is maintained at a constant value of 0.08.

(3) The landing maneuver ends with a rapid increase in the collective pitch when touchdown is imminent. This rapid control movement is a special feature in the landing flare phase of the optimal, autorotative descent of a helicopter with a descent velocity bound.

As was found in the case without a descent velocity bound, the horizontal component of the thrust coefficient C_{T_x}, shown in Figure (4.6.39) is initially positive for this particular case with a low entry speed. The helicopter is initially accelerated to a higher forward velocity. The thrust vector must eventually be rotated backward to decelerate the vehicle for a safe landing. This reversal in the sign of the horizontal thrust component has been delayed when compared with results found in the case without the descent velocity bound.

The time histories of the descent velocity, forward speed, rotor RPM, as well as the optimal trajectory obtained for the nominal case are given in Figures (4.6.42)-(4.6.43).

The time histories of the helicopter's descent velocity obtained from optimal control programs with and without an upper bound on the descent velocity is compared in Figure (4.6.44). Those for the helicopter's forward speed and the angular speed of the main rotor are compared in Figure (4.6.45). It is apparent from Figure (4.6.44), that "peaking" of the descent velocity has been effectively suppressed after the introduction of an upper bound on the descent velocity. To cover the same vertical distance of 423 feet, the flight time in the case with a $[V_D]_{max}$-bound has been lengthened. The touchdown time has increased from 11.3 seconds in the case without the $[V_D]_{max}$-bound to 16.3 seconds in the case with the bound.

The time variations of the helicopter's forward speed with and without the descent velocity bound are compared in Figure (4.6.45). These variations are qualitatively similar. In both cases, the forward speed of the helicopter first increases, reaches a maximum before it is decreased to near zero at touchdown. The time at which the maximum forward speed is reached in the case with the descent velocity bound has been delayed when compares with that without the descent velocity bound. This is due mainly to the late rotation of the thrust vector to the rearward direction as explained before.

Differences in the time variations of the main rotor RPM in cases with and without the $[V_D]_{max}$-bound are most significant. In the case without the $[V_D]_{max}$-bound, the peak angular speed of the rotor is about 30 percent higher than its nominal value of 353 *rpm*. Figure (4.6.45) clearly shows that this "peaking" in the angular speed of the rotor has been suppressed as a result of bounding the vertical sink-rate. The

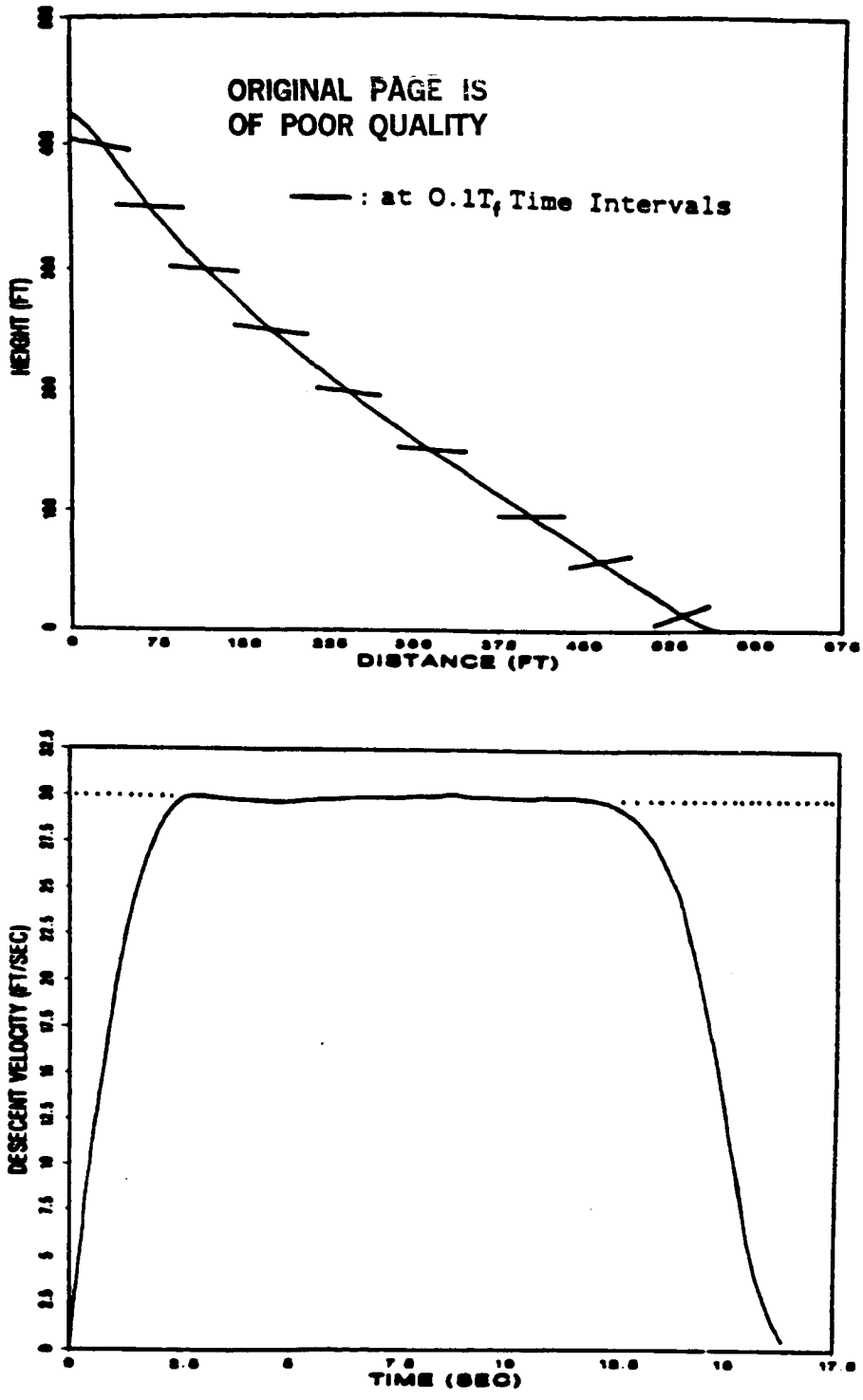

Figure 4.6.42 Time Variation of the Descent Velocity and the Optimal Flight Profile

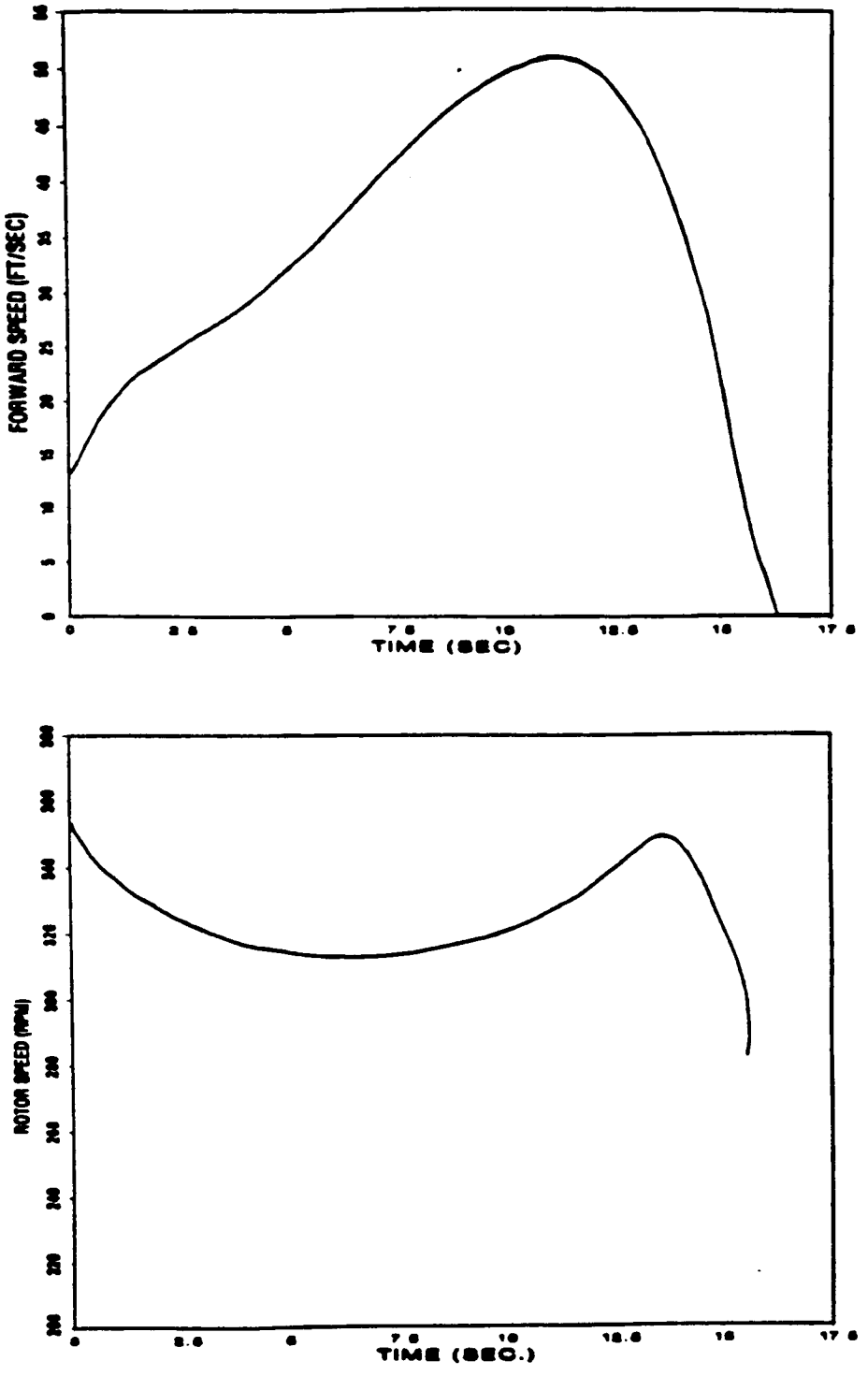

Figure 4.6.43 Time Variations of the Forward Speed and the Rotor RPM

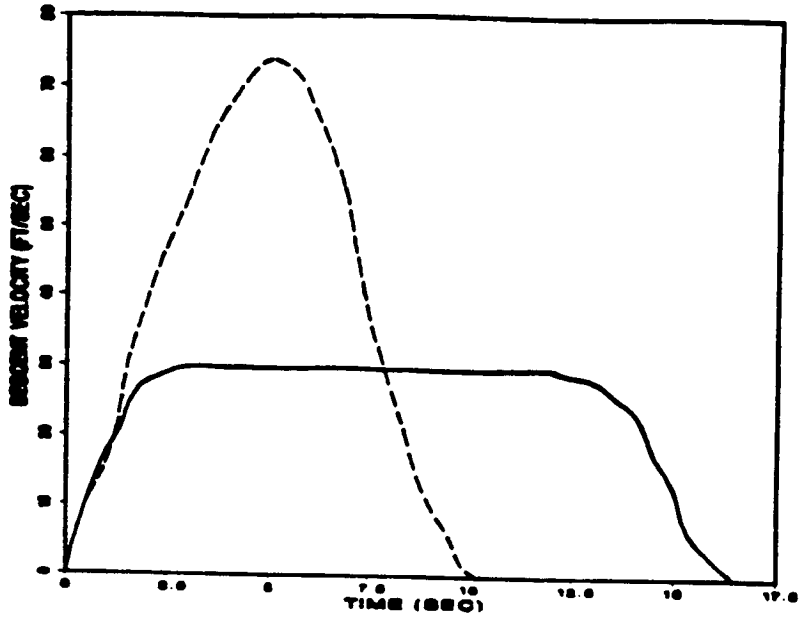

Figure 4.6.44 Comparison of the Time Variations of the Descent Velocity with and without a $[V_D]_{max}$-Bound

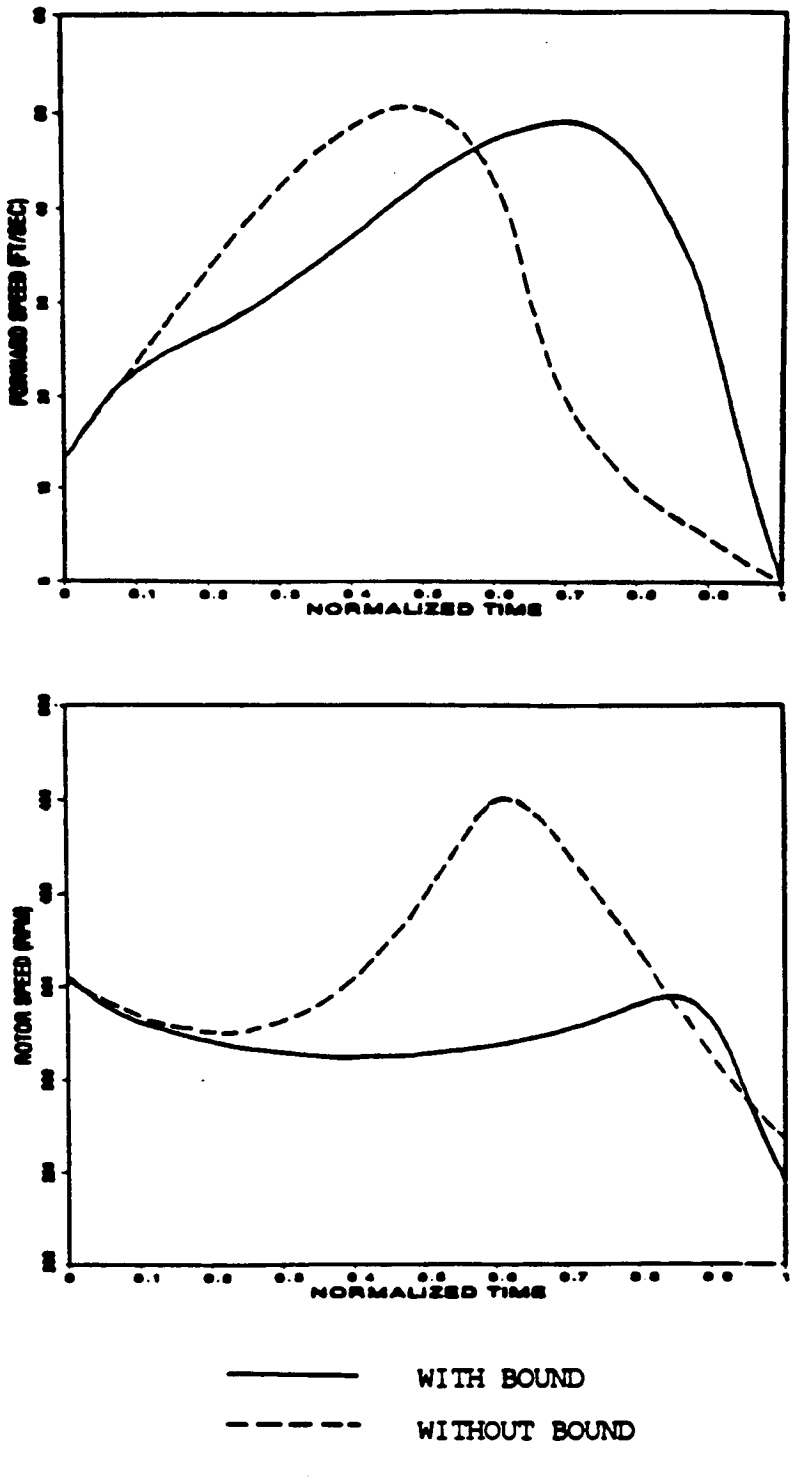

Figure 4.6.45 Comparison of the Time Variations of the Forward Speed and Rotor RPM with and without a $[V_D]_{max}$-Bound

peak value of the angular speed in the nominal case is actually less than the nominal value. This suggests that the peaking of the rotor RPM found in the solution of the problem without a descent velocity bound can be eliminated in two different ways. The overspeeding of the rotor can be removed either directly by the addition of an inequality constraint on the rotor RPM or indirectly through the use of an upper bound on the descent velocity.

4.6.3 Some Generalizations

If we impose path inequality constraints on both the descent velocity of the helicopter and the angular speed of the main rotor, the time variations of the descent velocity and the rotor angular speed in the optimal results might look like those shown in Figure (4.6.46). A plot of the angular speed of the rotor with respect to the descent velocity of the helicopter in the resultant optimal solution is as shown in Figure (4.6.46). Depending on values of $[V_D]_{max}$ and Ω_{max}, the V_D-Ω plot might consist of one or more "corner" points. In Figure (4.6.46), the entry phase starts from the initial entry condition (point 0) to the point when the upper bound on the descent velocity is reached (point 1). Thereafter, the descent velocity is maintained at a constant value while the angular speed of the rotor is increased till it reaches its upper bound Ω_{max}, at point 2. The angular speed of the rotor remains unchange from point 2 to 3 while the descent velocity of the helicopter is dropped. During this landing flare phase (from point 3 to 4), the descent velocity is being continuously reduced to its near zero value at touchdown. During the same period of time, the rotor RPM is also being reduced, indicative of the extraction of the stored rotational energy to cushion the landing.

4.6.4 Effects of Perturbed Initial or Terminal Conditions

The nominal case considered in the above subsections is with a 7.7-knots forward

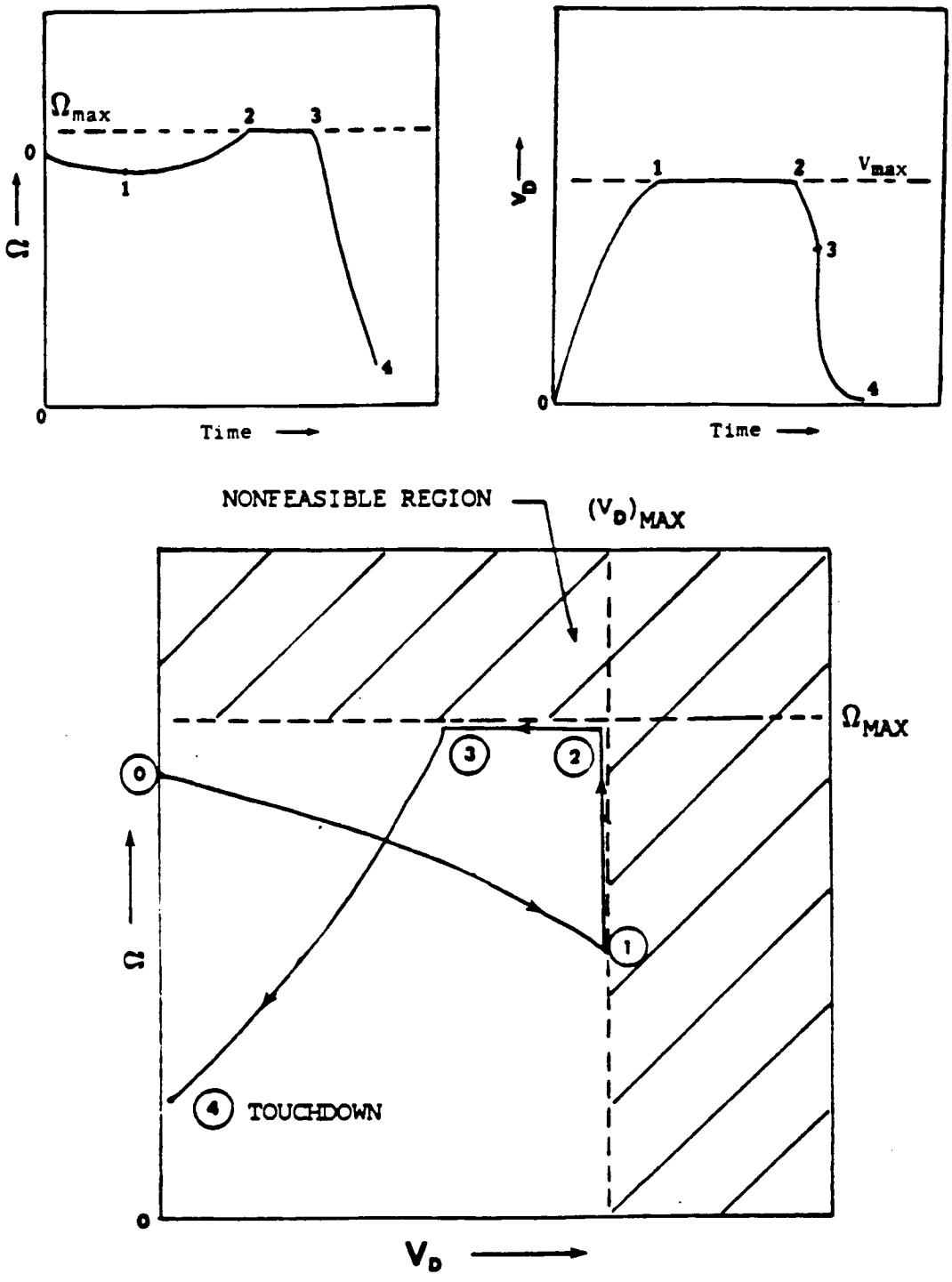

Figure 4.6.46 Ω versus V_D Plot showing Segments of the Optimal Control Scheme

airspeed and at an initial altitude of 423 feet. To investigate effects that initial and terminal conditions have on the control scheme, we consider the following three cases:

(1) The initial airspeed is increased from 7.7 knots to 15 knots.

(2) An additional terminal. horizontal distance constraint of 623 feet is added to the nominal problem (which is without a terminal distance constraint).

(3) The entry altitude is increased from 423 feet to 460 feet.

Results obtained for the first case are given in Figures (4.6.47)-(4.6.49). Those obtained for the second case are presented in Figures (4.6.50)-(4.6.53). Results obtained for the case with a change in the entry height are shown in Figures (4.6.54)-(4.6.57).

The optimal results obtained for these three cases agree qualitatively with those found in the nominal case. In all the cases considered, the path inequality constraint on the vertical sink-rate of the helicopter has been effectively enforced by the optimization algorithm. Since the perturbations in initial and terminal conditions are relatively small, only minor control adjustments are needed to accomodate these changes. It is also interesting to note that most of these control adjustments are made in the entry and/or landing flare phases of the descent maneuver. Both the horizontal and vertical components of the thrust coefficient in the steady descent phase of the maneuver remain practically unchanged with the perturbed boundary conditions.

The nominal problem (without a terminal, horizontal distance constraint) has a touchdown distance of about 560 feet. This horizontal distance has been extended to 635 feet in the second case. This extension in the horizontal distance has been achieved by an increase in the forward speed of the helicopter (see Figure (4.6.52)).

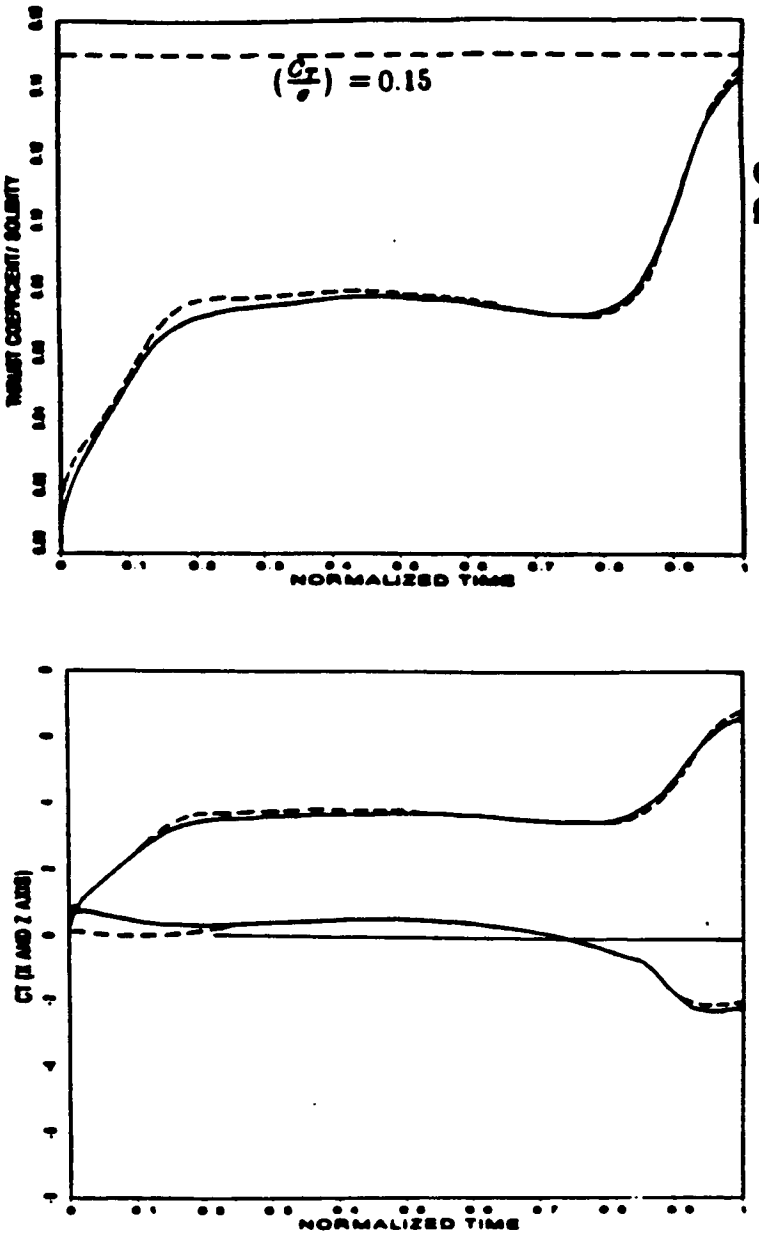

Figure 4.6.47 Comparisons of Optimal Results Obtained at Two Different Entry Airspeeds

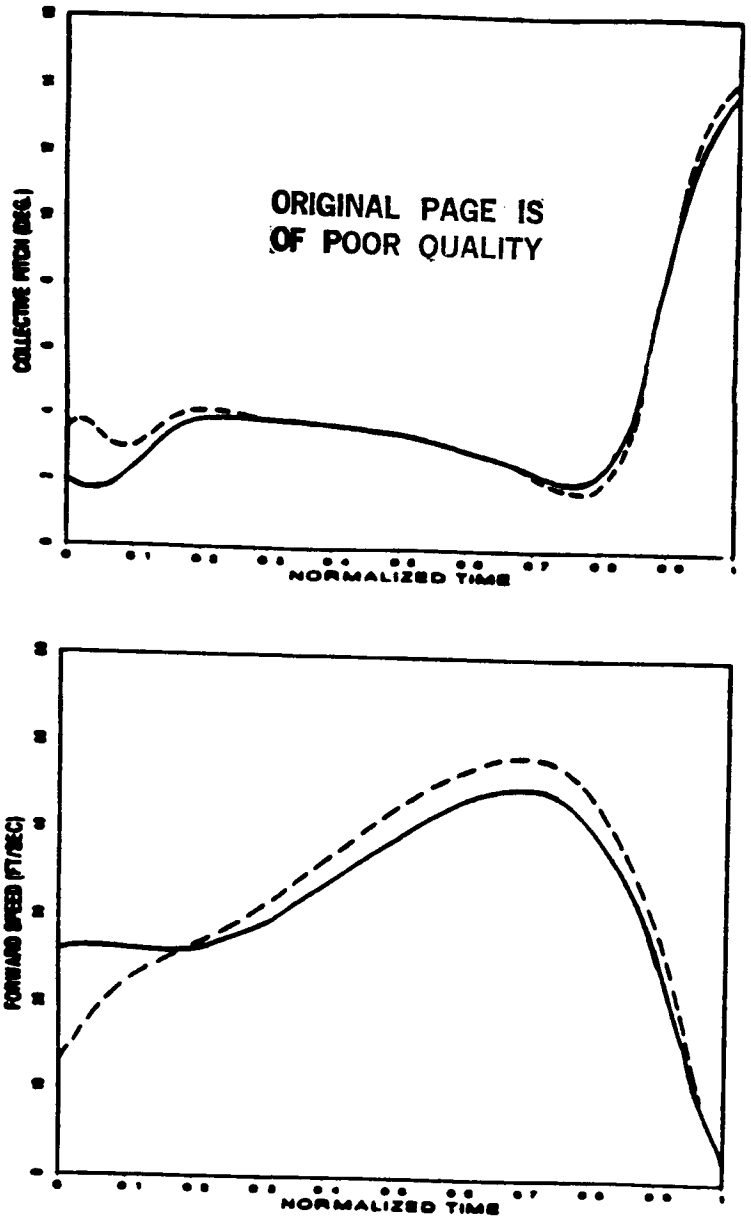

——— Initial Forward Speed = 26 fps

— — — Initial Forward Speed = 13 fps

Figure 4.6.48 Comparisons of Optimal Results Obtained at Two Different Entry Airspeeds

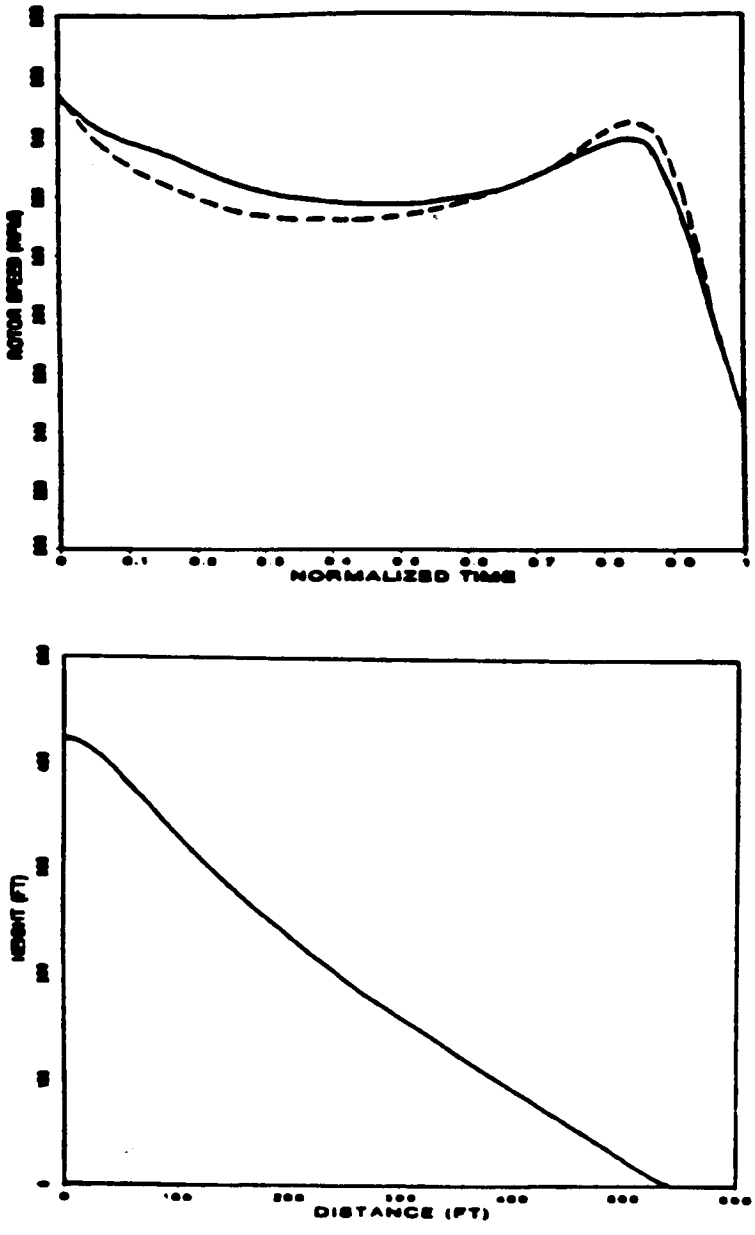

Initial Forward Speed = 26 fps

Initial Forward Speed = 13 fps

Figure 4.6.49 Comparisons of Optimal Results Obtained at Two Different Entry Airspeeds

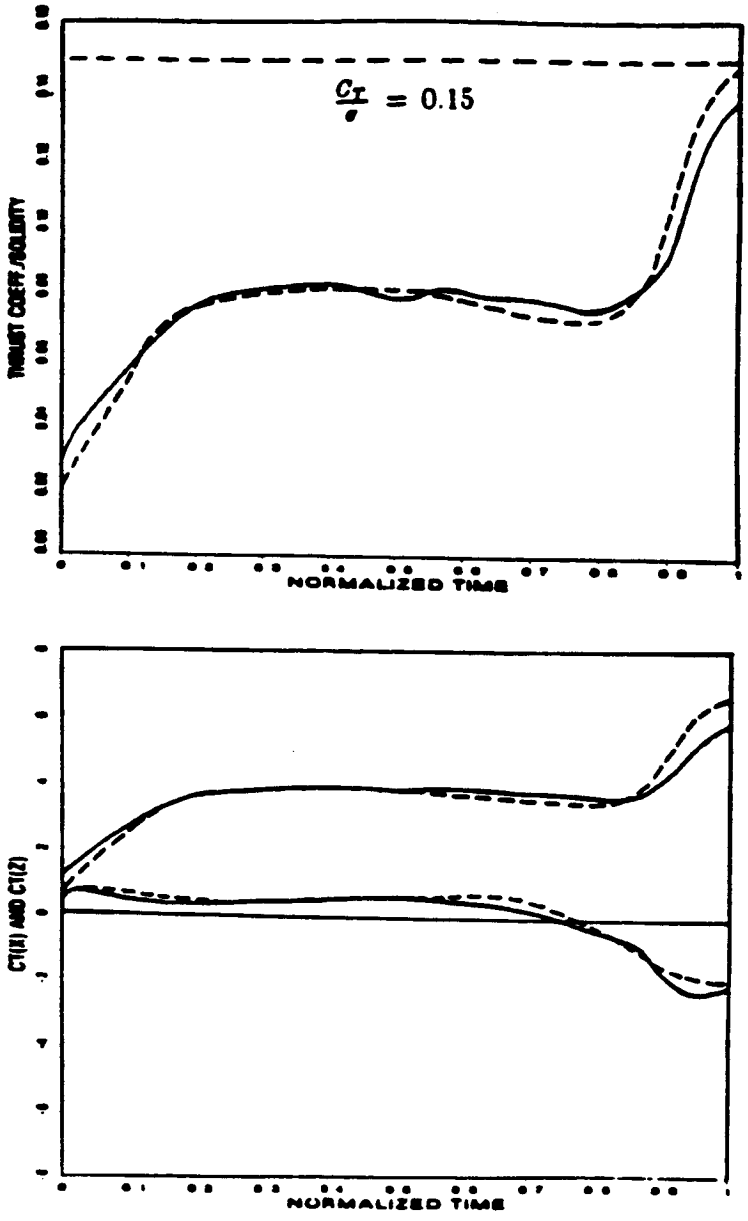

——— With Horizontal Distance Constraint at 635 feet

— — — Without Horizontal Distance Constraint

Figure 4.6.50 Comparisons of Optimal Results Obtained With and Without a Horizontal Distance Constraint

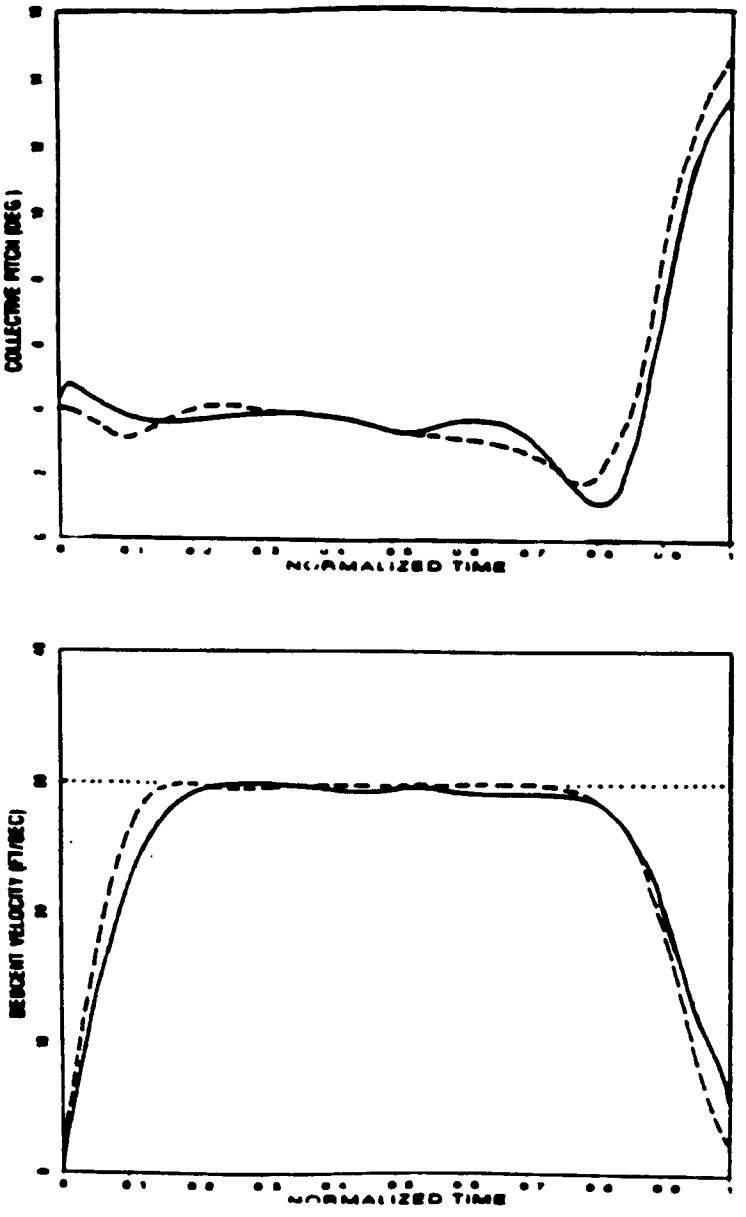

——— With Horizontal Distance Constraint at 635 feet

– – —– Without Horizontal Distance Constraint

Figure 4.6.51 Comparisons of Optimal Results Obtained With and Without a Horizontal Distance Constraint

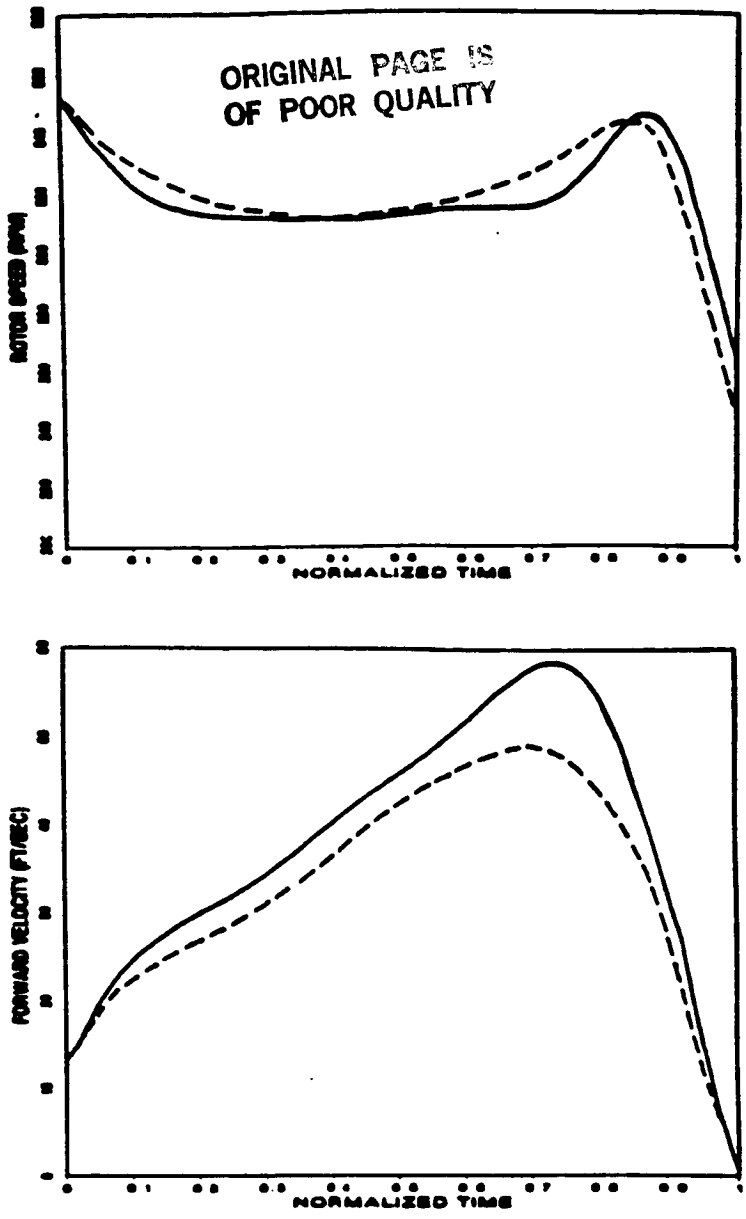

——— With Horizontal Distance Constraint at 635 feet

— — — Without Horizontal Distance Constraint

Figure 4.6.52 Comparisons of Optimal Results Obtained With and Without a Horizontal Distance Constraint

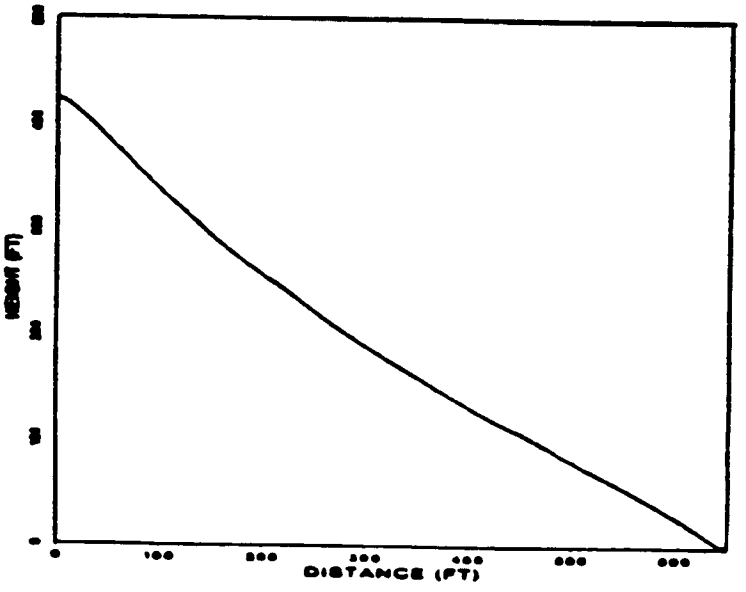

Figure 4.6.53 Optimal Results obtained with a Horizontal Distance Constraint

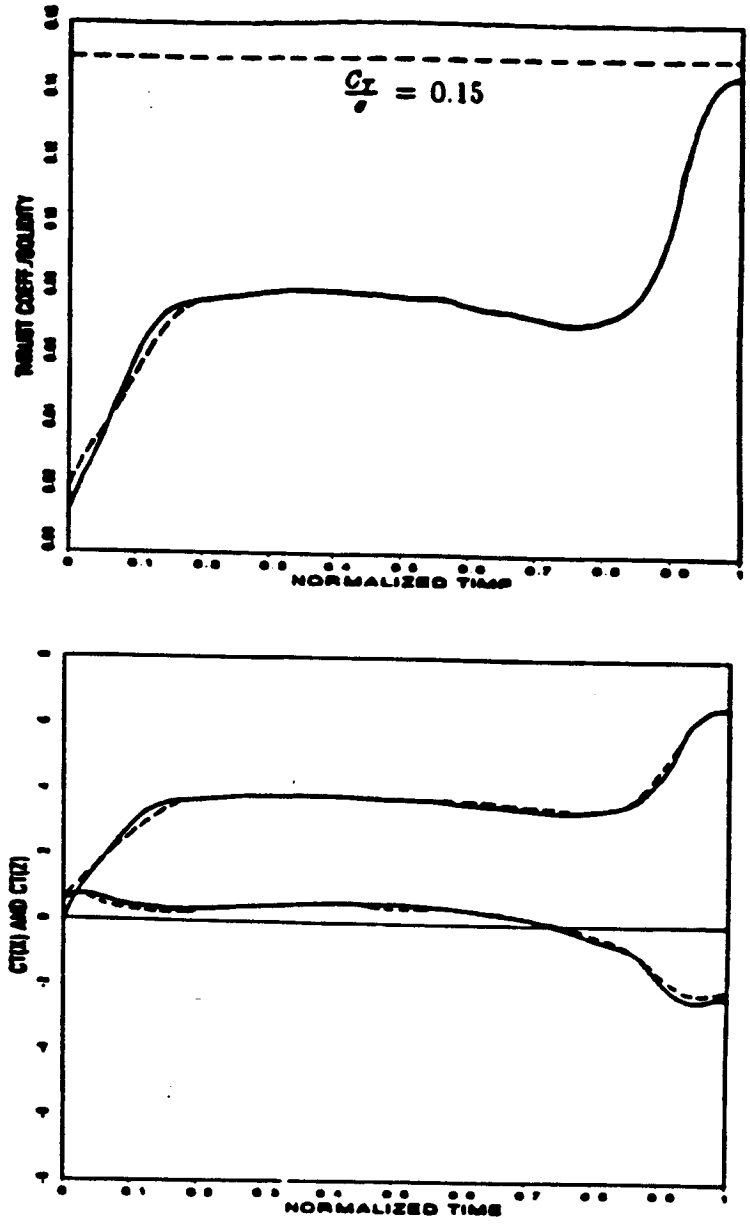

Figure 4.6.54 Comparisons of Optimal Results obtained at Two Different Entry Altitudes

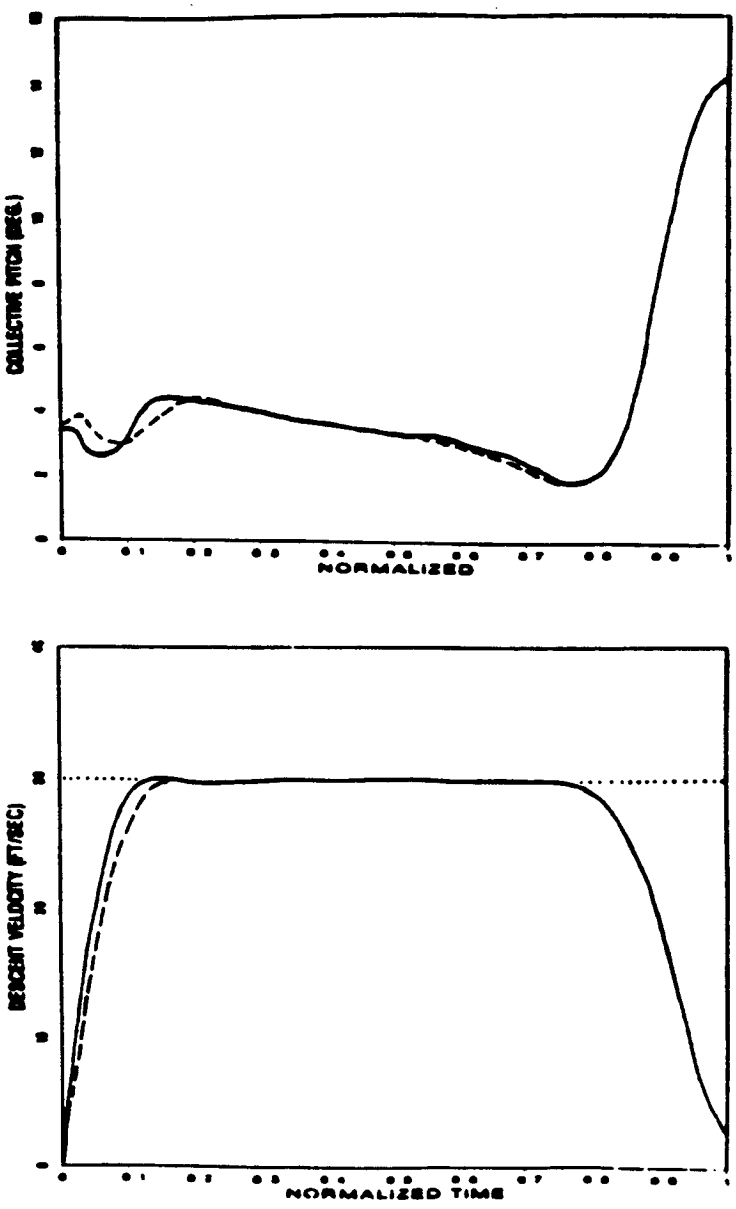

Figure 4.6.55 Comparisons of Optimal Results obtained at Two Different Entry Altitudes

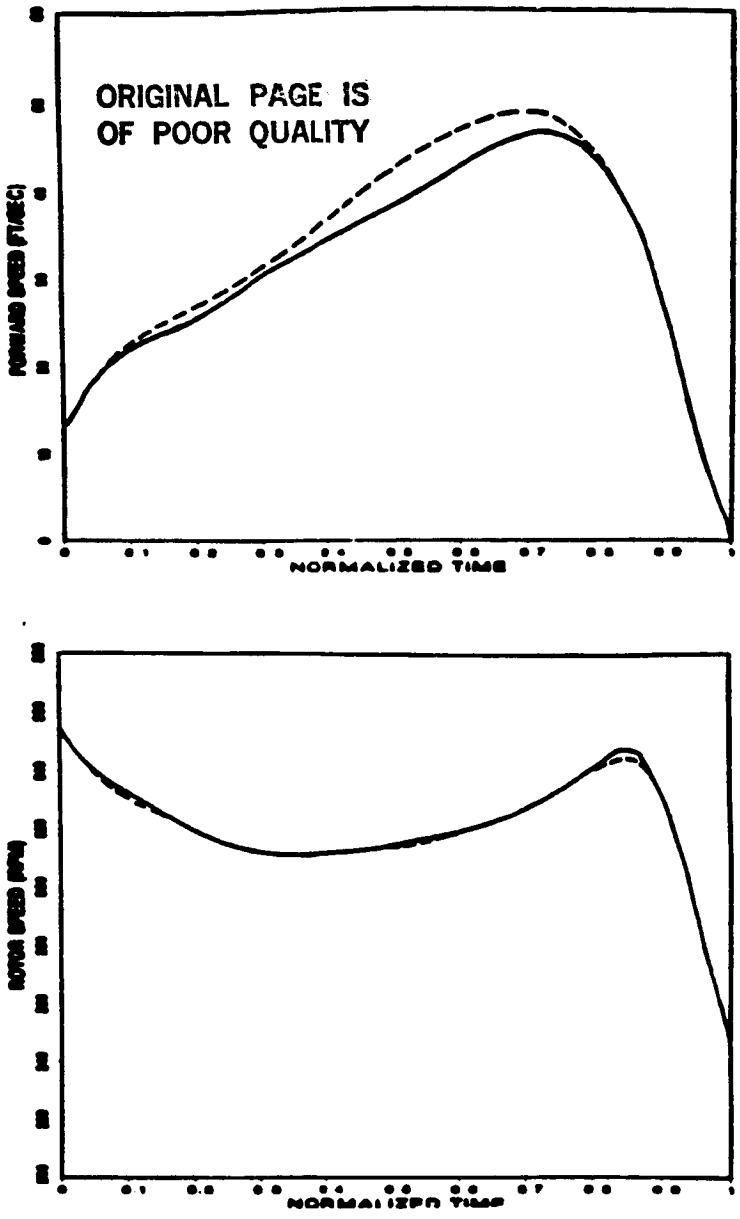

Figure 4.6.56 Comparisons of Optimal Results obtained at Two Different Entry Altitudes

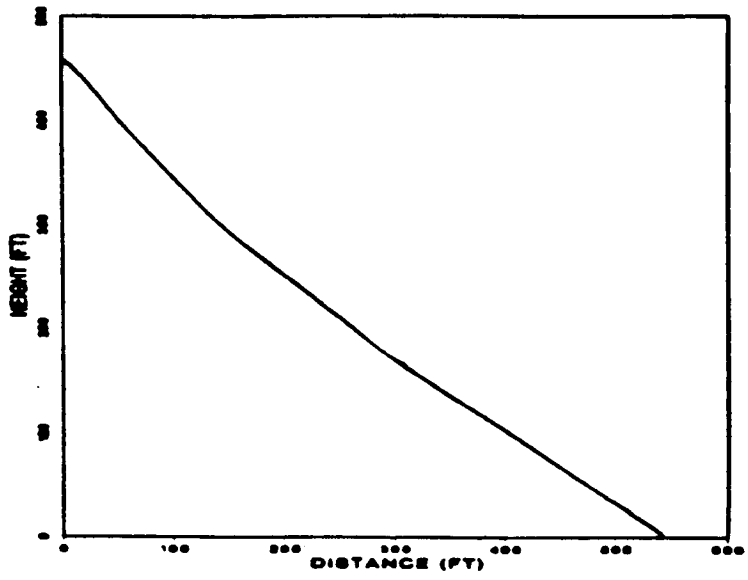

Figure 4.6.57 Optimal Results obtained at the Perturbed Entry Altitude

and by an increase in the overall flight time of the descent. The resultant flight profile is shown in Figure (4.6.53).

A summary of the optimal results obtained in these three cases are given in Table (4.6.5) together with that found in the nominal case.

4.6.5 General Conclusions

One of the distinct features in the optimal, autorotative control of a helicopter with a descent velocity bound is a clear division of the landing maneuver into phases. These control phases, resemble those practiced by helicopter pilots in their autorotational training. Therefore, this control scheme should be more acceptable to helicopter pilots.

A second feature of the control scheme is the suppression of the overspeed of the angular speed of the main rotor during the rearward cyclic flare. The increased flight time of the autorotational maneuver is an added benefit of putting a bound on the rate of descent.

One of the major disadvantages of the control scheme considered is the high rate of collective pitch input observed during the landing flare phase. Another disadvantage of the control scheme is in the use of a large amount of cyclic pitch during the last few seconds of the landing maneuver. This will cause a loss of all the ground references during the final touchdown. However, this will not create too much of a problem in a practical situation since the helicopter must always be rotated to its level attitude before a touchdown can be made.

CASE	DESCRIPTION	INITIAL CONDITIONS		TERMINAL CONDITIONS		
		SPEED (Knots)	HEIGHT (feet)	$[\frac{C_T}{\sigma}]_f$	ROTOR RPM	TOUCHDOWN TIME (sec.)
1	Nominal case with no bound on sink-rate	7.7	423	0.10	266	11.3
2	Nominal case with bound at 1800 ft/min.	7.7	423	0.15	246	16.3
3	Nominal case with different forward Speed	15.5	423	0.14	245	16.4
4	Nominal case with distance constraint	7.7	423	0.14	262	16.6
5	Nominal case with different entry height	7.7	460	0.14	247	16.9

Table 4.6.5 Summary of Results Obtained With and Without a Descent Velocity Bound

Chapter 5

Conclusions and Recommendations for Further Research

§5.1 Summary

5.1.1 Adequacy of a Point Mass Model in the Optimal Helicopter Landing Study

A point-mass model of an OH-58A helicopter was used in the optimal helicopter landing study. The states were vertical and horizontal velocities, vertical and horizontal displacements, and the rotor angular speed. The cost function was a weighted sum of the squared horizontal and vertical components of the helicopter velocity at touchdown. The controls were horizontal and vertical components of the thrust coefficient.

Optimal trajectories were calculated for entry conditions well within the H-V restriction curve, with the helicopter initially in hover or in forward flight. The optimal solutions exhibited control techniques similar to those used by helicopter pilots in actual autorotational landings. The results confirm the need to drop collective pitch immediately after engine failure. During the landing flare phase, the thrust vector

is rotated to the rear in order to reduce the forward velocity and, just before touchdown, the stored rotational energy in the rotor is traded for additional thrust to reduce the vertical velocity. The correlation between flight data and the optimal results establishes the adequacy of the use of a point mass model in the optimal helicopter landing study.

5.1.2 The Need for Path Inequality Constraints on Both the Control and the State Vectors

In order to minimize the cost function defined above, a larger rate of descent and a larger rotor RPM at the point of flare are desirable. However, a high rate of descent over a substantial period of time is unacceptable to helicopter pilots, while a large rotor RPM threatens the structural integrity of the rotor system. A unique feature of the present formulation is the addition of path inequality constraints on components of both the control and the state vectors. The control variable inequality constraint is a reflection of the limited amount of thrust that is available to the pilot in the autorotational maneuver without stalling the rotor. The state variable inequality constraint is an upper bound on either the vertical sink rate of the helicopter or the rotor angular speed during the descent.

With these bounds on the control and the state vectors, the optimal solutions obtained will realistically reflect the limitations of the helicopter and its pilot. The optimal solutions consist of subarcs which are connected at suitable corners. The subarcs are either unconstrained, or are on the upper bound of the thrust coefficient, or are on the bound on the vertical sink rate. The results exhibit division of the landing maneuver into entry, steady descent and landing flare/touchdown phases. This resembles the techniques taught to helicopter pilots, and so should be more acceptable to them.

5.1.3 Comments on the Sequential Gradient Restoration Technique

Slack variables were employed to convert the path inequality constraints mentioned above into path equality constraints. The resultant two-point boundary-value problem with path equality constraints was solved using the Sequential Gradient Restoration Technique. The effectiveness of the SGR technique for problems with of both control and state variable inequality constraints was demonstrated by the present study.

In general, the amount of computation involved with the use of the SGR algorithm is proportional to the square of the dimension of the state vector [42]. Therefore, the use of by auxiliary states in problems with state variable inequality constraints increases the computational requirements. In this regard, a transformation technique for optimal control problems with partially linear state variable inequality constraints is strongly recommended [43]. The transformation technique takes advantage of the partial linearity of the state inequality constraint so as to yield a transformed problem characterized by a new state vector of minimal size. Substantial savings in computer time can be achieved with this transformation technique.

5.1.4 Reduction in the H-V Restriction Curve and Other Potential Applications

Even though effects of the pilot time delay and other factors have not been taken into account, the present study indicates that a substantial reduction might be achievable in the H-V restriction zone using optimal control techniques. Results computed using the optimal technique thus provide a benchmark for comparisons with other control techniques. These optimization techniques could also be used to:

(1) help instruct pilots on good autorotation technique.

(2) reduce the risk/time/effort involved in establishing the H-V restriction

zones by flight tests.

(3) provide an objective comparison of the autorotation capabilities of different helicopter models.

(4) assess the influence of vehicle parameters on autorotation during preliminary design.

§5.2 Recommendations for Further Research

5.2.1 Refinements of the Mathematical Model

The accuracy of studies like this one could be improved by adding the following refinements to the mathematical model:

(1) induced velocity dynamics (cf. references [15], [19], [20] and [70]);

(2) ground effect (cf. references [15] and [71]);

(3) variation of the profile drag coefficient with rotor blade angle of attack (cf. reference [24]);

(4) rigid body dynamics, which would show the effects of pitch attitude during descent and at touchdown.

These refinements increase the dimension of the state vector (refinements (1) and (4)) and also the complexity of the analysis (refinements (2) and (3)). They are considered to be of secondary importance (cf. Section (2.2)), and should be included only if improvement in the accuracy of the optimal programs is required.

5.2.2 The Effects of the Engine Failure Mode (cf. [5])

The nature of the power reduction transient affects pilot technique and the response of the helicopter. Common causes of power loss are fuel starvation, fuel control malfunctions, engine deterioration, and damage from an external source. The transient nature of the power reduction varies greatly with the cause and directly influences

the necessary corrective pilot actions. The present study considered the most critical case of a sudden complete power loss, caused as a result of an engine seizure, disintegration, or drive system failure. It would be of interest to study other "less critical" cases.

5.2.3 The Effects of Pilot Time Delay (cf. [5])

The term "time delay" defines the time lag between the instant of power loss, and the time recovery action is initiated by the pilot. It consists of the recognition time and the reaction time of the pilot. Therefore, the amount of time delay involved is a strong function of both the engine failure cues (either audio, visual or kinesthetic signals) available to the pilot and the experience of the pilot involved.

A time delay on the order of 1.5-2 seconds is typically used in the establishments of the H-V restriction curves. It is recommended that effects of the pilot time delay on the autorotational landing of a helicopter from critical flight conditions be studied. This can be studied through the incorporation of a time delay into the helicopter landing problem formulated in Section (2.9).

5.2.4 Pilot-in-the-loop Simulation

The importance of pilot-in-the-loop simulations for helicopter research has been emphasized in references [4, 10, 15 and 65]. The usefulness of simulations in autorotation research has been confirmed in reference [15]. Simulations provide important information about pilot workload, pilot ability to track a given optimal flightpath, limitations of hardware involved, and the structural integrity of the vehicle. They may provide other information, such as whether a particular sink rate or pitch rate is acceptable to helicopter pilots. Data acquired from these flight simulations and comments from helicopter pilots should be studied carefully and appropriate

modifications made in the formulation of the optimal helicopter landing problem. Only through iterative cycles of this kind can a realistic optimal control program be established and implemented.

References

1. Graves, J.D., "Methods and Devices to Improve Helicopter Autorotational Characteristics," USAAVRADCOM-TR-82-D-38, Sep., 1983.

2. Hansen, K.C., "Single Rotor Helicopter Transient following a Power Failure at High Speed," presented at the 22nd Annual National Forum of the American Helicopter Society, 1966.

3. Jepson, W.D., "Some Considerations of the Landing and Take-Off Characteristics of Twin Engine Helicopters," Journal of American Helicopter Society, Vol.7, No.4, Oct.,1962.

4. Saunders, G.H., "Safety Column," Rotor and Wing, Jan./Feb., 1976.

5. Ferreel, K.R., Frederickson, A.C., and Shapley, J.J., "A Flight Test Investigation of Autorotational Performance and Height Velocity Testing of a Single Main Rotor, Single engine Helicopter," USAAEFA No. 68-25, Mar.,1976.

6. Segner, D.R., "AH-56A Compound Helicopter Autorotation Characteristics ," 1972 Report of the Society of Experimental Test Pilots, pp. 29-47.

7. Buss, M.W., "Sudden Engine Failure Problems of High Performance Attack Helicopters," 1971 Report of the Society of Experimental Test Pilots, pp. 173-188.

8. Davis, J.M., et al, "Study of Tandem Rotor Helicopter Dynamics following Power Failure at High Speed," USAAVLABS 65 72, Nov., 1965.

9. Cooper, D.E., et al, "Single Rotor Helicopter Dynamics following Power Failure at High Speed," USAAVLABS TR 66 30, Jun., 1966.

10. Watts, J.C., et al, "Engineering Flight Test of AH-1G Helicopter Autorotational Characteristics," USAASTA-74-10, May, 1974.

11. Wood, T.L., "High Energy Rotor System," presented at the 32nd Annual National Forum of the American Helicopter Society, Washington, D.C., May, 1976.

12. Dooley, L.W., and Yeary, R.D., "Flight Test Evaluation of the High Inertia Rotor System ," USARTL-TR-79-9, June,1979.

13. Pleasant, W.A.,III, and White, G.T.,III, "Status of Improved Autorotative Landing Research," Journal of American Helicopter Society, Vol. 128 , No. 1, Jan., 1983.

14. White, G.T., Logan, A.H., and Graves, J.D., "An Evaluation of Helicopter Autorotation Assist Concepts," presented at the 38th Annual Forum of the American Helicopter Society, May, 1982.

15. Johnson, W., "Helicopter Optimal Descent and Landing after Power Loss," NASA TM 73,244, May, 1977.

16. Bryson, A.E., Jr., "FCNOPT Computer Program," Department of Aeronautics and Astronautics, Guidance and Control Lab., Stanford University, Stanford, CA 94305.

17. Washizu, K., Azuma, A., Koo, J., and Oka, T., "Experiments on a Model Helicopter Rotor Operating in the Vortex Ring State," Journal of Aircraft, Vol. 3, No. 3, May-June, 1966.

18. Yamakawa, G.M., and Watts, J.C., "Airworthiness and Flight Characteristics Tests - Production OH-58A Helicopter Unarmed and Armed with XM27E1 Weapon System - Performance," USAAATA Technical Report 68-30, Sep., 1970, AD875793.

19. Decker, W.A., et al, "Model Development and the Use of Simulator for Investigating Autorotation," presented at FAA Conference on Helicopter Simulation,

Atlanta, Georgia, Apr.,1984.

20. Harris, F.D., "Articulated Rotor Blade Flapping Motion at Low Advanced Ratio," J. Am. Helicopter Soc., Vol. 17, Jan. 1972.

21. Hayden J.S., "The Effect of Ground on Helicopter Hovering Power Required," presented at the 32^{nd} Annual National Forum of the American Helicopter Society, May, 1976.

22. Sheridan, P.F., et al "Aerodynamics of Helicopter Flight near the Ground," Paper No. 77.30-04, 33^{rd} Annual National Forum of the American Helicopter Society, Washington, D.C., May, 1977.

23. Private communication with William A. Decker of NASA Ames Research Center, Moffet Field, California.

24. Gessow, A., and Myers,G.C., Jr., Aerodynamics of the Helicopter, Frederick Ungar Publishing Co., New York, 1952.

25. Stepniewski, W.Z., "Rotary Wing Aerodynamics," NASA Contractor Report 3083, Jan., 1979.

26. Jacoby, S.L.S., Iteration Methods for Nonlinear Optimum Problems, Prentice Hall, Inc., 1972.

27. Bryson, A.E., Jr., Denham, W.F. and Dreyfus, S.E., "Optimal Programming Problems with Inequality Constraints I: Necessary Conditions for Extremel Solutions," AIAA Journal, Vol. 1, No. 11, pp. 2544-2550, Nov., 1963.

28. Denham, W.F. and Bryson, A.E., Jr., "Optimal Programming Problems with Inequality Constraints II: Solution by Steepest-Ascent," AIAA Journal, Vol.2, No. 1, pp. 25-34, Jan., 1964.

29. Bryson, A.E., Jr., and Ho, Y.C., Applied Optimal Control, Hemisphere, Washington, 1975.

30. Bryson, A.E. Jr., and Denham, W.F., "A Steepest-Ascent method for Solving Optimal Programming Problems," J. of Applied Mechanics, 29, pp. 247-257, 1962.

31. Kelley, H.J., "Method of Gradients," Optimization Techniques, edited by G. Leitmann, Academic Press Inc., New York, 1962. (Chapter 6)

32. Kelley, H.J., Falco, M. and Ball, D.J., "Air Vehicle Trajectory Optimization," Symposium on Multivariable System theory, Fall meeting of Society of SIAM, Cambridge, Mass., 1962.

33. McGill, R., "Optimal Control, Inequality State Constraints, and the Generalized Newton Raphson algorithm," J. of SIAM, (Control), Series A, Vol. 3, No. 2, 1965.

34. Speyer, J.L. and Bryson, A.E.,Jr., "Optimal Programming Problems with Bounded State Space," AIAA Journal, Vol. 6, No. 5, pp. 1488-1491, Aug., 1968.

35. Chang, S.S.L., "Optimal Control in Bounded Phase Space," Automatica, Vol. 1, 1963, pp. 55-67; also TR-400-37, Aug., 1961, Department of Electrical Engineering, New York University.

36. Mehra, R.K. and Davis, R.E., "A Generalized Gradient Method for Optimal Control Problems with Inequality Constraints and Singular Arcs," IEEE Transactions on Automatic Control, Vol. AC-17, No. 1, Feb., 1972.

37. Maurer, H. and Gillessen, W., "Application of Multiple Shooting to the Numerical Solution of Optimal Control Problems with Bounded State Varibales," Computing 15, pp. 105-126, 1975.

38. Stoer, J., and Bulirsh, R., "Einfuhrung in die Numerische Mathematik II. (Heidelberger Traschenbuch 114) Berlin-Heidelberg-New York: Springer 1973.

39. Miele, A., "Method of Particular Solutions for Linear, Two-Point Boundary Value Problems," Journal of Optimization Theory and Applications, Vol. 2, No. 4, 1968.

40. Heideman, J., "Use of Method of Particular Solutions in Nonlinear, Two-point, Boundary Value Problems," JOTA, Vol. 2, No. 6, 1968.

41. Jacobson, D.H. and Lele, M.M., "A Transformation Technique for Optimal Con-

trol Problems with a State Variable Inequality Constraint," IEEE Transactions on Automatic Control, Vol. AC-14, No. 5, Oct., 1969.

42. Miele, A. et al, "Sequential Gradient-Restoration Algorithm for Optimal Control Problems with Non-differential Constraints," Journal of Optimization Theory and Applications, Vol. 13, No. 2, 1974.

43. Miele, A. et al, "A Transformation Technique for Optimal Control Problems with Partially Linear State Inequality Constraints," Journal of Optimization Theory and Applications, Vol. 28, No. 2, 1979.

44. Gonzalez, S. and Miele, A., "Sequential Gradient-Restoration Algorithm for Optimal Control Problems with General Boundary Conditions," Journal of Optimization Theory and Applications, Vol. 26, No. 3, 1978.

45. Miele, A., "Recent Advances in Gradient Algorithms for Optimal Control Problems - Survey Paper," Journal of Optimization Theory and Applications, Vol. 17, No. 5/6, 1975.

46. Sage, A.P. and White, C.C., III, Optimum Systems Control , second edition, Prentice-Hall, Inc., 1977

47. Weinreb, A., "Optimal Control with Multiple Bounded Inputs," SUDAAR Report No. 544, Department of Aeronautics and Astronautics, Stanford University, Stanford, CA 94395.

48. Miele, A., et al, "Sequential Gradient Restoration Algorithm for Optimal Control Problems with Non-differential Constraints," Journal of Optimization Theory and Applications, Vol. 13, No.2, 1974.

49. Miele, A., et al, "Modified Quasilinearization Algorithm for Optimal Control Problems with Non-differential Constraints, Part I, Theory," Rice University, Aero-Astronautics Report No. 112, 1973.

50. Miele, A., et al, "Modified Quasilinearization Algorithm for Optimal Control Problems with Non-differential Constraints, Part II, Example," Rice University, Aero-Astronautics Report No. 113, 1973.

51. Breakwell, J.V., Speyer, J.L., and Bryson, A.E., Jr., "Optimization and Control of Nonlinear Systems Using the Second Variation," Journal of SIAM Control, Series A, Vol. 1, No. 2, 1963, pp. 193-217.

52. Kelley, H.J., "An Optimal Guidance Approximation Theory," IEEE Transaction on Automatic Control, Oct. 1964, pp.375-380.

53. Hymas, C.E., Cavin, R.K., III, and Colunga, D., "Neighboring Extremals for Optimal Control Problems," AIAA Journal, Vol. 11, No. 8, pp. 1101-1109, August, 1973.

54. Johnson, W., Helicopter Theory, Princeton University Press, Princeton, New Jersey, 1980.

55. Bramwell, A.R.S., Helicopter Dynamics, A. Halsted Press Book, John Wiely and Sons, New York, 1976.

56. Wood, T.L., Bull, H., "Safety of Flight Data for the High Energy Rotor System of Flight Verification Review (SOFVR) Evaluation," Bell Helicopter Textron Report Number 699-099-051, Fort Worth, Texas, March 1977.

57. Watts, J.C., Condon, G.W., and Pincavage, J.V., "Height-Velocity Test of the OH-58A Helicopter," USAASTRA Technical Report Number 69-16, U.S. Army Aviation System Test Activity, Edwards Air Force Base, California, June 1971, AD884973.

58. Operator's Manual, Army Models UH-1D/H and EH-1H Helicopters, Technical Manual 55-1520-210-10, Headquarters, Department of the Army, Washington, D.C., May 1979.

59. Operator's Manual, Army Models OH-58A Helicopter, Technical Manual 55-1520-228-10, Headquarters, Department of the Army, Washington, D.C., Oct. 1970.

60. Operator's Manual, Army Models OH-58C Helicopter, Technical Manual 55-1520-235-10, Headquarters, Department of the Army, Washington, D.C., April 1978.

61. Operator's manual, Army Models AH-1S Helicopter, Technical Manual 55-1520-234-10, Headquarters, Department of the Army, Washington, D.C., Nov. 1976.

62. Training Circular, Rotary Wing Night Flight, TC 1-28, Headquarters, Department of the Army, Washington, D.C., Feb. 1976.

63. Field Manual, Rotary Wing Flight, FM 1-51, Headquarters, Department of the Army, Washington, D.C., April 1979.

64. Ferreel, K.R., et al, "A Flight Research Investigation of Autorotational Performance and Height Velocity Testing of a Single Main Rotor, Single Engine Helicopter," USAAEFA Project No. 68-25, US Army Aviation Engineering Flight Activity, Edwards Air Force Base, California 93523, March 1976.

65. Benson, G. et al, "Use of Helicopter Flight Simulation for Height-Velocity Test Predictions and Flight Test Risk Reduction," presented at the 34^{th} Annual National Forum of the American Helicopter Society, Washington, D.C., May, 1978.

66. Shapley, J.J., et al. "The Development of an Improved Method of Conducting Height-Velocity Testing on Rotary Wing Aircraft," Journal of American Helicopter Society, Vol. 15, No. 2, April 1970.

67. Roesch, P. and Samoni, G., "Applications of Energy to the Determination of Helicopter Flight Paths," Fifth European Rotorcraft and Powered Lift Aircraft Forum, Amsterdam, The Netherland, September 1979.

68. Private Communication with Mr. Bill S. Hindson, Senior Research Associate, Department of Aeronautics and Astronautics, Stanford University, Stanford, CA 94305.

69. Talbot, P.D. and Schroers, L.G., "A Simple Method for Estimating Minimum Autorotative Descent Rate of Single Rotor Helicopters," NASA-TM-78452, March 1978.

70. Carpenter, P.J. and Fridovich, B., "Effects of a Rapid Blade-Pitch Increase on the Thrust and Induced Velocity Response of a Full-Scale Helicopter Rotor," NACA-TN-3044, August 1953.

71. Cheeseman, I.C. and Bennett, W.E., "The Effect of the Ground on a Helicopter Rotor in Forward Flight," ARC R and M No. 3021, September 1955.

Appendix A

Verification of Point Mass Helicopter Model

§A.1 Introduction

A simple point mass helicopter model is used in the study of optimal autorotative control of the OH-58A helicopter. It includes the effects of gravity force, main rotor thrust, parasite drag (on the fuselage) and profile drag (on the rotor blades). The effects of increased induced power loss when the helicopter operates in the vortex-ring state have also been included. Secondary effects, such as induced velocity lag. ground effects etc. have been neglected.

Experimental data describing the steady state sink rate of the standard OH-58A helicopter in autorotation are given in References [12,18]. Fig.(A.1.1) (from Reference [18]) shows the steady autorotational sink rate of the standard OH-58A helicopter at a constant rotor speed of 354 rpm.. A comparison of these flight data with those computed by the simplified point mass model is made to establish the validity of the point mass model, at least in the steady state. The result of such a comparison is given here.

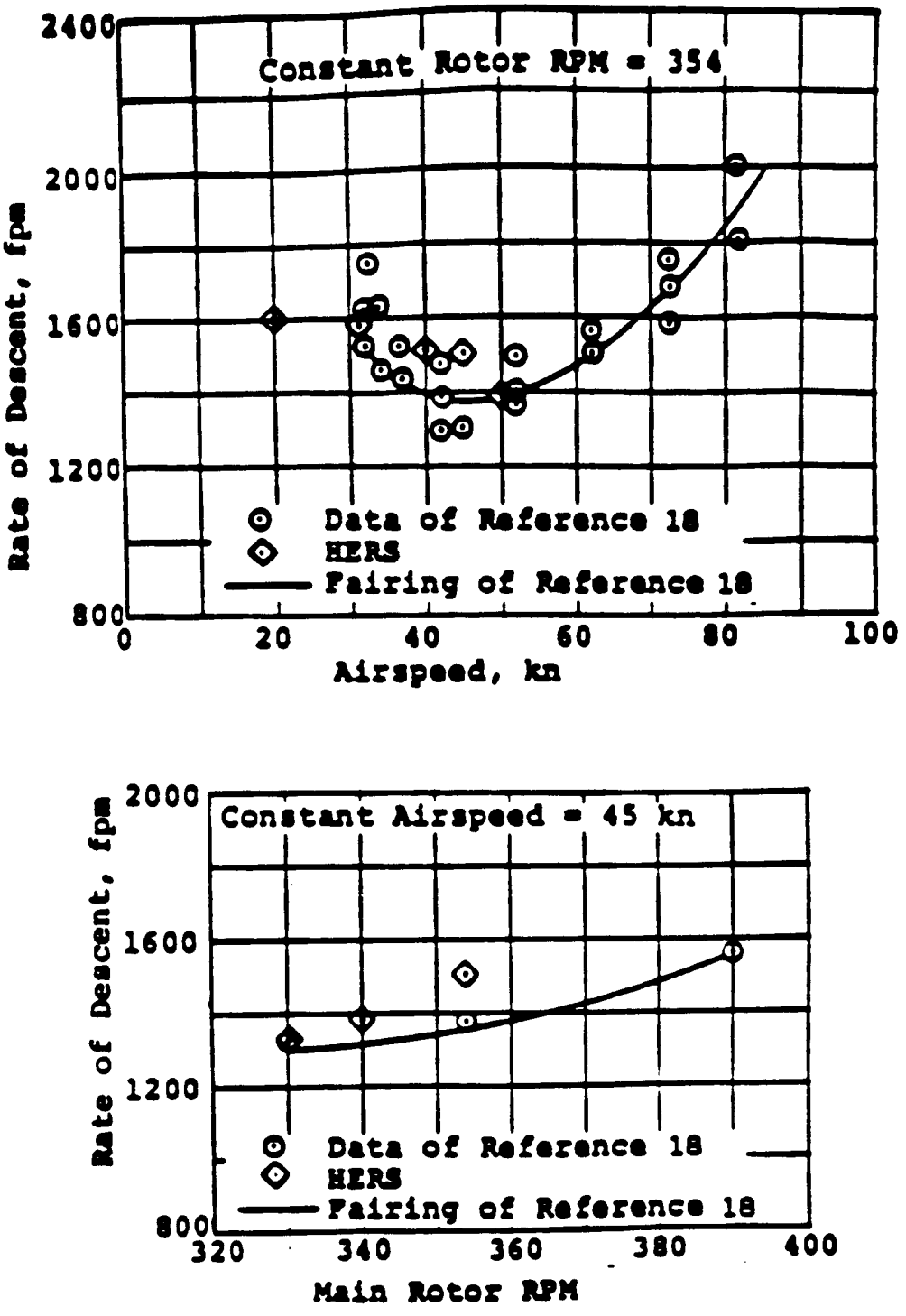

Figure A.1.1 Steady Autorotational Sink Rtae of the Standard OH-58A Helicopter

§A.2 Analysis

Table (A.2.1) contains a list of parameters and their values used in the point mass model. Other than the estimated values of 24 ft^2 for the equivalent flat plate area of the fuselage f_e, and 0.0087 for the mean profile drag coefficient of rotor blades δ_{e_0}, all the other values were taken from Reference 18. These two estimated values were obtained by fitting the flight data for steady sink rate with the steady sink rate from the point mass model.

In the steady state, the angular speed of the rotor, as well as the forward and vertical speeds of the helicopter are constant. We can therefore equate the first three of the five equations of motion derived in Chapter (2) to zero. The resulting equations are :

$$\begin{aligned} g_0 - m_0(C_{T_z}\omega^2 + \bar{f}w\sqrt{w^2+u^2}) &= 0, \\ C_{T_z}\omega^2 - \bar{f}u\sqrt{w^2+u^2} &= 0, \\ c_0 + 0.05(\frac{C_{T_z}u - C_{T_z}w}{\omega}) + k_0 f_l (C_{T_z}^2 + C_{T_z}^2)^{\frac{3}{4}} &= 0. \end{aligned}$$

where the definitions of the constants are :

$$\begin{aligned} g_0 &= \frac{2000g}{\Omega_0^2 R}, \\ m_0 &= \frac{2\rho\pi R^3}{m}, \\ \bar{f} &= \frac{5f_e}{4\pi R^2}, \\ i_0 &= \frac{\rho\pi R^5}{10 I_R}, \\ c_0 &= \frac{1}{8}\sigma\bar{c_d}(10^3), \\ k_0 &= \frac{K_{ind}}{\sqrt{2000}}, \\ p_0 &= 0.05(\sqrt{2000}). \end{aligned}$$

S/NO.	SYSTEM PARAMETER	VALUE USED
1	f_e. equivalent flat plate area (ft^2)	24.0
2	g. acceleration due to gravity (ft/sec^2)	32.17
3	ρ. air density ($slug/ft^3$)	0.002378
4	m. mass of helicopter (slug) (lb.wt.)	93.16 (3000.0)
5	σ. rotor solidity	0.048
6	K . induced velocity correction factor	1.13
7	a. $\frac{\partial}{\partial\alpha}(C_\ell)$	5.73
8	R. radius of main rotor (ft)	17.63
9	ω. nominal rotor speed (rpm)	354.0
10	δ_e. profile drag coefficient (NACA 0012 airfoil assumed)	0.0087
11	γ. rotor system Lock number	2.6

Table A.2.1 System Parameters

These three nonlinear algebraic equations, with their five unknown (u, w, ω, C_{T_x}, and C_{T_z}), must be solved simultaneously. By fixing the rotor speed at a constant value of 354 rpm., then for any given value of forward speed, u, the above system admits an unique solution for w, C_{T_x}, and C_{T_z}. Alternatively, the airspeed of the helicopter can be fixed at a constant value of 45 Knots and the variation of the steady state sink rate with the rotor rpm. can be studied. Computer programs have been written to solve these simultaneous nonlinear equations. The results are given in Tables (A.2.2)-(A.2.5).

§A.3 Comparison of Computed Results with Flight Data

The effects of parasite and profile drag on the steady-state sink rate of the OH-58A helicopter are given in Figs.(A.3.2) and (A.3.3) respectively. The profound effect of increased parasite drag at high speed can be seen clearly in Fig.(A.3.2). Fig.(A.3.3) shows the rise in the steady state sink rate needed to balance the higher profile power loss as the mean profile drag coefficient is increased.

By trial and error, it was determined that a good fit between the computed and measured sink rate is obtained with $\delta_{e_0} = 0.0087$ and $f_e = 16.0\ ft^2$. A comparison of the computed results with the flight data is given in Fig.(A.3.4). The scatter of the experimental data shown in the figure is possibly due to the variation of the side-slip angle of the helicopter during the tests. As can be seen, the computed sink rate falls within the range of the experimental data.

Further confirmation of these results can be obtained by fixing the forward speed at a constant value of 45 Knots, and computing the steady sink rate at different rotor speeds. The computed results, plotted in Fig.(A.3.5), compare well with those found experimentally (see also Fig.(A.1.1)).

SPEED (KNOTS)	SINK RATE (FPM)	CT(Z)	CT(X)	CT
15.4	2138	0.062	0.000	0.062
17.4	2018	0.062	0.001	0.062
19.3	1914	0.062	0.001	0.062
21.2	1825	0.062	0.001	0.062
23.2	1749	0.062	0.001	0.062
25.1	1683	0.062	0.001	0.062
27.0	1628	0.062	0.001	0.062
29.0	1581	0.062	0.001	0.062
30.9	1541	0.062	0.001	0.062
32.8	1508	0.062	0.001	0.062
34.8	1481	0.062	0.001	0.062
36.7	1459	0.062	0.002	0.062
38.6	1442	0.062	0.002	0.062
40.6	1429	0.062	0.002	0.062
42.5	1421	0.062	0.002	0.062
44.4	1417	0.062	0.002	0.062
46.4	1417	0.062	0.003	0.062
48.3	1421	0.062	0.003	0.062
50.2	1429	0.062	0.003	0.062
52.2	1440	0.062	0.003	0.062
54.1	1454	0.062	0.003	0.062
56.0	1472	0.062	0.004	0.062
58.0	1494	0.062	0.004	0.062
59.9	1519	0.062	0.004	0.062
61.9	1548	0.062	0.004	0.062
63.8	1581	0.062	0.005	0.062
65.7	1617	0.062	0.005	0.062
67.7	1657	0.062	0.005	0.062
69.6	1700	0.062	0.006	0.062
71.5	1748	0.061	0.006	0.062
73.5	1800	0.061	0.006	0.062

Table A.2.2 Variations of Steady State Sink Rate With Forward Speed at Constant Rotor Speed of 354 rpm [$f_e = 16\ ft^2$, $\delta_e = 0.0087$]

SPEED (KNOTS)	SINK RATE (FPM) DE=0.007	DE=0.0087	DE=0.010
0.00	2801	2843	2874
3.86	2760	2803	2834
7.73	2632	2679	2713
11.60	2409	2464	2503
15.47	2053	2138	2202
19.34	1808	1914	1993
23.21	1632	1749	1837
27.08	1505	1628	1721
30.95	1415	1541	1637
34.81	1352	1481	1579
38.68	1311	1442	1542
42.55	1290	1421	1522
46.42	1284	1417	1519
50.29	1295	1429	1531
54.16	1319	1454	1557
58.03	1359	1494	1598
61.90	1412	1548	1653
65.76	1480	1617	1722
69.63	1562	1701	1807
73.50	1660	1800	1907

Table A.2.3 Variation of Steady State Sink Rate With Forward Speed at Constant Rotor Speed of 354 rpm [constant $f_e = 16\ ft^2$]

SPEED (KNOTS)	SINK RATE (FPM) FA=16.0	FA=24.0	FA=32.0
0.00	2843	2835	2805
3.86	2803	2795	2787
7.73	2679	2671	2663
11.60	2464	2455	2447
15.47	2138	2134	2131
19.34	1914	1916	1918
23.21	1749	1757	1766
27.08	1628	1645	1662
30.95	1541	1569	1597
34.81	1481	1521	1563
38.68	1442	1498	1556
42.55	1421	1497	1576
46.42	1417	1517	1621
50.29	1429	1556	1691
54.16	1454	1616	1786
58.03	1494	1695	1909
61.90	1548	1795	2061
65.76	1617	1917	2246
69.63	1701	2063	2468
73.50	1800	2235	2733

Table A.2.4 Variation of Steady State Sink Rate With Forward Speed at Constant Rotor Speed of 354 rpm [constant $\delta_e = 0.0087$]

SPEED (KNOTS)	SINK RATE (FPM)	CT(Z)	CT(X)	CT
300	1155	0.086	0.003	0.086
303	1170	0.084	0.003	0.084
307	1185	0.082	0.003	0.082
310	1201	0.080	0.003	0.080
314	1217	0.079	0.003	0.079
317	1233	0.077	0.003	0.077
321	1250	0.075	0.003	0.075
325	1267	0.074	0.003	0.074
328	1284	0.072	0.003	0.072
332	1302	0.070	0.003	0.070
335	1320	0.069	0.003	0.069
339	1339	0.067	0.003	0.068
342	1358	0.066	0.003	0.066
346	1377	0.065	0.003	0.065
349	1397	0.063	0.002	0.063
353	1417	0.062	0.002	0.062
356	1438	0.061	0.002	0.061
360	1459	0.060	0.002	0.060
363	1480	0.059	0.002	0.059
367	1502	0.057	0.002	0.057
370	1524	0.056	0.002	0.056
374	1547	0.055	0.002	0.055
378	1570	0.054	0.002	0.054
381	1593	0.053	0.002	0.053
385	1617	0.052	0.002	0.052
388	1642	0.051	0.002	0.051
392	1667	0.050	0.002	0.050
395	1692	0.049	0.002	0.049
399	1718	0.049	0.002	0.049
402	1744	0.048	0.002	0.048
406	1771	0.047	0.002	0.047

Table A.2.5 Variation of Steady State Sink Rate With Rotor Speed at Constant Forward Speed of 45 Knots

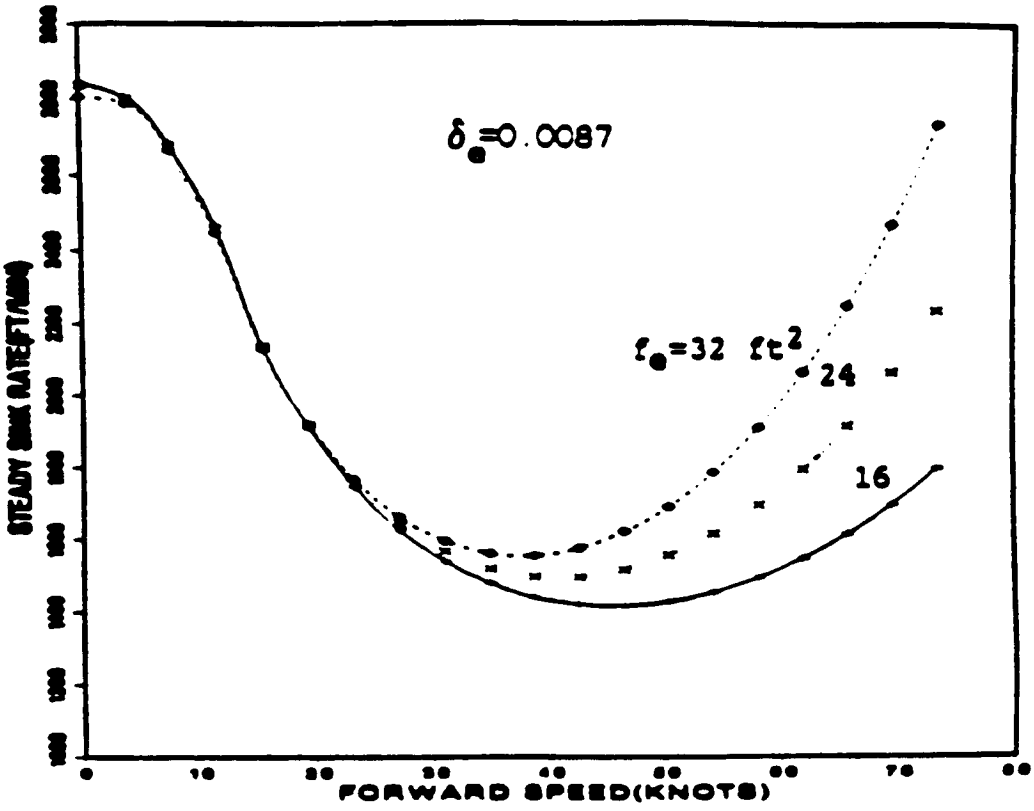

Figure A.3.2 Effects of Parasite Drag on Steady State Sink Rate of Standard OH-58A Helicopter

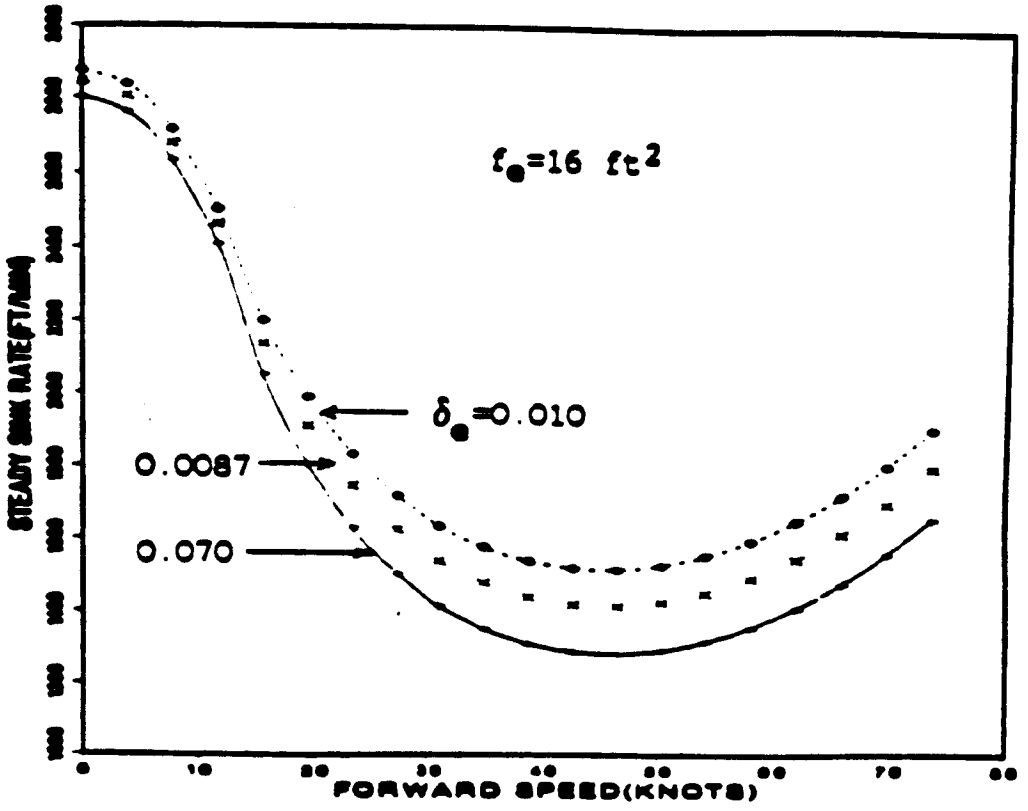

Figure A.3.3 Effects of Profile Drag on Steady State Sink Rate of Standard OH-58A Helicopter

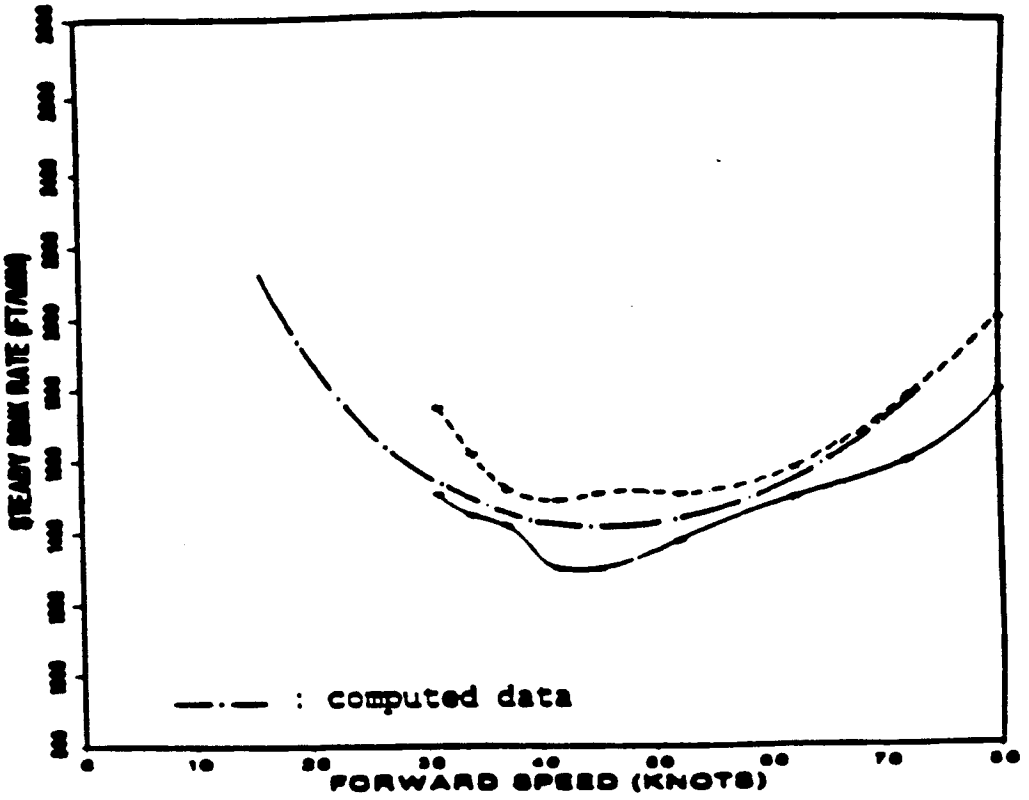

Figure A.3.4 A Comparison of Computed Sink Rate With Experimental Results of Reference [18]

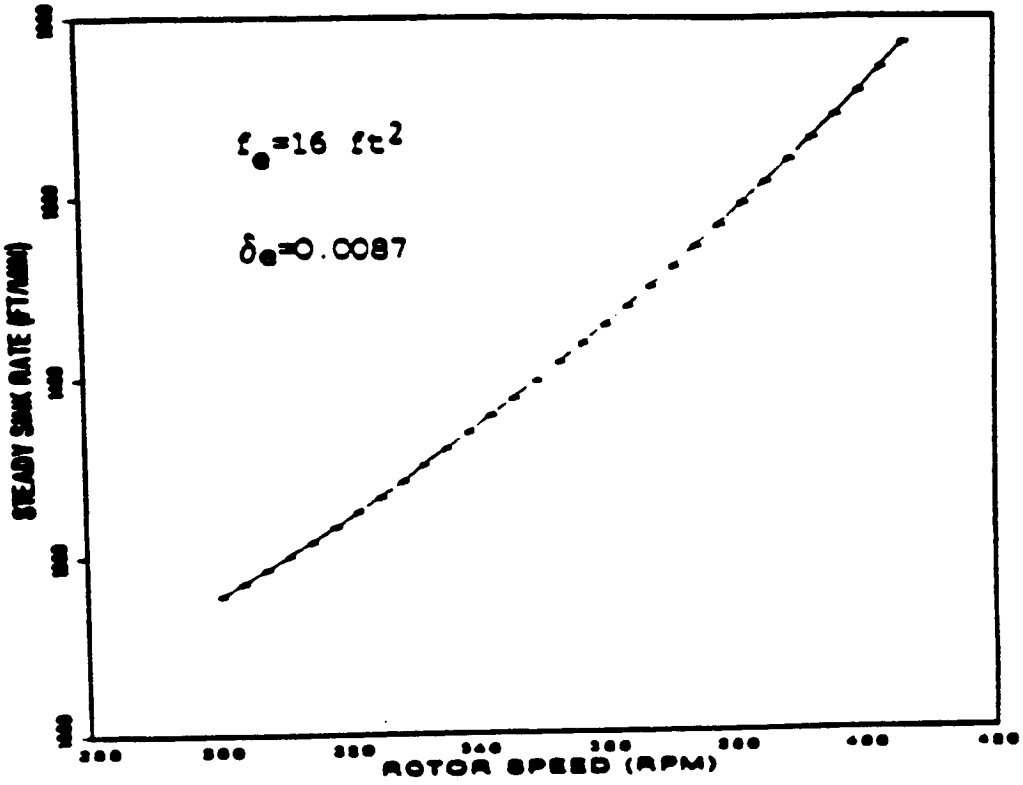

Figure A.3.5 Variation of Sink Rate With Rotor Speed at a Constant Forward Speed of 45 Knots

§A.4 Conclusions

The Flight test data were used to validate the point mass model and also to provide a basis for establishing values for certain parameters in the model. The confidence that can be placed in the results of the optimization programs is considerably enhanced.

Appendix B

Supporting Analysis

§B.1 Introduction

The landing of a helicopter after engine failure has been formulated as an optimal control problem with a path equality constraint (cf. equations (57-64) in Section (2.9)). The problem is repeated here for ease of reference:

$$\min_{\vec{U},\vec{\pi}} \quad I = \frac{1}{2}({x_1}_f^2 + W_x {x_2}_f^2) = \phi(\vec{X}_f),$$

$$\vec{X} = (x_1\ x_2\ x_3\ x_4\ x_5)^T,$$
$$\vec{U} = (u_1\ u_2\ u_3)^T,$$
$$\vec{\pi} = (\tau_f).$$

where $\vec{U}, \vec{X}$ *and* $\vec{\pi}$ are the control ,state and parameter vectors.

subjected to :

(1) equations of motion ($\vec{X}^{\nabla} = \vec{f}$):

$$x_1{}^{\nabla} = \tau_f(g_0 - m_0(u_1 x_3{}^2 + \bar{f} x_1\sqrt{x_1{}^2 + x_2{}^2})),$$

$$x_2{}^{\nabla} = \tau_f m_0(u_2 x_3{}^2 - \bar{f} x_2\sqrt{x_1{}^2 + x_2{}^2}),$$

$$x_3{}^{\nabla} = -\tau_f i_0 x_3{}^2(c_0 + \lambda\sqrt{u_1{}^2 + u_2{}^2}),$$

$$x_4{}^{\nabla} = 0.1\tau_f x_1,$$

$$x_5{}^{\nabla} = 0.1\tau_f x_2.$$

The initial condition of $\vec{X}$ is given by:

$$\vec{X}_0 = (0, \bar{u}_0, 1, 0, 0)^T.$$

(2) path equality constraint ($\vec{S}(\vec{X}, \vec{U}, \vec{\pi}) = 0$):

$$(u_1{}^2 + u_2{}^2) - (\frac{(u_1{}^2 + u_2{}^2)}{\bar{C}_{T_e}})^2 - u_3{}^2 = 0.$$

(3) terminal constraints ($\vec{\psi}(\vec{X}_f, \vec{\pi}) = 0$):

$$x_{4f} - \bar{h}_f = 0,$$

$$x_{5f} - \bar{d}_f = 0.$$

In this appendix, detailed expressions for $\frac{\partial \vec{f}}{\partial \vec{U}}$ (5×3 matrix), $\frac{\partial \vec{f}}{\partial \vec{X}}$ (5×5 matrix), $\frac{\partial \vec{f}}{\partial \vec{\pi}}$ (5×1 matrix), $\frac{\partial \vec{S}}{\partial \vec{U}}$ (1×3 matrix), $\frac{\partial \phi}{\partial \vec{X}_f}$ (1×5 matrix) and $\frac{\partial \vec{\psi}}{\partial \vec{X}_f}$ (2×5 matrix) are given.

§B.2 Determination of $(f_I)_\zeta$

The induced velocity parameter f_I is a function of x_1 and x_2 which in turn are funtions of u_1, u_2, x_1, x_2, and x_3. f_I is thus a function of these variables and the partial derivatives of f_I with respect to u_1,u_2,x_1,x_2 and x_3 are given below.

Let us first define β and γ as follows:

$$\beta = x_1 = p_0 \frac{x_2 u_2 - x_1 u_1}{x_3 (u_1^2 + u_2^2)^{\frac{1}{4}}}, \tag{1}$$

$$\gamma = x_2 = p_0 \frac{x_2 u_1 + x_1 u_2}{x_3 (u_1^2 + u_2^2)^{\frac{1}{4}}}. \tag{2}$$

Once again, the value of the induced velocity parameter f_I, is determined from the expressions:

$$f_I(\beta, \gamma) = \begin{cases} 1.0/\sqrt{(\gamma^2 + (\beta + f_I)^2)}, & \text{If } (2\beta + 3)^2 + \gamma^2 \geq 1; \\ \beta(0.373\beta^2 + 0.598\gamma^2 - 1.991), & \text{otherwise.} \end{cases} \tag{3}$$

In the region where the momentum theory is applicable, (i.e. when $(2\beta + 3)^2 + \gamma^2 \geq 1$) expressions for $f_{I\beta}$ and $f_{I\gamma}$ are given by the following expressions:

$$f_{I\beta} = (\frac{z}{1 - z}), \tag{4}$$

$$f_{I\gamma} = (\frac{z}{1 - z})(\frac{\gamma}{\beta + f_I}). \tag{5}$$

where
$$z = -\frac{(\beta + f_I)}{(\gamma^2 + (\beta + f_I)^2)^{\frac{3}{2}}},$$
$$= -(\beta + f_I) f_I^3. \tag{6}$$

In the vortex-ring state, the expressions of $f_{I\beta}$ and $f_{I\gamma}$ are given simply by:

$$f_{I\beta} = 1.119\beta^2 + 0.598\gamma^2 - 1.991, \tag{7}$$

$$f_{I\gamma} = 1.196\beta\gamma. \tag{8}$$

We can then use the chain-rule:

$$(f_I)_{(\,)} = f_{I\beta}(\beta)_{(\,)} + f_{I\gamma}(\gamma)_{(\,)} \tag{9}$$

where ( ) stands for u_1, u_2, x_1, x_2 or x_3. To determine $(f_I)_{(\,)}$, expressions of $\beta_{(\,)}$ and $\gamma_{(\,)}$ are therefore needed. These expressions, which are identical for both the vortex-ring and momentum theory states, are as given below:

$$
\begin{aligned}
\beta_{x_1} &= -\left(\frac{p_0 u_1}{x_3({u_1}^2+{u_2}^2)^{\frac{3}{4}}}\right),\\
\beta_{x_2} &= +\left(\frac{p_0 u_2}{x_3({u_1}^2+{u_2}^2)^{\frac{3}{4}}}\right),\\
\beta_{x_3} &= -\left(\frac{\beta}{x_3}\right),\\
\beta_{u_1} &= \left(\frac{p_0}{x_3({u_1}^2+{u_2}^2)^{\frac{3}{4}}}\right)\left(-x_1 - 1.5u_1\frac{(x_2u_2-x_1u_1)}{({u_1}^2+{u_2}^2)}\right),\\
\beta_{u_2} &= \left(\frac{p_0}{x_3({u_1}^2+{u_2}^2)^{\frac{3}{4}}}\right)\left(+x_2 - 1.5u_2\frac{(x_2u_2-x_1u_1)}{({u_1}^2+{u_2}^2)}\right),
\end{aligned}
\tag{10}
$$

similarly the expressions for $\gamma_{(\,)}$ are given by:

$$
\begin{aligned}
\gamma_{x_1} &= +\left(\frac{p_0 u_2}{x_3({u_1}^2+{u_2}^2)^{\frac{3}{4}}}\right),\\
\gamma_{x_2} &= +\left(\frac{p_0 u_1}{x_3({u_1}^2+{u_2}^2)^{\frac{3}{4}}}\right),\\
\gamma_{x_3} &= -\left(\frac{\gamma}{x_3}\right),\\
\gamma_{u_1} &= \left(\frac{p_0}{x_3({u_1}^2+{u_2}^2)^{\frac{3}{4}}}\right)\left(+x_2 - 1.5u_1\frac{(x_2u_1+x_1u_2)}{({u_1}^2+{u_2}^2)}\right),\\
\gamma_{u_2} &= \left(\frac{p_0}{x_3({u_1}^2+{u_2}^2)^{\frac{3}{4}}}\right)\left(+x_1 - 1.5u_2\frac{(x_2u_1+x_1u_2)}{({u_1}^2+{u_2}^2)}\right),
\end{aligned}
\tag{11}
$$

Expressions of $(f_I)_{x_1}$, $(f_I)_{x_2}$, $(f_I)_{x_3}$, $(f_I)_{u_1}$ and $(f_I)_{u_2}$ can therefore be computed using equations (4-11) for either the vortex-ring or momentum theory state. These results will be needed in equations (12) and (13) in the next two sections.

§B.3 Expressions for $\partial\vec{f}/\partial\vec{U}$, $\partial\vec{f}/\partial\vec{X}$ and $\partial\vec{f}/\partial\vec{\pi}$

$\frac{\partial\vec{f}}{\partial\vec{U}}$ is a (5×3) , $\frac{\partial\vec{f}}{\partial\vec{X}}$ a (5×5) and $\frac{\partial\vec{f}}{\partial\vec{x}}$ a (5×1) matrix. Detailed expressions of these matrices are as given in the following sub-sections. An individual element of a matrix is indicated (in the usual way) by its row and column position in the matrix. An element which is identically zero is not given.

B.3.1 Expressions for $\partial\vec{f}/\partial\vec{U}$.

$\frac{\partial\vec{f}}{\partial\vec{U}}$ is a (5×3) matrix. Non-zero elements of $\frac{\partial\vec{f}}{\partial\vec{U}}$ are given below:

$$
\begin{aligned}
(1,1) &= -\tau_f m_0 x_3{}^2, \\
(2,2) &= +\tau_f m_0 x_3{}^2, \\
(3,1) &= -\tau_f i_0 x_3{}^2\left(-\frac{0.01x_1}{x_3} + 1.5k_0 f_I\left(\frac{u_1}{(u_1{}^2+u_2{}^2)^{\frac{1}{4}}}\right) + k_0(u_1{}^2+u_2{}^2)^{\frac{3}{4}}(f_I)_{u_1}\right), \\
(3,2) &= -\tau_f i_0 x_3{}^2\left(+\frac{0.01x_2}{x_3} + 1.5k_0 f_I\left(\frac{u_2}{(u_1{}^2+u_2{}^2)^{\frac{1}{4}}}\right) + k_0(u_1{}^2+u_2{}^2)^{\frac{3}{4}}(f_I)_{u_2}\right).
\end{aligned}
\tag{12}
$$

B.3.2 Expressions for $\partial\vec{f}/\partial\vec{X}$.

$\frac{\partial\vec{f}}{\partial\vec{X}}$ is a (5×5) matrix. Non-zero elements of $\frac{\partial\vec{f}}{\partial\vec{X}}$ are given below:

$$
\begin{aligned}
(1,1) &= -m_0\tau_f\bar{f}\left(\sqrt{x_1{}^2+x_2{}^2} + \frac{x_1{}^2}{\sqrt{x_1{}^2+x_2{}^2}}\right), \\
(1,2) &= -m_0\tau_f\bar{f}\left(\frac{x_1x_2}{\sqrt{x_1{}^2+x_2{}^2}}\right), \\
(1,3) &= -2\tau_f m_0 u_1 x_3, \\
(2,1) &= -m_0\tau_f\bar{f}\left(\frac{x_1x_2}{\sqrt{x_1{}^2+x_2{}^2}}\right), \\
(2,2) &= -m_0\tau_f\bar{f}\left(\sqrt{x_1{}^2+x_2{}^2} + \frac{x_2{}^2}{\sqrt{x_1{}^2+x_2{}^2}}\right), \\
(2,3) &= 2\tau_f m_0 u_2 x_3, \\
(3,1) &= -\tau_f i_0 x_3{}^2\left(-\frac{0.01u_1}{x_3} + k_0(f_I)_{x_1}(u_1{}^2+u_2{}^2)^{\frac{3}{4}}\right), \\
(3,2) &= -\tau_f i_0 x_3{}^2\left(+\frac{0.01u_2}{x_3} + k_0(f_I)_{x_2}(u_1{}^2+u_2{}^2)^{\frac{3}{4}}\right),
\end{aligned}
\tag{13}
$$

$$(3,3) = -\tau_f i_0(2c_0 x_3 + 0.01(x_2 u_2 - x_1 u_1) + k_0 x_3 (u_1{}^2 + u_2{}^2)^{\frac{1}{4}}(2f_I + x_3(f_I)_{x_3})),$$

$$(4,1) = 0.1\tau_f,$$

$$(5,2) = 0.1\tau_f.$$

B.3.3 Expressions for $\partial\vec{f}/\partial\vec{\pi}$.

$\frac{\partial\vec{f}}{\partial\vec{\pi}}$ is a (5×1 matrix). Non-zero elements of $\frac{\partial\vec{f}}{\partial\vec{\pi}}$ are given below:

$$\begin{aligned}
(1,1) &= g_0 - m_0(u_1 x_3{}^2 + \bar{f} x_1\sqrt{x_1{}^2 + x_2{}^2}),\\
(2,1) &= m_0(u_2 x_3{}^2 - \bar{f} x_2\sqrt{x_1{}^2 + x_2{}^2}),\\
(3,1) &= -i_0\, x_3{}^2(c_0 + \lambda\sqrt{u_1{}^2 + u_2{}^2}),\\
(4,1) &= 0.1x_1,\\
(5,1) &= 0.1x_2.
\end{aligned} \tag{15}$$

Expressions for the inflow ratio (λ) and advance ratio (μ) are given by the following expressions:

$$\begin{aligned}
\lambda &= 0.01\left(\frac{x_2 u_2 - x_1 u_1}{x_3\sqrt{u_1{}^2 + u_2{}^2}}\right) + k_0 f_I (u_1{}^2 + u_2{}^2)^{\frac{1}{4}},\\
\mu &= 0.01\left(\frac{x_2 u_1 + x_1 u_2}{x_3\sqrt{u_1{}^2 + u_2{}^2}}\right).
\end{aligned} \tag{16}$$

The first equation of (16) on λ is needed in equation (15). The second expression on μ will be needed in equation (19) of Section (B.6).

§B.4 Expressions for $\partial\vec{S}/\partial\vec{U}$

The path equality constraint $\vec{S}$ is not a function of either $\vec{X}$ or $\vec{\pi}$ but only a function of $\vec{U}$. Expressions for $\frac{\partial\vec{S}}{\partial\vec{X}}$ and $\frac{\partial\vec{S}}{\partial\vec{\pi}}$ are therefore identically zero. $\frac{\partial\vec{S}}{\partial\vec{U}}$ is a (1×3) matrix.

Non-zero element of $\frac{\partial \vec{S}}{\partial \vec{U}}$ are as given below:

$$\begin{aligned}(1,1) &= 2u_1(1 - \frac{2({u_1}^2 + {u_2}^2)}{\bar{C}_{T_s}^2}),\\ (1,2) &= 2u_2(1 - \frac{2({u_1}^2 + {u_2}^2)}{\bar{C}_{T_s}^2}),\\ (1,3) &= -2u_3.\end{aligned} \tag{17}$$

§B.5 Expressions for $\partial\phi/\partial\vec{X}_f$ and $\partial\vec{\psi}/\partial\vec{X}_f$

The terminal cost (ϕ) (a scalar) and the hard terminal constraints ($\vec{\psi}$) (q×1 vector) are usually combined to form a ((q+1)×1) vector $\vec{\Phi}$. $\vec{\Phi}$ is not a function of either $\vec{U}$ or $\vec{\pi}$ but only a function of $\vec{X}_f$. $\frac{\partial\vec{\Phi}}{\partial\vec{U}}$ and $\frac{\partial\vec{\Phi}}{\partial\vec{\pi}}$ are therefore identically zero. $\frac{\partial\vec{\Phi}}{\partial\vec{X}_f}$ is a (3×5) matrix. Non-zero elements of $\frac{\partial\vec{\Phi}}{\partial\vec{X}_f}$ are given below:

$$\begin{aligned}(1,1) &= x_1,\\ (1,2) &= W_z x_2,\\ (2,4) &= 1,\\ (3,5) &= 1.\end{aligned} \tag{18}$$

§B.6 Determination of Collective pitch setting, θ_{75}

The collective pitch setting required to obtain a given amount of thrust may be obtained from blade element theory as [24]:

$$\theta_{75} = \frac{(1 + \frac{3}{2}\mu^2)(\frac{6C_T}{a\sigma}) + \frac{3}{2}\lambda(1 - \frac{1}{2}\mu^2)}{(1 - \mu^2 + \frac{9}{4}\mu^4)}$$

where θ_{75} is the rotor collective pitch angle at 75 percent chord, while σ and a are the rotor solidity ratio and rotor blade two dimensional lift curve slope respectively.

The quantities, μ and λ were defined by equations (16) of section (B.3.3). The collective pitch angle θ_{75} is therefore given by the following expression:

$$\begin{aligned}\theta_{75} &= \frac{(\frac{6C_T}{\sigma a})(1+\frac{3}{2}\mu^2)+\frac{3}{2}(1-\frac{\mu^2}{2})\lambda}{1-\mu^2}, \\ &= \frac{(1+\frac{3}{2}\mu^2)(\frac{6\times 10^{-3}\sqrt{u_1{}^2+u_2{}^2}}{\sigma a})+\frac{3}{2}(1-\frac{\mu^2}{2})\lambda}{1-\mu^2}.\end{aligned} \tag{19}$$

Appendix C

Example Problems Solved Using the CPF Algorithm

In the following section, three examples are described, all pertaining to problems with an unknown parameter. Problem (1) is a minimum time and energy problem with an unspecified terminal time. Problem (2) is a specified control law problem and Problem (3) is the classical Brachistochrone problem. These problems are solved numerically using the Combined Parameter and Function Optimization Algorithm developed in Section (3.2).

§C.1 Example Problems

PROBLEM (1) MINIMUM TIME/ENERGY CONTROL

Consider the following minimum time/energy problem:

$$\min_{u,t_f} I = {t_f}^{\alpha} + \frac{1}{2}\beta \int_0^{t_f} u^2 dt$$

The equation of motion is given by

$$\dot{x} = u$$

The initial condition is

$$x(0) = 1 .$$

The terminal condition is

$$x(t_f) = 0 .$$

Values of α and β are chosen to be

$$\alpha = 1 ,$$

$$\beta = 1 .$$

Initial guesses for $u(t)$ and t_f are

$$u(t) = 0 , \qquad \text{for} \qquad 0 \leq t \leq t_f$$

$$t_f = 1 .$$

The problem is first converted to one with fixed end-time (cf. equation (38) of Section (3.2)). The transformed problem with α=β=1 is

$$\min_{u,t_f} I = t_f + \frac{1}{2} t_f \int_0^1 u^2 d\tau$$

The independent variable is now τ which varies from 0 to 1.

The modified equation of motion is given by

$$\dot{x} = t_f u ,$$

where $\dot{(\ )}$ now denotes time differentiation with respect to τ.

The initial condition of $x(0)$ remains unchanged.

The transformed problem is one with an unknown parameter t_f. The problem can be solved using the Combined Parameter and Function optimization algorithm and the optimum solution found is

$$u(t) = -2^{\frac{1}{2}},$$

$$t_f = 2^{-\frac{1}{2}}.$$

The minimum value of the cost function is given by

$$I_{min} = 2^{\frac{1}{2}} = 1.4141.$$

PROBLEM (2) SPECIFIED CONTROL LAW PROBLEM

Consider the following optimization problem:

$$\min_u I = \frac{1}{2}\int_0^1 (x_1{}^2 + u^2)dt$$

subject to the following equations of motion

$$\dot{x}_1 = x_2 + 0.01x_2{}^3,$$

$$\dot{x}_2 = -4x_1 - 5x_2 + 4u.$$

Initial conditions are

$$x_1(0) = 2,$$

$$x_2(0) = 0.$$

There is no terminal condition.

The control law is specified to have the following form

$$u = bx_1,$$

where b is an unknown constant whose value is to be optimally selected. The *transformed* problem becomes

$$\min_b I = \frac{1}{2}\int_0^1 x_1^2 1 + b^2 dt$$

with the following equations of motion

$$\dot{x}_1 = x_2 + 0.01x_2^3,$$

$$\dot{x}_2 = 4x_1(b-1) - 5x_2.$$

while the initial conditions of $x_1(0)$ and $x_2(0)$ remain unchanged.

The transformed problem is a problem with an unknown parameter b but without any control. The problem can be solved using the Combined Parameter and Function optimization algorithm and the optimum value of b found is:

$$b = -0.23387$$

The minimum value of the cost function determined is:

$$I_{soc} = 1.14284.$$

Note that the value of I_{soc} is (slightly) larger than the minimum value of the original problem, where $u(t)$ is open, which is:

$$I_{min} = 1.13289.$$

PROBLEM (3) BRACHISTOCHRONE PROBLEM

Consider the Classical Brachistchrone Problem

$$\min_\theta I = t_f$$

The equations of motion are given by

$$\dot{x}_1 = x_3 \cos\theta\,,$$

$$\dot{x}_2 = x_3 \sin\theta\,,$$

$$\dot{x}_3 = \sin\theta\,.$$

The initial conditions are given by

$$x_1(0) = 0\,,$$

$$x_2(0) = 0\,,$$

$$x_3(0) = 0\,.$$

The terminal condition is given by

$$x_1(t_f) = 1\,.$$

This problem with an unspecified terminal time can be transformed into one with t_f as the unknown parameter (cf. Problem (1)). The transformed problem can be solved using the Combined Parameter and Function Optimization Algorithm. The minimum value of the cost function determined is

$$I_{min} = 1.7724$$

which is very close to the exact solution of $\sqrt{\pi}$.

Appendix D

Generalized Transversality Condition

§D.1 Introduction

In the classical calculus of variations problem, we seek to minimize a cost function J subject to a set of differential equations and terminal constraints: problem:

$$\min_{\bar{u}} J = \phi(\bar{x}_f, t_f) + \int_0^{t_f} L(\bar{x}, \bar{u}, t)dt,$$

$$\dot{\bar{x}} = f(\bar{x}, \bar{u}, t),$$

$$\bar{x}(0) = \text{given},$$

$$\text{and} \qquad \bar{\psi}(\bar{x}_f, t_f) = 0.$$

Here $\bar{x}(n \times 1)$, $\bar{u}(m \times 1)$, and $\bar{\pi}(p \times 1)$ are the state, control and parameter vectors. $\bar{\psi}(q \times 1)$ are the terminal constraint functions. t_f is the specified or unspecified end-time of the problem. If t_f is unspecified, first-order **necessary conditions** of the problem are given by the following relations:

$$
\begin{aligned}
\dot{\vec{x}} &= f(\vec{x},\vec{u},t)\,,\\
\vec{x}(0) &= given\,,\\
\dot{\lambda}^T &= -H_x\,,\\
\lambda^T(t_f) &= (\Phi_x)_{t=t_f}\,,\\
H_u &= 0\,,\\
\vec{\psi}(\vec{x}_f,t_f) &= 0\,.\\
\text{and}\quad (\frac{\partial\Phi}{\partial t} &+ H)_{t=t_f} = 0\,.
\end{aligned}
\tag{1}
$$

where for convenience, we have defined scalar functions H (the Hamiltonian function) and Φ as :

$$
\begin{aligned}
H(\vec{x},\vec{u},\vec{\lambda},t) &= L(\vec{x},\vec{u},t) + \lambda^T f(\vec{x},\vec{u},t)\,,\\
\Phi(\vec{x}_f,t_f,\vec{\mu}) &= \phi(\vec{x}_f,t_f) + \mu^T\psi(\vec{x}_f,t_f)\,.
\end{aligned}
$$

The last condition in (1) is the so called " transversality condition " in the classical literature. It determines the value of the unspecified terminal time, t_f.

The above problem with unspecified end-time can be converted into one with fixed end-time with the following change of independent variable:

$$
\tau = \frac{t}{t_f}\,.
$$

The transformed problem becomes:

$$
\begin{aligned}
\min_{\vec{u},t_f} J &= \phi_1(\vec{x}_f,t_f) + \int_0^1 t_f L(\vec{x},\vec{u},t_f\tau)d\tau,\\
(\vec{x})' &= t_f f(\vec{x},\vec{u},t_f\tau),\\
\vec{x}(0) &= given,\\
\text{and}\qquad \vec{\psi}(\vec{x}_f,t_f) &= 0.
\end{aligned}
$$

Here $(\,)'$ denotes differentiation with respect to the independent variable τ.

The characteristics of the transformed problem are that the end-time is now fixed at $\tau = 1$ but we have introduced into the problem an unknown parameter t_f that is to be "optimally" selected.

The first-order necessary conditions of the transformed problem are similar to those given for the original problem. If we define the following "transformed" functions:

$$\begin{aligned}\tilde{H}(\vec{x},\vec{u},\vec{\lambda}',t_f,\tau) &= t_f L(\vec{x},\vec{u},t_f\tau) + (\vec{\lambda}')^T t_f f(\vec{x},\vec{u},t_f\tau)\,,\\ &= t_f\,[L(\vec{x},\vec{u},t_f\tau) + (\vec{\lambda}')^T f(\vec{x},\vec{u},t_f\tau)]\,,\\ \tilde{\Phi}(\vec{x}_f,t_f,\vec{\mu}') &= \phi(\vec{x}_f,t_f) + (\vec{\mu}')^T\psi(\vec{x}_f,t_f)\,.\end{aligned}$$

Here $\vec{\lambda}'(\tau)$ and $\vec{\mu}'$ are the Lagrange multiplier function and Lagrange multiplier associated with the transformed problem.

The necessary conditions are given by the following relations:

$$\begin{aligned}(\vec{x})' &= t_f f(\vec{x},\vec{u},t_f\tau)\,,\\ \vec{x}(0) &= given\,,\\ \frac{d}{d\tau}(\lambda')^T &= -\tilde{H}_x\,,\\ (\lambda'_1)^T &= (\tilde{\Phi}_x)_1\,,\\ \tilde{H}_u &= 0\,,\\ \vec{\psi}(\vec{x}_f,t_f) &= 0\,,\end{aligned} \qquad (2)$$

$$\text{and} \qquad (\tilde{\Phi}_{t_f})_1 + \int_0^1 \tilde{H}_{t_f}\,d\tau = 0\,.$$

In this appendix we prove that necessary conditions (1) and (2) are equivalent to each other and that the last equation in (2) is a generalized transversality condition.

§D.2 Proof

The proof consists of four parts. The first two parts of the proof establish the facts that $\bar{\lambda}' = \bar{\lambda}$ and $\bar{\mu}' = \bar{\mu}$. The last two parts prove that in the special case when $\bar{\pi} = t_f$. the last equation of necessary conditions (2) becomes the classical transversality condition.

Part (1)

From the optimality condition of (2), we have:

$$\frac{\partial}{\partial u}\tilde{H}(\bar{x}, \bar{u}, \bar{\lambda}', t_f, \tau) = 0,$$
$$t_f \frac{\partial}{\partial u}[L(\bar{x}, \bar{u}, \tau t_f) + (\bar{\lambda}')^T f(\bar{x}, \bar{u}, \tau t_f)] = 0.$$

Since t_f is non-zero, we must have:

$$\frac{\partial}{\partial u}[L(\bar{x}, \bar{u}, \tau t_f) + (\bar{\lambda}')^T f(\bar{x}, \bar{u}, \tau t_f)] = 0 \tag{3}$$

From the optimality condition of the original problem, we have the following relation:

$$H_u = 0,$$
$$\frac{\partial}{\partial u}[L(\bar{x}, \bar{u}, t) + \lambda^T f(\bar{x}, \bar{u}, t)] = 0. \tag{4}$$

A comparison of equation (3) and (4) leads to the conclusion that:

$$\bar{\lambda}' = \bar{\lambda} \tag{4a}$$

The same conclusion can be reached by comparing the adjoint equation:

$$\dot{\lambda}^T = -H_x,$$
$$\text{with} \qquad \frac{\partial}{\partial \tau}(\lambda')^T = -\tilde{H}_x.$$

Part (2)

To prove that $\vec{\mu}' = \vec{\mu}$, we can compare the terminal conditions of the adjoint equations (i.e. the λ-equation and the λ'-equation). From Part (1) of the proof, we have:

$$\begin{aligned}(\vec{\lambda}')_1^T &= (\vec{\lambda}_1)^T , \\ &= (\frac{\partial \tilde{\Phi}}{\partial x})_1 , \\ &= [\frac{\partial}{\partial x}(\phi(\vec{x}_f, t_f) + (\vec{\mu}')^T \psi(\vec{x}_f, t_f))]_{\tau=1} .\end{aligned} \tag{5}$$

Whereas the terminal condition of the λ-equation is given by

$$\lambda^T(t = t_f) = [\frac{\partial}{\partial x}(\phi(\vec{x}_f, t_f) + \mu^T \psi(\vec{x}_f, t_f))]_{t=t_f} , \tag{6}$$

a comparison of equation (5) and (6) leads to the conclusion that

$$\vec{\mu}' = \vec{\mu} \tag{6a}$$

Part (3)

Here, we prove an intermediate result that is needed in part (4). To express $\int_0^1 \tilde{H}_{t_f} d\tau$ in terms of H, we note that:

$$\begin{aligned}\int_0^1 \tilde{H}_{t_f} d\tau &= \int_0^1 \frac{\partial}{\partial t_f}[t_f H(\vec{x}, \vec{u}, \tau t_f)] d\tau , \\ &= \int_0^1 [H(\vec{x}, \vec{u}, \tau t_f) + t_f \frac{\partial}{\partial t_f} H(\vec{x}, \vec{u}, \tau t_f)] d\tau , \\ &= \int_0^1 [H(\vec{x}, \vec{u}, \tau t_f) + t_f \frac{\partial}{\partial t}(H(\vec{x}, \vec{u}, t)) \frac{\partial t}{\partial t_f}] d\tau .\end{aligned}$$

But since:

$$\tau = \frac{t}{t_f} ,$$

$$\frac{\partial t}{\partial t_f} = \tau ,$$

and $$d\tau = \frac{dt}{t_f} .$$

Therefore the above equation can be simplified to:

$$\begin{aligned}\int_0^1 \tilde{H}_{t_f} d\tau &= \int_0^{t_f} [H(\bar{x},\bar{u},t) + t\frac{\partial H}{\partial t}(\bar{x},\bar{u},t)]\frac{dt}{t_f}, \\ &= \frac{1}{t_f}\int_0^{t_f}(H + t\frac{\partial H}{\partial t})dt, \\ &= \frac{1}{t_f}\int_0^{t_f}\frac{\partial}{\partial t}(tH)dt. \\ &= \frac{1}{t_f}(tH)_0^{t_f}, \\ &= (H)_{t=t_f}.\end{aligned} \tag{7}$$

This result is needed in the next part of the proof.

Part (4)

To express $(\tilde{\Phi}_{t_f})_1$ in terms of $(\frac{\partial\Phi}{\partial t})_{t=t_f}$, we note that:

$$\begin{aligned}(\tilde{\Phi}_{t_f})_1 &= (\frac{\partial\tilde{\Phi}}{\partial t_f})_{\tau=1}, \\ &= [\frac{\partial}{\partial t_f}(\phi(\bar{x}_f,t_f) - \mu^T\psi(\bar{x}_f,t_f))]_{\tau=1}, \\ &= [\frac{\partial}{\partial t}(\phi(\bar{x}_f,t) - \mu^T\psi(\bar{x}_f,t))]_{t=t_f}. \\ &= (\frac{\partial\Phi}{\partial t})_{t=t_f}.\end{aligned} \tag{8}$$

From equations (7) and (8), we obtain the final result:

$$\begin{aligned}(\tilde{\Phi}_{t_f})_1 + \int_0^1(\tilde{H}_{t_f})\,d\tau, & \\ &= (\frac{\partial\Phi}{\partial t} + H)_{t=t_f}, \\ &= 0.\end{aligned} \tag{9}$$

which completes the proof.

§D.3 Conclusion

In section (D.2). we have proved that the necessary conditions (2) for the general problem with fixed end-time (τ=1) but with an unknown parameter vector ($\bar{\pi}$) are equivalent to the necessary conditions (1) for problems without the unknown parameter vector $\bar{\pi}$ but with an unspecified end-time t_f. The necessary condition

$$(\Phi_\pi)_1 + \int_0^1 H_\pi d\tau = 0$$

in equation (2) that determines the value of $\bar{\pi}$ is in effect a more general form of the classical " transversality condition."

Appendix E

Definitions of Matrices used in Section (3.4)

§E.1 Introduction

In Section (3.4), we formulated a linear, time-varying Two-Point Boundary-Value Problem with integral path constraints. The problem was formulated in terms of the matrices S_i (where i = 1,...,13), A_{ij} and C_{ij} where i = 1,2 and j = 1, 2 and 3. These matrices themselves are functions of H_{uu}, $H_{u\pi}$, H_{zz}, H_{uz}, $H_{\pi z}$ and $H_{\pi u}$. Detailed expressions of S_i, A_{ij}, B_{ij} as well as those of H_{uu}, $H_{u\pi}$, H_{zz}, H_{uz}, $H_{\pi z}$ and $H_{\pi u}$ are given in this appendix.

§E.2 Expressions for $H_{(\ )}$

Expressions for H_{uu}, $H_{u\pi}$, H_{zz}, H_{uz}, $H_{\pi z}$ and $H_{\pi u}$ are given in this section. For brevity, we assume that the integral payoff L is zero. Cases when L is not zero can be treated in either of the following ways. The problem may be converted to one with only terminal payoff by the addition of an auxiliary state whose integral is L. Alternatively, the matrices $L_{uu}(m \times m)$, $L_{u\pi}(m \times p)$, $L_{zz}(n \times n)$, $L_{uz}(m \times n)$, $L_{\pi z}(p \times n)$ and $L_{\pi u}(p \times m)$ must be computed and added to the the appropriate $H_{(\ )}$

matrix. We have also assumed here that the path constraints $\bar{S}$ are not functions of $\bar{\pi}$. General expression of $H_{(\,)}$ is given by the following expression [29]:

$$H_{\alpha\beta} = \frac{\partial}{\partial\beta}(\frac{\partial H}{\partial\alpha})^T.$$

Without the integral payoff L, the Hamiltonian function H is given by the following expression:

$$H = \lambda^T f - \rho^T S$$

The H_{uu}, $H_{u\pi}$, H_{ux}, $H_{\pi x}$, $H_{\pi u}$, and H_{xx} matrices are given by the following expressions: $H_{uu}(m \times m)$

$$H_{uu} = \frac{\partial}{\partial u}(f_u^T\lambda + S_u^T\rho),$$
$$= \begin{pmatrix} \sum_{i=1}^{n}\lambda_i\frac{\partial^2 f_i}{\partial u_1^2} + \sum_{j=1}^{r}\rho_j\frac{\partial^2 S_j}{\partial u_1^2} & \cdots & \sum_{i=1}^{n}\lambda_i\frac{\partial^2 f_i}{\partial u_1\partial u_m} + \sum_{j=1}^{r}\rho_j\frac{\partial^2 S_j}{\partial u_1\partial u_m} \\ \vdots & \ddots & \vdots \\ symmetry & \cdots & \sum_{i=1}^{n}\lambda_i\frac{\partial^2 f_i}{\partial u_m^2} + \sum_{j=1}^{r}\rho_j\frac{\partial^2 S_j}{\partial u_m^2} \end{pmatrix}.$$

$H_{u\pi}(m \times p)$

$$H_{u\pi} = \frac{\partial}{\partial\pi}(f_u^T\lambda),$$
$$= \begin{pmatrix} \sum_{i=1}^{n}\lambda_i\frac{\partial^2 f_i}{\partial\pi_1\partial u_1} & \cdots & \sum_{i=1}^{n}\lambda_i\frac{\partial^2 f_i}{\partial\pi_p\partial u_1} \\ \vdots & \ddots & \vdots \\ \sum_{i=1}^{n}\lambda_i\frac{\partial^2 f_i}{\partial\pi_1\partial u_m} & \cdots & \sum_{i=1}^{n}\lambda_i\frac{\partial^2 f_i}{\partial\pi_p\partial u_m} \end{pmatrix}.$$

$H_{ux}(m \times n)$

$$H_{ux} = \frac{\partial}{\partial x}(f_u^T\lambda + S_u^T\rho)\,,$$
$$= \begin{pmatrix} \sum_{i=1}^{n}\lambda_i\frac{\partial^2 f_i}{\partial u_1\partial x_1} + \sum_{j=1}^{r}\rho_j\frac{\partial^2 S_j}{\partial u_1\partial x_1} & \cdots & \sum_{i=1}^{n}\lambda_i\frac{\partial^2 f_i}{\partial u_1\partial x_n} + \sum_{j=1}^{r}\rho_j\frac{\partial^2 S_j}{\partial u_1\partial x_n} \\ \vdots & \ddots & \vdots \\ \sum_{i=1}^{n}\lambda_i\frac{\partial^2 f_i}{\partial u_m\partial x_1} + \sum_{j=1}^{r}\rho_j\frac{\partial^2 S_j}{\partial u_m\partial x_1} & \cdots & \sum_{i=1}^{n}\lambda_i\frac{\partial^2 f_i}{\partial u_m\partial x_n} + \sum_{j=1}^{r}\rho_j\frac{\partial^2 S_j}{\partial u_m\partial x_n} \end{pmatrix}.$$

$H_{\pi x}(p \times n)$

$$H_{\pi x} = \frac{\partial}{\partial x}(f_\pi^T\lambda)\,,$$
$$= \begin{pmatrix} \sum_{i=1}^{n}\lambda_i\frac{\partial^2 f_i}{\partial x_1\partial \pi_1} & \cdots & \sum_{i=1}^{n}\lambda_i\frac{\partial^2 f_i}{\partial x_n\partial \pi_1} \\ \vdots & \ddots & \vdots \\ \sum_{i=1}^{n}\lambda_i\frac{\partial^2 f_i}{\partial x_1\partial \pi_p} & \cdots & \sum_{i=1}^{n}\lambda_i\frac{\partial^2 f_i}{\partial x_n\partial \pi_p} \end{pmatrix}.$$

$H_{\pi u}(p \times m)$

$$H_{\pi u} = (H_{u\pi})^T$$

$H_{xx}(n \times n)$

$$H_{xx} = \frac{\partial}{\partial x}(f_x^T\lambda + S_x^T\rho)\,,$$
$$= \begin{pmatrix} \sum_{i=1}^{n}\lambda_i\frac{\partial^2 f_i}{\partial x_1^2} + \sum_{j=1}^{r}\rho_j\frac{\partial^2 S_j}{\partial x_1^2} & \cdots & \sum_{i=1}^{n}\lambda_i\frac{\partial^2 f_i}{\partial x_1\partial x_n} + \sum_{j=1}^{r}\rho_j\frac{\partial^2 S_j}{\partial x_1\partial x_n} \\ \vdots & \ddots & \vdots \\ \textit{symmetry} & \cdots & \sum_{i=1}^{n}\lambda_i\frac{\partial^2 f_i}{\partial x_n^2} + \sum_{j=1}^{r}\rho_j\frac{\partial^2 S_j}{\partial x_n^2} \end{pmatrix}.$$

Here the time-varying functions $\vec{\lambda}(\tau)$, $\vec{\rho}(\tau)$, $\frac{\partial}{\partial u}(f_u)^T$, $\frac{\partial}{\partial u}(S_u)^T$, $\frac{\partial}{\partial \pi}(f_u)^T$, $\frac{\partial}{\partial x}(f_u)^T$, $\frac{\partial}{\partial x}(S_u)^T$, and $\frac{\partial}{\partial x}(f_\pi)^T$ are evaluated on the nominal optimal path.

§E.3 Expressions for $S_{(\ )}$

The dimensions and detailed expressions of S_i, where i = 1,...,13 (note that S_9 is not defined) are given by the following relations:

$$
\begin{aligned}
S_1(r \times n) &= S_u H_{uu}^{-1} H_{ux} - S_x \,. \\
S_2(r \times p) &= S_u H_{uu}^{-1} H_{u\pi} - S_\pi \,. \\
S_3(r \times n) &= S_u H_{uu}^{-1} f_u^T \,, \\
S_4(r \times r) &= S_u H_{uu}^{-1} S_u^T \,, \\
S_5(p \times p) &= (\Phi_{\pi\pi})_1 + \int_0^1 H_{\pi\pi} d\tau \,, \\
S_6(m \times n) &= -H_{uu}^{-1}(H_{ux} - S_u^T S_4^{-1} S_1) \,, \\
S_7(m \times n) &= -H_{uu}^{-1}(f_u^T - S_u^T S_4^{-1} S_3) \,, \\
S_8(m \times p) &= -H_{uu}^{-1}(H_{u\pi} - S_u^T S_4^{-1} S_2) \,, \\
S_{10}(p \times 1) &= (\Phi_{\pi x})_1 (\delta\vec{x})_1 + (\psi_\pi^T)_1 (\delta\vec{\mu})_1 \,, \\
S_{11}(p \times p) &= S_5 + \int_0^1 [H_{\pi u} S_8 - S_\pi^T S_4^{-1} S_2 \, d\tau \,, \\
S_{12}(p \times n) &= H_{\pi x} + H_{\pi u} S_6 - S_\pi^T S_4^{-1} S_1 \,, \\
\text{and } S_{13}(p \times n) &= H_{\pi u} S_7 + f_\pi^T - S_\pi^T S_4^{-1} S_3 \,.
\end{aligned}
$$

Note that S_1 to S_4 are defined only when the matrix H_{uu} is non-singular. This is referred to as the **convexity condition** (or strengthened Legendre- Clebsch condition) in calculus of variations. The existence of the matrices S_6 to S_8 and S_{11} to S_{13} also depends on the non-singularity of both H_{uu} and S_4 $(= S_u H_{uu}^{-1} S_u^T)$. The latter condition is in effect a modified form of the convexity condition for problems with path equality constraints $\vec{S}$. It requires that all the path equality

constraints $\bar{S}$ must involve some components of the control vector $\bar{u}$ so as to ensure that $det(S_4) \neq 0$.

§E.4 Expressions for A_{ij}

In terms of the matrices S_i defined in the last section, expressions for A_{ij} are given below :

$$\begin{aligned} A_{11}(m \times n) &= S_6 , \\ A_{12}(m \times n) &= S_7 , \\ A_{13}(r \times n) &= -S_4^{-1} S_1 , \\ A_{21}(r \times n) &= -S_4^{-1} S_3 , \\ A_{22}(m \times p) &= S_8 , \\ \text{and } A_{23}(r \times p) &= -S_4^{-1} S_2 . \end{aligned}$$

These expressions for A_{ij} are needed in the computations of the neighboring optimal feedback gains, Λ_i (where $i = 1, 2$ and 3) in Section (3.4).

§E.5 Expressions for C_{ij}

In terms of the matrices S_i defined in section (E.3), expressions of C_{ij} are given by the following relations:

$$\begin{aligned} C_{11}(n \times n) &= f_x + f_u S_6 , \\ C_{12}(n \times n) &= f_u S_7 , \\ C_{13}(n \times p) &= f_\pi + f_u S_8 , \\ C_{21}(n \times n) &= -H_{xx} - H_{xu} S_6 + S_x^T S_4^{-1} S_1 , \\ C_{22}(n \times n) &= -f_x^T - H_{xu} S_7 + S_x^T S_4^{-1} S_3 , \\ \text{and } C_{23}(n \times p) &= -H_{x\pi} - H_{xu} S_8 + S_x^T S_4^{-1} S_2 . \end{aligned}$$

These expressions for C_{ij} are needed in the solution of time- varying Two-Point Boundary-Value Problem formulated in Section (3.4).

Appendix F

Iterative Solution for TPBVPs with Integral Path Constraints

In Section (3.4), we consider small deviations from a nominal path produced by small perturbations in $\delta\vec{x}(0)$ and $\delta\vec{\psi}$. These perturbations give rise to $\delta\vec{x}(\tau)$, $\delta\vec{\lambda}(\tau)$, $\delta\vec{u}(\tau)$, $\delta\vec{p}(\tau)$ and $\delta\vec{\psi}$. The perturbed quantities are determined by a linear, time-varying Two-Point Boundary-Value Problem (TPBVP) with integral path equality constraints. The general form of the problem is given by equations (3-6) of Section (3.4).

When ϕ, $\vec{\psi}$, $\vec{S}$ and f_π are not functions of $\vec{\pi}$, the TPBVP can be simplified and solved using the **Backward Sweep Method** of reference [29]. The resultant neighboring optimal feedback law has the form

$$\delta\vec{u} = -\Lambda_1\delta\vec{x} - \Lambda_2\delta\vec{\psi} - \Lambda_3\delta\vec{\pi}.$$

The values of $\delta\vec{\pi}$ needed in the above feedback law can be obtained from the solution of integral path equality constraints. An iterative procedure which imbeds the solution of $\delta\vec{\pi}$ in the solution of the TPBVP is described in this appendix.

§F.1 Problem Formulation

The TPBVP consists of the following differential relations:

$$\begin{pmatrix} \delta\dot{\vec{x}} \\ \delta\dot{\vec{\lambda}} \end{pmatrix} = \begin{pmatrix} C_{11} & C_{12} & C_{13} \\ C_{21} & -C_{11}^T & C_{23} \end{pmatrix} \begin{pmatrix} \delta\vec{x} \\ \delta\vec{\lambda} \\ \delta\vec{\pi} \end{pmatrix} \tag{1}$$

and path equality constraints

$$\vec{\Omega} = S_{11}\delta\vec{\pi} + \int_0^1 (S_{12}\delta\vec{x} + S_{13}\delta\vec{\lambda})\, d\tau = 0. \tag{2}$$

The end-conditions of (1) are

$$\begin{aligned} &\delta\vec{x}(0) = \textit{given}, \\ &(\delta\vec{\psi})_1 = (\psi_x)_1(\delta\vec{x})_1 = \textit{given}, \\ &(\delta\vec{\lambda})_1 = (\Phi_{xx})_1(\delta\vec{x})_1 + (\psi_x^T)_1\delta\vec{\mu}. \end{aligned} \tag{3}$$

Here $\delta\vec{x}(\tau)(n \times 1)$, $\delta\vec{\lambda}(\tau)(n \times 1)$ and $\delta\vec{\pi}(p \times 1)$ are variations in the state $x(\tau)$, Lagrange multiplier $\lambda(\tau)$, and the unknown parameter $\vec{\pi}$ from their nominal values. The matrices $C_{ij}(\tau)$ and $S_i(\tau)$ are defined in Appendix (E).

Solution of the TPBVP with path equality constraints can be obtained using a modified form of the backward sweep method. The solution of the problem is given by the following relations:

$$\begin{aligned} \delta\vec{\lambda} &= T\,\delta\vec{x} + R\,\delta\vec{\mu} + P\,\delta\vec{\pi}, \\ \delta\vec{\psi} &= R^T\,\delta\vec{x} + Q\,\delta\vec{\mu} + H\,\delta\vec{\pi}. \end{aligned} \tag{4}$$

where $T(n \times n)$, $R(n \times q)$, $P(n \times p)$, $Q(q \times q)$ and $H(q \times p)$ are matrices that satisfy the following differential equations

$$\dot{T} = -TC_{11} - C_{11}^T T - TC_{12} T + C_{21},$$

$$\dot{R} = -(C_{11}^T + TC_{12})R,$$

$$\dot{P} = C_{23} - C_{11}^T P - T(C_{12}P + C_{13}),$$

$$\dot{Q} = -R^T C_{12} R,$$

$$\text{and } \dot{H} = -R^T(C_{12}P + C_{13}).$$

and with the following terminal conditions

$$T(1) = (\Phi_{xx})_1,$$

$$R(1) = (\psi_x^T)_1,$$

$$P(1) = (\Phi_{xx})_1 = 0,$$

$$Q(1) = 0,$$

$$\text{and } H(1) = (\psi_x)_1 = 0.$$

Using these terminal conditions, the matrix time histories can be obtained by backward integrations of the differential equations given above. The task remains to find the value of $\delta\vec{\pi}$ that also satisfies the integral path equality constraints

$$\vec{\Omega} = S_{11}\delta\vec{\pi} + \int_0^1 (S_{12}\delta\vec{x} + S_{13}\delta\vec{\lambda})\, d\tau = 0.$$

Once determined, $\delta\vec{\pi}$ can be used in the neighboring optimum feedback law

$$\delta\vec{u} = -\Lambda_1\delta\vec{x} - \Lambda_2\delta\vec{\psi} - \Lambda_3\delta\vec{\pi} \qquad (5)$$

where the time-varying gains, Λ_i ($i = 1, 2$ and 3) are given by the following relations:

$$\Lambda_1(m \times n) = -[A_{11} + A_{12}(T - RQ^{-1}R^T)],$$

$$\Lambda_2(m \times q) = -A_{12}RQ^{-1},$$

$$\text{and } \Lambda_3(m \times p) = -[A_{13} + A_{12}(P - RQ^{-1}H)].$$

§F.2 Solution method

An iterative procedure can be constructed for the solution of the problem posed in the last section. We first note from equation (4) that

$$\delta\vec{\lambda} = [T - RQ^{-1}R^T]\delta\vec{x} + [RQ^{-1}]\delta\vec{\psi} + [P - RQ^{-1}H]\delta\vec{\pi}.$$

Therefore the initial conditions needed for the forward integration of equation (1) are given by the following relations:

$$\begin{aligned} (\delta\vec{x})_0 &= \textit{given}, \\ (\delta\vec{\lambda})_0 &= [T - RQ^{-1}R^T]_0(\delta\vec{x})_0 + [RQ^{-1}]_0\delta\vec{\psi} + [P - RQ^{-1}H]_0\delta\vec{\pi}. \end{aligned} \tag{6}$$

If we denote the value of $\delta\vec{\pi}$ at the i^{th} iteration by $\delta\vec{\pi}_i$, we can substitute this value of $\delta\vec{\pi}$ into equation (6) and integrate equation (1) forward to obtain time histories of $[\delta\vec{x}(\tau)]_i$ and $[\delta\vec{\lambda}(\tau)]_i$ of the i^{th} iteration. These time histories can then be substituted into equation (2) to obtain the value of $\vec{\Omega}$ at i^{th} iteration

$$\vec{\Omega}_i = S_{11}[\delta\vec{\pi}]_i + \int_0^1 (S_{12}(\tau)[\delta\vec{x}(\tau)]_i + S_{13}(\tau)[\delta\vec{\lambda}(\tau)]_i)\, d\tau.$$

If all the components of $\vec{\Omega}_i$ is less than ϵ, i.e. $|\,[\vec{\Omega}_i]_j\,| \leq \epsilon$, where $j = 1,...,p$ and ϵ is a small, pre-selected quantity (for example $\epsilon = 10^{-4}$), then the value of $\delta\vec{\pi}$ used in the present iteration is close enough to the correct value and can be used in the feedback law. Otherwise, $[\delta\vec{\pi}]_i$ must be improved to better satisfy path equality constraints in the next (i.e. $(i+1)^{th}$) iteration.

To construct an iterative procedure, let us define the following vectors/matrices:

$$\begin{aligned}
\vec{y} &= \begin{pmatrix} \delta\vec{x} \\ \delta\vec{\lambda} \end{pmatrix}, \\
\vec{p} &= (\delta\vec{\pi}), \\
A &= \begin{pmatrix} C_{11} & C_{12} \\ C_{21} & C_{22} \end{pmatrix}, \\
B &= \begin{pmatrix} C_{13} \\ C_{23} \end{pmatrix}, \\
C &= \begin{pmatrix} (\delta\vec{x})_0 \\ [T - RQ^{-1}R^T]_0(\delta\vec{x})_0 + [RQ^{-1}]_0\delta\vec{\psi} \end{pmatrix}, \\
D &= \begin{pmatrix} 0 \\ [P - RQ^{-1}H]_0 \end{pmatrix}
\end{aligned} \tag{7}$$

Equations (1) and (6) can now be written in more compact forms as follow:

$$\begin{aligned}
\dot{\vec{y}}(\tau) &= A(\tau)\vec{y} + B(\tau)\vec{p}, \\
\vec{y}(0) &= C + D\vec{p}.
\end{aligned} \tag{8}$$

from which we note that $\vec{p}$ $(=\delta\vec{\pi})$ enters into both the differential equation and its initial condition **linearly**.

Now consider the effect of variation in $\vec{p}$, i.e.

$$\vec{p} \rightarrow \vec{p} + \Delta\vec{p},$$

(where $\Delta\vec{p}$ is not small) on the solution of equation (8). Let the corresponding change in $\vec{y}$ be

$$\vec{y} \rightarrow \vec{y} + \Delta\vec{y}.$$

If we substitute the last two equations into equation (8), we obtain the following relation between the Δ-quantities

$$\Delta\vec{y} = f(\tau)\Delta\vec{p}, \tag{9}$$

where $f(\tau)$ is a $(2n \times p)$ matrix that satisfies the following first-order, linear, time-varying differential equation

$$\dot{f} = A(\tau)f + B(\tau)\,, \tag{10}$$

and with the following initial condition

$$f(0) = [D]\,.$$

The result given in equation (9) is needed in our subsequent analysis.

§F.3 Iterative Procedure

If we denote the value of $\vec{p}$ at the i^{th} iteration by $\vec{p}_i$, and if $\vec{p}_i$ does not meet the path equality constraints, then

$$\vec{\Omega}_i = S_{11}\vec{p}_i + \int_0^1 (S_{12}, S_{13})\,\vec{y}_i d\tau \neq 0\,,$$

To come closer to satisfying the constraints, we change $\vec{p}_i$ by $\Delta\vec{p}_i$ in our next iteration. The corresponding change in $\vec{y}_i$ is given by equation (9). The path constraints at the $(i+1)^{th}$ iteration are

$$0 = \vec{\Omega}_{i+1} = S_{11}(\vec{p}_i + \Delta\vec{p}_i) + \int_0^1 (S_{12}, S_{13})\,[\vec{y}_i + f(\tau)\Delta\vec{p}_i]d\tau\,, \tag{11}$$

where $\Delta\vec{p}_i$ is selected in such a way that path equality constraints at the $(i+1)^{th}$ are satisfied exactly.

If we substract the $\vec{\Omega}_{i+1}$- equation from the $\vec{\Omega}_i$- equation, we get the following relation that can be used to solve for $\Delta\vec{p}_i$:

$$-\vec{\Omega}_i = [S_{11} + \int_0^1 (S_{12}, S_{13})f(\tau)d\tau](\Delta\vec{p}_i)\,, \tag{12}$$

$$\text{therefore}\quad \Delta\vec{p}_i = -K\,\vec{\Omega}_i\,.$$

where

$$K = [S_{11} + \int_0^1 (S_{12}, S_{13}) f(\tau) d\tau]^{-1} \tag{13}$$

Since $S_{11}(\tau)$, $S_{12}(\tau)$, and $S_{13}(\tau)$ can be computed (cf. Appendix (E)) and $f(\tau)$ is the solution of equation (10), the $(p \times p)$ gain matrix K can be computed.

Once the value of $\Delta\vec{p}_i$ is computed, the value of $\vec{p}$ for the $(i+1)^{th}$ iteration can be computed as

$$\begin{aligned} \vec{p}_{i+1} &= \vec{p}_i + \Delta\vec{p}_i, \\ &= \vec{p}_i - K\vec{\Omega}_i. \end{aligned} \tag{14}$$

The path constraints are satisfied "exactly" if we use this value of $\vec{p}$ for the $(i+1)^{th}$ iteration.

Alternatively, an iterative procedure can be constructed as follow. Here instead of finding the value of K from equation (13) and using it in the computation of $\vec{p}_{i+1}$ for the $(i+1)^{th}$ iteration, we choose to compute the value of $\vec{p}_{i+1}$ as follow:

$$\begin{aligned} (\vec{p})_{i+1} &= \vec{p}_i - \tilde{K}[\vec{\Omega}]_i, \\ \text{or} \quad (\delta\vec{\pi})_{i+1} &= (\delta\vec{\pi})_i - \tilde{K}[\vec{\Omega}]_i. \end{aligned} \tag{13}$$

Equation (13) states that the correction that has to be made after the i^{th} iteration is proportional to the negated value of the constraint violation $\vec{\Omega}_i$. $\tilde{K}(p \times p)$ is an arbritarily selected, positive gain matrix. Now instead of meeting the path constraints in one single step (with substantial amount of calculation in that one step), we meet them iteratively in several steps. The iterative procedure ends when the conditions $| [\vec{\Omega}_i]_j | \leq \epsilon$ for $j = 1,...,p$ are met (this also means that the correction to $\vec{p}$ in the next iteration is going to be insignificantly small). A flow chart of this iterative procedure for the case when $p = 1$ is shown in Figure (F.3.1).

Once determined, the value of $\delta\vec{\pi}$ can be used in the neighboring optimal feedback law and the TPBVP with path equality constraints is solved.

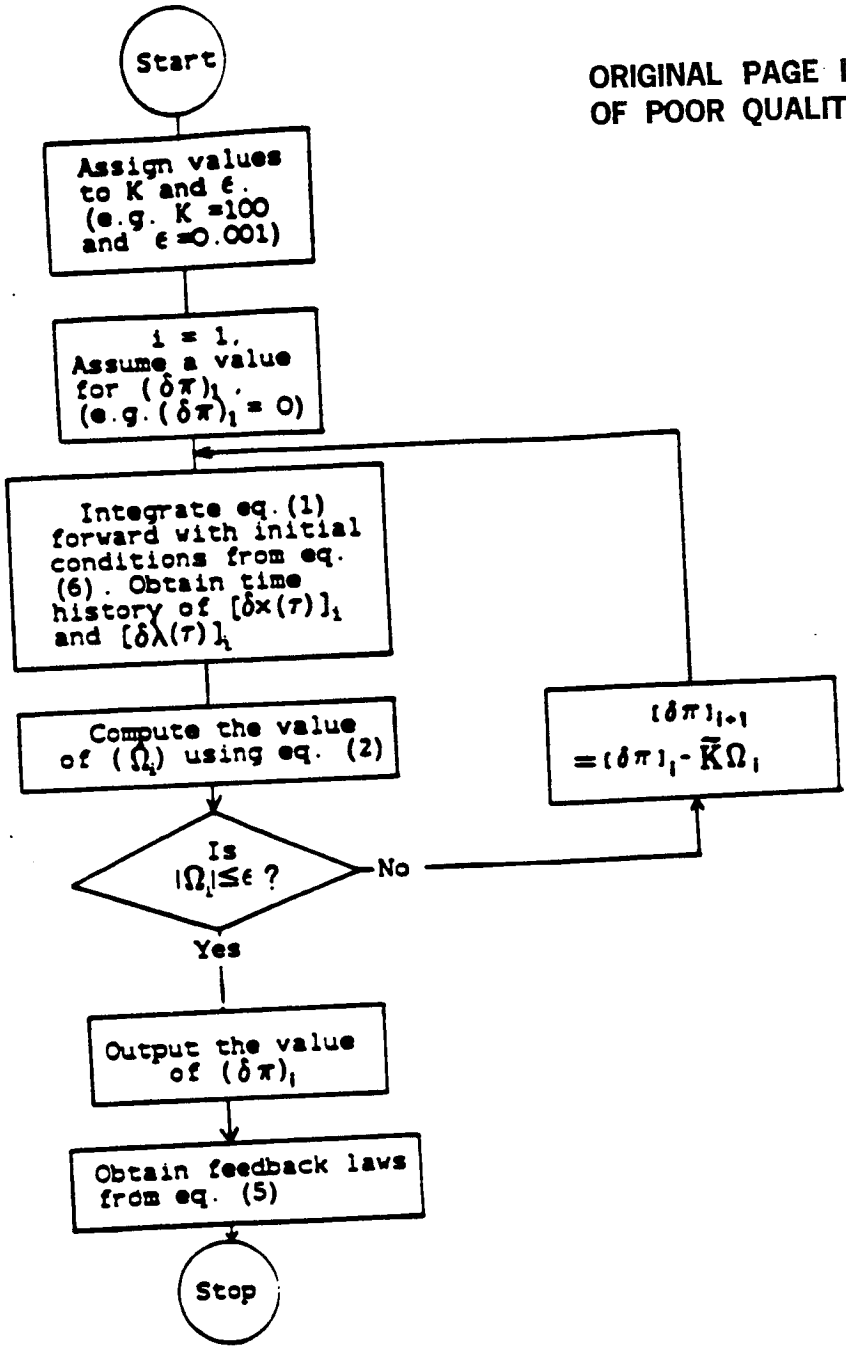

Figure F.3.1 An iterative procedure to find $\delta\bar{\pi}$

Appendix G

Example Problems Solved Using the SGR Technique

Four example applications of the Sequential Gradient Restoration Optimization Algorithm are given in this chapter. Example (1) has a state variable inequality constraint. Example (2) has a bound on the control. Example (3) is one with multiple path constraints involving both the state and the control vectors. Lastly, Example (4) involves a situation where there is a bound on the time rate of change of one of the states. Whenever necessary, the path inequality constraints are first converted to equality constraints that involve the controls. The Sequential Gradient Restoration (SGR) method is then used to solve the optimal control problem with nondifferential constraints.

§G.1 BOUNDED BRACHISTOCHRONE PROBLEM [29]

Consider the following optimization problem:

$$\min_{u} I = t_f$$

The equations of motion are given by

$$\dot{V} = g \sin\gamma ,$$

$$\dot{x} = V \cos\gamma ,$$

$$\dot{y} = V \sin\gamma ,$$

The initial conditions are :

$$V(0) = 0 ,$$

$$x(0) = 0 ,$$

$$y(0) = 0 .$$

The terminal condition is :

$$x(t_f) = 1 .$$

The minimum time problem is further subjected to a state variable inequality constraint of the following form :

$$y \leq \frac{x}{2} + 0.2 .$$

The above problem is the same as the one posed in Chapter (3) of Reference [29] (pps 119-120) with $h = 0.2$ and $\tan\theta = \frac{1}{2}$.

The inequality constraint can be converted into a path constraint with the use of a Valentine-type auxiliary state z

$$\frac{x}{2} + 0.2 - y - z^2 = 0 .$$

The initial condition of the auxiliary state z is given by

$$z(0) = +\sqrt{0.2} .$$

If we take the first time derivative of the path constraint and substitute for $\dot{x}$ the dynamic equation of x, we obtain a path equality constraint which involves the control

$$\frac{1}{2}V\cos\gamma - V\sin\gamma - 2zw = 0,$$

where the auxilliary control w is defined as the time derivative of the auxillary state z

$$\dot{z} = w.$$

Therefore the transformed problem is given by

$$x' = t_f V\cos\gamma,$$

$$y' = t_f V\sin\gamma,$$

$$z' = t_f w,$$

$$V' = t_f g\sin\gamma.$$

Since the end-time ofthe problem is not specified, we have made a change in the independent variable from t to τ where

$$\tau = \frac{t}{t_f}.$$

The "new" independent variable of the problem is now τ (which varies from 0 to 1); and $(\,)'$ denotes differentiation with respect to τ.

The initial conditions of the transformed problem are

$$x(0) = 0,$$

$$y(0) = 0,$$

$$z(0) = +\sqrt{0.2},$$

$$V(0) = 0,$$

and the terminal condition is

$$x(1) = 1.$$

The path equality constraint of the transformed problem is

$$\frac{1}{2}V\cos\gamma - V\sin\gamma - 2zw = 0.$$

The minimum-time of this problem for the special case when $g = 1$ and $l = 1$ is found to be 1.7741. This minimum time compares well with that computed using the formula given in [29] ($t_f = 1.7795$).

The optimal trajectory of the above problem is given in Figure (G.1.1).

§G.2 BOUNDED CONTROL OF DOUBLE INTEGRATOR PLANT [29]

$$\min_u I = t_f$$

The equations of motion are given by

$$\dot{x} = y,$$

$$\dot{y} = u.$$

The initial conditions are :

$$x(0) = 0,$$

$$y(0) = 0.$$

The terminal conditions are :

$$x(t_f) = 1,$$

$$y(t_f) = 0.$$

The minimum-time problem is subjected to a bound on the control u

$$-1 \leq u \leq 1.$$

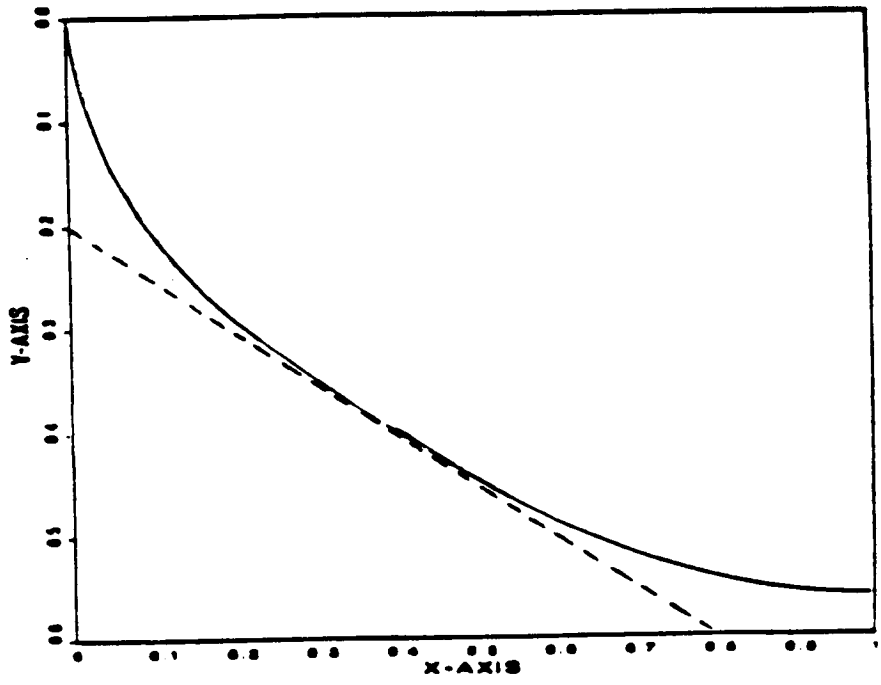

Figure G.1.1 Bounded Brachistochrone Problem

The above problem is the same as the one posed in Chapter (3) of Reference [29] (pps 112-114). Solution of this optimization problem involves "bang-bang" control, i.e. the control "bang" from u = -1 to u = +1 and vice versa.

The inequality constraint on the control can be converted into a path equality constraint with the use of an auxilliary control v

$$u^2 + v^2 - 1 = 0.$$

Therefore the transformed problem is given by

$$x' = t_f y,$$

$$y' = t_f u.$$

Once again, since the end-time of the problem is not specified, we have made a change in the independent variable like the one used in Example (1).

The initial conditions of the transformed problem are

$$x(0) = 0,$$

$$y(0) = 0,$$

and the terminal conditions are :

$$x(1) = 1,$$

$$y(1) = 0.$$

The path equality constraint of the transformed problem is

$$u^2 + v^2 - 1 = 0.$$

The minimum-time of this problem is found numerically to be 2.0041. This minimum time compares well with that obtained analytically (cf. [29], t_f = 2.0000).

The "Bang-bang" control of the problem and the optimal trajectory in the distance-velocity phase-plane is given in Figure (G.2.2).

§G.3 A GEODESIC PROBLEM [42]

$$\min_{u} I = t_f$$

The equations of motion are

$$\dot{x} = u\,,$$

$$\dot{y} = v\,,$$

$$\dot{z} = w\,.$$

The initial conditions are :

$$x(0) = 1\,,$$

$$y(0) = 0\,,$$

$$z(0) = 0\,.$$

The terminal condition are :

$$x(t_f) = \frac{1}{\sqrt{3}}\,,$$

$$y(t_f) = \frac{2}{\sqrt{3}}\,,$$

$$z(t_f) = \frac{3}{\sqrt{3}}\,.$$

Here u, v, and w are the components of the velocity vector in a 3-D Cartesian space. The idea here is to transfer between end points on an ellipsoid, moving at constant velocity, in minimum time without leaving the surface of the ellipsoid.

Thus, the minimum-time problem is subjected to the following state and control path equality constraints

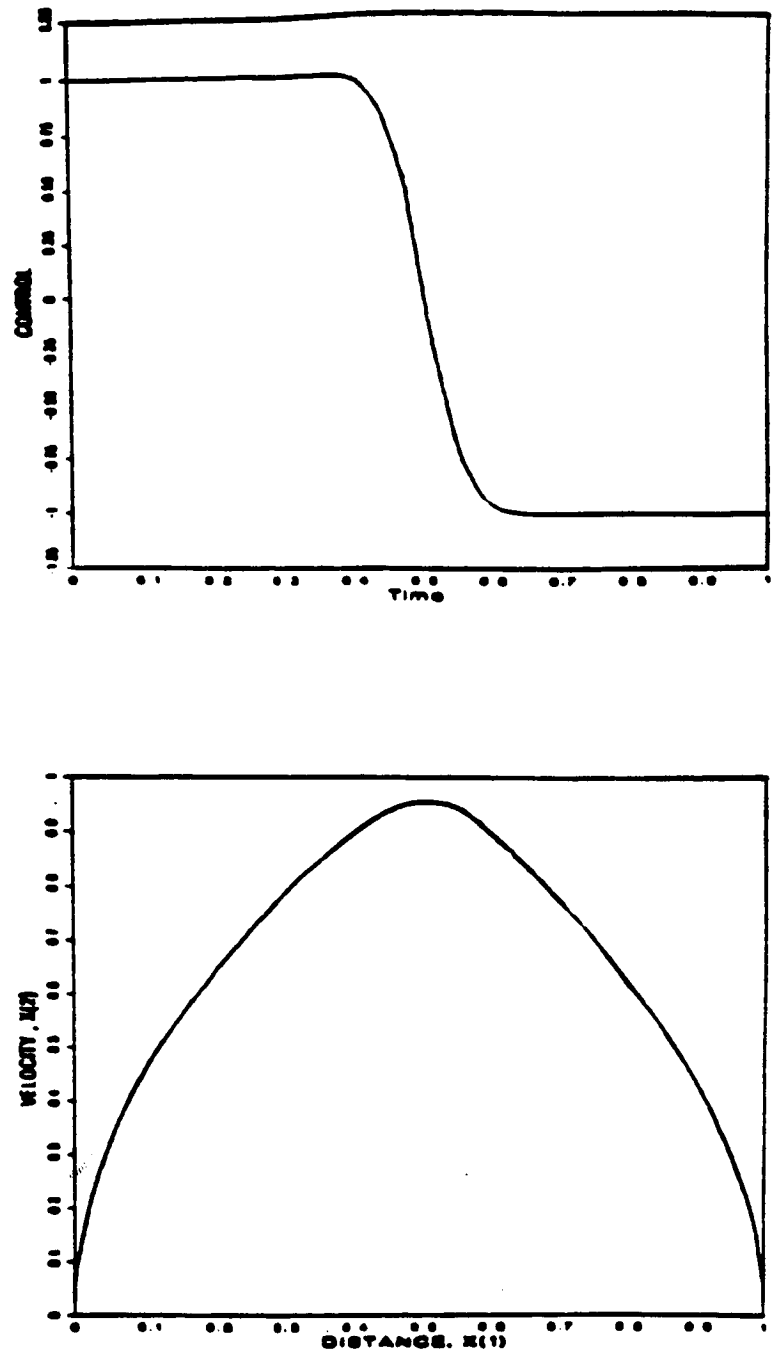

Figure G.2.2 Bounded Control of $\frac{1}{s^2}$ Plant

$$u^2 + v^2 + w^2 = 1,$$
$$x^2 + \frac{y^2}{4} + \frac{z^2}{9} = 1.$$

The first constraint states the fact that the magnitude of the velocity is unity. The second constraint requires that the travel be made on the surface of an ellipsoid with semiaxes $a = 1$, $b = 2$ and $c = 3$.

Since the first constraint of the problem is already a path *equality* constraint, further transformation is not necessary. If we take the time derivative of the second constraint equation and substitute into the resultant equation dynamic relations given by the equations of motion, we obtain an alternative form of the path equality constraint

$$xu + \frac{yv}{4} + \frac{zw}{9} = 0$$

Therefore the tranformed problem is given by

$$x' = t_f u,$$
$$y' = t_f v,$$
$$z' = t_f w.$$

Note the change in the independent variable from t to τ for the reason explained before.

The initial conditions of the transformed problem are

$$x(0) = 1,$$
$$y(0) = 0,$$
$$z(0) = 0,$$

and the terminal conditions are :

$$x(1) = \frac{1}{\sqrt{3}},$$
$$y(1) = \frac{2}{\sqrt{3}},$$
$$z(1) = \frac{3}{\sqrt{3}}.$$

In view of the need to stay on the surface of the ellipsoid at all times, one of the above three initial and terminal conditions is redundant.

The path equality constraints of the problem are

$$u^2 + v^2 + w^2 - 1 = 0,$$
$$xu + \frac{yv}{4} + \frac{zw}{9} = 0.$$

The minimum-time of this problem is found to be **2.1443.** this minimum time compares well with that obtained using the quasilinearization technique of References [49-50] ($t_f = 2.1439$).

Optimal trajectories in the $x - y$, $x - z$ and $y - z$ coordinate planes are given in Figure (G.3.3). Note that the first two trajectories are part of an ellipse while the last one is a straight line. This result is analogous to the shortest path "great-circle" travel on the surface of a sphere.

§G.4 BOUNDED TIME RATE OF CHANGE OF STATE

$$\min_u I = t_f :$$

The equations of motion are given by

$$\dot{x} = u,$$
$$\dot{y} = u^2 - x^2 - 0.5.$$

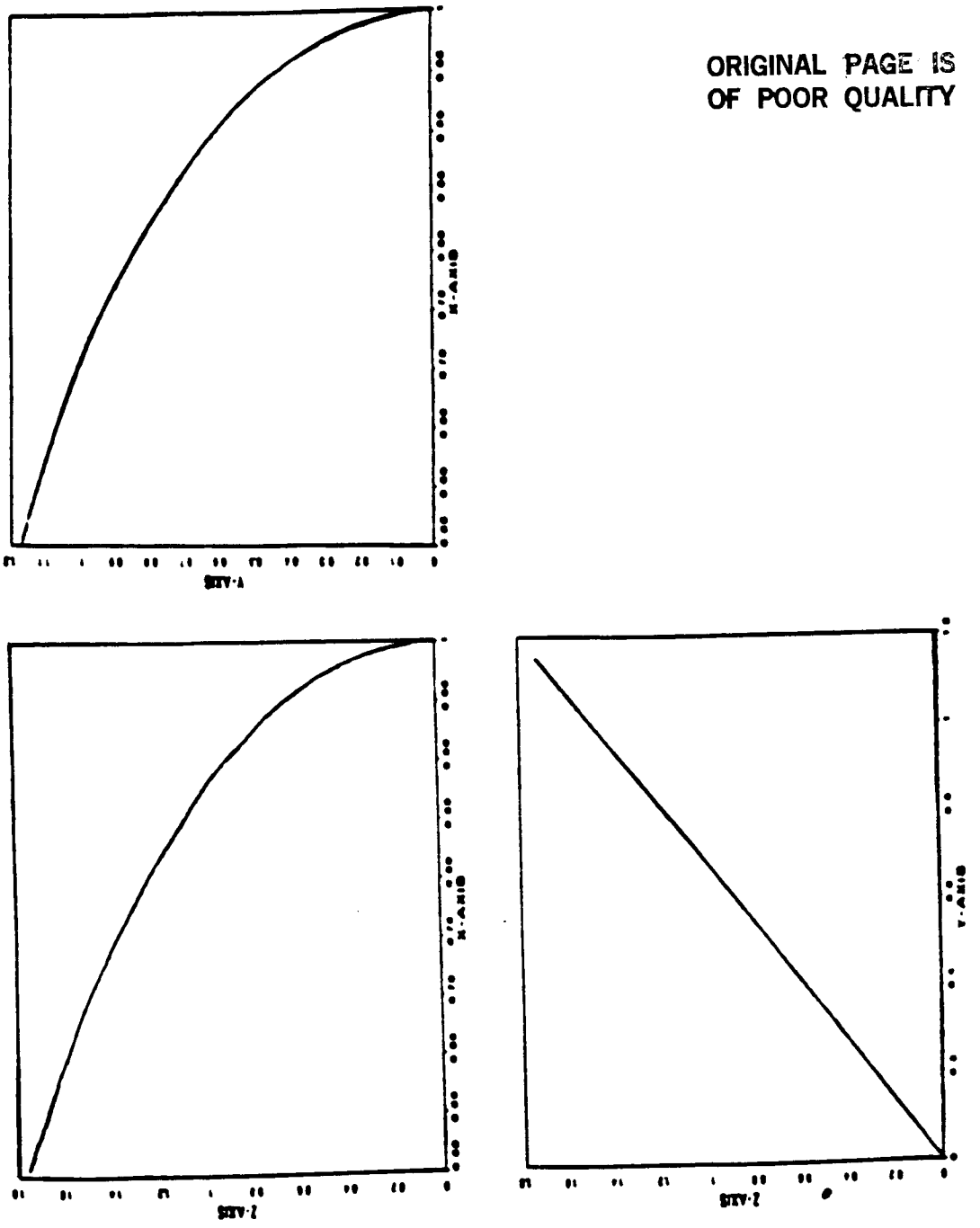

Figure G.3.3 A Geodesic Problem

The initial conditions are :

$$x(0) = 0,$$

$$y(0) = 0.$$

The terminal conditions are :

$$x(t_f) = 1,$$

$$y(t_f) = -\frac{\pi}{4}.$$

This minimum-time problem is subjected to a bound on the time rate of change of the state y from below

$$\dot{y} \geq -0.5$$

The inequality constraint can be converted into a path equality constraint by the use of the dynamic equation of y. The result is

$$u^2 - x^2 \geq 0.$$

The inequality can be further transformed into a path equality constraint with the use of an auxiliary control v

$$u^2 - x^2 - v^2 = 0.$$

Therefore the transformed problem is given by

$$x' = t_f u,$$

$$y' = t_f(u^2 - x^2 - 0.5).$$

Note the change in the independent variable from t to τ for the reason given before.

The initial conditions of the transformed problem are :

$$x(0), = 0,$$

$$y(0) = 0,$$

and the terminal conditions are :

$$x(1) = 1,$$
$$y(1) = -\frac{\pi}{4}.$$

The path equality constraint of the transformed problem is

$$u^2 - x^2 - v^2 = 0.$$

The minimum-time of this problem is found to be 1.8191, which compares well with that computed using the quasilinearization technique of Referene [49-50] and reported in Reference [48] ($t_f = 1.8222$).

The optimal time history of the state and the control of the problem are given in Figure (G.4.4). Note that in order to satisfy the bound on the time rate of change of y, the control u must at all times be larger or equal to x.

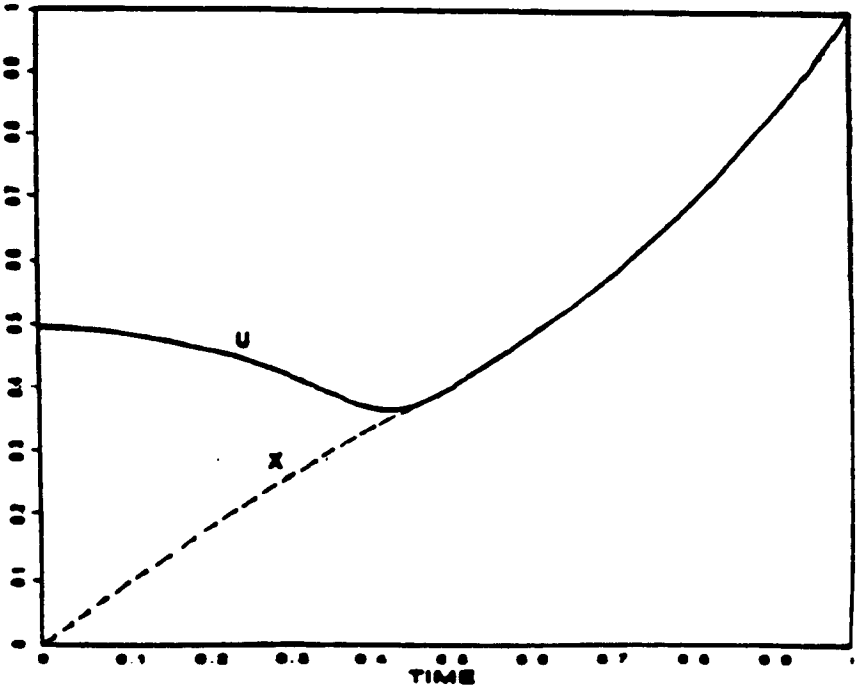

Figure G.4.4 Bounded Time-rate-of-change of State Control